

FORMULATION AND STABILITY
OF
MODEL FOOD FOAM MICROSTRUCTURES

by
Ernest Alexander Kristian Heuer

A thesis submitted to
The University of Birmingham
for the degree of

ENGINEERING DOCTORATE

School of
Chemical Engineering
The University of Birmingham

March 2009

UNIVERSITY OF
BIRMINGHAM

University of Birmingham Research Archive

e-theses repository

This unpublished thesis/dissertation is copyright of the author and/or third parties. The intellectual property rights of the author or third parties in respect of this work are as defined by The Copyright Designs and Patents Act 1988 or as modified by any successor legislation.

Any use made of information contained in this thesis/dissertation must be in accordance with that legislation and must be properly acknowledged. Further distribution or reproduction in any format is prohibited without the permission of the copyright holder.

ABSTRACT

Many foods contain large amounts of saturated fatty acids (SaFa), which are considered unhealthy, and their presence in the diet is one of the contributing factors of cardio-vascular disease, obesity and the inherent risk of diabetes. It has become the driver of food producers to manufacture products with as little of these oils as they can. Reformulation work based on Elmlea whipping creams sought to address this issue, by which the ingredients of the principal formulation were taken and ever increasing levels of liquid oil were added, but keeping the total oil concentration at 34%. Many of its' properties were tested and the optimum formulation was found to be that containing 20% hydrogenated and 14% liquid oil.

Further formulation work was associated with another product: ice-cream. Ice-cream distribution, particularly with its transport over the Rocky Mountains in the US, poses a large problem. Taking ice cream across the Mountains involves travelling at altitudes in excess of 2000 metres and this leads to its expansion due to the reduced air pressures. The product can spoil in transit. Further instabilities arise when extruded from a freezer. This instability was studied extensively in this work. It was seen that larger drops in pressure and at a slower rate were more detrimental to the model foam structure than small pressure differences and a fast rate. The fast pressure release seemed to have less of a detrimental effect on the resultant bubble foam microstructure.

***Gutta cavat lapidem non vi sed semper cadendo,
sic fit homo sapiens, non vi sed saepe legendo.***

Acknowledgments

To my life-coach, my late grandfather N. E. Cox: I owe it all to you. Thanks!

The Latin phrase above is one he liked quoting behind the cover of all his books, and I could not think of a more fitting place in which to be able to use it.

My eternal cheerleader, late U.M. Cox: I miss our interesting chats.

My forever interested and always enthusiastic late grandmother Uja Cox: she was always interested to know what I was doing and how I was proceeding, although might not have always grasped what it was all about!

I will miss your squeals of joy whenever a significant milestone was reached and also just your general cheekiness.

To both my sibling and also my mother, Natalie and Vivien respectively: your moral and emotional support has been invaluable.

And also to all my family and friends who have supported me along the way.

A very special gratitude goes out to all down at Colworth and also Vlaardingen for helping and providing the funding for the work.

With a special mention to Andrew Cox, Scott Singleton, Dudley Ferdinando, Michael van-Ginkel, Matt Golding, Mark Kirkland, the pilot plant team, Ice-foods, UFHRI and MSU in general. It was fantastic to be able to do a great part of my thesis work down there. What a cracking place to work!

On the Birmingham side, great thanks also to Ian Norton, Phil Cox, Peter Fryer, Richard Greenwood and Mostafa Barigou, for their unfailing support and assistance and the EPSRC for funding the Eng.D.

To Sam and Stu for a Tribometer graph (oil and water comparison).

And finally, last but by no means least, also to everyone in lab G10... it was great sharing lab-space with all of you.

Thanks for all your encouragement!

Index

CHAPTER 1

| | | |
|---------|--|----|
| 1.1 | Introduction | 1 |
| 1.1.1 | Business drivers for the research topic | 1 |
| 1.1.2 | Project objectives | 4 |
| 1.1.3 | Summary | 4 |
| 1.2 | Literature review | 5 |
| 1.2.1 | Bubble formation and definition of a liquid foam | 5 |
| 1.2.2 | Role of different molecules and proteins in foam formation and foamability | 7 |
| 1.2.2.1 | Proteins | 8 |
| 1.2.3 | Bubble Sizing | 9 |
| 1.2.4 | Tribology | 12 |
| 1.2.5 | Imaging by Confocal Scanning Laser Microscopy (CSLM) | 14 |
| 1.2.6 | Foam destabilisation | 15 |
| 1.2.7 | Mixed interfaces | 16 |
| 1.2.8 | Disproportionation | 17 |
| 1.2.9 | Food foams | 18 |
| 1.2.9.1 | Stabilisation of ice-cream | 18 |
| 1.2.9.2 | Manufacture of ice-cream | 19 |
| 1.2.9.3 | Intrinsic characteristics of ice cream | 21 |
| 1.2.9.4 | Stabilisation of whipped cream | 28 |
| 1.2.9.5 | Process of stabilisation | 34 |
| 1.2.10 | Lab-scale testing and production of foam microstructures | 35 |
| 1.2.11 | Choice of Model Mix for the food foam microstructures | 36 |
| 1.3 | Micrographs | 39 |
| 1.4 | Conclusions | 41 |

CHAPTER 2, Part I - Whipping of creams

| | | |
|-----|---|----|
| 2.0 | Whipping of creams | 42 |
| 2.1 | Ingredients and nutritional information of the commercial whipping cream. | 43 |
| 2.2 | Composition of the reformulated mixes | 44 |
| 2.3 | Preparation of the re-formulated mixes | 45 |
| 2.4 | Whipping and fat separation | 48 |

| | | |
|------|--|----|
| 2.5 | Whipping method | 50 |
| 2.6 | Slumping | 52 |
| 2.7 | Light microscopy of whipped structures | 56 |
| 2.8 | Cryo-SEM | 57 |
| 2.9 | Rheology | 57 |
| 2.10 | Tribology measurements | 58 |
| 2.11 | Differential Scanning Calorimetry | 59 |
| 2.12 | Closing remarks | 60 |

CHAPTER 2, Part II - Foaming of the ice-cream Model Mix

| | | |
|----------|--|----|
| 2.13 | Mix preparation and formulation | 62 |
| 2.14 | Preparation of a foam for the master batch method | 65 |
| 2.15 | Foam stability experiments | 66 |
| 2.15.1 | Creaming | 66 |
| 2.15.2 | Shear characterisation and stability | 66 |
| 2.15.2.1 | Bulk Rheology | 66 |
| 2.15.2.2 | Shear stage | 68 |
| 2.15.3 | Principles of Confocal Scanning Laser Microscopy | 69 |
| 2.15.4 | Confocal imaging of the model mix | 73 |
| 2.15.5 | Selection of riboflavin (Vitamin B ₂) as a fluorophore and comparison to other dyes | 74 |
| 2.15.6 | Intrinsic characteristics of Riboflavin | 76 |
| 2.15.7 | Bubble sizing | 77 |
| 2.15.8 | Bulk pressurisation | 79 |
| 2.15.9 | Pressurisation on a ‘micro’ scale | 80 |
| 2.15.10 | Disproportionation of foams under five different gases: Air, Nitrous Oxide (N ₂ O), Helium, Argon and Carbon Dioxide (CO ₂) | 82 |
| 2.15.11 | Pressure release | 85 |
| 2.15.12 | Pressure Cycling | 86 |
| 2.16 | Closing remarks | 88 |

CHAPTER 3 - Properties of dairy and vegetable whipping creams

| | | |
|-------|--------------|----|
| 3.1 | Introduction | 89 |
| 3.1.1 | Emulsions | 91 |

| | | |
|--------|---|-----|
| 3.1.2 | Whipped cream | 92 |
| 3.2 | Analysis of commercially available creams | 98 |
| 3.2.1 | Overrun of commercially available products | 98 |
| 3.2.2 | Optical microscopy of Elmlea Light samples | 103 |
| 3.2.3 | Bubble Sizing in Elmlea Light | 107 |
| 3.2.4 | Bubble sizing with the three commercial creams | 108 |
| 3.2.5 | Fat particle sizing with a Mastersizer | 108 |
| 3.2.6 | Bulk rheology | 109 |
| 3.2.7 | Thin Film Rheology | 112 |
| 3.2.8 | Oscillatory rheology with aerated samples at 10 °C | 116 |
| 3.2.9 | Oscillatory rheology with aerated samples at 25 °C | 119 |
| 3.2.10 | Analysis of fat content by Differential Scanning Calorimetry | 121 |
| 3.2.11 | Slumping behaviour of the whipped creams | 125 |
| 3.2.12 | Micrographs of commercial samples | 130 |
| 3.2.13 | Closing remarks | 133 |
| 3.3 | Analysis of reformulated whipping cream with a vegetable oil base. Elmlea patent. | 135 |
| 3.3.1 | Overrun Assessment of six reformulated creams | 135 |
| 3.3.2 | Bubble sizing and characterisation of reformulated mixes | 141 |
| 3.3.3 | Bulk rheology of the reformulated mixes | 151 |
| 3.3.4 | Thin film rheology of the reformulated mixes | 154 |
| 3.3.5 | Fat particle sizing with a Mastersizer | 159 |
| 3.3.6 | Slumping behaviour of the reformulated cream | 161 |
| 3.4 | SEM images of all the whipping creams studied | 164 |
| 3.4.1 | Comments on unaerated micrographs of all the whipping creams | 173 |
| 3.4.2 | Comments on micrographs of the aerated commercial samples | 178 |
| 3.4.3 | Comments on Mix 1 micrographs | 182 |
| 3.4.4 | Comments on Mix 3 micrographs | 185 |
| 3.4.5 | Comments on Mix 6 micrographs | 188 |
| 3.5 | General discussion | 189 |
| 3.6 | Conclusion | 198 |

CHAPTER 4 - Model foam and its pressure stability

| | | |
|-------|---|-----|
| 4.1 | Introduction | 200 |
| 4.2 | Results and Discussion | 202 |
| 4.2.1 | Dynamic video sequence and bubble imaging | 202 |
| 4.2.2 | Quiescent foam stability and drainage | 206 |
| 4.2.3 | Single pressure cycle | 213 |
| 4.2.4 | 5-bar consecutive pressure cycles from 1 to 6 bar {C}. Analysing the effect of air phase volume. | 220 |
| 4.2.5 | Bulk pressurisation: single cycle and three cycles | 225 |
| 4.2.6 | 5-bar pressure cycles. A comparison of 6 to 11 bar {B} with 1 to 6 bar {C} | 228 |
| 4.2.7 | Comparison of pressure cycling events from 1 to 11 bar {A} and from 1 to 6 bar {C} | 231 |
| 4.3 | Concluding remarks | 234 |

CHAPTER 5 - Effect of pressure release, foam structure and gas solubility

| | | |
|---------|---|-----|
| 5.1 | Introduction | 238 |
| 5.2 | Release Rate and disproportionation | 240 |
| 5.3 | Pressure release | 241 |
| 5.4 | Results | 242 |
| 5.4.1 | Pressure Analysis | 242 |
| 5.4.1.1 | Release rate | 242 |
| 5.4.2 | Disproportionation of foam microstructures under: Air, Nitrous Oxide, Carbon Dioxide, Helium and Argon | 252 |
| 5.4.2.1 | Disproportionation with Air | 253 |
| 5.4.2.2 | Disproportionation with Nitrous Oxide (N ₂ O). | 256 |
| 5.4.2.3 | Disproportionation with Helium | 258 |
| 5.4.2.4 | Disproportionation with Argon | 261 |
| 5.4.2.5 | Disproportionation with Carbon Dioxide (CO ₂) | 263 |
| 5.4.3 | Aeration times and textures of the foams with the different gases | 267 |
| 5.4.4 | Shear Analysis | 269 |
| 5.4.4.1 | Vane rheometry | 269 |
| 5.4.4.2 | Linkam shear stage | 277 |
| 5.5 | Discussion | 280 |
| 5.6 | Concluding remarks | 290 |

| | | |
|-----|--------------|-----|
| 6.0 | Conclusions | 293 |
| 7.0 | Further Work | 294 |
| | References | 297 |

List of Figures

CHAPTER 1

| | |
|--|----|
| Figure 1.1 Diagram of Bubbles. With particular reference to the lamellae and Plateau borders. | 6 |
| Figure 1.2 Stribeck curves obtained for Guar Gum solutions at 35 °C | 13 |
| Figure 1.3 Model for behaviour of Guar Gum | 13 |
| Figure 1.4 AFM data showing displacement of a β -lactoglobulin protein film (green) from an air-water interface by progressive addition of surfactant Tween 20 (black). Image sizes: (a) $1.0 \times 1.0 \mu\text{m}$, (b) $1.6 \times 1.6 \mu\text{m}$, (c) $3.2 \times 3.2 \mu\text{m}$ and (d) $10.0 \times 10.0 \mu\text{m}$. A schematic model of the displacement is illustrated below the images. The red rods are surfactants and the grey is protein. | 35 |
| Figure 1.5 Diagram of the Model Mix bubble interface | 37 |
| Figure 1.6 Confocal micrographs of a model foam undergoing a pressure cycle. Top Left: 1 bar absolute, before the experiment began. Bottom left: 1 bar absolute after the experiment finished. Top Right: 6 bar absolute on the pressurisation side, Bottom Right: 6 bar absolute on the depressurisation side. 10 \times magnification | 39 |
| Figure 1.7 Light microscope image of a model foam undergoing coalescence | 40 |
| Figure 1.8 Microstructure taken from a whipped non dairy whipping cream | 40 |
| Figure 1.9 Microstructures from a dairy whipping cream. In both cases the fat particles can be seen on the air interface of the bubble. | 41 |

CHAPTER 2, Part I

| | |
|--|----|
| Figure 2.1 Armfield FT9 homogeniser, with a diagram of the flow field created by the screw that sits behind the black turning wheel. | 48 |
| Figure 2.2 Schematic example of the sample layout within the Perspex box and lid for one experimental run at e.g. 25 °C and T = 0 minutes | 53 |
| Figure 2.3 Example of sampling error in the cream slumping experiment | 55 |
| Figure 2.4 Schematic of the MTM Tribometer | 59 |

CHAPTER 2, Part II

| | |
|---|----|
| Figure 2.1 Summary of Master Batch Method | 66 |
| Figure 2.2 Layout of Small vane with serrated cup and foam sample. | 68 |
| Figure 2.3 Internal layout of Linkam shear cell | 68 |
| Figure 2.4 Principles of CSLM | 70 |

| | |
|---|----|
| Figure 2.5 Absorption and emission spectra of (a) Nile Blue suspended in ethanol and (b) Rhodamine B. (absorption red / emission green), | 75 |
| Figure 2.6 Absorption and Emission spectra of Riboflavin for comparison | 75 |
| Figure 2.7 Structure of (a) Nile Blue and (b) Rhodamine B. | 75 |
| Figure 2.8 Absorption and Emission Spectra of Riboflavin, Vitamin B2. | 76 |
| Figure 2.9 Structure of Riboflavin | 76 |
| Figure 2.10 A representative example of a correctly tessellated image with a guard-frame (left). In comparison a raw un-tessellated image (right). | 79 |
| Figure 2.11 A representative example of a rejected and in-correctly tessellated image with a guard-frame. Included is the raw un-tessellated image for comparison. Sometimes incorrect tessellation could be fixed with the water-shed function. At other times though, it is irredeemable and the image and data-set had to be disregarded and the analysis repeated. | 79 |
| Figure 2.12 Binks Pressure pot. Capable of pressures up to 10 bar absolute. | 80 |
| Figure 2.13 Pressure cell setup | 81 |
| Figure 2.14 Pressure cell setup with a dedicated gas line attached to the chamber via the blue flex-hose. The image also shows the quartz crucible that holds the sample. The Black hose and pressure gauge are there for the pressure read-out. | 84 |
| Figure 2.15 Metallic frit and rod setup used for sparging the sample prior to aeration. | 85 |
| Figure 2.16 Summary of three different pressure cycling experiments. | 87 |

CHAPTER 3

| | |
|---|-----|
| Figure 3.1 Overrun curves of the three different double cream samples. The samples were stopped and started, and the Overrun was measured every 30 seconds. | 101 |
| Figure 3.2: Overrun curves of the three different double cream samples. The samples were whipped continuously until the desired time-point was reached. The stopped/started whip curves are included as a reference. Each data point was gathered in triplicate, for which, a fresh sample was used each time. | 103 |
| Figure 3.3 Representative micrographs of Emlea Light whipping cream, aerated for different time periods. Imaged with a Polyvar and the 10× Objective. | 105 |
| Figure 3.4 Representative micrographs of Elmlea Light whipping cream, aerated for two different lengths of time, either 60 seconds or 150 seconds. Imaged with a Polyvar and a 10× Objective (left micrographs) and 25× Objective (right micrographs). The higher | |

| | |
|---|-----|
| magnification image is from the same field of view as the one from low magnification. | 106 |
| Figure 3.5 Bubble sizing of the Elmlea light whipping cream which had been aerated for different time periods and imaged with a 10× objective. | 107 |
| Figure 3.6 Bubble sizing of the three commercial samples which had been aerated for 150 seconds and imaged with a 10× objective | 108 |
| Figure 3.7 Elmlea Light Emulsion particle analysis | 109 |
| Figure 3.8 Elmlea Full Fat emulsion particle analysis | 109 |
| Figure 3.9 J. Sainsbury's full fat whipped cream emulsion particle analysis. | 109 |
| Figure 3.10 Viscometry of the three different double whipping creams performed at 25°C. Samples whipped for 150 seconds. | 112 |
| Figure 3.11 Viscometry of the three different double whipping creams performed at 10°C. | 112 |
| Figure 3.12 Thin Film Rheology with a comparison of Distilled water and Rapeseed Oil. Stribeck curve at 37 °C, 50% SRR, 3N Ball Load. | 113 |
| Figure 3.13 Thin Film Rheology on the unaerated commercial mixes. Stribeck curves for Ball on disc at 37°C, 50% SRR, 3 N. | 114 |
| Figure 3.14 Thin Film Rheology on the aerated commercial mixes. Mixes aerated for 150 seconds. Stribeck curves for Ball on disc at 37°C, 50% SRR, 3 N | 115 |
| Figure 3.15 Elmlea Full Fat oscillatory rheology taken at 10 °C after 150 seconds whipping time | 116 |
| Figure 3.16 Elmlea Light oscillatory rheology taken at 10 °C after 150 seconds whipping time | 117 |
| Figure 3.17 J. Sainsbury's whipping cream oscillatory rheology taken at 10 °C after 150 seconds whipping time. | 118 |
| Figure 3.18 Oscillation rheology on triplicate measurements on aerated J. Sainsbury's cream at 25°C. Sample aerated for 150 seconds. Bohlin Rheometer, parallel plate geometry and a 2000 µm gap size. | 119 |
| Figure 3.19 Oscillation rheology on triplicate measurements on aerated Elmlea creams at 25 °C. Sample aerated for 150 seconds. Bohlin Rheometer, parallel plate geometry and a 2000 µm gap size. | 119 |
| Figure 3.20 DSC measurement of Elmlea light cream at a sampling rate of 5 °C per minute. Traces include baseline subtraction. | 121 |
| Figure 3.21 DSC measurement of Elmlea full fat cream at a sampling rate of 5 °C per minute. Traces include baseline subtraction. | 121 |
| Figure 3.22 DSC measurement of J. Sainsbury's cream at a sampling rate of 5 °C per minute. Traces include baseline subtraction. | 122 |
| Figure 3.23 Loss of visible area of samples relaxing under gravity at 25 °C. The trendline is a moving average. | 126 |

| | |
|---|-----|
| Figure 3.24 Loss of visible area of samples relaxing under gravity at 30 °C. The trendline is a moving average. | 127 |
| Figure 3.25 Loss of visible area of samples relaxing under gravity at 35 °C. The trendline is a moving average. | 128 |
| Figure 3.26 Loss of visible area of samples relaxing under gravity at 40 °C. The trendline is a moving average | 129 |
| Figure 3.27 Full Fat Elmlea sample aerated for 150 seconds and imaged with a 10× Objective. | 130 |
| Figure 3.28 Elmlea Light sample aerated for 150 seconds and imaged with a 10× Objective. | 130 |
| Figure 3.29 J. Sainsbury's cream sample aerated for 150 seconds and imaged with a 10× Objective. | 130 |
| Figure 3.30 Overrun characterisation of six different mix emulsions with varying hard palm oil and liquid rape-seed oil concentration. Always making up a 34% total oil phase, e.g. Mix1 – 10% and 24%, is 10% hard oil and 24% liquid oil. The mix overrun was measured every minute, for 30 minutes and then every 5 minutes, to make one hour aeration. The arrow demarcates the skip from 1 minute to 5 minute aeration. | 137 |
| Figure 3.31 Bar graph of Mix 1 with the highest proportion of liquid oil, illustrates the normalised bubble size distribution as a function of whipping time. Hard oil and liquid oil are 10 and 24 percent respectively. | 141 |
| Figure 3.32 Bar graph of Mix 2 with the next highest proportion of liquid oil, illustrating the normalised bubble size distribution as a function of whipping time. Hard oil and liquid oil are 15 and 19 percent respectively. | 142 |
| Figure 3.33 Whipping graph of Mix 2 and representative images of the aeration process at the selected imaging points. Scale bar is 25 µm. | 143 |
| Figure 3.34 Representative micrographs of mix 3 (20% hard oil and 14% liquid oil) and the whipping behaviour at the different phases. Taken at the start (Initial phase) image (a), 2 images in the middle (one from Phase I, b, & one from II, c) and at the end of the whipping curve (Phase IV), image d. They were imaged with a Polyvar and a 25× Objective. Scale bar = 25 µm | 145 |
| Figure 3.35 Micrograph of Mix 1 aerated for 11 minutes, reaching an Overrun of 168%. The image was taken with a 10× Objective. Visible liquid oil pooled at the bubble interface (arrows) can be seen. Scale bar = 50 µm. | 146 |
| Figure 3.36 Micrograph of Mix 3 aerated for 7 minutes, reaching an Overrun of 91.7%. The image was taken with a 10× Objective. Scale bar = 50 µm | 146 |

| | |
|--|-----|
| Figure 3.37 Micrograph of Mix 6 aerated for 4 minutes, reaching an Overrun of 77.7%. The image was taken with a 10× Objective. Scale bar = 50 µm. | 146 |
| Figure 3.38 Comparison bar graph of three mixes, illustrating the normalised bubble size distribution as a function of formulation at the optimum whip time, in minutes. Optimum whip is the highest Overrun achievable of each mix. | 147 |
| Figure 3.39 Average bubble size taken at the different time points within the entire whipping process. The ratio of hard oil to liquid oil in percent is included in the parenthesis (e.g. 34/00). The first is the hard oil the second the liquid oil | 149 |
| Figure 3.40 Average bubble size taken at the different time points, for Mix 1 and 6. | 149 |
| Figure 3.41 Un-aerated mix Instantaneous viscosity on triplicate measurements at 25°C with a Bohlin Rheometer, parallel plate geometry and a 1000 µm gap size. | 151 |
| Figure 3.42 Un-aerated mix Oscillation rheology on triplicate measurements at 25°C with a Bohlin Rheometer, parallel plate geometry and a 1000 µm gap size. | 151 |
| Figure 3.43 Aerated mix Oscillation rheology on triplicate measurements at 25°C with a Bohlin Rheometer, parallel plate geometry and a 1000 µm gap size. Total whipping time is indicated in square brackets. | 152 |
| Figure 3.44 Thin Film Rheology on the un-aerated reformulated mixes. Stribeck curves for Ball on disc at 37°C, 50% SRR and 3N ball loading. | 154 |
| Figure 3.45 Effect of Aeration and the Thin Film Rheological response on the reformulated mixes. The aeration time for each mix was different. The mixes were aerated to the point of maximum overrun. Stribeck curves for Ball on disc at 37°C, 50% SRR and 3N loading | 154 |
| Figure 3.46 a,b,c) Re-plotted data from Figure 3.44 and Figure 3.45 to allow the comparison of the aerated and un-aerated mixes side by side. | 155 |
| Figure 3.47 Average Ball Load on the disc (in N), with samples of different thickness. Either aerated or un-aerated. The results are based on triplicate read-outs. Error bars have been omitted for clarity purposes. | 159 |
| Figure 3.48 Mix 1 Emulsion particle analysis. | 160 |
| Figure 3.49 Mix 6 Emulsion particle analysis | 160 |
| Figure 3.50 Mix 3 Emulsion particle analysis | 160 |
| Figure 3.51 Slumping at 25°C of self made whipped vegetable oil emulsions, optimally whipped. Whipping time indicated next to | |

| | |
|---|-----|
| each mix. | 161 |
| Figure 3.52 Slumping at 25°C of self made whipped vegetable oil emulsions, overwhipped. Overwhipped samples were taken either at 55 minutes or 60 minutes. | 161 |
| Figure 3.53 Mix 6, 34% hard oil only and no liquid oil (34/00) with overnight ageing at 25°C. The overwhipped sample (left) aerated for 60 minutes and the peak whipped cream (right) aerated for 4 minutes. | 164 |
| Figure 3.54 J. Sainsbury's unaerated | 167 |
| Figure 3.55 J. Sainsbury's unaerated | 167 |
| Figure 3.56 Elmlea Full Fat unaerated | 168 |
| Figure 3.57 Elmlea Full Fat unaerated | 168 |
| Figure 3.58 Elmlea Light unaerated | 169 |
| Figure 3.59 Elmlea Light unaerated | 169 |
| Figure 3.60 Mix 1 unaerated | 170 |
| Figure 3.61 Mix 1 unaerated | 170 |
| Figure 3.62 Mix 3 unaerated | 171 |
| Figure 3.63 Mix 3 unaerated | 171 |
| Figure 3.64 Mix 6 unaerated | 172 |
| Figure 3.65 Mix 6 unaerated | 172 |
| Figure 3.66 J. Sainsbury's aerated for 150 seconds | 175 |
| Figure 3.67 J. Sainsbury's aerated for 150 seconds | 175 |
| Figure 3.68 Elmlea Full Fat aerated for 150 seconds | 176 |
| Figure 3.69 Elmlea Full Fat aerated for 150 seconds | 176 |
| Figure 3.70 Elmlea Full Fat aerated for 150 seconds | 177 |
| Figure 3.71 Elmlea Light aerated for 210 seconds | 177 |
| Figure 3.72 Mix 1, peak whip, aerated for 11 minutes | 180 |
| Figure 3.73 Mix 1, peak whip, aerated for 11 minutes | 180 |
| Figure 3.74 Mix 1, overwhipped, aerated for 30 minutes | 181 |
| Figure 3.75 Mix 1, overwhipped, aerated for 30 minutes | 181 |
| Figure 3.76 Mix 3, peak whip, aerated for 7 minutes | 183 |
| Figure 3.77 Mix 3, overwhipped, aerated for 30 minutes | 183 |
| Figure 3.78 Mix 3, peak whip, aerated for 7 minutes | 184 |
| Figure 3.79 Mix 3, overwhipped, aerated for 30 minutes | 184 |
| Figure 3.80 Mix 6, peak whip, aerated for 4 minutes | 186 |
| Figure 3.81 Mix 6, peak whip, aerated for 4 minutes | 186 |
| Figure 3.82 Mix 6, overwhipped, aerated for 30 minutes | 187 |
| Figure 3.83 Mix 6, overwhipped, aerated for 30 minutes | 187 |

CHAPTER 4

Figure 4.1 Captured coalescence events and time evolution from the first

| | |
|--|-----|
| observed coalescence event captured within a dynamic video sequence. The video sequence was obtained during depressurisation from 3 bar absolute pressure to 1 bar absolute. Total run time of the video was 90 seconds. Scale bar is 200 μm . | 204 |
| Figure 4.2 3-D sectional slice at 40 \times magnification of a foam with an air phase volume $\phi = 0.6$. Each step in the reconstruct is 15 μm . 30 images were taken for the reconstruct. Displacement between images was 1 μm . Image dimensions were 768 \times 512 pixels (each pixel 0.46 μm in size). | 205 |
| Figure 4.3 Achievement of different Overrun levels through the use of different sized Hobart mixers with different maximum speeds (in brackets) | 208 |
| Figure 4.4 Foam creaming and collapse of the formulations over time. $H_0 = 100$ ml. H_0 the initial level of the foam before the creaming experiment began, and H is the top level of the foam minus the serum level collected at the bottom of the measuring cylinder. | 208 |
| Figure 4.5 Drainage evidence. The sample once aerated was placed in multiple vane inserts which were sampled every 30 minutes up to a maximum of 5 hours. The results were gathered through oscillatory rheology at 1 Hz. Only the results for the start of the experiment, 2 hours and 5 hours are shown for clarity. | 210 |
| Figure 4.6 Vane Rheometer cup and geometry after carrying out an experiment with a “dry” foam from Figure 4.5. The coarsened structure of the foam can clearly be seen where it has left holes on the shaft of the vane. The foam is so dry that even the well that the vane created within the cup remains after the insert has been taken out. | 211 |
| Figure 4.7 The samples for this experiment were taken from a bulk master batch. This was held in three 500 ml Nalgene bottles and inverted every 15 minutes for a maximum of 5 hours. Samples were assessed every 30 minutes. The results were taken straight after the foam was made, 2 hours and 5 hours after aeration and assessed with oscillatory rheology at 1 Hz. | 212 |
| Figure 4.8 Confocal Scanning Laser Micrographs showing the pressure response of the model foam. The foam was pressurised to 11 bar absolute and the pressure gradually released in 1 bar steps. A confocal image was captured on each bar released, representative images are shown here. Experiment {A} | 214 |
| Figure 4.9 Single pressure cycle experiment, pressurising to 11 bar and de-pressurising to ambient pressure, carried out on three different samples with the same air phase volume, ϕ (in brackets). The graph above is an average of three experiments and shows the volumetric | |

| | |
|--|-----|
| dependence of the optimised model foam corrected for universal gas law, where $p \times V = \text{const}$. Experiment {A}. It also shows the number of bubbles counted per mm^2 of image. | 217 |
| Figure 4.10 Single pressure cycle experiment, pressurising to 11 bar and de-pressurising to ambient pressure, carried out on four different samples with different air phase volume, ϕ (in brackets). All four traces show a reproducible onset of coalescence at the 2 bar pressure point. The trace is a volumetric dependence of the optimised model foam corrected for universal gas law, where $p \times V = \text{const}$. Experiment {A} | 217 |
| Figure 4.11 Sub-sampling Figure 4.10 to deduce the actual shape of the first part of the graph (without the coalescence) | 218 |
| Figure 4.12 The coalescence section of the sub-sampled graph Figure 4.10 | 218 |
| Figure 4.13 The graph summarises the results obtained for 12 samples pressurised from 1 bar absolute to 6 bar absolute. Each trace comprises 3 averaged experiments per air phase volume ϕ (in brackets). Each fresh sample was subjected to three full cycles with a maximum Δp of 5 bar from the start pressure. The curves show the volumetric dependence of the optimised model foam corrected for universal gas law, where $p \times V = \text{const}$. There's almost complete structure collapse by the end of the third cycle. Experiments {C}. For clarity purposes error bars were omitted. | 221 |
| Figure 4.14 The results show the number of bubbles counted per mm^2 of image. Each sample was analysed in triplicate. The counting corresponds to experiments described in Figure 7a. (Experiments {C}) In sample 4 partial creaming could be observed. Error bars have been omitted for clarity purposes. | 222 |
| Figure 4.15 Mean area fraction for actual measured results versus those that might be expected. The results are those for Sample one, the sample with the highest air phase volume, ϕ (0.62) | 224 |
| Figure 4.16 Mean area fraction for actual measured results versus those that might be expected. The results are those for Sample four, the sample with the lowest air phase volume, ϕ (0.35) | 224 |
| Figure 4.17 Vane rheology measurements taken at 22°C of the model foam, $\phi = 0.60$. Experiments were performed after bulk pressurisation and release to a maximum of 6 bar absolute pressure. | 226 |
| Figure 4.18 Vane rheology measurements taken at 22°C of the model foam, $\phi = 0.66$. Experiments were performed after bulk pressurisation and release to a maximum of 6 bar absolute pressure. The foam was cycled 3 times to the specified pressure | 227 |
| Figure 4.19 The experiments described are matched for their air phase volume ϕ (in brackets). Each sample was subjected to three full | |

| | |
|--|-----|
| cycles with a maximum Δp of 5 bar from the start pressure (i.e. from 6 bar absolute for Experiment {B} and from 1 bar absolute for Experiment {C}). The curves show the volumetric dependence of the optimised model foam corrected for universal gas law, where $p \times V = \text{const.}$ and the evolution of bubble density per mm^2 of the captured images | 229 |
| Figure 4.20 In contrast to Figure 4.19, this graph shows the average surface area change for the bubbles at each given pressure. The samples were matched for their air phase volume ϕ (in brackets). Each sample was subjected to three full cycles with a maximum Δp of 5 bar from the start pressure (i.e. from 6 bar absolute for Experiment {B} and from 1 bar absolute for Experiment {C}) | 230 |
| CHAPTER 5 | |
| Figure 5.1 Different pressure release rates. Each column at each Δp is a fresh sample. The target pressure is pumped into the cell for each Δp which is then released using different release rates. The time indicated in the legend is the time taken to release the air per bar (e.g. two minutes, is two minutes per bar released). | 243 |
| Figure 5.2 Second image, taken after a waiting period after full pressure release of 4 minutes for the 2 minute release rate data and 2 minutes for the 30 second and 10 second release rate data. Coalescence events continued for a long time after the whole pressure had been released, this second image was taken to see how much the volume had changed over that extra time period. | 245 |
| Figure 5.3 1 Second per bar pressure release. Comparison of total bubble numbers from the field of view before and after the pressure release event has taken place and a comparison of the change in measured mean bubble volume, before and after the pressure release event. | 246 |
| Figure 5.4 10 seconds per bar pressure release. Comparison of total bubble numbers from the field of view before and after the pressure release event has taken place and a comparison of the change in measured mean bubble volume, before and after the pressure release event. A third measurement was included which involved leaving the sample to rest. | 247 |
| Figure 5.5 30 seconds per bar pressure release. Comparison of total bubble numbers from the field of view before and after the pressure release event has taken place and a comparison of the change in measured mean bubble volume, before and after the pressure release event. | 248 |
| Figure 5.6 2 minutes per bar pressure release. Comparison of total bubble numbers from the field of view before and after the pressure release | |

| | |
|---|-----|
| event has taken place and a comparison of the change in measured mean bubble volume, before and after the pressure release event. | 249 |
| Figure 5.7 In this figure the results for the starting mean bubble volume were divided by the mean bubble volume at the end, once the foam had undergone the pressure release regime. | 250 |
| Figure 5.8 In this figure the number of Bubbles counted at the beginning of the experiment in one field of view, was divided by the number of bubbles that were left once the pressure release event had taken place. | 252 |
| Figure 5.9 Air: CSLM imaging in air of disproportionation behaviour for 5 hours of the model mix sample under 3 different pressure regimes. Imaging took place at ½ hour intervals. Initial air phase volume of the mix shown in brackets (ϕ). The volumetric dependence of the foam was corrected using the universal gas law, where $p \times V = \text{const}$. | 254 |
| Figure 5.10 Bubble Count per mm^2 of image captured for a 5 hour experiment in Air | 255 |
| Figure 5.11 Sample aerated with air. Oscillatory vane rheology measurement on a fresh sample and a master batch sample after 5 hours disproportionation. | 255 |
| Figure 5.12 <i>Nitrous Oxide</i> CSLM imaging in Nitrous oxide (N_2O) of disproportionation behaviour for 5 hours of the model mix sample under 3 different pressure regimes. Imaging took place at ½ hour intervals. Initial air phase volume of the mix shown in brackets (ϕ). The volumetric dependence of the foam was corrected using the universal gas law, where $p \times V = \text{const}$. | 257 |
| Figure 5.13 Bubble Count per mm^2 of image captured for a 5 hour experiment in Nitrous Oxide | 257 |
| Figure 5.14 Sample aerated with nitrous oxide. Oscillatory vane rheology measurement on a fresh sample and a master batch sample after 5 hours disproportionation. | 258 |
| Figure 5.15 <i>Helium</i> CSLM imaging in Helium of disproportionation behaviour for 5 hours of the model mix sample under 3 different pressure regimes. Imaging took place at ½ hour intervals. Initial air phase volume of the mix shown in brackets (ϕ). The volumetric dependence of the foam was corrected using the universal gas law, where $p \times V = \text{const}$ | 259 |
| Figure 5.16 Bubble Count per mm^2 of image captured for a 5 hour experiment in Helium | 260 |
| Figure 5.17 Sample aerated with Helium. Oscillatory vane rheology measurement on a fresh sample and a master batch sample after 5 hours disproportionation. | 260 |

| | |
|--|-----|
| Figure 5.18 <i>Argon</i> CSLM imaging in Argon of disproportionation behaviour for 5 hours of the model mix sample under 3 different pressure regimes. Imaging took place at ½ hour intervals. Initial air phase volume of the mix shown in brackets (ϕ). The volumetric dependence of the foam was corrected using the universal gas law, where $p \times V = \text{const}$. | 261 |
| Figure 5.19 Bubble Count per mm ² of image captured for a 5 hour experiment in Argon | 262 |
| Figure 5.20 Sample aerated with Argon. Oscillatory vane rheology measurement on a fresh sample and the same sample after 5 hours disproportionation. | 262 |
| Figure 5.21 <i>Carbon Dioxide</i> CSLM imaging in Carbon Dioxide of disproportionation behaviour for 5 hours of the model mix sample under 3 different pressure regimes. Imaging took place at ½ hour intervals. Initial air phase volume of the mix shown in brackets (ϕ). The volumetric dependence of the foam was corrected using the universal gas law, where $p \times V = \text{const}$. | 264 |
| Figure 5.22 Bubble Count per mm ² of image captured for a 5 hour experiment in Carbon Dioxide | 264 |
| Figure 5.23 Sample aerated with Carbon Dioxide. Oscillatory vane rheology measurement on a fresh sample and the same sample after 5 hours disproportionation. | 265 |
| Figure 5.24 <i>Carbon Dioxide</i> The sample was shaken overnight for 17 hours. Subsequent imaging a day later took place at ½ hour intervals, up to a total of 5 hours. The sample was at ambient pressure. Initial air phase volume of the mix is shown in brackets (ϕ). The volumetric dependence of the foam was corrected using the universal gas law, where $p \times V = \text{const}$. | 265 |
| Figure 5.25 Shear rate and time evolution of foam sample on a linear shear regime. Air phase volume (ϕ) of the sample is given in square brackets. | 270 |
| Figure 5.26 Linkam shear stage data at two different speeds | 270 |
| Figure 5.27 Dependence of sheared foam sample on sampling time-point and shearing time | 272 |
| Figure 5.28 Shear rheometry, (sheared using a linear ramp) of a foam sample for 10 minutes using four different shear rates: 50 s ⁻¹ , 100 s ⁻¹ , 150 s ⁻¹ and 200 s ⁻¹ | 273 |
| Figure 5.29 Shear rheometry of a foam sample for 10 minutes using four different shear rates 50 s ⁻¹ , 100 s ⁻¹ , 150 s ⁻¹ and 200 s ⁻¹ . Sheared using continuous shear at the set shear rate | 275 |
| Figure 5.30 Shear rate and time evolution of foam sample on a continuous shear regime. Air phase volume (ϕ) of the sample is given in square | |

brackets.

276

Figure 5.31 a) shear breakdown of the model mix as seen under the Linkam shear stage. The graph is shear rate against ‘breakdown time’ b) Representative images of the initial foam microstructure and the image which was taken at the time which was considered as the point of shear “breakdown”.

278

List of Tables

CHAPTER 2

| | |
|--|----|
| Table 2.1 Nutritional Composition, per 100 ml of product, as described on the original packaging: | 43 |
| Table 2.2 Kenwood chef mixer speed settings | 49 |

CHAPTER 3

| | |
|--|-----|
| Table 3.1 Peak analysis of the thermal behaviour of the commercial creams within the DSC | 124 |
| Table 3.2 Representative photos of cream samples relaxing under gravity at 25 °C | 126 |
| Table 3.3 Representative photos of cream samples relaxing under gravity at 30 °C | 127 |
| Table 3.4 Representative photos of cream samples relaxing under gravity at 35 °C | 128 |
| Table 3.5 Representative photos of cream samples relaxing under gravity at 40 °C | 129 |
| Table 3.6 Cream behaviour during the main stages of whipping with a description of the phenomena taking place | 140 |

CHAPTER 4

| | |
|---|-----|
| Table 4.1 Cross-over point of G' and G'' at given oscillatory stresses for the 3 samples assessed in Figure 4.5 | 211 |
| Table 4.2 Increase in Measured Mean Bubble Volume relative to starting mean bubble volume during three consecutive pressure cycles | 231 |

CHAPTER 5

| | |
|---|-----|
| Table 5.1 Henry's law constants, taken at 25 °C in water | 241 |
| Table 5.2 Disproportionation histograms for the foams with five different gases. They were studied at three different pressures and the data represented is the initial foam condition and its evolution after 5 hours. The graphs are plots of normalised bubble frequency against bubble size, measured in mean bubble surface area. | 266 |
| Table 5.3 Visual assessment of Aeration textures | 268 |

CHAPTER 1

1.1 Introduction

1.1.1 Business drivers for the research topic

Unilever's mission is to add vitality to life. Meeting the everyday need for nutrition, hygiene and personal care with brands that help people feel good, look good and get more out of life. Each day, around the world, consumers are said to make 160 million decisions to purchase Unilever products. The company in its portfolio includes brand icons such as: Axe, Ben & Jerry's, Bertolli, Breyers, Country Crock, Degree, Dove (personal care products), Elmlea, Hellmann's, Klondike, Knorr, Lipton, Promise, Skippy, Slim-Fast, Snuggle, Suave, Sunsilk and Vaseline (Business Wire web, 2008).

Peter Ter Kulve, Category Senior Vice President of Ice-cream Global, is of the opinion that Ice cream is the core strategic category for Unilever, generating more than \$6 billion in global annual sales for the company (Business Wire web, 2008).

Unilever's market share of global ice cream production is 17% which corresponds to an annual world-wide output in excess of 5 billion litres. The US comes top of the ice cream league in consumption, where an excess of 20 litres are consumed per capita per year (Business Wire web, 2008).

In addition to the highest consumption, the US also faces one of the most unusual transport issues which confront ice cream distributors in the whole world, as transporting ice cream across the Rocky Mountains involves travelling at altitudes in excess of 2000 metres. This leads to the expansion of the ice cream due to reduced air pressures. Since ice cream is compositionally 50% air, a great deal of the dairy products can spoil in transit (Cosway, 2008). Ice-cream packaged in tubs may blow their lids and run down the sides with a loss of product as a consequence and in addition damaged packaging. The transport problem can be exemplified by another ice-cream, Magnum. This particular product could expand inside its chocolate couverture, leading it to crack and break, contributing to an organoleptically unacceptable product. Placing this for sale would lead to persistent customer complaints. Various suggestions to circumvent this problem have been proposed but would prove just too costly. One of the suggestions would involve building a tunnel through the Rocky Mountains themselves, or building a production and distribution warehouse on either side of the mountains. Both of these suggestions have been dismissed out of hand. The company instead employs fairly simple strategies to by-pass the problem (Business Wire web, 2008). If the products are to be transported in this way, the ice-cream in the tubs is not filled up to the top, leaving a head-space for it to be allowed to expand into.

A further ice-cream instability issue arises when the product is dispensed from the ice-cream freezer wherein it undergoes a pressure gradient as it is extruded from a nozzle. It is going from a pressurised system, with the product being released from pressurised conditions of around 6 bar, to ambient pressure. The patent filed by Windhab and Wildmoser, (2005, number: WO/2005/070225) describes the problem in greater detail.

Understanding and helping to solve bubble stability issues within ice-cream be it due to low pressure and mimicking its transport route over the Rocky Mountains, or the change of pressure it undergoes when it is released and dispensed from the freezer, would be of great benefit to Unilever.

There's also an increasing demand for products with less hydrogenated oils (Golding and Pelan, 2008) and Unilever would like to meet this demand by seeking to market their products containing higher levels of 'healthier' oils. Perneti et al., (2007) mention that the most common way to provide texture to the lipid phase of food products is by including a crystalline hardstock. These hardstocks contain large amounts of saturated fatty acids (SaFa), which are considered unhealthy, since their presence in the diet is among one of the contributing factors of cardio-vascular disease (Keys et al, 1965), obesity and the inherent risk of diabetes. Work in this thesis tackles this problem; firstly by analysing two commercially available products that Unilever have on the market, two (non-dairy) double whipping creams, which trade under the name

Elmlea. For comparison purposes a dairy cream from J. Sainsbury's (of the double whipping kind) was also analysed.

By reformulating the cream to include healthier oils which would reduce the amount of saturated fat within the whipping cream, healthier products could be manufactured which would in turn increase the concerted efforts being taken to tackle global obesity issues.

1.1.2 Project objectives

The project was set up to create an in depth understanding of the formation, stability and mechanisms involved in the formulation and creation of whipping creams containing ever higher amounts of healthier (liquid) oils.

The additional inherent instability of food foams was also studied. A model mix similar to an ice-cream base mix was created. All foams created for this purpose were made so that they should be ambient stable. Of particular interest were the processing parameters that are used to create food foams. Perhaps the two most important parameters that will be investigated in this thesis are shear and pressure.

1.1.3 Summary

The Literature review summarises the conditions required for foam formation, with particular reference to the type of bubble instabilities that exist. Factors required for the processing of both ice-cream and whipped cream are

enumerated. Sample micrographs of bubbles, foams and whipped cream are also included.

The thesis contains two materials and methods sections, Part I (the whipping one) describes the work covered in the first results chapter (chapter 3) and whipped cream as its subject. Part II of the methods and materials section, titled foaming, covers the work of the final two chapters, which are concerned with the shear and pressure work (chapters 4 and 5).

1.2 Literature review

1.2.1 Bubble formation and definition of a liquid foam

Almost all the foam systems (bar a few exceptions) have one thing in common; they all require agitation of some kind to be created. Upon removal of this agitation the created structure deteriorates. The timescale at which it does this is very much dependent on the make-up of the dispersed and continuous phases.

Perry and Green (1997) give the definition of a bubble as a globule of gas or vapour surrounded by a mass or thin film of liquid. By extension, globular voids in a solid are sometimes called bubbles. Foams are a group of bubbles separated from one another by thin films, the aggregation having a finite static

life. Although non-technical dictionaries do not distinguish between foam and froth, a technical distinction is often made. A highly concentrated dispersion of bubbles in a liquid is considered a froth even if its static life is substantially nil (i.e. it must be dynamically maintained). Thus, all foams are also froths, whereas not all froths are foams. The definition of a foam according to Bergman and Egloff (1941) (*in* Perry and Green, 1997) is that it can only be produced in systems possessing the proper combination of interfacial tension, viscosity, volatility, and concentration of solute or suspended solids.

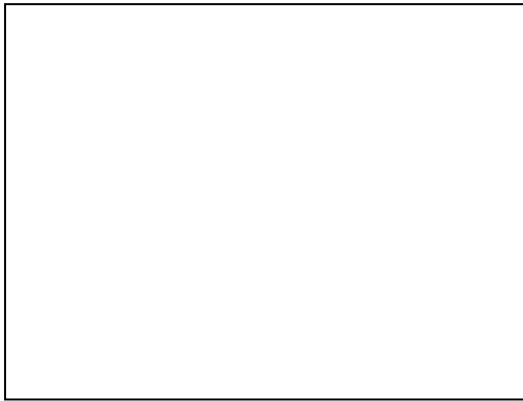


Figure 1.1 Schematic diagram of Bubbles showing the lamellae and plateau borders.

The thin walls of bubbles comprising a foam are called laminae or lamellae. Bubbles in a liquid originate from one of three general sources: (1) they may be formed by de-supersaturation of a solution of a gas or by the decomposition of a component in the liquid (2) They may be introduced directly into the liquid by a bubbler or sparger or by mechanical entrainment through mixing (of different kinds); and (3) they may result from the disintegration of larger bubbles already in the liquid (Perry and Green, 1997). Instability of foam is covered in section 1.26 together with the description of Plateau borders.

1.2.2 Role of different molecules and proteins in foam formation and foamability

Proteins and emulsifiers are both surface active ingredients, reducing the surface tension at an interface and therefore alleviating the thermodynamic tendency to minimise the interfacial area. However, they have very different chemical structures, and the mechanism by which they stabilise bubbles in food products differs widely. Typical emulsifiers are small fatty acid chains with a polar head. Once in solution and at a bubble interface, the water-loving polar moiety will sit in the aqueous liquid, while the hydrophobic lipid chain sticks out into the air.

Proteins, by contrast, are long chain molecules made up of amino acid units. Some parts of the protein molecule are hydrophobic, other parts hydrophilic. The molecule can therefore unfold at a bubble interface, such that the hydrophilic portions are in the water and the hydrophobic portions in the air (Stauffer, 1999).

Bubbles will burst or coalesce if the interface thins excessively. Emulsifiers stabilise bubbles by the Gibbs-Marangoni effect which can be described as a rapid diffusion of a surfactant into a depleted area when local thinning of a bubble occurs (Stauffer, 1999) ; (Campbell and Mougeot, 1999). This diffusion onto the bubble surface sweeps liquid in with it which then re-thickens the thinned region of the bubble. In contrast, proteins have low rates of surface

lateral diffusion, and instead stabilise bubbles primarily by forming a rigid layer of interlinked proteins at the interface. A mixed system of protein and surfactant can be unstable, as the surfactant dilutes the proteins and prevents their interlinking, while the proteins interfere with rapid surface diffusion of the emulsifier (Campbell and Mougeot, 1999).

The mode of action within this mixed system, it is assumed, is that there is an incompatibility between the protein systems within the bubble wall. Individually the protein and surfactant are capable of forming stable foam-stabilising networks, through polypeptide–polypeptide interactions but also through linkages with other key foam components, but when they are present together, the same interactive opportunities are negated. Either type of molecule individually is capable of producing a stable foam, whereas, when mixed together, they are incompatible and neither agent can establish a stable foam according to its given mechanism (Bamforth and Milani, 2004)

1.2.2.1 Proteins

In principle, proteins are polyampholytes, composed of a linear polypeptide backbone to which amino-acid side chains with various degrees of polarity and charge are attached (van Aken et al., 2003b) ; (Belitz et al., 2004). In the dissolved state, the polypeptide chain is often folded, structuring the molecules at different levels of organisation. The primary structure refers to the amino acid sequence. The secondary structure corresponds to regular arrangements of the

polypeptide backbone in elements, such as α -helices, β -sheets and random coil segments. Super-secondary structures correspond to combinations of secondary elements, such as coiled-coil α -helices and β -strands. The tertiary structure corresponds to compact highly structured domains along the polypeptide chain, which are loosely connected to each other. The quaternary structure of a molecule is given by the assembly of non-covalently linked sub-units, which is often found in larger proteins, such as glycinin.

In many proteins, the structure is stabilised by intramolecular disulfide bonds (van Aken et al., 2003a).

Protein conformational changes resulting from adsorption of the protein molecules to an interface are usually referred to as ‘surface denaturation’. For many globular proteins, surface denaturation leads to an increased exposure of non-polar and sulfhydryl containing amino acids to the aqueous phase (McClements, 2004). Examples of disordered and globular proteins are given in the Appendix section A1.

1.2.3 Bubble Sizing

Calvert and Nezathi (1987) review the different bubble sizing options available, at the time of writing their publication. The techniques within these standard sizing methods have not changed significantly since then.

They mention that remote measuring systems are usually either optical, requiring a reasonably transparent material, or ultrasonic, which is unlikely to have the resolution required for sizing. They further mention that a method using techniques similar to those used in laser Doppler velocimetry could give a continuous indication of bubble size and bulk foam velocity. They speculate that such a system might be used to make measurements a short distance inside the bulk of the foam (Calvert and Nezhati, 1987)

A number of approaches to obtaining average values over a relatively large volume are possible. For example, the electrical conductivity of a foam is a function of both bubble size and expansion ratio. Similarly, the speed of sound in a foam might be useable. However, both these approaches would need further development. They are unlikely to be able to give bubble size distributions, or measurements in a small enough region to obtain variations across a flow field. The authors argue that to achieve these results, it is necessary to examine the foam at the individual bubble level, rather than the bulk fluid level, but that a method which has been used in gas-liquid dispersions is to use electrodes to detect the passage of individual bubbles and could be employed (Calvert and Nezhati, 1987).

However, this method is not likely to be so effective at high bubble densities, and Calvert and Nezhati (1987) argue that in fact it could modify the

flow it is trying to observe and in addition could not be used for stationary foams (Calvert and Nezhati, 1987).

In general the properties of a foam are usually not satisfactorily characterised, because the liquid and gas distribution in the foam is only partly measured or not at all. Bisperink et al., (1992) described two methods with which to measure foams and several of their properties: like the collapse of a foam, the rate of drainage, the gas fraction in the foam, and the bubble-size distribution. One method is based on an optical glass-fibre technique and the other is a Foam Analyser. The difference between the two is that the Foam analyser is based on the use of a single probe that is moved through immobile bubbles in a foam whereas the glass fibre method is based on the use of a stationary multi glass-fibre probe with which the velocity and the size of passing bubbles is measured (Bisperink et al., 1992).

Macroscopic detection of creaming can in principle be done by visual observation; however, in turbid systems substantial gradients of the droplet concentration may already exist long before they become apparent to the eye. The detection can be improved by using acoustic measurements (ten Grotenhuis et al., 2000). The velocity of ultrasound is sensitive to the droplet concentration, and therefore the transmission of sound waves through a sample as a function of the height in the sample can be used to detect creaming. Similar information is obtained by scanning the turbidity and reflectivity of

light as a function of the height in the sample, and various commercial analysers exist which can perform this task (ten Grotenhuis et al., 2000), one of them made and marketed by Turbiscan (Formulaction, Hemel Hempstead, UK). Structural changes at colloidal scale will precede an actual phase separation, and monitoring these changes may therefore be useful for predicting stability (ten Grotenhuis et al., 2000).

1.2.4 Tribology

Tribology (or thin film rheology) is the science of adhesion, friction and lubrication and has, in the past, been used to try and correlate in-mouth response of food materials. Malone et al., (2003) attempted to correlate friction measurement with perceived slipperiness of a series of guar gum solutions (0.05, 0.2, 0.4, 0.6%). They found that a significant level of correlation between fluid lubricant properties and oral slipperiness perception took place in the mixed lubrication regime which occurs at entrainment speeds between 10 and 100 mm s⁻¹. This suggests that this regime is the one most relevant to describe in-mouth processes associated with slippery mouthfeel.

The Stribeck curves shown in Figure 1.2 demonstrate that the biopolymer significantly reduces the friction coefficient in the mixed regime.

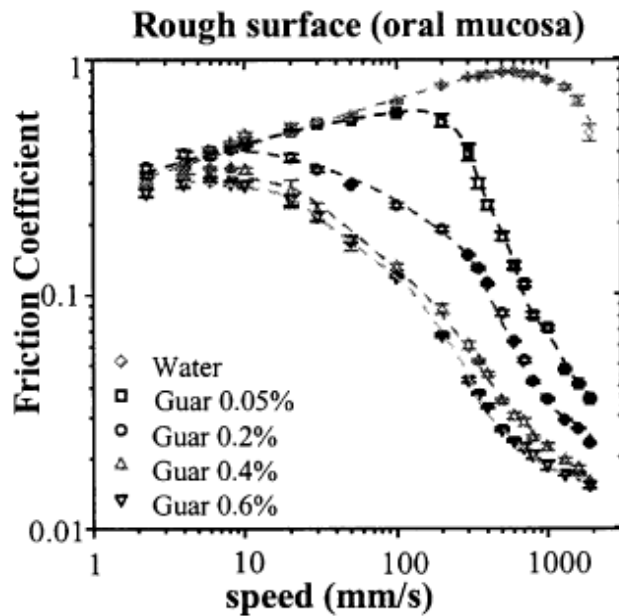


Figure 1.2 Stribeck curves obtained for Guar Gum solutions at 35 °C (Malone et al., 2003).

The authors elucidate the mechanism by which guar forms a lubricating film between the surfaces. They illustrate the principle in Figure 1.3, where at low speed, the non-absorbing polymer cannot fit into the gap and is therefore excluded.

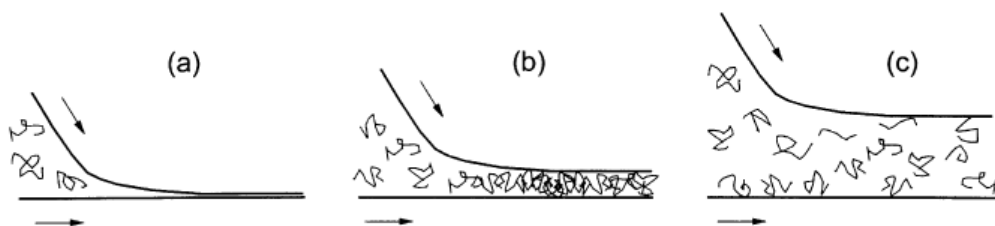


Figure 1.3 Model for behaviour of Guar Gum.

Legend

- (a) In the boundary regime the film thickness is too small for the non-adsorbed polymer to enter in the contact zone;
- (b) The polymer can fit in the gap. Confinement of the polymer in the contact zone increases the inlet viscosity;
- (c) at higher speeds the inlet viscosity is based on that of the base fluid.

Source: (Malone et al., 2003)

As the entrainment speed is increased and the surfaces start to part, the guar polymer fills the gap as a viscous film and becomes effective at reducing the friction coefficient (shown by the Stribeck curve in Figure 1.2).

Malone et al., (2003) further hypothesise about the two mechanisms that could explain the reduction in friction with high viscosity fluids. One is that the presence of a layer of polymer in the contact zone physically stops the solid surfaces from contacting; and the second is that the high viscosity of the fluid leads to the suppression of turbulent flow in the contact zone, and therefore limits drag. At the much higher speed the guar polymer is no longer confined within the contact zone and the film in the gap is dominated by the bulk fluid viscosity. Therefore at higher speed the effect of the polymer on the lubrication properties tend to be negligible. (Malone et al., 2003).

1.2.5 Imaging by Confocal Scanning Laser Microscopy (CSLM)

The improvement in the quality of products already in the food market (frozen foods, meat and dairy products), the design of new food commodities (e.g. spreads of different formulations, duplex emulsions, etc.) and the modification of properties of products directly derived from animal and plant tissues (e.g. intermediate moisture products) are all based on changes in the microstructure; their control and analysis must be done at microscopic level. The technique of light microscopy is subjected to a serious limitation arising from the difficulty in obtaining sharply delineated images along the viewing (z-axis), or depth, of the specimen. Good quality images of the microstructure are

obtained only from thin sections of the sample, however, slicing may cause damage to the product structure by shear and compression forces. Moreover, sectioning requires tedious fixation and embedding, which may introduce artifacts. The introduction of confocal scanning laser microscopy (CSLM) meant a major advance in microscopy. CSLM greatly enhances the ability to obtain sharp, well resolved images from selected levels within relatively thick, three dimensional objects (Ferrando and Spiess, 2000)

1.2.6 Foam destabilisation

Foams are principally unstable, meaning that foam properties vary with time as a result of shifts in the distribution of gas and liquid within it. Three different processes contribute to the instability of foams i.e. drainage, coalescence and disproportionation.

Drainage is the liquid flow from a foam as a result of gravity and capillary forces. As a consequence of drainage a foam becomes dryer and bubbles may become distorted. In that case foams change from spherical foams to polyhedral foams. Coalescence is the merging of two bubbles as a result of the rupture of the film between them. Larger bubbles appear in the foam and the number of bubbles decreases. Disproportionation is described as interbubble gas diffusion. As a result of gas diffusion larger bubbles grow at the expense of smaller bubbles. Smaller bubbles shrink and may finally disappear (Bisperink et al., 1992). The driving force is the Laplace pressure, which for a spherical particle is given by $2\gamma/r$, where γ is the interfacial tension and r is the radius

(Ettelaie et al., 2003). All these processes affect the distribution of the liquid and gas phase and thus alter the foam properties (Bisperink et al., 1992).

Film thicknesses at a given height were measured in steady state foams that are generated by passing nitrogen through a collection of equal sized orifices (to give an approximately monodisperse foam). The liquid phase was a mixture of water, glycerol and sucrose with Aerosol as a surfactant (Garrett, 1993). Once a foam is formed then the geometry of the bubbles is determined by the gas phase volume. When this exceeds a certain critical value, distortion of bubbles occurs, so that planar films and plateau borders form. In these circumstances the process of drainage of liquid out of the foam is influenced by the capillary pressure in the foam (Garrett, 1993).

1.2.7 Mixed interfaces

There are several ways to control emulsion destabilisation: the most popular way is to add low molecular weight emulsifiers to the recipe. The idea is that in the presence of these components a mixed interfacial layer consisting of proteins and low molecular weight emulsifiers is formed. Although alone, both low molecular weight emulsifiers and proteins can stabilise foams and emulsions, it is known that only small quantities of emulsifier added to a protein-stabilised interface reduce rather than enhance emulsion stability. This is because low molecular weight surfactants and proteins stabilise interfaces by different mechanisms. Surfactants generally stabilise an interface by the Gibbs-

Marangoni mechanism that relies on the surfactant having a high degree of lateral mobility involving minimal interactions of surface adsorbed molecules. Conversely, proteins stabilise an interface by forming a strong visco-elastic network in which the protein molecules are essentially immobile and interacting with each other. The two mechanisms are incompatible and in the absence of intermolecular protein-surfactant attractive forces at the interface, addition of surfactant leads to competition between the two amphiphilic molecules for the interface during or after emulsification, giving rise to instability. The net result is that the interfacial protein layer is weakened and the stability of the emulsion is reduced, generally by induced flocculation (Leser and Michel, 1999)

1.2.8 Disproportionation

Dutta et al., (2004) mention that very little work has been done to study the disproportionation process in aerated food products where air is the dispersed phase. The process of gas diffusion owes its origin to the fact that the pressure inside a bubble is greater than the atmospheric pressure, due to the surface tension and curvature of the bubble. Due to this pressure difference, gas diffuses out of a bubble when the aerated food system is in contact with the atmosphere and as a result, the bubble size as well as the overrun (the amount of incorporated air) would decrease with time. As the bubble size decreases, the pressure difference increases and an acceleration of gas loss with time could be

expected, this is if only the gas diffusion mechanism was at play (Dutta et al., 2004).

In their conclusion, Kokelaar and Prins (1995) mention that surface properties are important in determining the rate of disproportionation of gas bubbles directly after mixing, and they may be important in determining the film stability against rupture for very thin films.

1.2.9 Food foams

1.2.9.1 Stabilisation of ice-cream

The ice cream system can be considered as an aerated suspension of crystallised fat and water in a highly concentrated sugar solution containing hydrocolloids, casein micelles and proteins. During manufacture fat agglomeration occurs depending on process conditions and the type of emulsifier used. This has an impact on the stabilisation of the ice cream foam, especially in the molten state during consumption. For example smaller dispersed air cells lead to a more stable foam and a creamier mouthfeel of the product (Eisner et al., 2005).

Ice cream is produced in two main steps. In the first step a premix is prepared, which is then aerated and frozen in the second step. The premix contains mainly fat, proteins, sweeteners and water. A typical recipe contains

10% fat from milk, cream or vegetable sources, 10% nonfat milk solids which are mainly proteins from milk or whey powders and 15% sweeteners (Eisner et al., 2005).

In ice-cream the milk-solids-no-fat (msnf) phase contains the lactose, casein micelles, whey proteins, minerals (ash), vitamins, acids, enzymes and gases of the milk or milk products from which they were derived. Proteins contribute much to the development of structure in ice cream, including emulsification, whipping and water holding capacity (Goff, 1997).

Emulsification properties of proteins in the mix arise from their adsorption to fat globules at the time of homogenisation (Goff, 1997). Whipping properties of proteins in ice cream contribute to the formation of the initial air bubbles in the mix (Goff, 1997). The water holding capacity of proteins leads to enhanced viscosity in the mix, which imparts a beneficial body to the ice cream, increases the meltdown time of ice cream and contributes to reduced iciness (Goff, 1997).

1.2.9.2 Manufacture of ice-cream

The following paragraphs summarise in detail the ice-cream making process as it takes place at the Ben and Jerry's factory. In one of the first steps of manufacture all the liquid ingredients go into the blending tank, which holds 1000 gallons. The blending tanks have mixers and agitators; from there the mix goes through strainers which then lead it to a surge tank. From the surge tank it

then proceeds to the pasteurisers and homogenisers. Two processes which in this factory happen co-currently. The pasteurisation of the mix in the Ben and Jerry's setup takes place at HTST (high temperature and short time) which equates to the mix being heated to 83 °C for 20 seconds. When the mix reaches 63 °C this is then the approximate temperature at which it is homogenised, and this process is undertaken at 2000 psi. Homogenisation is carried out at this higher temperature as the mix can be processed with less difficulty than at colder temperatures. As mentioned earlier, the process of homogenisation and pasteurisation take place at the same time. Once homogenisation has taken place, the mix is re-circulated back to the cooling section of the pasteurisation process and cooled to a specified temperature of 3 °C. After homogenisation the mix is then aged for a minimum of 4 hours, although it is not uncommon to age the mix for longer, sometimes this might take place overnight with the mix being stored in the tank room. In the tank room the mix cools by a further fraction down to 2 °C. After ageing, the mix can be processed and it is usually processed using a continuous freezer (which at Ben and Jerry's is a Hoyer freezer). It is able to process 750 gallons of mix per hour. In the freezer the base mix is cooled from the holding temperature of 2 °C to about -5 °C. The mix is pumped into the freezer at a constant and controlled rate and in addition air is pumped into the freezer barrel at a constant and controlled rate as well. The mix is processed at a pressure of about 5 bar. The agitators in the freezer whip the mix at a constant speed while the outer cylinder is being cooled by the liquid ammonia refrigerant. Once frozen the dashers scrape off the mix and it

can then be extruded. After extrusion the ice-cream gets packaged and sent to the hardener (Ben and Jerry web, 2006).

1.2.9.3 Intrinsic characteristics of ice cream

Ice-cream if characterised, could be described as a partly frozen four-phase system consisting of air bubbles, ice crystals, emulsified fat and a continuous serum phase containing dissolved and colloidal sugars, salts, proteins and stabilisers. Typical ice cream formulations may contain some of the following ingredients (by weight): 6 – 12% fat, 7.5 – 11.5% milk solids not fat, 13 – 18% sweeteners, less than 0.3% emulsifiers and stabilisers and about 64% water, making up the rest. These ingredients are blended to form the premix, which is then pasteurised, homogenised and cooled again before an ageing period of several hours. During subsequent freezing in a scraped surface heat exchanger, 40% to 55% air (by volume) are simultaneously whipped into the mixture to form the final structure. During homogenisation the pre-emulsion is formed by dispersing the molten liquid fat at high temperature in order to obtain droplet sizes below 2 μm (Eisner et al., 2007). This reduction in droplet size results in not only an increase in surface area but also in a new surface devoid of any membrane material. Surface active molecules present in the continuous aqueous phase and from the disrupted membrane immediately start to adsorb to these interfaces. In ice cream mix these are mainly casein, casein micelles, whey proteins, phospholipids, lipoprotein molecules, components of the original milk fat membrane and any added emulsifiers. The immediate

membrane formed is mainly dependent on the micro-environment around the fat globule with a probability of casein micelles spreading out to subunits over the surface. Since concentration of protein is high, the fat droplet sizes are independent of changes in protein concentration in the range relevant to ice cream. The protein surface concentrations after homogenisation of typical mixes are around 10-15 mg m⁻². Additional emulsifiers are not necessary to stabilise the emulsion and also have no impact on the particle sizes of the homogenised mix. Emulsifiers like mono- and di-glycerides or polysorbates lower the interfacial tension between fat and aqueous phase further than the proteins and are preferably adsorbed at the fat interface. During aging, fat crystallises, hydrocolloids and proteins are hydrated and the fat globule membranes rearrange in order to form the final membrane. Rearrangements in the membrane are directed towards the lowest possible energy state with a high competition of the different surface active molecules. While protein adsorption after homogenisation is very fast, unrolling of proteins on the fat surfaces happens within the order of minutes. Cooling makes the fat droplets crystallise and changes the affinity of emulsifiers and proteins to the fat globule interface. Hydrophobic parts of proteins have a much lower affinity to crystallised lipids as compared to liquid fat (Eisner et al., 2007) and the concentration of unadsorbed proteins increases steadily during ageing. Crystallisation of the fat also lowers the surface concentration of proteins. Further reduction of the protein coverage of the fat globules could be reached by Tween 60 or Tween 80 but on the other hand oil soluble surfactants increase the protein load on the

surface. It was shown that the changes can not only be explained by the displacement of proteins by polysorbate, but rather a complex interaction between proteins and the surfactant and that these were in charge of changing the properties of the interfacial layers (Eisner et al., 2007).

After initial freezing in a scraped surface freezer (SSF), the packaged ice cream is hardened to -18 °C or ideally to -25 to -30 °C. The physical structure of ice cream is then composed of air, ice, fat, and an unfrozen serum phase, which consists of the proteins, emulsifiers, stabilisers, milk salts, lactose and sweeteners within the unfrozen water (Drewett and Hartel, 2007).

Drewett and Hartel (2007) studied the effect of process variables on ice crystal size, and residence time in the freezer had the largest effect on its mean size. At shorter residence times, heat was removed from the freezer more rapidly, producing smaller ice crystals. When ice cream was in the freezer barrel for a longer time, at low throughput rates (long residence times), there was more time at the warmer temperatures where recrystallisation occurred quickly. By reducing the residence time in the freezer, smaller ice crystals will be produced due to the rapid heat removal. Lower draw temperatures cause larger subcoolings and a higher nucleation rate at the barrel surface resulting in smaller ice crystals. Another benefit of lower draw temperatures was the reduction in recrystallisation rates, which helped to keep the ice crystals small (Drewett and Hartel, 2007).

High shear forces at low temperatures result in a finely dispersed ice cream microstructure (ice crystals, air cells and fat globules). In order to obtain optimum product quality with respect to creaminess, slow melting, heat shock resistance and structure stability, it is of importance to generate the smallest ice crystals and air cells as is reasonably possible (Wildmoser et al., 2004).

In microstructuring related studies the influence of the Low-Temperature extrusion (LTE) process on the ice crystal size in comparison to conventional freezer processing was investigated (Wildmoser et al., 2004). It was shown that the mean ice crystal size in the freshly produced ice cream after additional hardening was significantly reduced by means of the LTE process. Sensorial properties like consistency, melting behavior, coldness and scoopability were found to be improved (Wildmoser et al., 2004).

Studies on ice cream have shown that hydrocolloids exert a cryoprotective effect which is mainly due to the inhibition of ice crystal growth in the freezer and in the hardening step and also by inhibiting ice recrystallisation throughout frozen storage (Camacho et al., 2001).

Beside the ice crystals, the size and distribution of air cells play an important role in ice cream especially on the sensorial aspect of creaminess (Wildmoser et al., 2004). The smaller the air bubble sizes the more pronounced

was the sensorial sensation of creaminess. A strongly pronounced correlation between ice cream (mix) viscosity and the resulting air bubble size was found by Chang and Hartel in a batch ice cream freezer (Chang & Hartel, 2002) (*in* Wildmoser et al., 2004). The ice cream viscosity increased with decreasing product temperature and simultaneously air cell sizes also decreased. Dynamic rheological measurements were used for the characterisation of texture and structure in foamed dairy emulsions (Stanley et al., 1996), (Wildmoser et al., 2004). At low deformation amplitudes the unstable foam microstructure is maintained during the rheological measurement. Smith et al., (2000) investigated the microstructure influence of whipped cream on the dynamic oscillatory moduli G' and G'' . The storage and loss moduli apparently decreased with a coarser foam structure due to increasing air bubble sizes during storage.

It was shown that the storage modulus G' strongly increases with decreasing ice cream temperature and hence increasing ice fraction in ice cream (Stanley et al., 1996).

Due to its sensitivity to mechanical and thermal treatment the small deformation oscillation test is a good means to study the microstructure of ice cream. Quantitative analysis of air bubble sizes of a Low Temperature Extruded ice cream in comparison to Freezer extruded ice cream directly after draw, showed that the air cell size largely decreased because of the low

temperature treatment. The median air cell diameter decreased from 36 μm (Freezer) to 16 μm (LTE). A narrow size distribution of air cells of LTE ice cream in comparison to Freezer ice cream could be observed. Air cell size is hence strongly affected by the LTE. The difference of air bubble sizes of Freezer extruded in comparison to LTE ice cream directly after draw is certainly of significance with regard to the ice cream microstructure after the final hardening process. Air bubbles were better stabilised in LTE ice cream at the relatively low draw temperature (-13 $^{\circ}\text{C}$), because of the high ice cream viscosity in comparison to the viscosity of Freezer ice cream at draw (-5 $^{\circ}\text{C}$). A narrow and monomodal size distribution of air cells lead also to smaller disproportionation rates during storage time, in which large air bubbles grow at the expense of smaller air bubbles (Laplace pressure dependent on air bubble size). LTE ice cream seemed to be preferable to Freezer ice cream with respect to the narrow air cell size distribution (Wildmoser et al., 2004).

The less air that is added to the ice cream, the better the heat conductivity will be and the colder the sensorial sensation will be during the melting phase of the ice cream. Correspondingly ice cream with a high overrun is evaluated less cold than low Overrun ice cream (Wildmoser et al., 2004).

In the comparison of LTE and Freezer processed ice cream the difference of the rheological behaviour could only be attributed to a difference in microstructures as the same ice cream mix was used by Wildmoser et al. (2004)

in both cases, and the final overrun level was fixed. The mean ice crystal size was considerably reduced by the LTE process compared to that by conventional freeze-hardening. Smaller ice crystals, however, led to a smaller degree of connectivity of the ice crystals and therefore to a less stiff product. In the molten state ($T > 0^{\circ}\text{C}$) higher storage moduli were measured for LTE processed ice cream compared to Freezer ice cream, indicating a higher ice cream foam elasticity. Increased elastic behaviour (G') could be attributed to the smaller air cell sizes and a higher degree of fat globule aggregation in the low temperature treated LTE ice cream (Wildmoser et al., 2004).

The impact of the ice cream microstructure on the rheological behaviour and the quality characteristics of ice cream were investigated by Wildmoser, Scheiweiller and Windhab (2004) and they conclude that in the low temperature range, the ice crystal microstructure governs the rheological behaviour of ice cream. The higher the degree of connectivity of ice crystals, the higher are the resultant storage and loss moduli (lower flowability) at temperatures below -10°C . The storage modulus G' of LTE ice cream was reduced by a factor of 10 compared to that for conventionally processed Freezer ice cream at a temperature of -15°C . Small and homogeneously distributed ice crystals in LTE ice cream caused an improved scoopability. Besides the ice crystal microstructure, the air fraction also influenced the rigidity/stiffness of ice cream at low temperatures. The higher the Overrun and the more finely dispersed the air bubbles, the lower are the storage and loss

moduli. The ice crystal microstructure is interrupted by the air bubbles resulting in a better scoopability of the ice cream. In the temperature range above 0 °C, the ice crystals in ice cream are completely melted and therefore air and fat phases play a major role in the rheological behaviour (Wildmoser et al., 2004). The loss modulus G'' increased by a factor of about 10 when the air content was increased from 0% to 100% (Wildmoser et al., 2004).

As the ice cream without air might be sensorially evaluated as watery, the creaminess was improved in ice cream with a high overrun. Smaller air bubble sizes in ice cream produced by means of LTE process also led to an increase of G'' by approximately 100%. Increased fat globule aggregation with increasing overrun and due to LTE processing contributed also to increased storage and loss moduli as measured for ice cream in the molten state ($T > 0$ °C) (Wildmoser et al., 2004).

1.2.9.4 Stabilisation of whipped cream

From a consumer point of view, the ideal qualities that a whipped cream should have would include the following attributes: be acceptable physically, microbiologically and organoleptically. In addition, good quality whipping creams with a fat content of around 30–40% must be easy to whip and produce a fine foam with a high value of overrun (over 80–90%). The final product must be long lasting and stable during storage (Prentice, 1992) (*in* Jakubczyk and Niranjana, 2006). Bubble mechanics can be used to estimate the shelf-life of

whipped cream, since the textural appearance and mouth-feel are a direct consequence of the complex interactions between bubble mechanics and our senses (Niranjan, 1999).

Whipped cream is a dispersion of gas bubbles surrounded by fat at the air/serum interface that has only partially coalesced and which is supported by a serum phase with a high viscosity. Several factors affect the structural properties of whipped cream, some of which are: the fat content, processing conditions and the addition of stabilisers and emulsifiers (Bruhn & Bruhn, 1988). In order for a cream without stabilisers or thickeners to be whippable, the cream must have a fat content of at least 30% to support rigid foam formation. Graf and Müller (1965) reported that a fat globule size of 15-20 μm is ideal for whipping creams.

It is for this reason that whipping cream has traditionally been processed without homogenisation, which as a process may reduce the size of fat globules to the point where they resist partial coalescence and inhibit stiff foam formation (Graf and Müller, 1965). At least 40% of the fat must be crystalline (Smith et al., 2000) in order to promote partial coalescence and add rigidity to the air bubble interface. In Ultra-high-temperature (UHT) sterilisation of whipping cream, a process which is desirable to increase the shelf-life also results in changes in whipping properties when compared to high-temperature-short-time (HTST)-processed cream (Bruhn & Bruhn, 1988) (Graf and Müller,

1965). Comparisons have been made based on whipping time, overrun, drainage and viscoelastic properties. UHT treatment resulted in lower Overrun and increased whipping time when compared to cream whipped after HTST pasteurisation (Bruhn & Bruhn, 1988) (Graf & Müller, 1965). This is because processing at temperatures above 70°C causes denaturation of β -lactoglobulin (Smith et al., 2000), a milk protein.

It was noticed that thermal analysis of β -lactoglobulin showed two denaturation temperatures, one near 80 °C, and another near 140 °C, indicating that more denaturation was occurring during UHT processing (Smith et al., 2000).

Denatured β -lactoglobulin may form complexes with κ -casein and α -lactalbumin resulting in a higher viscosity in the serum phase (Smith et al., 2000). Changes in membrane structure at the MFGM (milk fat globule membrane) and at the air/fat interface may help explain changes in viscoelastic properties associated with destabilisation of whipped cream. Smith et al., (2000) reported a delay in fat globule adsorption at the air/serum interface when that interface was stabilised with whey proteins. The initial delay in air bubble stabilisation may be indicative of a more stable interface in fully whipped cream. A fine balance must be achieved for proper structure development and integrity; fat globule membranes must be destabilised to support partial coalescence, MFGM must interact with proteins in the air serum

interface during whipping and the resulting foam structure must resist collapse (Smith et al., 2000).

Emulsifier/stabiliser formulations added to cream, improve the whipping behaviour and enhance foam stability. Addition of low molecular weight emulsifiers promote adsorption of partially coalesced fat at the air/serum interface through a lowering of interfacial tension (Smith et al., 2000).

The main structural component of foam is the network of air bubbles with their interface of protein and partially coalesced fat. In the absence of bubbles the serum phase becomes the measurable quantity. However, the foam is a combination of these structural elements, which are not being measured in isolation. Therefore, in samples with a lower Overrun, measurements are based more strongly on the viscosity of the serum, which minimizes anticipated differences (Smith et al., 2000).

The rheological measurements G' and G'' of whipped fresh foams differing in heat treatment or the addition of stabiliser were not significantly different, even though physical properties of the foams showed variations in whipping time and Overrun (Smith et al., 2000).

Foams were whipped to the point of maximum Overrun to compare whipping properties. Results showed that unstabilised HTST and UHT creams

required similar whipping times to reach maximum Overrun and confirmed that the addition of stabiliser resulted in a significant increase in whipping time, within heat treatments (Bruhn & Bruhn, 1988). Stabilised UHT-processed cream required longer whipping times than the stabilised HTST treatment. Stabiliser was added to increase foam stability through increased serum/phase viscosity, but also increased resistance to shear during whipping which explains the longer whipping times (Stanley et al., 1996) required to reach maximum Overrun. Unstabilised HTST cream whipped to a significantly higher Overrun than unstabilised UHT sterilised cream. Addition of stabiliser resulted in a significant decrease in Overrun for both heat treatments. HTST and UHT stabilised creams had similar Overrun values. The increase in viscosity of the serum phase, because of the added stabiliser, also reduced the ability to incorporate air during whipping (Smith et al., 2000).

Unstabilised whipped foams did not exhibit significant differences in rheological measurements when freshly whipped or after 24 h of refrigerated storage regardless of heat treatment. Foam persistence is related to strength and flexibility, that is, a balance between viscous and elastic components. The result of the imbalance is the breaking of air/serum interfaces that will lead to the loss of air in UHT-processed stabilised foams. A stabiliser/emulsifier mix would need to be designed to account for compositional differences caused by protein denaturation in UHT sterilised whipping cream, and also provide a foam with greater visco-elasticity (Smith et al., 2000).

In model emulsion systems sheared in the absence of air under conditions of gradually increasing applied stress, Allen et al. (2008) saw that the onset of partial coalescence was accompanied by a sudden increase in the measured apparent viscosity (Davies, Dickinson, & Bee, 2001) and in the fat particle structure (Xu, Nikolov, & Wasan, 2005). With air incorporation, once substantial fat globule clumping has taken place, the dairy cream is converted from a viscous liquid emulsion into an aerated viscoelastic solid with an optimum overrun of 100–120% (Graf & Müller, 1965). The high fat content of whipping cream (ca. 35%) yields a sufficiently clumped structure during aeration to facilitate rapid and complete stabilisation of the incorporated air bubbles. In contrast, for ice-cream mix which has a considerably lower fat content (7-10%), the emulsion partial coalescence by itself was not enough to stabilise the aerated microstructure; additional structural contributions to ice-cream stabilisation were provided at low temperature by ice crystals, as well as by a combination of sugars, emulsifiers and hydrocolloid thickeners (Allen et al., 2008).

Whipping changes the properties of cream by rendering it more viscoelastic than unwhipped cream. Both G' and G'' increase with whipping time up to a point beyond which they do not change significantly. Jakubczyk and Niranjana (2006) mention that the Overrun also increases until this whipping time, but decreases thereafter as fat globules aggregate and the foam collapses. Bubble

size distributions indicate that the highest number frequency shifts towards lower diameter values, as whipping progresses. In other words, progressive whipping results in the formation of a greater proportion of smaller bubbles until the overrun attains a maximum value. Thereafter, the bubble size distribution changes from being log-normal to a bimodal population (Jakubczyk and Niranjana, 2006).

1.2.9.5 Process of stabilisation

In food colloids such as ice-cream and whipped cream, the air–water and oil–water interfaces are stabilised by adsorbed layers of protein and low-molecular-weight (LMW) surfactants (emulsifiers). The response of these adsorbed layers to large deformations is of practical significance during the processing of many industrial products. The large rapid deformations of interfaces are induced during whipping, stirring, shaking, etc. During product storage, phenomena such as the disproportionation of air bubbles and the Oswald ripening of oil droplets induce large, albeit comparatively slow, changes in the area of adsorbed layers. Compression of adsorbed protein layers is also induced during the process of competitive displacement by LMW surfactants. Surfactant molecules form islands in the protein network which grow and compress the initial protein film at the interface. This mechanism has been termed “orogenic displacement.” (Pugnaloni et al., 2005), an example of this process taking place is depicted in Figure 1.4.

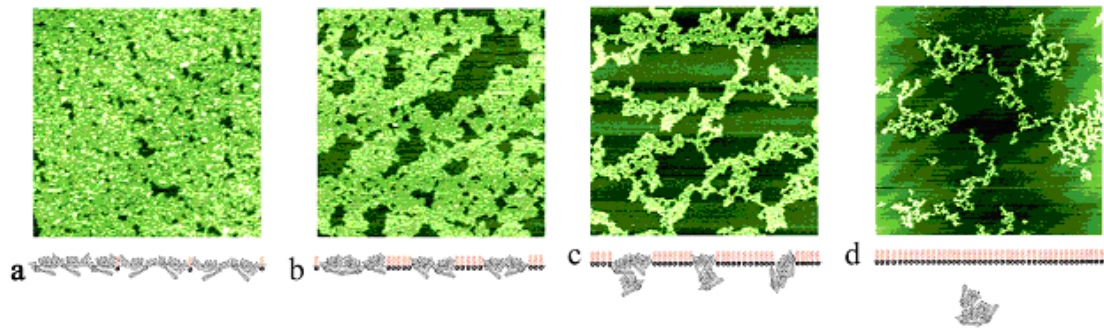


Figure 1.4: AFM data showing displacement of a β -lactoglobulin protein film (green) from an air-water interface by progressive addition of surfactant Tween 20 (black). Image sizes: (a) $1.0 \times 1.0 \mu\text{m}$, (b) $1.6 \times 1.6 \mu\text{m}$, (c) $3.2 \times 3.2 \mu\text{m}$ and (d) $10.0 \times 10.0 \mu\text{m}$. A schematic model of the displacement is illustrated below the images. The red rods are surfactants and the grey is protein. (Source: IFR web, 2009)

1.2.10 Lab-scale testing and production of foam microstructures

Balerin et al. (2007) describe a pilot scale foaming line that was equipped with a range of on-line probes, including flow-meters, pressure, temperature and multiple light scattering sensors. They note that the combination of these sensors allowed them to measure bubble size under pressure, at different stages of the foaming process (Balerin et al., 2007).

Richardson et al. (2004) on the other hand, formulated the foam under different pressures, but visualised the extruded and resultant foam, under atmospheric pressure. In their experiments the vessel was pressurised with air (1–5 bar absolute pressure), the foam was stirred at 2000 rpm for 1 min, after which the stirrer was stopped and the air let out slowly through a valve. The resultant foam was analysed with confocal microscopy (Richardson et al., 2004).

In the first setup described above the foam needs to be stopped during flow, before it can be imaged. This could bring with it inherent problems with instability as the foam is halted mid-flow. Another problem might be the disruption of the bubbles with the instrumentation meant to measure them. In the experiment described by Richardson, the foam is created under pressure before it is released to ambient conditions. The coalescence profile in their case will be very different from a foam which is formed under ambient conditions and then pressurised.

1.2.11 Choice of Model Mix for the food foam microstructures

Used separately both surfactants and proteins are able to stabilise foams and emulsions. However, small quantities of surfactant added to a protein-stabilized interface may reduce rather than enhance its stability. It is believed to be because surfactants and proteins stabilise the interfaces by different mechanisms. Surfactants stabilise an interface by using the Gibbs–Marangoni mechanism, which relies on the surfactant having a high degree of lateral mobility. Conversely, proteins stabilise an interface by forming a strong viscoelastic network in which the protein molecules are essentially immobile. It is the action of this network that slows drainage and resists stretching of the film.

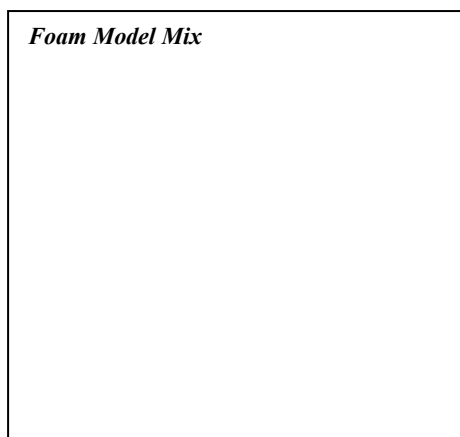


Figure 1.5 Diagram of the Model Mix bubble interface

The two mechanisms are each incompatible and addition of surfactant leads to competition between the two mechanisms which results in the displacement of protein from the interface: adsorption of surfactant weakens the protein network and reduces the stability of the foam. At present the exact mechanism of protein displacement by surfactant is still unclear, despite the fact that the adsorption of proteins to various interfaces has been studied widely and the displacement of protein films from interfaces by competitive adsorption has also been investigated (Mackie et al., 1999).

The studies that Mackie et al. (1999) looked at provide direct visual evidence, for the first time, of protein *gel-like* networks at the air/water interface. The results they obtained, suggests that surfactant molecules adsorb at vacant (or vacated) holes or defects in the protein network. These nucleated sites grow, compressing the protein network. The initial stage involves compression of the protein network without displacement of the proteins from the interface. The second stage involves buckling of the monolayer and reordering of the molecules as the protein film gets thicker in response to the

decreasing surface coverage. Finally, at sufficiently high surface pressures the protein network begins to fail, freeing proteins which then desorb from the interface. Such a model allows an explanation of the differences in behaviour observed between spread and adsorbed films. The final failure of the protein film will depend on the type of protein structure, the extent of unfolding upon adsorption, and the type and strength of intermolecular interaction. Different protein networks show different failure mechanisms, confirming the importance of protein secondary structure in determining interfacial stability (Mackie et al., 1999).

1.3 Micrographs

Some images will be shown of characteristic micrographs depicting processes that will be studied further and will form the main body of work in this thesis. They were taken using three different microscope techniques. The work they formed part of will be discussed in greater detail in the subsequent chapters.

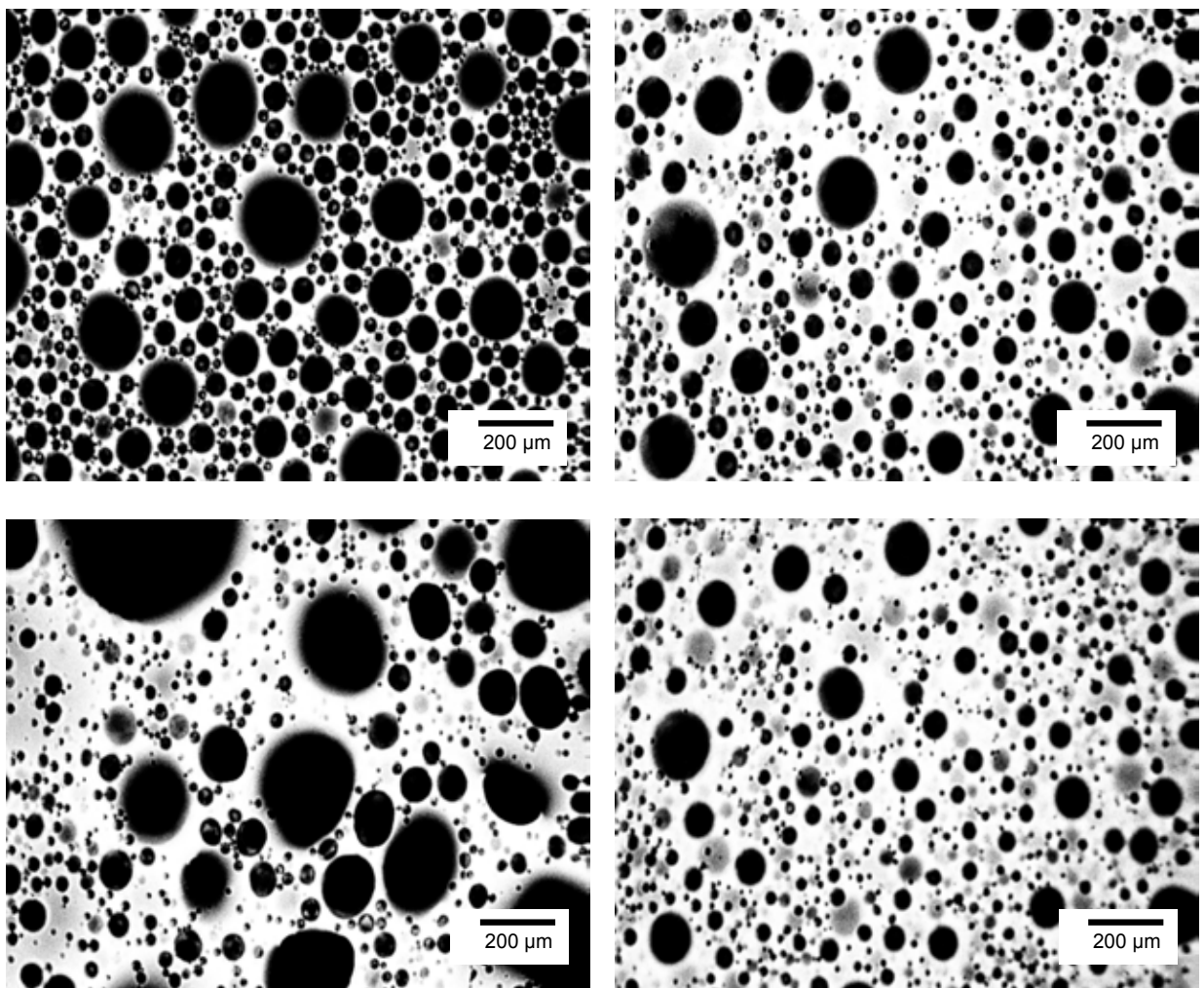


Figure 1.6: Confocal micrographs of a model foam undergoing a pressure cycle. Top Left: 1 bar absolute, before the experiment began. Bottom left: 1 bar absolute after the experiment finished. Top Right: 6 bar absolute on the pressurisation side, Bottom Right: 6 bar absolute on the depressurisation side. 10× magnification.

Figure 1.6 was taken with a Confocal Scanning Laser Microscope with a foam undergoing a pressure drop.

Figure 1.7 was captured with Light microscopy during steady shear.

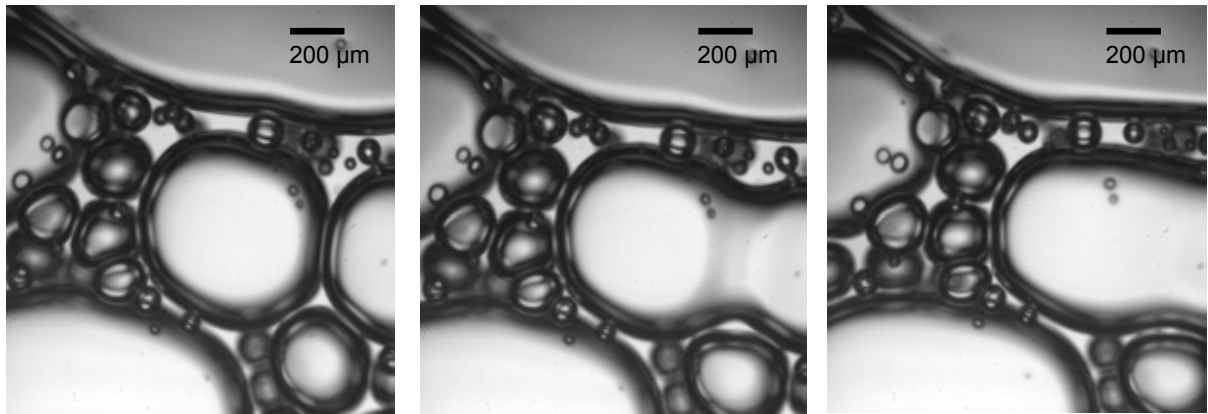


Figure 1.7: Light microscope image of a model foam undergoing coalescence.

Figure 1.8 and Figure 1.9 are comparisons of two different whipping cream types, taken by cryo-Scanning Electron Microscopy. The micrographs display the fat particle distribution at the air interface of the two creams.

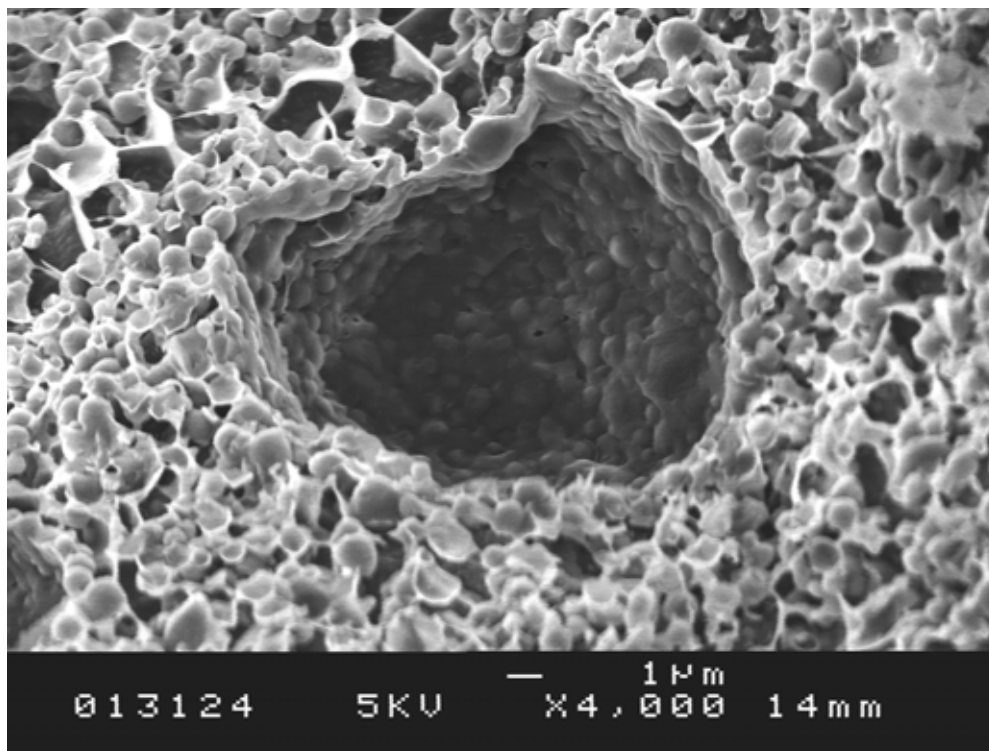


Figure 1.8: Microstructure taken from a whipped non dairy whipping cream

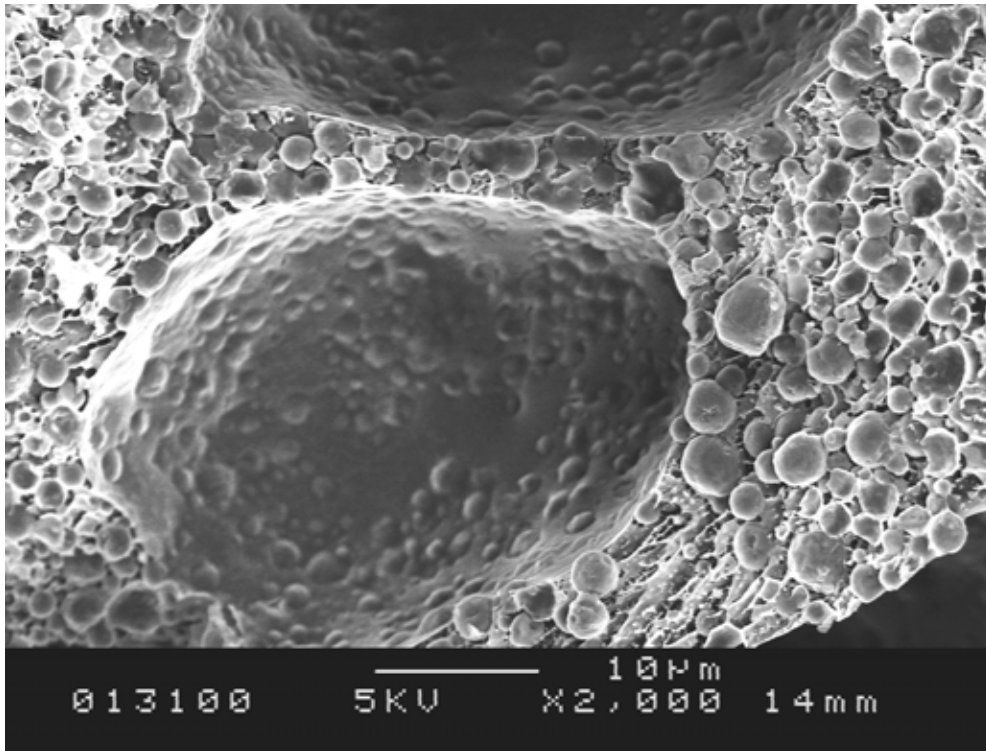


Figure 1.9: Microstructures from a dairy whipping cream. In both cases the fat particles can be seen on the air interface of the bubble.

1.4 Conclusions

Using the imaging capabilities displayed in section 1.3 it is possible to identify the microstructure and its response to shear and pressure events, which will be studied and elucidated further.

CHAPTER 2 – Methods and Materials

PART I

2 (1) Whipping of creams

The following section will describe the methods used throughout chapter 3 which incorporates an in depth understanding and thorough analysis of whipping creams, which is achieved through a range of different tests.

All the cream samples were placed in a “Beko” refrigerator (Beko, Herts., UK) for analysis when required. The refrigerator was running at 6°C according to a measurement taken with a Cole Parmer (London, UK) thermocouple.

The experiments undertaken either investigated (i) 3 commercially available creams or (ii) six in-house reformulated whipping emulsions. Of the commercial creams one was a dairy cream and the other two were vegetable oil whipping creams, marketed under the Elmlea brand. They were either of a Light or Full Fat double whipping variety.

2.1 *Ingredients and nutritional information of the commercial whipping cream.*

The ingredients contained within the commercially available Elmlea whipping creams were:

Elmlea double (full fat):

[claiming: 33% less fat than double cream]

- 63% Buttermilk
- 26% Hydrogenated vegetable oil
- 8.8% Vegetable Oil
- Buttermilk powder
- Lactose
- Emulsifiers: E435 (Polysorbate 60), E322 (Soya Lecithin)
- Stabilisers: E412 (Guar Gum), E410 (Locust Bean / Carob gum)
- Colour: E160a (Carotenes)

Elmlea double (light):

[claiming: 55% less fat than double cream]

- 75% Buttermilk
- 12% Vegetable Oil
- 11% Hydrogenated vegetable oils
- Buttermilk powder
- Emulsifiers: E435 (Polysorbate 60), E322 (Soya Lecithin)
- Stabilisers: E412 (Guar Gum), E410 (Locust Bean / Carob gum), E407 (Carageenan gum)
- Colour: E160a (Carotenes)

Table 2.1: Nutritional Composition, per 100 ml of product, as described on the original packaging:

| | Elmlea Light | Elmlea Full Fat | J. Sainsbury's cream |
|---------------------------|---------------------|------------------------|---|
| Energy | 246 kcal | 349 kcal | 445 kcal |
| Protein | 2.8 g | 2.4 g | 1.7 g |
| Carbohydrate | 4.1 g | 3.9 g | 2.6 g |
| <i>of which sugars</i> | 4.1 g | 3.9 g | 2.6 g |
| Fat | 24.3 g | 36 g | 47.5 g |
| <i>of which saturates</i> | 19 g | 26.8 g | 29.7 g 13.8 g (mono-unsat.) 1.4 g (poly-unsat.) |
| Fibre | 0.3 g | 0.3 g | 0 g |
| Sodium | 0.1 g | 0.1 g | Trace |

2.2 Composition of the reformulated mixes

The composition of the reformulated mixes was based primarily on the Elmlea prior art document following the recommended formulation space of the patent (number: 005149557 A, by Morrison et al. 1992). This was done in order to follow the preferred use and recommended concentrations of each of the ingredients. The patent was partly adapted, and the following mixes were a result of the reformulation, with the base formulation always containing:

- 5% Buttermilkpowder, BMP (Dairycrest, Stonehouse, Gloucester, UK) with 49.7% lactose, 34.3% Protein, 7.4% Ash, 3.5% Moisture and at least a minimum of 5% Butterfat, giving 0.25% of Butterfat in the total mix.
- 2% Sodium Caseinate (DMV International, Veghel, Netherlands)
- 1% Lactem (Grindsted, Danisco, Denmark), Emulsifier from lactic acid ester.
- 0.5% Xanthan (CP, Kelco, Knowsley, UK)
- 0.35% Lecithin (from Soya, Holland & Barrett, Warwickshire, UK) with each gram of granules equivalent to 1.5 grams of liquid Soya Lecithin

And each mix containing varying concentrations of:

- Silpalm, hardened palm oil (Silbury, Warwickshire, UK) with less than 0.1% free fatty acid as oleic acid and 99.9% fat content, of which (49% saturates, 40% mono-unsaturates, 11% polyunsaturates and less than 1% trans-fatty acids).
- Vegetable Rapeseed oil from *Brassica napus* (Sainsbury's, Holborn, London, UK) with less than 0.1% protein, 91.7% total fat content (of which, 6.1% saturated fat, 54.4% mono-unsaturated fat, 26.9% polyunsaturated fat) and 0.1% sodium.

The following ratios of hard Silpalm oil to liquid vegetable oil were investigated:

- **Mix 1:** 10% hard oil and 24% liquid oil
- **Mix 2:** 15% and 19%
- **Mix 3:** 20% and 14%
- **Mix 4:** 25% and 9%
- **Mix 5:** 30% and 4%
- **Mix 6:** 34% hard oil only

All the ingredients were food grade, although some emulsifier levels selected for this work might not be allowed due to maximum upper limits set out for certain foodstuffs in UK and European legislation. The emulsions were all manufactured with food grade ingredients and thus can potentially be eaten.

2.3 Preparation of the re-formulated mixes

In the reformulated mix, firstly the Silpalm hardened palm oil (Silbury, Warwickshire, UK) was weighed out and placed in a conical flask and then in a beaker Bain-Marie style at 50 °C until the opaque coloured paste had dissolved and ran 'clear'. Following this the weighed liquid oil (Sainsbury's, Holborn, UK) and the Lactem (Danisco, Denmark) were added together and also heated to 50 °C, which was the emulsifiers' Krafft point according to manufacturers' instructions (pers. comm. Danisco). Krafft point is defined as the narrow temperature range above which the solubility of a surfactant rises sharply and it is at this temperature that the solubility of the surfactant becomes equal to the critical micelle concentration (c.m.c.) (IUPAC web, 1997). The c.m.c. is a characteristic value of the emulsifier which decreases as the hydrophobic part

of the molecule increases. It is also influenced by the temperature, pH value and electrolyte concentration. Crystals, micelles and the dissolved emulsifier are in equilibrium at the Krafft point (Belitz et al., 2004).

The emulsifier was heated within the oil in order to dissolve the emulsifier 'prills' in it. It was important to wait for complete incorporation of the emulsifier in the oil, or else its functionality would have been compromised. While these other ingredients were melting and dissolving, the BMP (Dairycrest, Gloucester, UK) was dissolved in de-ionised water together with the Lecithin (Holland & Barrett, Warwickshire, UK) under constant stirring with a magnetic flea. The lecithin was fully dissolved in the water after about 15 to 20 minutes. This was evident by no more yellow droplets being dispersed in the mix. A slightly yellow coloured liquid is obtained at this stage. Then the oil was added to this mix, followed by the Sodium caseinate (DMV, Veghel, Netherlands) and finally the Xanthan (CP, Kelco, Knowsley, UK) in quick succession, still under constant agitation of the magnetic flea. The agitation speed was increased to account for the increase in viscosity after the addition of the Xanthan. The caseinate at this stage builds distinct pillow like structures in the water, which do not re-suspend easily. They only get re-suspended when the mix gets sheared at higher speeds in subsequent steps. The final step of the mix involved adding the molten Silpalm to the mix by pouring it straight into the beaker.

For the subsequent processing of the mixes, use was made of an FT9 Homogeniser (Armfield Ltd, Ringwood, England, UK) and a Silverson mixer (Chesham, Bucks., UK). The homogeniser was operated at a working pressure of 1000 pounds per square inch (69 bar) and the Silverson was capable of a maximum speed of 13500 rpm dependent on mix viscosity. Initially the Silverson was used to create a pre-emulsion of all the mixed ingredients described above, and this was then followed on with the Homogeniser. The mix was added to the homogeniser and it was allowed to ‘pass’ through it a few times up to a maximum of 10 times. After loading the initial mix into the homogeniser, the first few millilitres of mix (left over from previous washes and purges) were allowed to flow to waste, immediately catching the following mix. This was done in order not to dilute the mix unduly with the wash-water. The homogeniser was operated at ambient temperature. Once prepared and homogenised, the emulsion was flash quenched in an ice-bath with salt. The coarse ground sea salt to ice ratio comprised about 80 grams to every 2 litres of ice. The samples were then stored in the refrigerator until required. It must be stressed that aeration was not performed until the sample had at least been overnight in the refrigerator to allow the fat phase to crystallise.

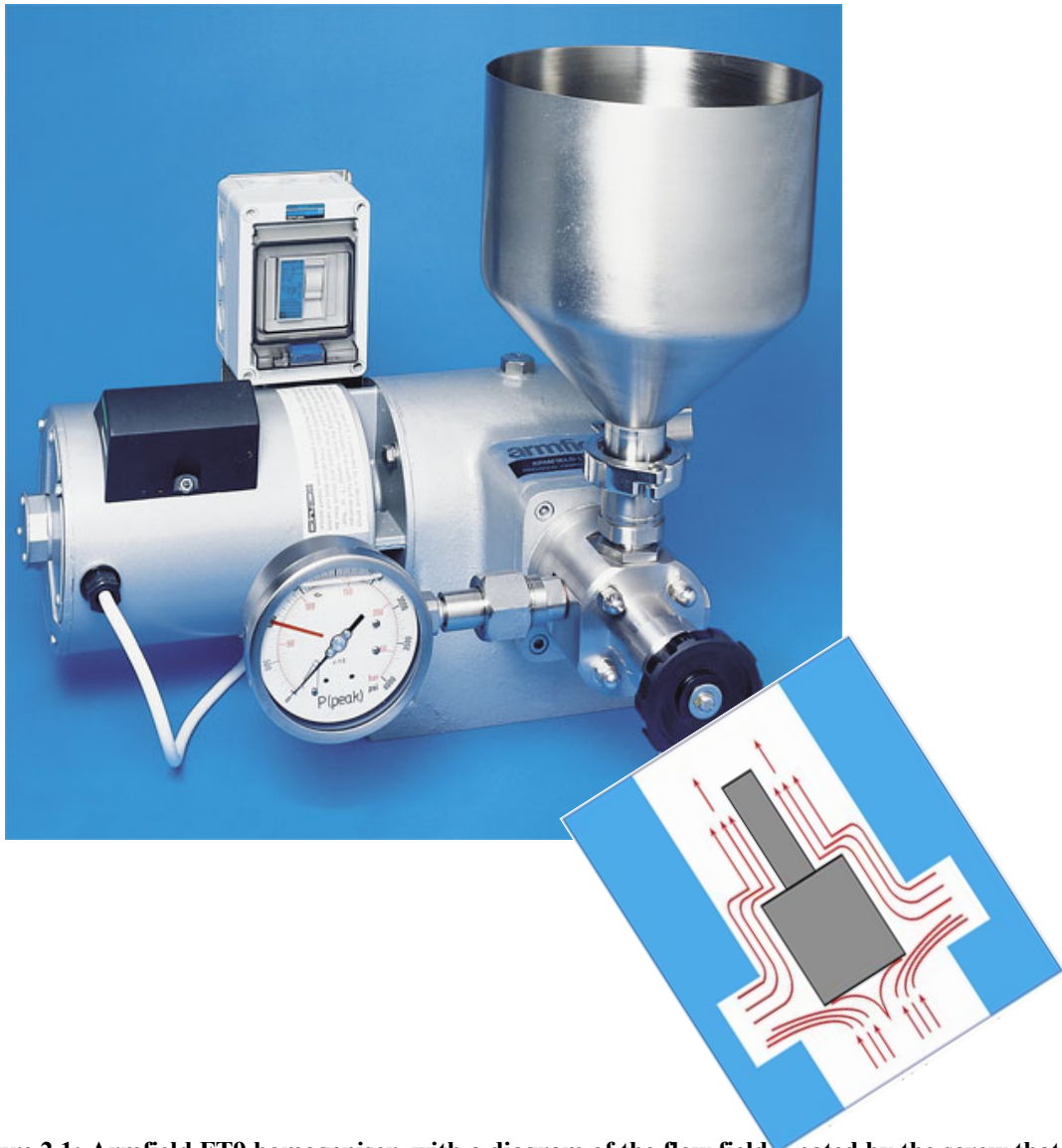


Figure 2.1: Armfield FT9 homogeniser, with a diagram of the flow field created by the screw that sits behind the black turning wheel.

2.4 *Whipping and fat separation*

A Kenwood Chef mixer KM300 (Kenwood, Havant, Portsmouth, UK) which had a 700 W rating was used with a wire whip attachment and planetary motion whipping. The cream was mixed using the sixth and “maximum” speed setting.

The six different approximate speeds of the mixer (according to the manufacturer) are as follows:

Table 2.2: Kenwood chef mixer speed settings

| <i>Speed Setting</i> | <i>rpm</i> |
|----------------------|------------|
| minimum | 42 |
| [1] | 80 |
| [2] | 98 |
| [3] | 120 |
| [4] | 145 |
| [5] | 170 |
| [6] | 190 |
| Reverse – “boost” | 200 |

An attempt was made at initial separation for fat characterisation of the commercial product but proved difficult.

To separate and obtain the oil phase of the whipped creams a Sci-quip centrifuge (Sci-quip, Sigma Scientific Laboratory Supplies) (Shrewsbury, Shropshire, UK) was used. The creams were centrifuged for 15 minutes at the maximum speed of 4000 rpm with an equivalent centrifugal force of 2400 g. For this purpose the samples were placed in two plastic test tubes of 15 ml each. Prior to centrifugation the cream was heated for up to 4 hours in two beakers on a hot-plate as a way of a Bain-Marie and held at a constant 80 °C throughout. The oil layer that formed on the cream was scooped off and spun down as it began appearing. Once finished, the test tubes were allowed to cool down at ambient on the bench until all the contents, including the top-most layer of liquid had congealed. Subsequently the test-tubes were placed in the refrigerator until required. Before they were required the top-most layer was

scraped off and re-heated under moderate heat until the congealed oil pellets re-melted. This was then transferred to a clean vessel, again left to congeal at ambient and then transferred to the refrigerator once solid.

2.5 *Whipping method*

Two main methods of aerating the creams were used. In the first method the creams were whipped intermittently (i.e. stopped and started) and the Overrun measured every 30 seconds. Overrun is defined as the percentage increase in the volume of the final mix over the volume of the initial mix due to the incorporation of air. Overrun can be expressed as a percentage of the volume of the mix and it can either be calculated by volume or by weight (Arbuckle, 1986). For percentage Overrun by weight, the following applies:

$$\text{OR (\%)} = \frac{(\text{weight of fixed un-aerated volume} - \text{weight of fixed aerated volume})}{(\text{weight of fixed aerated volume})} \times 100$$

equation 2.1

The whipping in this case was performed by keeping the same sample. The entire whipping cycle was not stopped until the cream was either severely overwhipped and a lot of liquid began to appear at the bottom of the bowl (in the case of the Elmlea), or the cream had completely ‘buttered’ in the case of the real whipping cream (J. Sainsbury’s cream). Whipping curves of percentage Overrun against whipping time were constructed with the values obtained. Each curve was composed of triplicate results, averaged and with error bars. In

the second method, selected points on the whipping curves were investigated further, but in this case the cream was aerated without stopping and starting and only one fresh sample was used for each data point. Each data point for this 'continuous' regime was formed of three separate readings for that time-point. This led to a completely different Overrun value than that obtained for the initial 'stop-start' whipping curves.

For the reformulated mixes the stop start method was used throughout the aeration process with all the mixes. For the Overrun assessment, whipping was stopped and the weight of a fixed amount of the cream was noted every minute. It was then re-started and aerated for a further minute. This was done for a total of 60 minutes. In order to gather the SEM images, this stop-start method was also used, even if the Overrun was not noted each time the mixer was stopped. The aerated mixes were refolded into the mix, as this was also done for the overrun assessment.

In addition to the SEM micrographs, the reformulated mixes and the commercial samples were also investigated under the light microscope. For microscope specifications, see section 2.7.

The creams were also investigated rheologically using a Bohlin Gemini HR Nano Rheometer (Malvern Instruments, Malvern, Worcs., UK). Thin film

rheology on the tribometer manufactured by PCS Instruments (London, UK) was also carried out, see section 2.9 and 2.10.

A test for creaming was carried out. The creaming experiment was performed by using 100 ml of the whipped cream, in a 250 ml volumetric glass cylinder with gradation every 2 ml. But results were inconclusive. No serum separation took place on any of the samples, and further investigation would have proved pointless.

2.6 *Slumping*

A stand-up/slumping test can be defined by the rigidity exhibited of a whipped cream and its ability to retain a pre-formed shape. This test was performed in order to analyse the creams' behaviour under the influence of gravity at different temperatures (later referred to simply as stand-up or preferably slumping, but used interchangeably). The temperatures investigated for the commercial samples were: 25 °C, 30 °C, 35 °C and 40 °C. For the reformulated mixes only 25 °C was chosen.

These tests are important as in a domestic or catering setting it is paramount to have a cream that can retain its shape for at least a short length of time after whipping, during serving and before eating (especially important if there is a time lag between whipping and eating).

Pictures were taken every 30 minutes for the 3 commercial stand-up samples at 25 °C and 30 °C (or every 20 minutes in the case of the 35 °C and 40 °C experiments). They were taken with a digital Olympus SLR E-500 camera (Olympus, Watford, Herts, UK). The camera was capable of taking pictures at a resolution of 8 Mega-pixels and was mounted on a Manfrotto tripod.

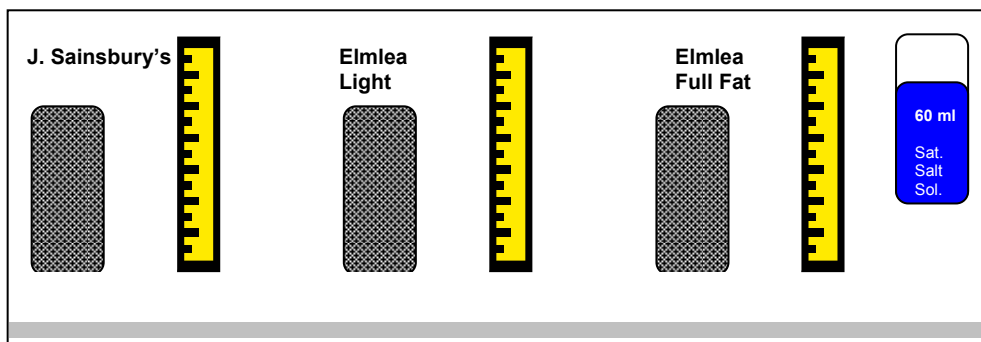


Figure 2.2: Schematic example of the sample layout within the Perspex box and lid for one experimental run at e.g. 25 °C and $T = 0$ minutes

For the re-formulated whipped creams placed at 25 °C, 20 minutes was taken as the interval between each of the images. Images were taken for a total of 4 hours during the sampling day. They were left in the incubator overnight to allow one image to be taken the following day too.

The commercial samples were first aerated for 150 seconds and their Overrun noted. The re-formulated mixes were aerated according to the time-point of maximum overrun (also termed ‘peak whip’). Each sample was carefully placed in round plastic containers capable of holding 60 ml of liquid sample. The container was filled to the top and each of the samples weighed.

The commercial samples were then carefully extracted from the containers with a metallic spatula and placed in an airtight sealed Perspex box with 9 cm plastic rulers for reference purposes. 60 ml of a saturated salt (NaCl) solution was added to the box to maintain a relative humidity at the four chosen temperatures of 25, 30, 35 and 40 °C giving a theoretical relative humidity of 75.3%, 75.1%, 74.9% and 74.7% respectively. The re-formulated mixes, before they could be extracted from the plastic cylinder to carry out the tests, were placed in a refrigerator until they were harder. The samples were left in the refrigerator to harden for at least 2 hours. It would have been impossible to make a stand-up shape with a freshly aerated re-formulated mix. The samples would have been too soft and would not have retained the shape of the mould upon extraction from the cylinder. Two whipping stages were analysed with the reformulated mixes: a 'peak whipped' sample and an overwhipped one. If the peak-whipped sample would have been left out of the refrigerator, while the overwhipped sample was prepared, this would have led to a dramatic loss of structure in the cream. This way, most of the sample integrity was conserved, albeit with some settling taking place. The reformulated mixes were only tested at 25 °C because the samples would have melted too quickly at the other temperatures. The samples were imaged in the time-frames indicated above. The photographs were digitised and printed out. Each digitised image once printed out on white 80 gsm paper had the same length to width ratio of 9.6 cm×7.65 cm. The print-outs of the cream outline were then cut-out and weighed. The individual weight of each cream 'tower' was noted. A reference

measure of 1 cm^2 was cut-out (relative to the size of the object in the picture, hence the need for a ruler in the picture!). This too was weighed on a Sartorius Microbalance (Epsom, UK). The relative loss of visible sample (expressed in cm^2) was then computed. In this experiment 1 digitised centimetre was equivalent to 1 actual centimetre. It was fortunate that this was the case, but this may not necessarily have remained the case during re-sizing or if a different zoom-level would have been selected on the camera lens.

In some cases the sample fell out of the field of view that was imaged, for example like in table 3.1 or 3.2. Here an estimate of the sample size lost, was given (and included in the error bars on the graph). The error bars are only in one direction, as the loss of area due to the towers' collapse could only have been under-estimated from the pictures and not over-estimated too. A diagram showing this problem is given in Figure 2.3.

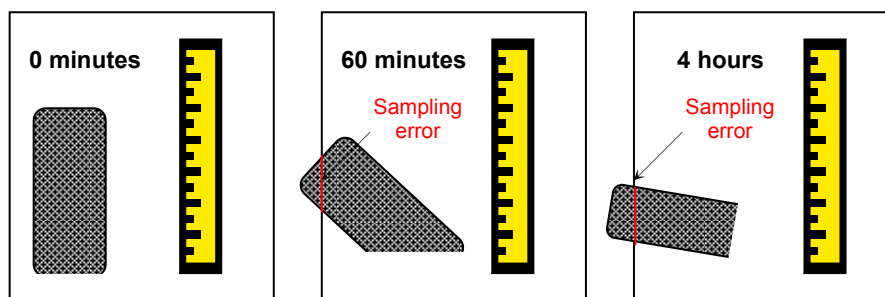


Figure 2.3 Example of sampling error in the cream slumping experiment

Ideally the stainless steel bowl of the mixing vessel would have been cooled down in a refrigerator prior to each use. This method was not practical, as at least 3 different samples needed aerating back to back. There were only 2

bowls available, and therefore, for consistency purposes, cooling was not undertaken.

Pre-cooling of a whipping bowl would not have been undertaken in a domestic setting either, so this step was omitted.

2.7 *Light microscopy of whipped structures*

Images were collected by using a Reichert-Yung Polyvar light microscope (Vienna, Austria) and an attached Photonic Science Camera (Millham, East Sussex, UK). The objectives supplied with the microscope were all Plan Fl Apo with either a 10×, 25×, 40× or 100× magnification and the following Numerical Apertures (NA: 0.30, 0.45, 0.70 and 30).

The whipped creams were prepared for microscopy by sampling the mixing bowl in the centre of the whisk with a fine pipette tip. A small cream sample was spread then on a glass microscope slide, ensuring (1) that the creams' structure was not destroyed and (2) that the cream was not applied too thickly or thinly onto the slide. To obtain a flat imaging plane a glass coverslip was placed over the sample and a little pressure applied to it.

Bubble sizing was performed with an image analysis tool within the PC attached to the Polyvar Microscope that was running the following software, Image Pro Plus Version 3.0.01.00 for Windows 95 (Media Cybernetics, L.P.

1993-1997, Bethesda, Maryland, USA). Bubble sizing was performed manually by measuring the bubble radii. All visible bubbles in an image were sized and the spreadsheet of bubbles sized and counted were downloaded to Excel for further manipulation.

2.8 *Cryo-SEM*

For the Scanning Electron Microscope micrographs the creams were whipped to the target Overruns for the time-frame required. The samples were then stored in a refrigerator until they were sampled, sectioned and prepared. It was ensured that sampling took place almost straight after aeration. Use was made of a Gatan Alto2500 low temperature preparation system. This was linked to a Jeol 6301F field emission SEM.

Small aliquots of cream were mounted onto SEM stubs and rapidly frozen in nitrogen slush. The sample was then fractured at -90 °C. It was subsequently etched for 30 seconds and then cooled to -110 °C. The prepared sample was then coated with a 2 nm thick layer of Au/Pd prior to examination at -150 °C.

2.9 *Rheology*

Oscillatory and viscometry tests were performed on a controlled stress Bohlin HR Nano 150 rheometer, from Malvern Instruments (Malvern, Worcestershire, UK). An amplitude sweep at a fixed frequency of 1 Hz was

performed. The gap loading conditions were 2 mm or 1 mm dependent on sample thickness and the geometry chosen was 40 mm parallel plate. The temperature of each of the test runs was either 10 °C or 25 °C.

In general a sample loading gap of 2 mm was used with the commercial samples and 1 mm with the reformulated mixes. All samples were tested at 25 °C but only the commercial samples were additionally tested at 10 °C.

For viscometry the samples' instantaneous viscosity was tested as a function of shear stress. The samples were tested on a shear stress from 1 to 1000 Pa. Parallel plate geometry was also used here.

The commercial samples were tested at 10 °C and 25 °C and the reformulated ones only at 25 °C.

2.10 Tribology measurements

Use was made of an MTM2 device (mini-traction machine) developed by PCS Instruments (London, UK). The results were gathered at 37 °C to reproduce conditions in the mouth. A Stribeck curve formed of variable speeds from 1 mm/s to 1000 mm/s in ascending order and using the ball-on-disc method was carried out. Throughout the process 28 sample points were gathered in a logarithmic fashion. For this purpose a drilled 3/4" AISI 52100 precision steel ball was used, together with a 46 mm diameter silicon sheet of 60 shore hardness and 4 mm thickness (Samco, Warwickshire, UK). Before the

sample reached the required temperature the machine was set to an idle speed of 1 mm/s where the ball applied no load to the sample or disc, but where both ball and disc rotated at the selected speed until the samples' temperature equilibrated. Once the desired temperature was reached, the ball applied the selected load (which in this case was 3 N) and the test run began. Each test was carried out in triplicate, with a fresh sample each time. A new silicon sheet was used for each new triplicate. Before use the disc required cleaning in detergent to remove any grease residue that may have been left after manufacture. The sample pot of the tribometer together with the disc was also rinsed with hot water and cleaned with ethanol after each run.

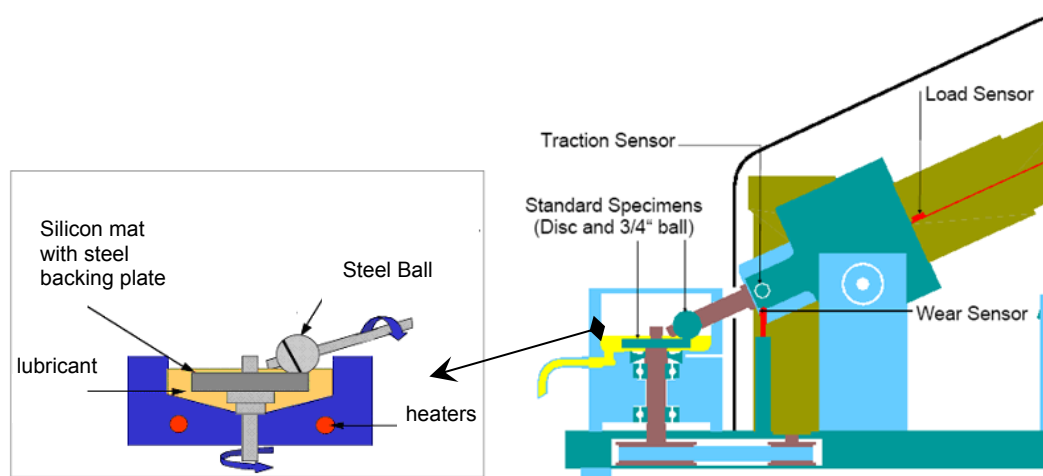


Figure 2.4 Schematic of the MTM Tribometer

Source: (PCS web, 2008).

2.11 Differential Scanning Calorimetry

Differential Scanning Calorimetry analyses were undertaken using a Perkin Elmer, DSC 7 (Perkin Elmer, Mass. USA) running the Pyris Software. The samples to be analysed were placed in aluminium sample pans with a diameter

of 0.15 mm. The sample pan can hold a total of 40 μl of liquid sample. The emulsion sample was weighed and crimped inside the aluminium pans. The sample pan was placed inside the DSC machine alongside an empty sealed reference pan. Nitrogen was continually purged at a rate of 20 ml per minute through the DSC sample holding well.

The cycle that was chosen for the DSC analysis cooled the sample from ambient temperature to 0 °C at 5 °C per minute, then held the sample at 0 °C for a minute subsequently heating it to 60 °C and holding it at this temperature for 1 minute. This cycle was then repeated three times at the same rate with the same sample. In the results these are labelled Scan 1 through to Scan 3 respectively.

2.12 *Closing remarks*

Following the methods outlined in this section should enable a complete study of whipping creams to take place. The creams under scrutiny are off-the-shelf commercially available formulations; and once the knowledge-base was built up, reformulated creams could be studied in more depth. The ultimate goal was to create a whipping cream that explored the ‘softening limit’ of a vegetable oil formulation. For this, the base formulation and recommendations contained within the Elmlea prior art document were used. Within the reformulated cream the ratio of liquid oil to ‘hard’ hydrogenated palm oil was

altered and resulted in six different reformulated mixes. These were studied extensively throughout the thesis.

CHAPTER 2 – Methods and Materials

Part II

2 (2) Foaming of the ice-cream Model Mix

The following section summarises all the methods employed in the experiments of Chapters 4 and 5. The next segments will deal with formulation space optimisation for the experiments. A detailed description given of the equipment and methods that were used throughout the two chapters will be given. Principally, the methods employed to test for the initial robustness of the model mix will be elucidated. A detailed description of the methods used and the rheometer is also described. Two Linkam cells that were extensively used are described. One is a shear cell, with two parallel glass plates and the other, a Linkam custom built pressure cell. All the gases used for long term disproportionation of the foams are also listed.

2.13 Mix preparation and formulation

The development of an ‘optimised’ base mix for the creation of aerated microstructures that are stable in the medium term will be described. The creation of the microstructures is brought about through whipping. When aerated, the foam is stable for at least 24 hours. This means that there is no significant bubble coarsening or any visual collapse over this time period when stored at chill temperatures. The viscosity of the system is such that no significant bubble creaming occurs. At ambient, limited creaming occurs over the same time period. However, the same foam would show some instability

when subjected to pressure or shear changes. In some respects it can be considered a model food foam, with a formulation space not too dissimilar to that of an ice-cream base mix.

The base mix is described as optimised, as the resultant foam created from it, unites the ideal properties of reasonably long range stability when stored at quiescent conditions, but short range stability when disturbed or in dynamic conditions. The mix contains both a protein and an emulsifier as both aerating and stabilising agents. A foam created with only one of the two would be either too unstable if it were only created by a protein, or far too stable, if only the emulsifier were present. By having both substances present, it creates a foam of mid-range stability, and hence it is 'optimised' to meet the specific requirements of the experiments. For the experiments a very stable foam where no coalescence could be observed was not desired, but it needed to be robust enough to last the day.

The model foam consisted of 70% w/w corn syrup (C-Sweet F 017Y4 LF9, Cerestar, Trafford Park, Manchester) (with a water content of 22% and dry substance of 78%, and LF9 in the product code, refers to its Low Fructose content at 9%), 0.2% w/w PGE-55 (Poly-glycerol esters of fatty acids) (Danisco Cultor, Wellingborough, Northampton) and 3% w/w Whey Powder (with a protein content of 12%, moisture of 2.5%, 1% fat, 74% lactose and 8% ash) (GFT 530, Glanbia Plc, Kilkenny, Ireland). This gives the final model mix

a total protein content of 0.36%. The mix was prepared by heating the PGE to 60 °C in de-ionised water making the total mix up to 96% w/w. In this case 60 °C is the Krafft point of PGE. It was then allowed to cool and the whey powder added into the liquid mix using a hand whisk. To allow the whey powder to dissolve properly, it was left in water for upwards of 30 minutes. This liquid mixture was then added and folded into the weighed corn syrup, ensuring that both ingredients were fully mixed. The mix was aged at chill temperatures (5 °C) until required (upwards of 24 hours). A stock solution of Riboflavin (Vitamin B₂) at 0.05% w/w concentration (Sigma Aldrich, Gillingham, Dorset) was prepared. From this fluorescent stock solution 4% w/w was added to the system as a fluorophor to enable confocal imaging and to complete the mix. The mix was aerated in a N50 Hobart planetary mixer, with a “D” wire whisk, on power setting 3, running at 500 rpm (Hobart Corp., Troy, Ohio, USA). The mix was aerated for up to 30 minutes or until the desired Overrun was achieved.

For the purposes of the experiments, the model foam microstructures were created noting the final volume of incorporated air as Overrun (OR). Overrun is defined in Chapter 2, Section I, equation 2.1.

In addition, the air phase volume can be calculated from the Overrun as described below:

$$\text{Air phase volume} = \phi = \text{OR} / (\text{OR} + 100) \quad \text{equation 2.2}$$

(Campbell and Mougeot, 1999).

2.14 *Preparation of a foam for the master batch method*

Preparation of a master batch foam for repeated analyses throughout any day was made by aerating the model mix and noting its final Overrun (the master batch method was not employed if only one sample was required, *e.g.* for the disproportionation experiments within the pressure cell). For a master batch, the mix was then placed in 3 plastic 500 ml wide mouthed Nalgene bottles (Nalge Europe, Hereford, UK). These were inverted every 15 minutes throughout the day until all the required analyses had been carried out, and to absolutely ensure that no drainage phenomena take place. Sampling always took place from the same bottle (bottle 1); this was then re-filled by the second bottle which in turn was topped up by the third, to avoid any dilution effects taking place (through eventual creaming in the half empty bottle).

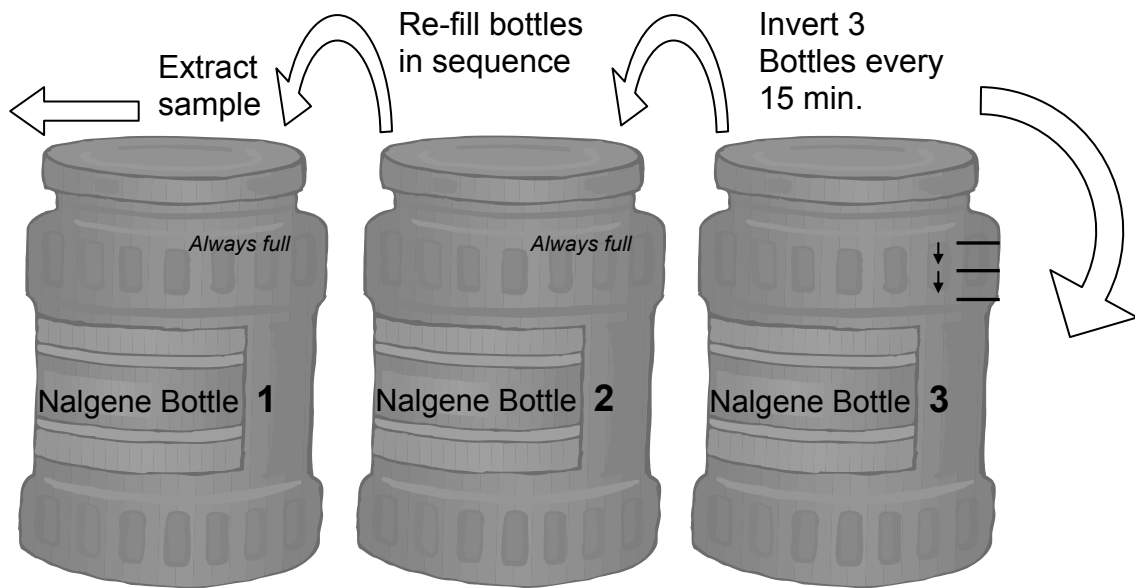


Figure 2.1 Summary of Master Batch Method

2.15 Foam stability experiments

2.15.1 Creaming

To confirm the initial bulk foam stability, a visual assessment of the aerated mix was carried out. This was performed by placing the mix in a glass volumetric cylinder with a total graduation of 100 ml in 1 ml steps. The sample was left at room temperature. Serum volume and foam collapse were noted for a total time of 48 hrs.

2.15.2 Shear characterisation and stability

2.15.2.1 Bulk Rheology

Rheological analysis of the foam in oscillatory and continuous shear mode was carried out on an AR 2000 controlled stress / controlled rate rheometer from TA Instruments (Crawley, West Sussex, UK). This was done by using the small vane and serrated cup geometry. The small vane insert was 38 mm in

length and 15 mm in diameter and contained four vanes. The internal diameter of the serrated cup with the measurement taken from the tips of the grooves was 30 mm and had a depth of 70 mm. The oscillatory procedure was a ramped log oscillatory stress sweep from 0.0258 Pa to 100 Pa, with a 5 minute pre-conditioning step which enabled the sample to stabilise and its temperature to equilibrate to room temperature (22 °C).

In the shear ramp experiments, the shear rate was increased linearly with time until the target shear rate was achieved at the end of the run. In the experiments this was 200 s^{-1} , 150 s^{-1} , 100 s^{-1} and a ‘no shear’ control. The whole continuous ramp consisted of 60 sampling points in total, and the sample was sheared for between 10 and 60 minutes, in 10 minute steps. Another shearing regime (using the same shear rates and times as the other experiment) was also used which consisted of continuous shear but it was not ramped. The shear rate set, is used by the rheometer for the duration of the experiment. Once the sample was sheared, $2 \times 1.5 \text{ ml}$ ‘spoonfuls’, were extracted from the top-most layer of the foam within the vane insert and these were discarded, to mitigate the negative influence of large, creamed bubbles on the surface, skewing the data, and also to sample from a uniform layer of foam.

Once a sheared foam sample was obtained, a sheared and non-sheared control sample were placed inside 30 mm disposable plastic petri dishes (Bibby Sterilin, Stone, Staffs., UK) and the foam was covered with a 16 mm round

coverslip (Chance Proper Ltd.) (West Midlands, UK). Two images were taken of each sample using the Biorad Confocal Scanning Laser Microscope (CSLM) setup.



Figure 2.2: Layout of Small vane with serrated cup and foam sample.

2.15.2.2 Shear stage

Use was made of a Linkam Shear Stage (CSS 450 Optical Shearing System) (Tadworth, Surrey, UK), to assess microstructural stability of the model foam, through steady shear experiments. The Shear Stage is capable of three modes of operation: oscillatory, step and steady shear. All experiments used the steady shear mode. The stage was equipped with Parallel plate geometry. The parallel plates were flat glass plates. The foam was loaded into the cell and sheared for a maximum period of 45 minutes. It was stopped every 5 minutes for image capture.



Figure 2.3: Internal layout of Linkam shear cell

2.15.3 Principles of Confocal Scanning Laser Microscopy

In Confocal Scanning Laser Microscopy (CSLM) optical sectioning is one of the main advantages. CSLM can be used in transmission and reflection modes, but fluorescence imaging has been proven to be the most powerful microscopic technique in biological applications and in microscopy of food materials. In confocal scanning microscopy, the sample is scanned by a focused spot of light; the light emitted through the interaction of the scanning light with focused areas can be recorded using a non-imaging photodetection device such as a photomultiplier (Figure 2.4). An excitation beam from the laser is reflected by the dichroic mirror (a chromatic beam splitter) and focused by the objective lens to a limited spot in the specimen. Fluorescent light is emitted from the irradiated spot, passing through the dichroic mirror and an adjustable imaging aperture or pinhole which is placed confocally with respect to the illumination aperture, and is collected by a photomultiplier. The instantaneous response of the light detector at all points of this scan must be displayed with the equivalent spatial position and relative brightness on a monitor screen. To build up a two-dimensional image, either the beam or the microscope stage has to be scanned in a raster pattern, with simultaneous accumulation of a digitised image (Ferrando and Spiess, 2000).

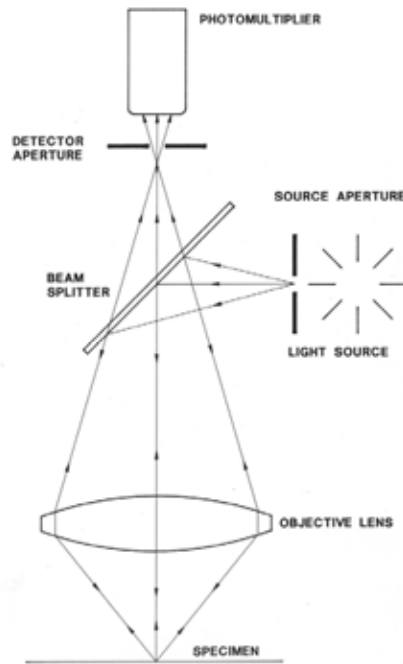


Figure 2.4: Principles of CSLM (from: Bio-Rad Handbook, Hemel-Hempstead, Herts., UK)

One of the main advantages of the confocal microscope is the exclusion of out-of-focus blur. The fluorescence emissions from the illuminated regions of the specimen above and below the in-focus point are not allowed to reach the photomultiplier, as a pinhole in front of the detector ensures that only light from the in-focus point is collected (Figure 2.4). Addressing different focus levels allows optical sectioning and it is possible to image a thick sample in three dimensions, this is one of the most useful properties of CSLM. Through combination of the information on several focal planes, optical slices stored on a computer, a three dimensional image that describes the object can be built up. Another benefit of the rejection of light which is not directly associated to the focal plane being imaged enhances the signal-to-noise ratio of the technique when compared to conventional fluorescence microscopy (Ferrando and Spiess, 2000).

Fluorescent dyes with a small shift between the maxima of the excitation and emission spectra (i.e. with small Stokes shift) are recommended because the resolution is proportional to a combination of the emitted and incident wavelength. Stokes shift will be covered later on in section 2.15.6.

The resolution in confocal microscopy can also be limited by the number of photons which reach the photomultiplier. The incident photon flux has to be high enough to produce a visible signal with efficient precision (in other words, an adequate imaging), but not too strong to produce a fading of the fluorophore. This vanishing of the fluorescence emission or photobleaching involves the irreversible chemical transformation of a dye molecule to a non-fluorescent species as a consequence of the exposure to emission light. In order to obtain an image of good quality without subjecting the specimen to extremely high levels of exciting light, two parameters must be set up in CSLM: zoom magnification and pinhole size. The zoom setting controls the size of the area scanned on the specimen. The optimal setting for zoom magnification depends on the resolution limit of the optical system, an optimum existing for each incident wavelength and objective lens used. Likewise, the optimal size of the pinhole to obtain both a high signal-to-noise ratio and a low blur of additional signal from other planes (high z-resolution) is a sensitive function of the wavelength, and the objective lens Numerical Aperture (NA) and magnification. According to these factors, usual values of

the pinhole diameter can be between 10 and 1000 micrometers (Ferrando and Spiess, 2000).

The imaging depth or the distance below the surface of the specimen which can be accurately imaged is restricted, first of all, by the working distance of the objective, i.e. the distance between the focal plane and the objective. Its value can be hundreds of microns or some millimetres depending on the Numerical Aperture (NA) and magnification of the lens, and also the immersion medium. However, the real limitation of the imaging depth is imposed by the opacity and inhomogeneity of the sample. These cause a reduction of the signal intensity detected as the focal plane penetrates deeper in the specimen. The illuminating beam is scattered or absorbed as it passes through the upper layers of the specimen, limiting it from reaching a further focus plane in the specimen. Likewise, fluorescent emission from within the sample, which is dispersed or absorbed between the focal plane and the detector, can then not be detected (Ferrando and Spiess, 2000).

In addition, any optical inhomogeneity in the specimen above the focal plane will tend to defocus the beam of illumination and the returning signal, thus decreasing the signal which can pass through the pinhole (Ferrando and Spiess, 2000).

The penetration depth can be several hundred micrometers, but is reduced in samples with an imbibing medium having an index of refraction very different to the solid components of the specimen. The use of a low magnification with immersion objectives with a $NA < 0.8$ can increase the penetration because the defocusing effects are less serious. In conclusion, although a minimum number of working conditions are required to obtain the best performance of a CSLM, in some cases a balance needs to be found between resolution and penetration depth (Ferrando and Spiess, 2000) This trade off will depend to some extent on the specific objectives of each job and the requirements of each image.

2.15.4 Confocal imaging of the model mix

In most of the experiments that required the capture of foam images, a Biorad MRC-600 Confocal Scanning Laser Microscope (CSLM) (Hemel Hempstead, Herts., UK) containing a Krypton / Argon Laser was used. The laser illuminates the sample at a wavelength of 488 nm. Sample fluorescence was imaged using a Leitz 10 \times objective (Wetzlar, Germany) with a Numerical Aperture, NA of 0.30 giving images of 768 \times 512 pixels (with each pixel 1.87 μm in size) and with a theoretical axial resolution of 5 μm . A further objective was sometimes used, a Leitz 40 \times objective (Wetzlar, Germany) with a NA of 1.30 giving (0.46 μm pixel size) and a theoretical axial resolution of 0.45 μm . For all experiments using the pressure cell, the sample was imaged about 10 μm below the surface of the coverslip.

2.15.5 Selection of riboflavin (Vitamin B₂) as a fluorophore and comparison to other dyes

One of the confocal lasers on the Biorad MRC-600 works at 488 nm. This is the one provided by the Argon Channel. The other laser line available (but which remained unused throughout the study) was capable of illuminating the sample at 568 nm and was the Krypton Channel. Riboflavin was used as a fluorescent marker and it is a food-grade ingredient which could be incorporated into the mixes within the pilot plant prior to aeration. It would thus get incorporated in the mix at the same time this was aerated. Riboflavin is a hydrophilic substance and completely unreactive with any of the other substances contained in the mix. It is mainly reactive with other aromatic compounds (Bolotin P.A. et al., 2007) which the system does not otherwise contain. It suffers from moderate photobleaching, but bleaching which should not be of undue concern.

Other markers such as Nile Blue or Rhodamine (with a smaller Stokes shift than riboflavin) could have been used instead, but would have required mixing into the foams after aeration took place. Their use in the pilot plant would have been forbidden as they are not food grade substances. These two markers were trialled with a few samples and they were very unsatisfactory as they did not mix well into the system, giving as a consequence a streaky appearance and non uniform fluorescence. By folding the marker into the foam after aeration, the bubble structure is disturbed, bringing with it local coalescence of the bubbles and the breaking of bigger bubbles. By doing this the mix is also

further diluted through the addition of more liquid. In a system holding only a sample of 0.5 ml, such disturbances should be kept to a minimum. Mixing in the sample pot was also unsatisfactory, as it too lead to many of the above mentioned problems. A further problem with staining in the pot was that the flourophore penetrated the delicate foam structure and sank to the bottom without staining the sample at all.

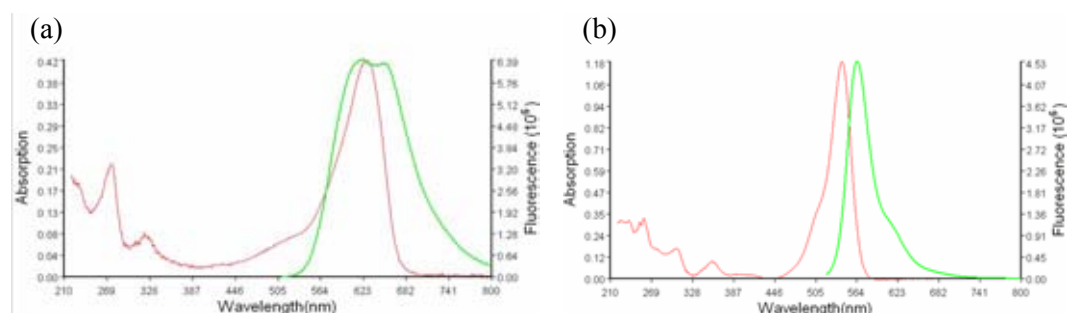


Figure 2.5 Absorption and emission spectra of (a) Nile Blue suspended in ethanol and (b) Rhodamine B. (absorption red / emission green),

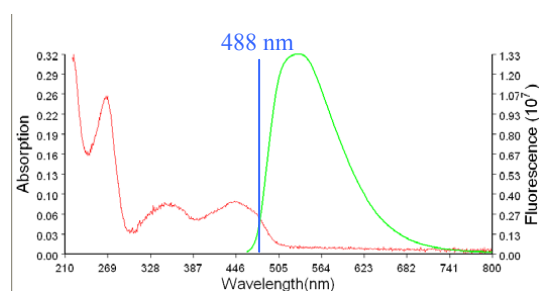


Figure 2.6: Absorption and Emission spectra of Riboflavin for comparison

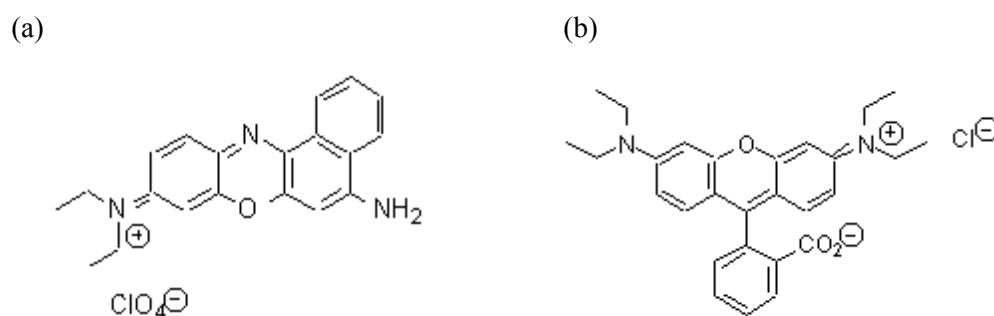


Figure 2.7 Structure of (a) Nile Blue and (b) Rhodamine B.

2.15.6 Intrinsic characteristics of Riboflavin

Fortunately the absorption and emission spectra of Riboflavin overlap at the excitation energy of 488 nm. If this did not happen Riboflavin would have been a poor confocal marker for the experiments with the confocal setup described in 2.15.3 and 2.15.4 (Photochemcad web, 2008). Other markers such as Nile Blue or Rhodamine (with a smaller Stokes shift than riboflavin, see previous section) might have been used instead.

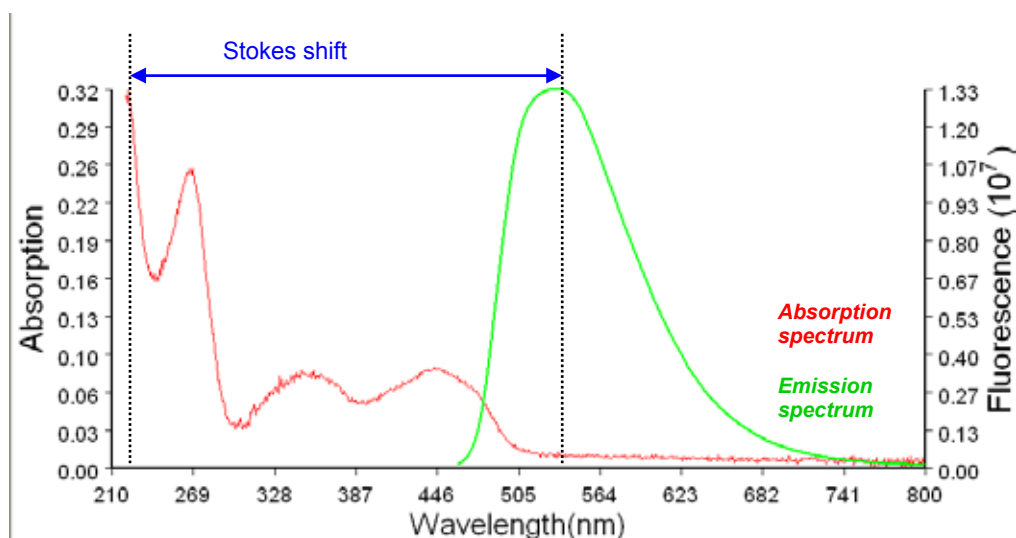


Figure 2.8: Absorption and Emission Spectra of Riboflavin, Vitamin B₂.
from: PhotochemCAD web, (2008)

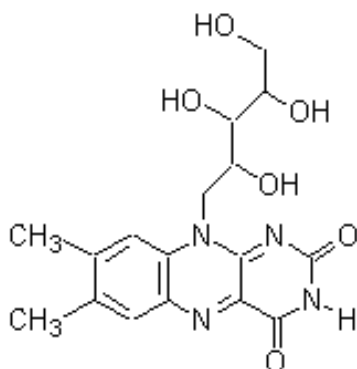


Figure 2.9: Structure of Riboflavin
from: PhotochemCAD web, (2008)

Fluorescence emission intensity can be seriously restricted due to poor overlap of the excitation wavelengths with the fluorophore absorption band. In addition, the confocal pinhole aperture, critical in obtaining thin optical sections at high signal-to-noise ratios, is said to be responsible for a 25 to 50 percent loss of emission intensity, regardless of the best attempts in alignment of the microscope optical system to prevent this. Photomultiplier tubes are the most common detectors in confocal microscopy, but suffer from a quantum efficiency that varies as a function of wavelength (especially in the red and infrared regions), further contributing to a wavelength-dependent loss of signal across the emission spectrum. Collectively, the light losses in confocal microscopy can result in a reduction of intensity exceeding 50 times the level typically observed in widefield fluorescence instruments. Fluorophore selection is one of the most critical aspects of confocal microscopy, and in addition instrumental efficiency must be carefully considered as well, in order to produce high quality images (Olympus web, 2008).

2.15.7 Bubble sizing

The images of the foams captured for bubble sizing were analysed with an image analysis script developed in-house at Unilever Colworth Park, using the DIPimage (Luengo Hendriks et al., 2006) toolbox running under MATLAB (Matlab ver.7, The Mathworks Inc. 2004). The gas cells are identified by first computing the gradient magnitude image, which extracts the edges of the gas cells. The gradient magnitude image is then tessellated using a watershed

algorithm (Soille, 1999). The edges of the tiles coincide with the edges of the underlying gas cells with the complication that the method tends to produce too many tiles and mostly with multiple adjacent tiles covering a single gas cell. To overcome this, an operator-set significance threshold was introduced, which ensures that the tiles cover an area with sufficient underlying contrast (*i.e.* whole gas cells which have not been segmented). The result is a tessellation of the entire image, of both gas cells and the background. To distinguish tiles corresponding to a gas cell from those covering the background a simple threshold on the average intensity within each of the tiles was used. The sizing itself was simple in that the number of pixels within each of the detected gas cells were counted, which could be transformed to give a size range in microns. In order to get an unbiased estimate of the size distribution, it is necessary to deal properly with cells touching the border of the image. This was achieved by using a guard frame technique (Russ, 1995). For each run on average a total of approximately 1500 bubbles were counted and sized within a defined area of about 1 mm².

The collected raw data was gathered in a range of ways, including the normal frequency distribution method and the cumulative distribution method. Hence, the size data shown here is comprised of the number $h(R)$ of bubbles with radius R , or alternatively the number of bubbles with a radius x satisfying $R - \Delta R < x < R + \Delta R$, with ΔR being half the spacing of the points in $h(R)$.

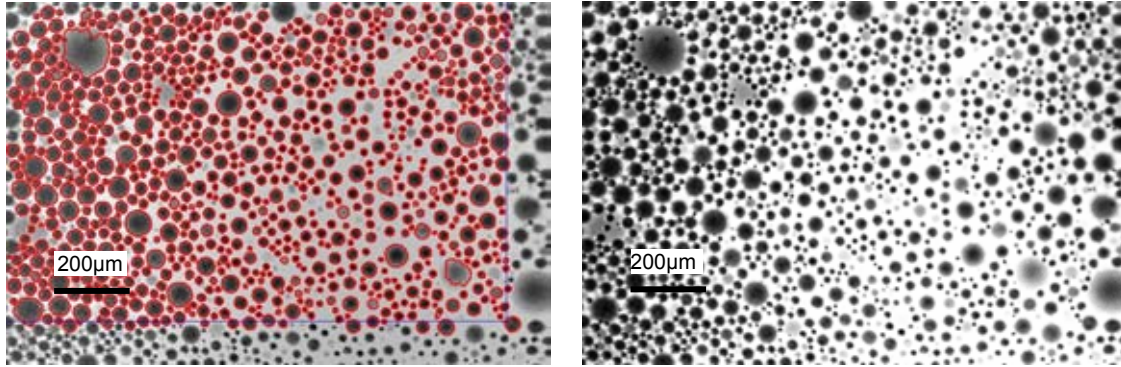


Figure 2.10: A representative example of a correctly tessellated image with a guard-frame (left). In comparison a raw un-tessellated image (right).

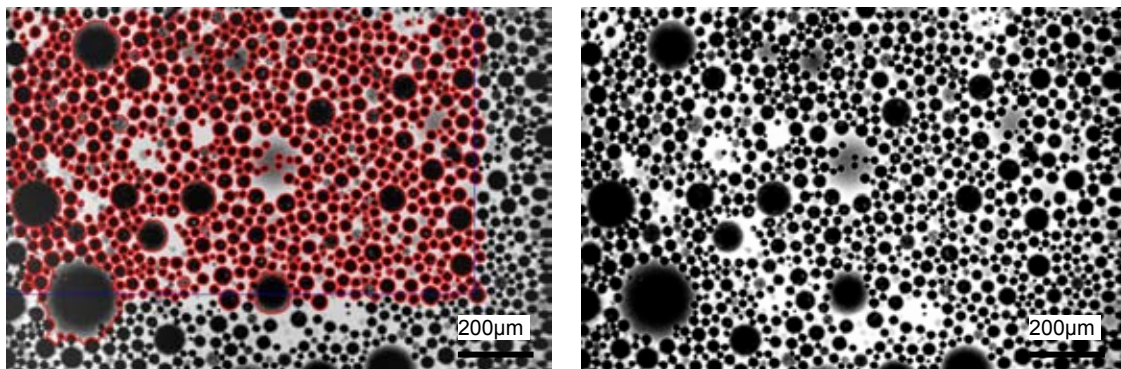


Figure 2.11: A representative example of a rejected and in-correctly tessellated image with a guard-frame. Included is the raw un-tessellated image for comparison. Sometimes incorrect tessellation could be fixed with the water-shed function. At other times though, it is irredeemable and the image and data-set had to be disregarded and the analysis repeated.

Note the different size of the guard-frame, which is adjusted automatically by the software, it does this to take into account the increase in mean bubble diameter between the images in Figure 2.10 and these.

2.15.8 Bulk pressurisation

Bulk pressurisation experiments of the foam were carried out by placing a sub-sample of the master batch foam in the serrated inserts of the vane rheometer (inserts described in section 2.15.2.1). These in turn were then placed inside a 3 gallon pressurisation tank, which was pressurised up to a maximum pressure of 6 bar absolute (Binks, Glendale Heights, Illinois, USA). The tank was capable of pressurisation up to 11 bar absolute, but the fixed air lines were only able to pressurise the system to 6 bar.



Figure 2.12: Binks Pressure pot. Capable of pressures up to 10 bar absolute.

2.15.9 Pressurisation on a 'micro' scale

In order to image the foam under quiescent and pressure fluctuating conditions, in a small scale, use was made of a Linkam Pressure Cell (THMS600) (Tadworth, Surrey, UK). The pressure cell is capable of pressurising the sample chamber up to an absolute pressure of 11 bar, with a GE-Druck gauge (Groby, Leicester, UK) and a pneumatic hand pump. Alternatively different gas bottles and an air line (BOC specialty gases, Guildford, Surrey) could be attached and the pressure cell pressurised this way. To be able to take images in the cell, it was coupled to a Biorad confocal microscope.

For each analysis, a foam sample was carefully spooned out of the sample pot and placed inside the quartz crucible of the pressure cell (THMS-Q)

(Tadworth, Surrey, UK). The crucible has a holding capacity of 0.5 ml. The sample was covered carefully with a round coverslip, 14 mm in diameter (Chance Propper Ltd.) (West Midlands, UK), avoiding excessive disturbance of the sample or trapping any bubbles. It is also vital to ensure that when the sample is loaded, no concave or convex meniscus is formed between the sample and the crucible side-walls. The preferred option is to have a completely flat surface, as otherwise the coverslip is liable to slip and lead to imaging a blurred interface. If the coverslip is left at an angle, when imaged, part of the sample remains in focus, while the other is imaged out of focus. In addition, if it remains slanted, when the sample is pressurised or depressurised it has as a consequence some sample loss out of the sides.

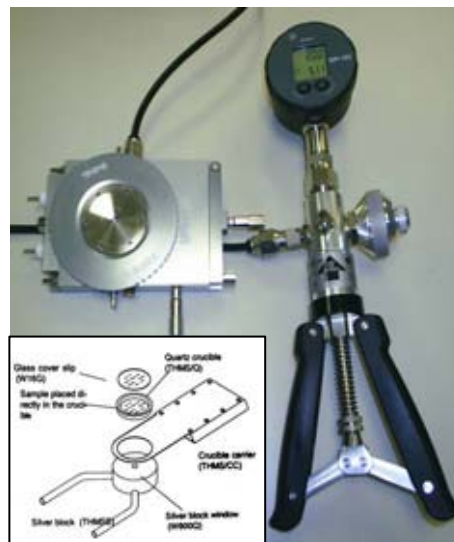


Figure 2.13: Pressure cell setup

Pressurisation of the Linkam cell and subsequent image capture with the Confocal Microscope, for each increase of one bar in pressure, took between 30

to 60 seconds to achieve with a pneumatic hand-pump. This was quicker if a gas bottle was used. The release of 1 bar pressure (allowing the system to stabilise) and the time taken for image capture was in the same order as above (30-60 seconds). To achieve an increase of one bar in pressure typically required three pumps of the pneumatic hand pump.

Through a very slow release in pressure it was possible to capture a dynamic video using the CSLM setup. The pressure was released slowly and continually from 3 bar to 1 bar absolute over a 90 second time-frame. The timescale involved in releasing the air for the capture of this video bears no relation to the actual release rates employed in most of the experiments (i.e. cycling, single cycle, or pressure release). The release-rate used in this experiment was slow, purely to allow the capture ‘in real time’, of the dynamics taking place when the last few bar are released from the pressure chamber.

2.15.10 Disproportionation of foams under five different gases: Air, Nitrous Oxide (N₂O), Helium, Argon and Carbon Dioxide (CO₂)

The disproportionation experiments in section 5.4.2, used three different pressures of 1 bar, 6 bar and 11 bar absolute (where the foams were left for 5 hours at this pressure). For these experiments, different foams were prepared, containing either: air, argon, nitrous oxide, helium or carbon dioxide (BOC specialty gases, Guildford, Surrey). See also Chapter 5, section 5.2 for the

different solubilities of the 5 gases. If the model mix included just air, it was prepared using the procedure outlined in ‘mix preparation and formulation’ (Section: 2.13). On the other hand if the model mix required any of the other four gases the only modification undertaken was to cover the mixing bowl with aluminium foil and to cover the whole mixer in a plastic bag to contain the gases. The gas was allowed to fill the bag before mixing commenced. The gas release rate from the bottle throughout the experiment was between 7 and 10 litres per minute. It was assumed that (1) as nitrous oxide is heavier than air, that it would remain contained within the bowl during mixing. (2) helium being lighter than air, would fill the bag around it and the aluminium foil only serving to prevent further extra atmospheric air from mixing into the bowl. One could describe the procedure as “mixing in a nitrous oxide, helium, argon or carbon dioxide enriched environment”. The prepared samples were then placed in the Linkam sample chamber, purging the sample chamber with the desired gas before closing the lid, and were then left for a total of 5 hours. During this time the sample was imaged every 30 minutes. For the samples with different gases from air, a cylinder containing that gas was attached to the pressure cell and the cell purged with the gas to obtain the desired pressure. For 1 bar the cell was just purged of the air and the cell lid closed tightly, and for 6 bar and 11 bar the cell was purged and then pressurised to these target pressures.



Figure 2.14: Pressure cell setup with a dedicated gas line attached to the chamber via the blue flex-hose. The image also shows the quartz crucible that holds the sample. The Black hose and pressure gauge are there for the pressure read-out.

For all gases (especially those with low solubility in an aqueous environment, prior to aeration in the mixer) it was necessary to sparge the gases through the sample for 5 minutes using a porous metallic frit. Due to the insoluble nature of Helium, and its rapid volatility, helium gas was sparged through the pre-mix for 20 minutes instead of 5 minutes. The metallic-frit setup was prepared in-house by the Engineering Department (Unilever R&D, Colworth Science Park, Bedford, UK).



Figure 2.15: Metallic frit and rod setup used for sparging the sample prior to aeration.

2.15.11 Pressure release

For the duration of the experiment, the samples were handled, using the master batch method described in section 2.14. For the release rate experiments, the foamed and prepared sample was placed within the pressure cell. A range of pressures were analysed (Δp 1 bar to Δp 6 bar) which will be described in the following paragraphs. For the release rate analysis the chamber was pressurised from 2 bar absolute (Δp of 1 bar) up to 7 bar absolute (Δp of 6 bar), in one bar steps. For each final target pressure, a new sample was used. Once the target pressure was reached (i.e. 7 bar) the pressure was released using the knob on the side of the handle. The pressure was released manually using four rates: 2 minutes, 30 seconds, 10 seconds or less than 1 second. Each release rate was used on a fresh sample, for each different Δp . Each bar of

pressure was released by using the release rates indicated next to each sample on the graph. So for a Δp of 6 bar with a release rate of 2 minutes per bar, it took 12 minutes to empty the whole chamber. No images were taken while the pressure was being released, the only images that were taken were those taken once the pressure had been fully released.

2.15.12 Pressure Cycling

For microstructural analysis the aerated mixes were subjected to one of three different pressure regimes, or cycles, as summarised diagrammatically in Figure 2.16. and summarised below:

- (1) One was a simple cycle with pressurisation from 1 bar to 11 bar absolute, followed by a complete release of the pressure {A}.
- (2) A second regime, a pressure cycle at elevated pressures, involved pressurising from 6 bar to 11 bar absolute, releasing the pressure to 6 bar, but then re-pressurising back to 11 bar. This was done a total of three times with the same sample {B}.
- (3) A low pressure cycle, the third regime, involved pressurising the chamber from 1 bar to 6 bar absolute, releasing the pressure back to ambient and re-pressurising, repeating this procedure twice more using the same sample {C}.

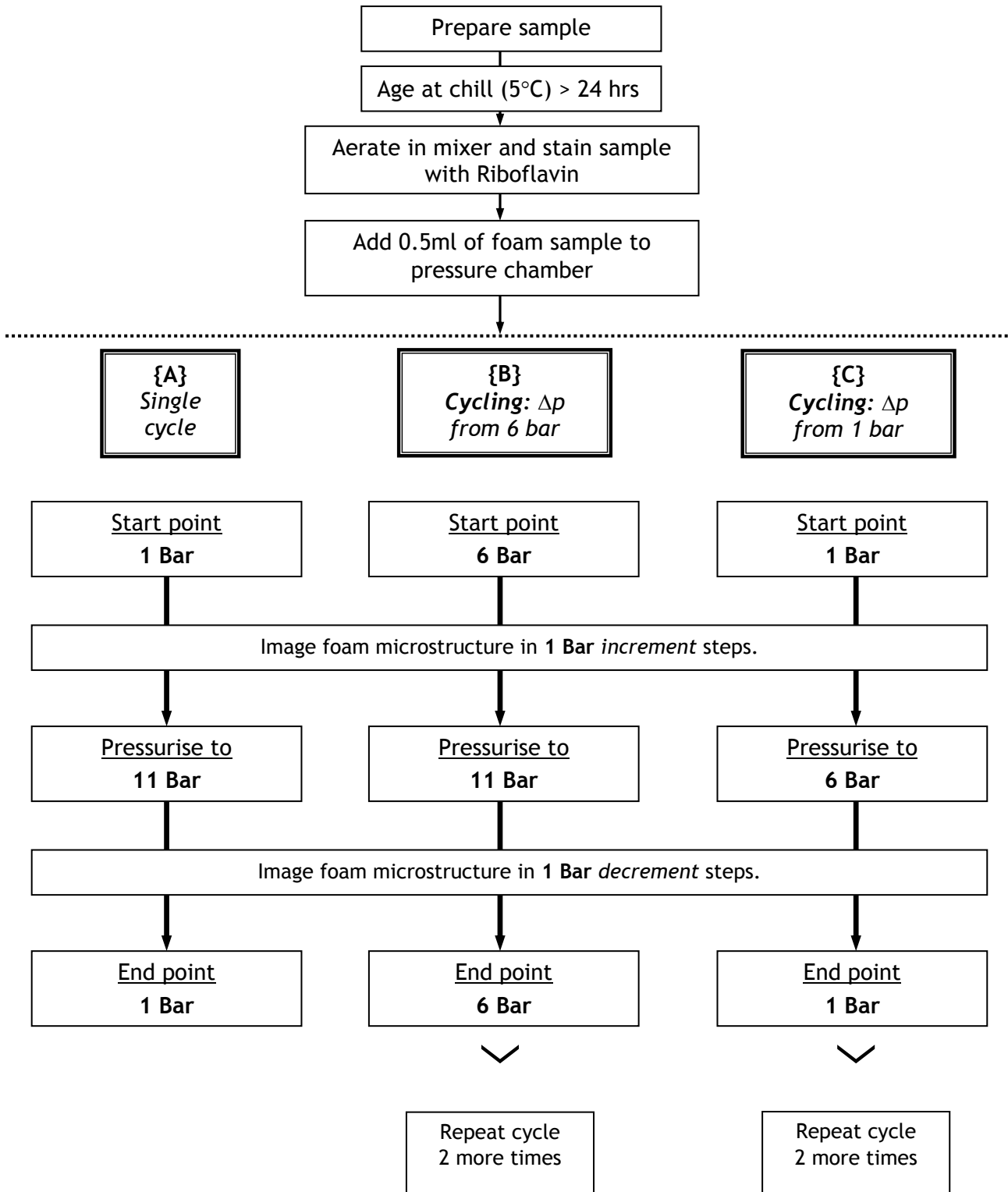


Figure 2.16: Summary of three different pressure cycling experiments.

2.16 Closing remarks

The experiments carried out using the methods outlined above should better the understanding and intricate response of a thick foamed mix exposed to extraneous disturbances acting on it. These might be those associated with its manufacture, such as shear or changes in pressure. The thick model food foam that was created for these purposes ideally suited the current investigation. It was neither too stable (where no coalescence events would be seen) neither was it so unstable that it collapsed straight after whipping. It showed excellent mid-term stability. The foam response to the tests described in Figure 2.16, will be formulation specific, but the techniques employed would allow great scope for further formulation space exploration. Due to the cooling capability of the pressure cell, further tests could involve cooling the mix and thus understand the viscosity dependency of the pressure mediated coalescence events. Ultimately one would then end up by studying a completely frozen mix, although the ice particles in such a studied system would add a whole new order of magnitude and complexity to the system.

CHAPTER 3

Properties of dairy and vegetable whipping creams

3.1 *Introduction*

Unilever, like other food manufacturers, continually strive to make products that contain healthier ingredients. The work in this chapter will cover one part of this, working with whipping creams. There is an increasing demand for products with less hydrogenated oils (Golding and Pelan, 2008) and Unilever would like to meet this demand by seeking to market their products containing higher levels of ‘healthier’ oils. Perneti et al., (2007) mention that the most common way to provide texture to the lipid phase of food products is by including a crystalline hardstock. These hardstocks contain large amounts of saturated fatty acids (SaFa), which are considered unhealthy, since their presence in the diet is among one of the contributing factors of cardio-vascular disease (Keys et al, 1965) obesity and the inherent risk of diabetes.

In this chapter two distinct themes predominate. The first part characterises commercially available whipping creams whilst the second then endeavours to create a vegetable oil whipping cream, building on the knowledge gained with the work undertaken in the first part.

The chapter describes the whipping characterisation of three commercially available double whipping creams. One of them is dairy-based and the other two are vegetable oil emulsions, which have been tempered and reformulated to whip and react like their dairy counterparts. In the second part of this chapter whipped emulsions were produced, based on the Elmlea formulation, taken

from the patent granted to Unilever (Whippable Non-dairy creams by Morrison, A. et al. (1992), US Patent number, 005149557 A). All systems studied, were reliant on partial crystallisation of the fat phase to allow the cream to be whipped. The variable that was changed within the re-formulated creams was the ratio of hardened palm oil to liquid rapeseed oil, described in Section 2.2. The aim of the work in section 3.2 that preceded that in the reformulation stage of section 3.3 was to build an understanding of the whipping properties of complex whipped creams. The parameters studied were; aeration as a function of time and collapse as a function of temperature (taken at 25 °C, 30 °C, 35 °C and 40 °C).

The oscillatory and viscometry response of these commercial samples was also measured as a function of shear and temperature (at 10 °C and 25 °C). These parameters were investigated with the re-formulated mixes too, although for the collapse work it was only carried out at 25 degrees. The rheological response was also only carried out at 25 degrees. All samples were investigated using Differential Scanning Calorimetry (DSC) to characterise the constituent fat phase in the cream. As described in the Prior Art document granted to Unilever for the Elmlea non dairy cream, the tempering step, (to which the Elmlea samples were subjected so they could be whipped in less than 4 minutes) is evident in the behaviour of the thermal peaks between 16 and 25 °C. In the tempering step, the emulsion is normally warmed to a temperature of 15 °C to 25 °C and it is held at this temperature for 18 to 30 hours. Finally, both the reformulated mixes and the commercial samples were also studied

using tribology. In both cases the samples were tested aerated and unaerated. The trends seen with the samples coincided with the viscometry response, as will be shown in figure 3.10, figure 3.11 and figure 3.41. For the re-formulated mixes the difference between the traction coefficients of the aerated and unaerated samples of the softest mix (number 1), remains the same, without much change at all. The slightly harder sample (mix number 3) has a slightly higher traction coefficient towards the higher speed of 100 mm/s, falling off after that, when compared to the unaerated mix. All creams scrutinised in this work were also analysed with cryo-SEM to understand the main stabilisation effects of the fat phase in the formulation of each cream.

3.1.1 Emulsions

It is usually assumed that the rheological properties of the adsorption layers of a protein on an air bubble are of primary importance for protein stabilisation (formation of mechanically stable adsorption layers), see also section 1.2.9.5 (Damodaran, 2004). Following this reasoning, Graham and Phillips (1976) (*in* Tcholakova et al., 2006) reported a certain correlation between the rheological properties of the protein adsorption layers (dilatation and shear elasticity) and foam stability. However, the authors did not find a direct correlation between emulsion stability and the rheological properties of the respective adsorption layers. The absence of such a correlation was also found in a study discussed in Tcholakova et al. (2006), which showed that ageing (which in this case consisted of shelf-storage at room temperature) and heating, of β -lactoglobulin (BLG) stabilised emulsions, lead to opposite effects on the emulsions stability

to coalescence— the ageing decreased stability, whereas heating increased it, although both treatments were known to increase the elasticity of the BLG adsorption layers. These show that the relationship between the visco-elastic properties of the protein adsorption layers and the subsequent emulsion stability are not always straightforward (Tcholakova et al., 2006).

Dimitreli and Thomareis (2008) mention that the fat content also reduces the elastic and the viscous modulus, the complex modulus and complex viscosity and increases the loss tangent, exhibiting a more liquid-like behaviour for the samples. They argue that this is due to the action of fat as a lubricant. Similar observations have been reported by Subramanian et al. (2006) who concluded that fat reduction results in increased viscoelastic properties in processed cheese. The softening effect of fat on the texture of processed cheese generally has also been observed using other methods (Subramanian et al., 2006). Dimitreli and Thomareis (2008) fail to mention in their conclusion that whipping, churning or mixing in addition to the softening will also affect the rheological response of cheeses.

3.1.2 Whipped cream

From a consumer point of view, the ideal qualities that a whipped cream should have would include: be acceptable physically, microbiologically and organoleptically. In addition, good quality whipping creams will be composed of a fat content of around 30 – 40% but which must be easy to whip. They should be capable of producing a fine foam with a high level of overrun (over

80 – 90%). The final product must be long lasting and stable during storage (Prentice, 1992 discussed in Jakubczyk and Niranjana, 2006). Bubble mechanics can be used to estimate the shelf-life of whipped cream, since the textural appearance and mouth-feel are a direct consequence of the complex interactions between bubble mechanics and our senses (Niranjana, 1999).

Whipped cream is a dispersion of gas bubbles that are surrounded by partially coalesced fat at the air/serum interface, and supported by high viscosity in the serum phase. Several factors affect the structural properties of whipped cream, which amongst them are: the fat content, processing conditions and the addition of stabilisers and emulsifiers (Bruhn and Bruhn, 1988). Without additives, the cream must have a fat content of at least 30% to support rigid foam formation. Graf and Mueller, (1965) reported an ideal fat globule size of 15-20 μm for whipping cream.

It is for this reason that whipping cream has traditionally been processed without homogenisation, which as a process may reduce the size of fat globules to the point where they resist partial coalescence and inhibit stiff foam formation (Graf and Mueller, 1965). At least 40% of the fat must be crystalline (Smith et al., 2000) to promote partial coalescence and add rigidity to the air bubble interface. In Ultra-high-temperature (UHT) sterilisation of whipping cream, a process which is desirable to increase the shelf-life also results in changes in whipping properties when compared to high-temperature-short-time (HTST)-processed cream (Graf and Mueller, 1965) (Bruhn and Bruhn, 1988).

Comparisons have been made based on whipping time, overrun, drainage and viscoelastic properties. UHT treatment resulted in lower overrun and increased whipping time when compared to cream whipped after HTST pasteurisation (Bruhn and Bruhn, 1988). This is because processing at temperatures above 70 °C causes denaturation of β -lactoglobulin (Smith et al., 2000) and also causes this to complex with other compounds.

Denatured β -lactoglobulin may form complexes with κ -casein and α -lactalbumin resulting in a higher viscosity in the serum phase (Smith et al., 2000). Changes in membrane structure at the MFGM (milk fat globule membrane) and at the air/fat interface may help explain changes in viscoelastic properties associated with destabilisation of whipped cream.

Emulsifier/stabiliser formulations added to cream, improve the whipping behaviour and enhance foam stability. Addition of low molecular weight emulsifiers promote adsorption of partially coalesced fat at the air/serum interface through a lowering of interfacial tension (Anderson & Brooker, 1988; Paquin & Dickinson, 1991 in Smith et al., 2000).

The main structural component of foam is the network of air bubbles with their interface of protein and partially coalesced fat. In the absence of bubbles the serum phase becomes the measurable quantity. However, the foam is a combination of these structural elements, which are not being measured in isolation. Therefore, in samples with a lower overrun, measurements are based

more strongly on the viscosity of the serum, which minimizes anticipated differences (Smith et al., 2000).

The rheological measurements (G' and G'') for fresh foams differing in heat treatment or the addition of stabiliser were not significantly different, even though physical properties of the foams showed variations in whipping time and overrun (Smith et al., 2000).

In the experiments of Bruhn and Bruhn (1988) the foams were whipped to the point of maximum overrun to compare whipping properties. Results showed that unstabilised HTST and UHT creams required similar whipping times to reach maximum overrun and confirmed that the addition of stabiliser resulted in a significant increase in whipping time, within heat treatments (Bruhn and Bruhn, 1988). Stabilised UHT-processed cream required longer whipping times than the stabilised HTST treatment. Stabiliser was added to increase foam stability through increased serum/phase viscosity but also increased resistance to shear during whipping which explains the longer whipping times (Stanley et al., 1996) required to reach maximum overrun. Unstabilised HTST cream whipped to a significantly higher overrun than unstabilised UHT sterilised cream. Addition of stabiliser resulted in a significant decrease in overrun for both heat treatments. HTST and UHT stabilised creams had similar overrun values. The increase in viscosity of the serum phase, because of the added stabiliser, also reduced the ability to incorporate air during whipping (Smith et al., 2000).

Unstabilised whipped foams in Smith et al. (2000) did not exhibit significant differences in rheological measurements when freshly whipped or after 24 h of refrigerated storage regardless of heat treatment. Foam persistence is related to strength and flexibility, that is, a balance between viscous and elastic components. The result of the imbalance is the breaking of air/serum interfaces that will lead to the loss of air in UHT-processed stabilised foams. A stabiliser/emulsifier mix would need to be designed to account for compositional differences caused by protein denaturation in UHT sterilised whipping cream, and also provide a foam with greater visco-elasticity (Smith et al., 2000).

Allen et al. (2008), backed up by statements from other authors, saw that in model emulsion systems sheared in the absence of air under conditions of gradually increasing applied stress the onset of partial coalescence was accompanied by a sudden increase in the measured apparent viscosity (Davies et al., 2001) and in the fat particle structure (Xu et al., 2005). They mention that with air incorporation, once substantial fat globule clumping has taken place, the dairy cream is converted from a viscous liquid emulsion into an aerated viscoelastic solid with an optimum overrun of 100–120% (Graf and Mueller, 1965). The high fat content of whipping cream (ca. 35%) yields a sufficiently clumped structure during aeration to facilitate rapid and complete stabilisation of the incorporated air bubbles. In contrast, for an ice-cream mix which has a considerably lower fat content (7-10%), the emulsion partial coalescence by

itself was not enough to stabilise the aerated microstructure; additional structural contributions to ice-cream stabilisation were provided at low temperature by ice crystals, as well as by a combination of sugars, emulsifiers and hydrocolloid thickeners (Allen et al., 2008).

Whipping changes the properties of cream by rendering it more viscoelastic than unwhipped cream. Both G' and G'' increase with whipping time up to a point beyond which they do not change significantly. Jakubczyk and Niranjana (2006) mention that the overrun also increases until this whipping time, but decreases thereafter as fat globules aggregate and the foam collapses. Bubble size distributions indicate that the highest number frequency shifts towards lower diameter values, as whipping progresses. In other words, progressive whipping results in the formation of a greater proportion of smaller bubbles until the overrun attains a maximum value. Thereafter, the bubble size distribution changes from being log-normal to a bimodal population (Jakubczyk and Niranjana, 2006).

3.2 Analysis of commercially available creams

Through the use of multiple techniques it was possible to characterise the microstructural properties of three different commercial whipped creams and six different reformulated ones.

The techniques comprised: using light microscopy for imaging, bulk rheological analysis of the samples, analyses of the fat phase of the sample with a Differential Scanning Calorimeter and testing the formulations using thin film rheology. The destruction of the samples under gravity was analysed at four different temperatures and at one temperature with the re-formulated mixes (as described in section 2.6). Overrun measurements at set time-points were also performed. In addition use was made of a Malvern Mastersizer for fat droplet sizing. SEM micrographs were also gathered of some representative structures of all the whipping creams.

3.2.1 Overrun of commercially available products

In the following experiments the whippability and therefore the Overrun level that can be achieved with the 3 commercially available double whipping creams will be assessed. The method for calculating Overrun is given in equation 2.1 in Chapter 2 Part I.

The full formulation and ingredients list and nutritional information of the commercial samples was included in methods and materials, Chapter 2 Part I.

Figure 3.1 is a graph of a whipping curve of commercially available whipping creams (whipping method as described in section 2.5). From the position of the maxima it can be seen that the J. Sainsbury's whipping cream obtained the maximum Overrun after 120 seconds, whilst the Elmlea Light cream exhibited maximum Overrun after 210 seconds and the Elmlea Full Fat version reached the highest Overrun after 240 seconds.

Both Elmlea variants do not react like the J. Sainsbury's whipping cream because the Elmlea formulations have been softened with liquid vegetable oils. In contrast the J. Sainsbury's sample shows a fast onset of overwhipping. Elmlea Light has a higher percentage of liquid oil when compared to the full fat version, as noted in section 2.1. The Full Fat Elmlea reaches a higher Overrun level as its total fat content is much higher than the Light version. The Full Fat Elmlea contains 34.8 percent total oil whereas the Light version in comparison only has 23 percent. In the Full Fat cream 26 percent of the total oil content is hydrogenated and in the light version only 11 percent is hydrogenated. The Elmlea Light therefore has a higher vegetable oil content, at 12 percent (which is rapeseed oil and therefore liquid, *personal communication* Elmlea) than the Full Fat which has a higher hydrogenated component and only 8.8 percent vegetable oil.

Elmlea Light overwhips faster as shown in Figure 3.1 due to the higher

content of vegetable oil. It would be unfair to compare both creams side by side, because in addition to having different oil ratios, Elmlea Light has one more stabiliser that is not included in the Full Fat version (Carageenan gum) and also has 12 percent more buttermilk than the Full Fat version. This difference between the samples tested will be eliminated in Section 3.3 by preparing cream formulations that have an identical continuous phase (of proteins, emulsifiers and stabilisers), but where only the oil ratios (hard oil to liquid oil) are varied.

Most of the subsequent experiments performed on the creams, like the melting behaviour, the bubble sizing and the representative micrographs were captured after 150 seconds aeration. This time-point was chosen as all three creams exhibited nearly equal Overrun values at this stage. In the case of the J. Sainsbury's (dairy) whipped cream, slight overwhipping of the sample may have already taken place. It was nevertheless decided that having the same Overrun values and equal aeration times for all experiments was of more importance for the elucidation of a change in behaviour.

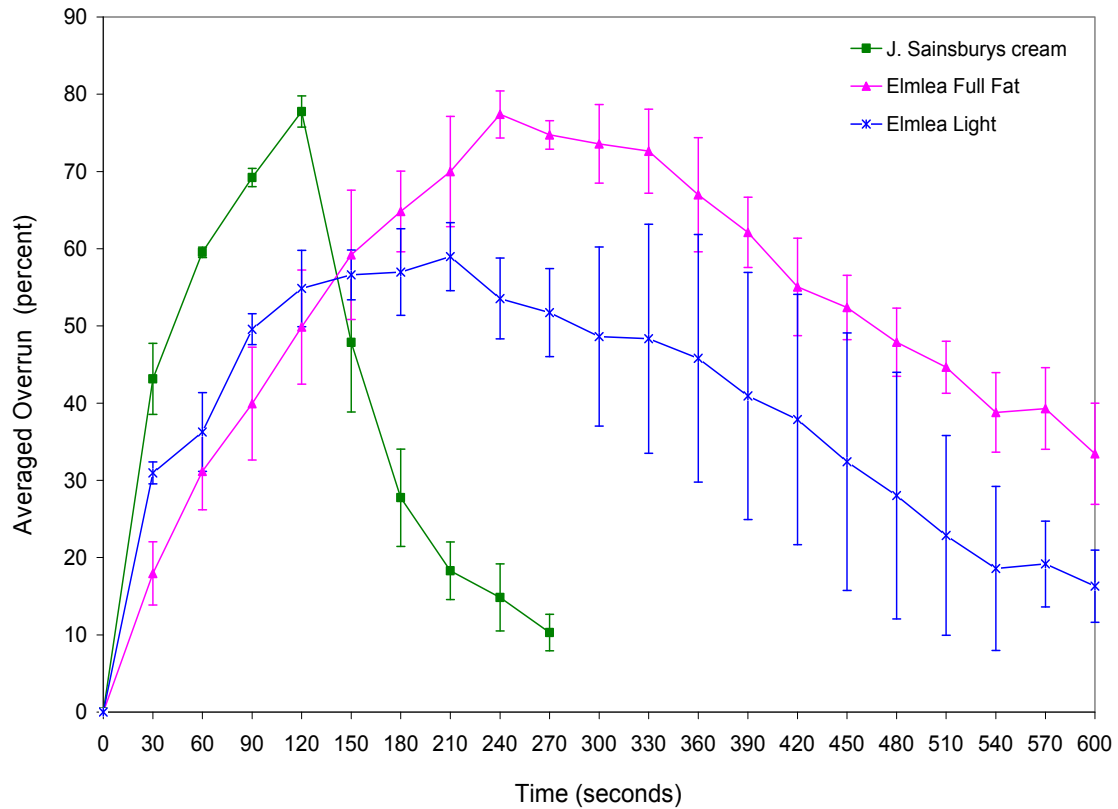


Figure 3.1: Overrun curves of the three different double cream samples. Each trace is an average of three measurements. The samples were stopped and started, and the Overrun was measured every 30 seconds.

Figure 3.2 shows the whipping curve for the same 3 commercially available whipping creams as in Figure 3.1, but they were whipped continuously for the time-period indicated on the x-axis. The results from Figure 3.1 (the stop-start method) are included for comparison as a discontinuous dashed line.

Throughout the continuous process the achieved Overrun values in Figure 3.2 remain nearly the same throughout the entire period for each of the creams. The only one that follows a similar trend as the stop-start method is the J. Sainsbury's cream.

The full fat Elmlea with the continuous method attains a lower level of Overrun throughout, in comparison to the stop-start method.

The light version attains a higher level of Overrun with the continuous aeration than with the stop-start method.

But both creams attain an Overrun level similar to that of the stop-start method if one factors in the margin of error, indicated by the error bars.

The stop-start method seems to show more consistent and reproducible results than the continuous method. It is perhaps not surprising as the stop-start method in some ways mimics more closely what takes place inside a domestic environment.

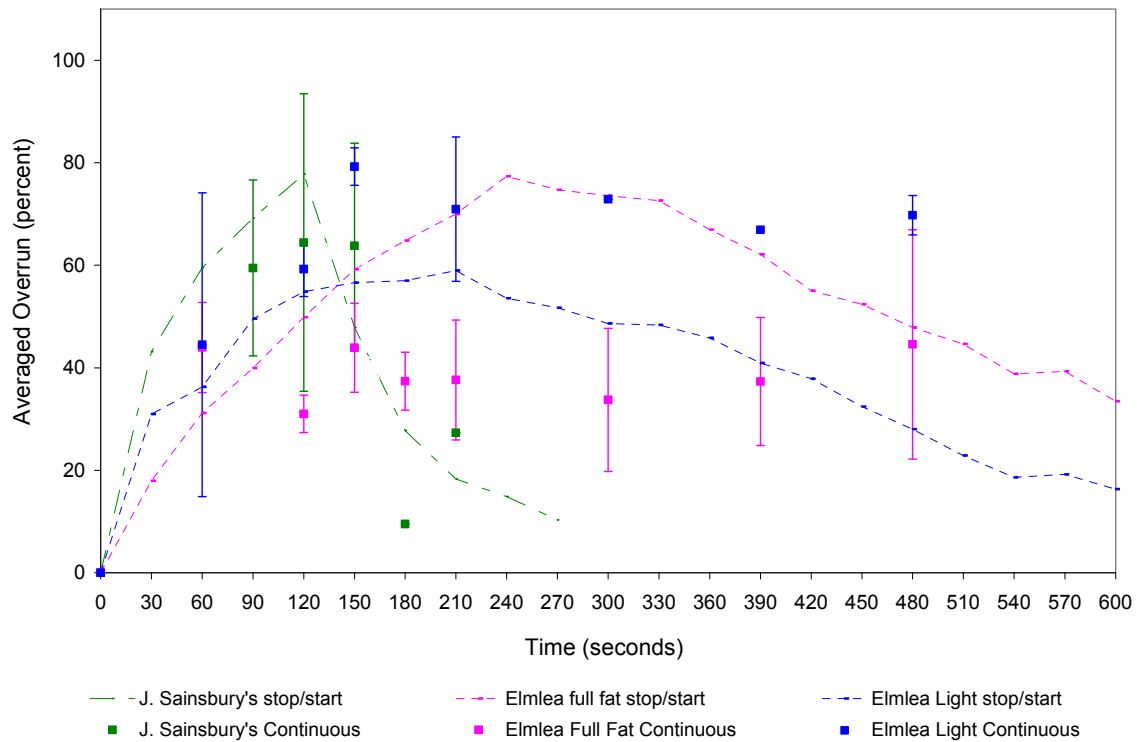


Figure 3.2: Overrun curves of the three different double cream samples. The samples were whipped continuously until the desired time-point was reached. The stopped/started whip curves (as seen in Figure 3.1) are included here as a reference, and their error bars omitted for clarity purposes. Each data point was gathered in triplicate, for which, a fresh sample was used each time.

3.2.2 Optical microscopy of Elmlea Light samples

Four representative micrographs of the Elmlea Light cream taken during aeration after 60, 90 and 150 seconds, together with an unaerated control have been included in Figure 3.3.

Later in the chapter, in section 3.2.12, micrographs of whipped structures were gathered for the three commercial formulations at the 150 second time-point only. They were gathered to show the difference in the microstructure between the three samples.

The work in this section and also in 3.2.3 is a one-off developmental test for a randomly chosen cream sample chosen to gain a visual insight into bubble structural development over time. In this case it happened to be with Elmlea light.

In addition to the low magnification micrographs (in Figure 3.3), which were taken at 10× magnification, some further micrographs of the Elmlea light formulation were gathered at a higher magnification (25×) after 60 seconds and 150 seconds aeration. At this higher magnification the partially coalesced fat is visible at the bubble interface (Figure 3.4). It is this fat layer that is responsible for giving whipping cream its structure, texture and which also allows it to be whipped in the first instance (see further descriptions in section 1.2.9.4). Jakubczyk and Niranjana, (2006) mention that for a cream to be whippable, in itself a minimum of 30% of the formulation needs to be a fat component. If the cream has less than this level, it requires stabilisers and emulsifiers to be whippable and remain stable. This is the case with the reformulated mixes and with the Elmlea creams. They both contain emulsifiers and stabilisers, although it is only Elmlea light that contains less than the 30% ‘critical’ fat composition to be whippable without the stabilisers and thus contains no less than 3 different stabilisers.

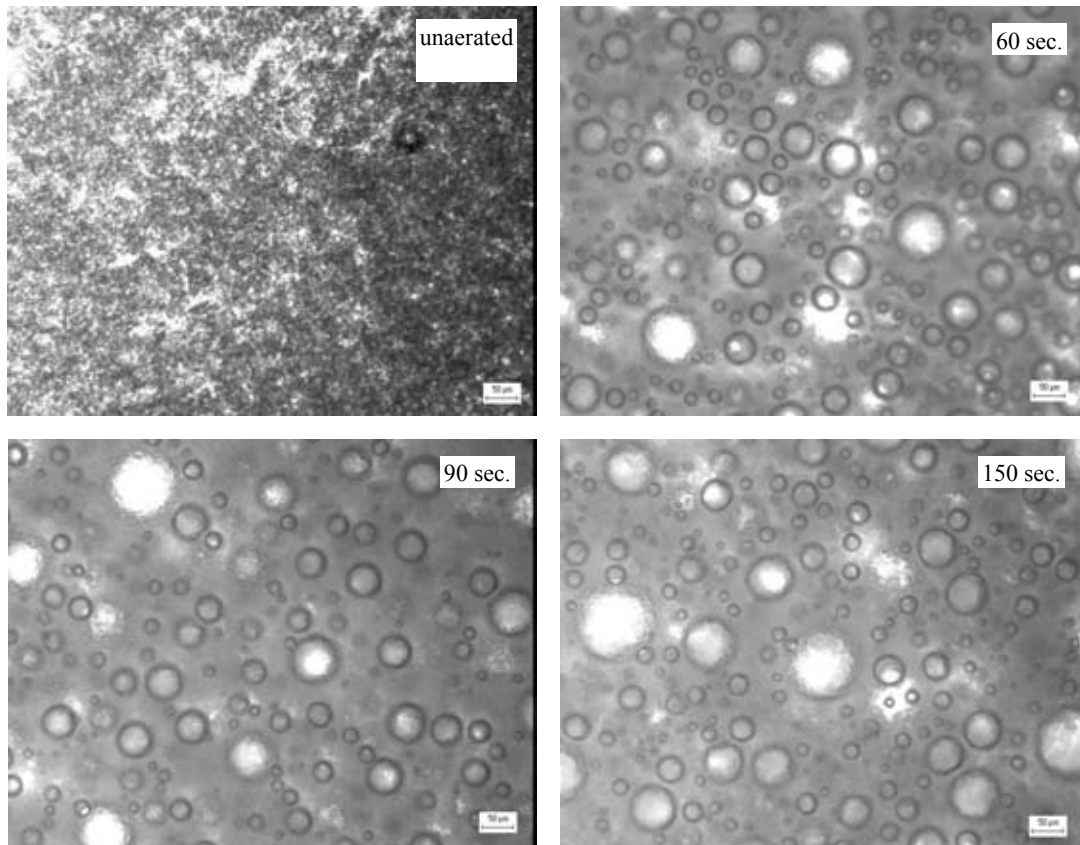


Figure 3.3 Representative micrographs of Elmlea Light whipping cream, aerated for different time periods. Imaged with a Polyvar and the 10× Objective. Quantitative data also represented in Figure 3.5. Scale bar is 50 µm.

The micrographs in Figure 3.3, chosen up to the time-point of optimum whipping, 150 seconds, show the structural development within Elmlea light cream. Bubble structure is very similar over the time periods chosen. Quantitative evidence of this can be seen in the bubble sizing experiments in section 3.2.3. Similar work with the reformulated creams in section 3.3.2 shows the same, little evolution in bubble size despite further whipping. In both cases, the average bubble size does not change, despite continued aeration.

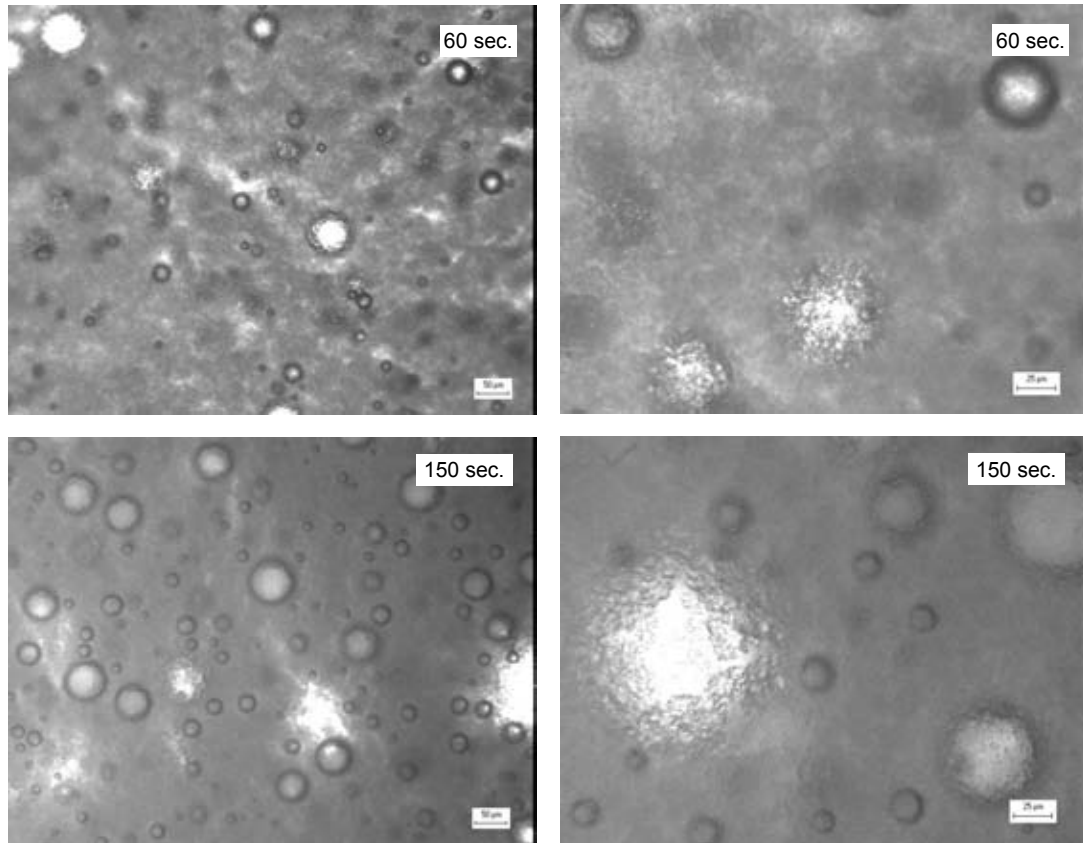


Figure 3.4 Representative micrographs of Elmlea Light whipping cream, aerated for two different lengths of time, either 60 seconds or 150 seconds. Imaged with a Polyvar and a 10× Objective, scale bar = 50 µm (left micrographs) and 25× Objective, scale bar = 25 µm (right micrographs). The higher magnification image is from the same field of view as the one from low magnification.

Figure 3.4 shows representative micrographs of whipped Elmlea Light cream with two magnified micrographs which show the characteristic partially coalesced fat at the air interface.

3.2.3 Bubble Sizing in Elmlea Light

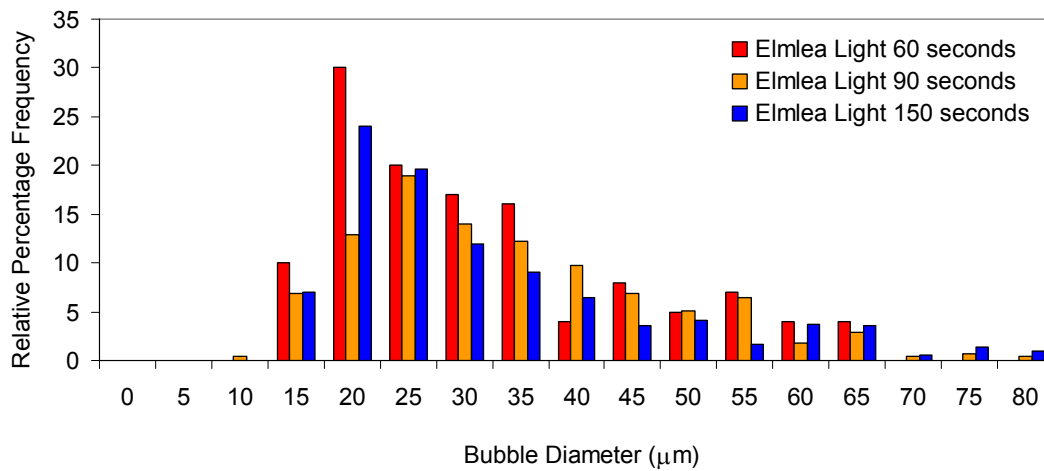


Figure 3.5 Bubble sizing of the Elmlea light whipping cream which had been aerated for different time periods and imaged with a 10× objective.

The data in Figure 3.5 was gathered to test Jakubczyk and Niranjana's (2006) theory of bubble size evolution during whipping; which predicts that the bubble diameters get smaller with an increase in aeration time. Here the average bubble sizes for the timepoints are: 30.1 μm +/- 15.1 μm S.D at the 60 second whipping time then an average bubble size of 32.1 μm +/- 14.2 μm S.D at the 90 second whipping time and the final bubble average is 31.1 μm +/- 18 μm S.D at the 150 second whipping time. Given the large Standard Deviations at each of the timepoints it is fair to conclude that the mean bubble size is constant at 30 μm. Jakubczyk and Niranjana (2006) state that bubbles get smaller with an increase in aeration time, but these datasets suggest the opposite. Although it could be said that the changes are necessarily not very marked between the three different aeration times, but work in this chapter on the whole will only look at the optimum aeration time of 150 seconds with the commercial whipped creams. The work was performed to understand bubble

evolution throughout the whipping process, up to the time of sampling.

3.2.4 Bubble sizing with the three commercial creams

Despite the “crudity” of the preparation of the samples for imaging and bubble sizing and the lack of reproducibility in the preparation of the slides (in the quantity of cream applied, the thickness of sample etc.), the results nevertheless seem robust. In each of the three creams in Figure 3.6 the highest percentage of bubbles fall in the 20 and 25 μm range.

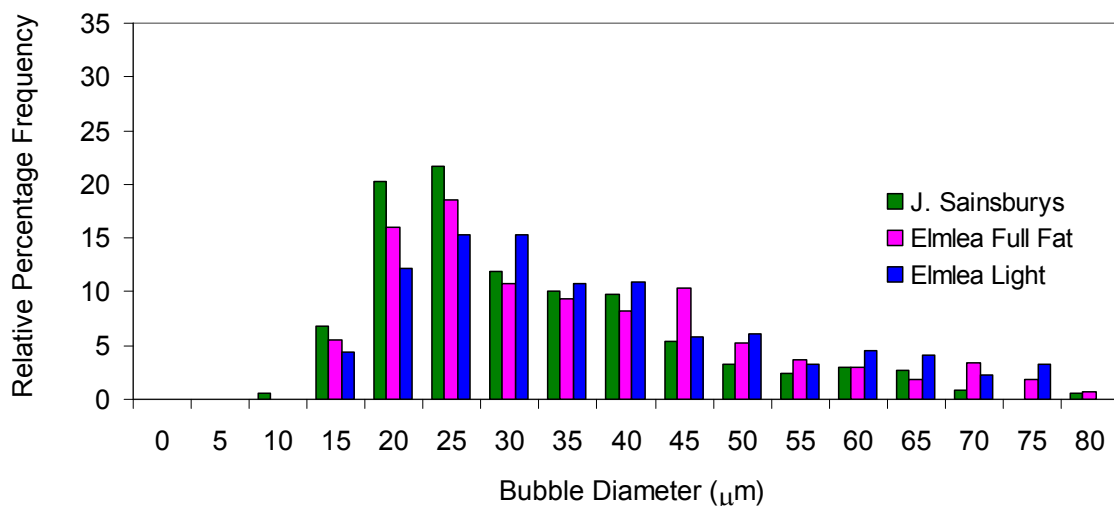


Figure 3.6 Bubble sizing of the three commercial samples which had been aerated for 150 seconds and imaged with a 10 \times objective.

3.2.5 Fat particle sizing with a Mastersizer

Particle sizes in the three commercial creams that were used were compared using a Mastersizer. Both Elmlea Light and Elmlea Full Fat show a bimodal particle size distribution around 10 μm . It is only the J. Sainsbury’s cream that shows a smaller but monomodal particle size distribution around 4 μm . The reason for a bimodal distribution is possibly due to the liquid oil content of both Elmlea formulations.

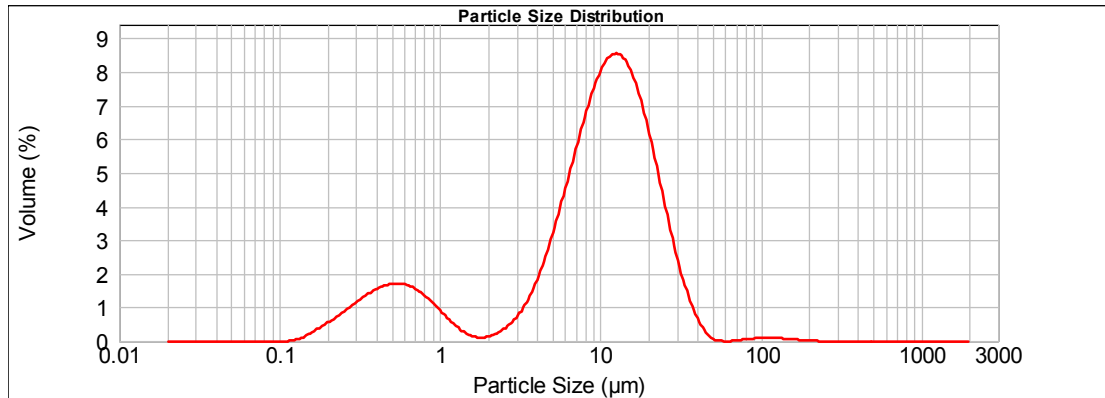


Figure 3.7 Elmlea Light Emulsion particle analysis

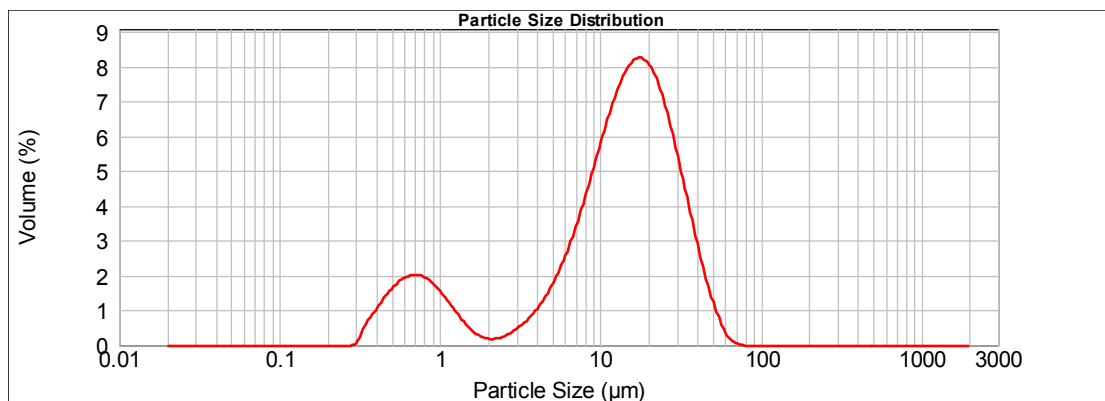


Figure 3.8 Elmlea Full Fat emulsion particle analysis

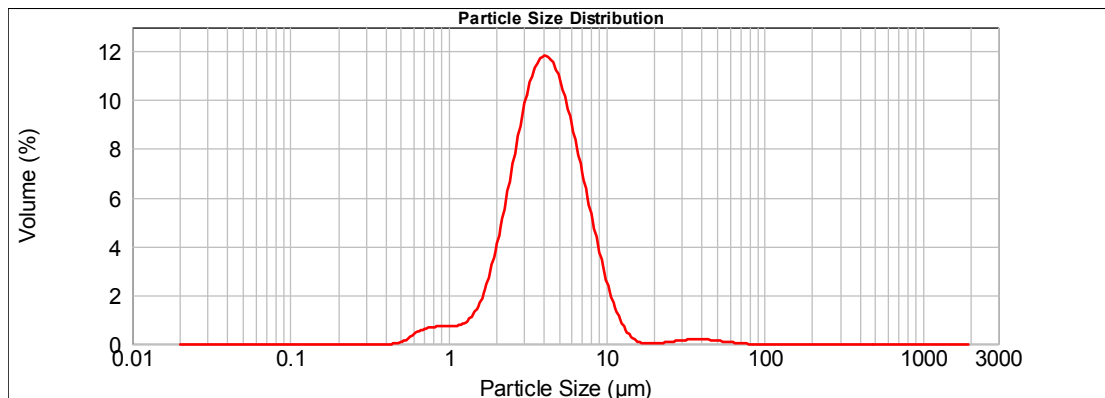


Figure 3.9 J. Sainsbury's full fat whipped cream emulsion particle analysis.

3.2.6 Bulk rheology

Results are displayed for the viscosity of the two Elmlea samples and the J. Sainsbury's cream as a function of shear stress in Figure 3.10 and Figure 3.11. Viscometry experiments using a Bohlin Rheometer (as described in section 2.9) were carried out on the commercial products at both 10 °C and 25 °C, to

test for temperature dependency of the three products.

The η_0 (low shear rate limiting viscosity) of Elmlea light is about four orders of magnitude higher at 10 °C than it is at 25 °C (temperature dependence is significant), whilst the η_0 (zero-shear) viscosity of Elmlea full fat at 10 °C is about two orders of magnitude higher than it is at 25 °C and the J. Sainsbury's cream is one order of magnitude higher at 10 °C than it is at 25 °C. This implies that all the creams are more structured at 10 °C than they are at 25 °C.

The shear dependence effect of the samples (seen in Figure 3.10 and Figure 3.11), with temperature, is as follows: Elmlea Light \ll Elmlea Full Fat \ll J. Sainsbury's cream, meaning that the effect on Elmlea Light with a change in temperature is stronger than with the J. Sainsbury's cream that sees the least effect.

Conventionally the 'yield stress' of a material can be calculated by generating a shear-rate shear-stress curve on a viscometer and subsequently extrapolating to zero shear, with the point at which the curve intercepts the stress axis taken as its yield stress. This value could be used to predict how the material would behave at low stresses. However, this is known not to be entirely satisfactory and could lead to misleading interpretations of the data. In a controlled stress rheometer (further described in section 2.9) it is possible to measure the yield stress directly and Bohlin rheometers come equipped to

perform the yield stress experiment whereby the stress is ramped from a low value and the resulting deformation is monitored. The resultant ‘instantaneous’ viscosity (η_i) is calculated and increases up until the stress at which the material starts to flow (i.e. its yield stress) (Malvern Instruments web, 2009).

The sudden change in viscosity seen with J. Sainsbury’s cream in Figure 3.10 goes some way to explain why the cream overwhips the fastest (in comparison to the Elmlea creams which take a long time to overwhip). With the J. Sainsbury’s cream only a small change in shear stress results in dramatic rupturing of the structure (analogous to overwhipping of this cream after only little added whipping). The softening of the Elmlea formulation with liquid oils and the addition of stabilisers to their mix means that they do not shear thin as strongly or dramatically as the J. Sainsbury’s cream does. The fact that Elmlea Light, shear thins more quickly at both temperatures when compared to the Full fat version, is due to the fact that Elmlea light has a higher proportion of liquid oil in the mix. Elmlea Full Fat has more than double the amount of hydrogenated vegetable oil in the mix, making it a lot thicker which the viscosity measurements show.

Shear thinning of Elmlea Light at 25 °C is two orders of magnitude lower than that for Elmlea Full Fat, which is indicative of the higher level of liquid oil contained within the Light sample.

At 10 °C the difference in the degree of shear thinning between the two

Elmlea samples is only one order of magnitude.

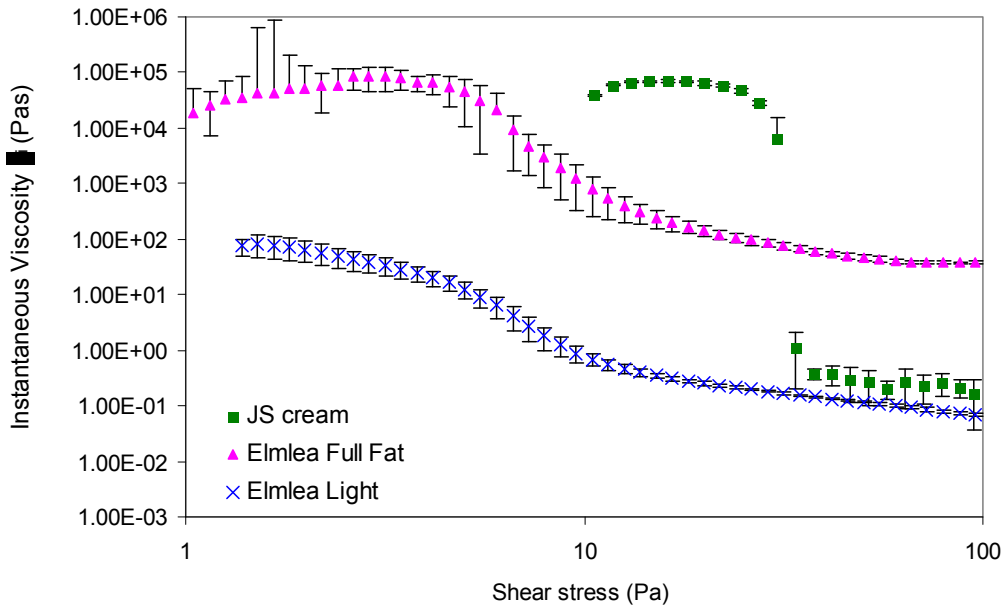


Figure 3.10 Viscometry of the three different double whipping creams performed at 25°C. Samples whipped for 150 seconds.

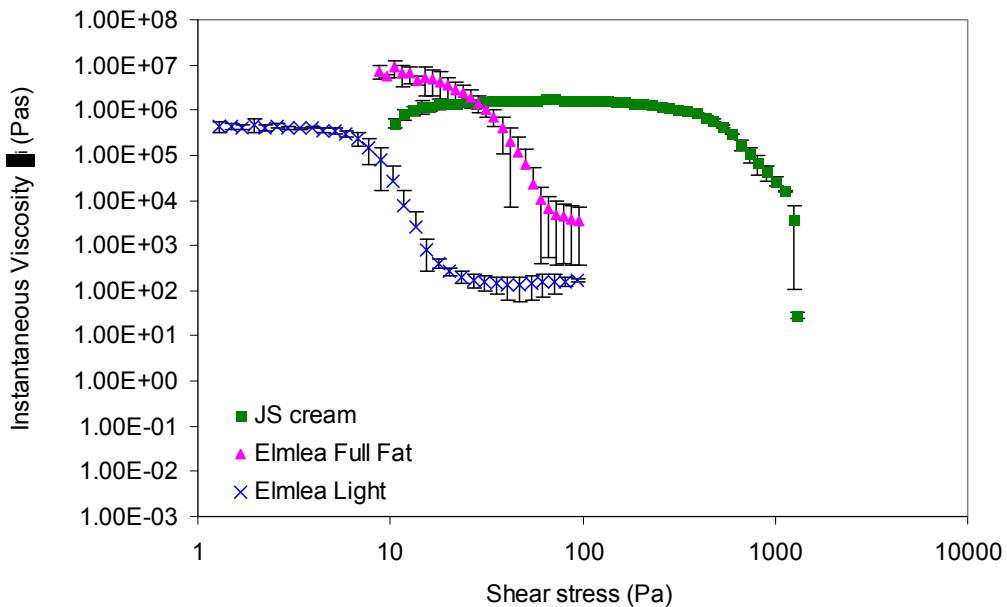


Figure 3.11 Viscometry of the three different double whipping creams performed at 10°C. Samples whipped for 150 seconds.

3.2.7 Thin Film Rheology

While setting up the tribometer, triplicate experiments were carried out purely with distilled water and separately with oil alone, to test the response to

simple systems. In Figure 3.12 the response of the machine to each of these can be seen. Oil shows very little traction throughout the speed ranges and water shows considerably more. The fact that the error bars with the water sample are large is because the silicon backing mat was used too many times. With the cream samples it was decided to change the mat after assessment of each triplicate was undertaken.

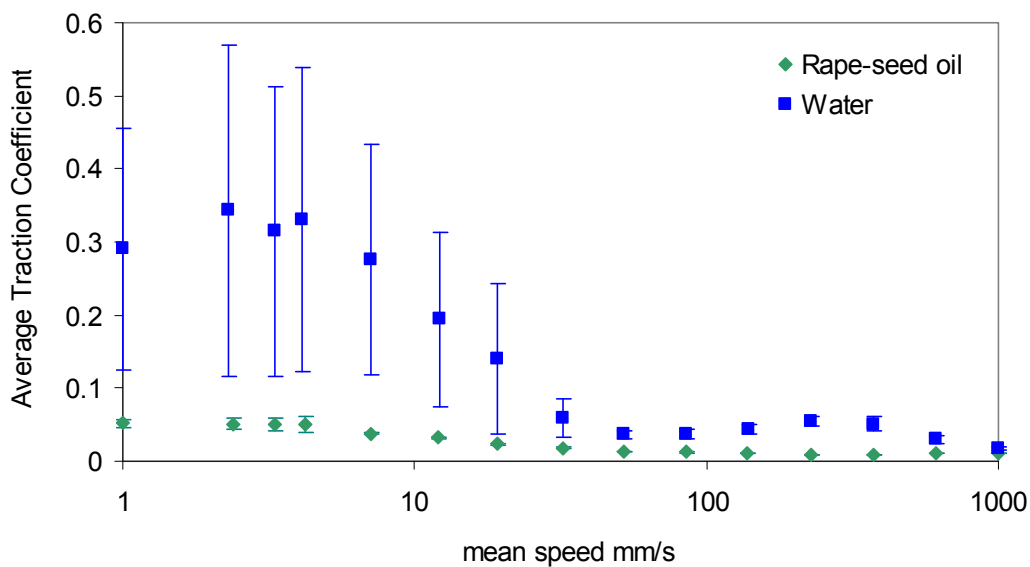


Figure 3.12 Thin Film Rheology with a comparison of Distilled water and Rapeseed Oil. Stribeck curve at 37 °C, 50% SRR, 3N Ball Load.

The tribometer results of the unaerated commercial whipping creams are shown in Figure 3.13.

In the mixed regime (from 10 mm/s to about 100 mm/s) all three creams behave differently. Only later again in the hydrodynamic regime at around 1000 mm/s do all three creams begin to show the same traction coefficient again.

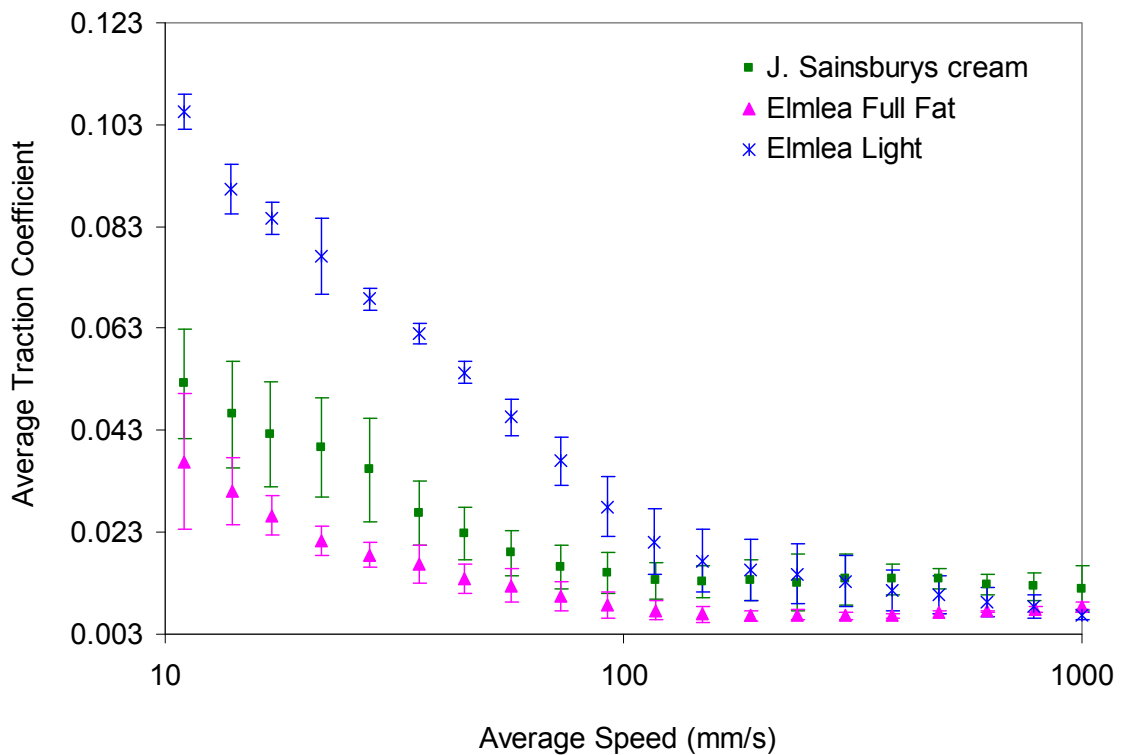


Figure 3.13 Thin Film Rheology on the unaerated commercial mixes. Stribeck curves for Ball on disc at 37°C, 50% SRR, 3 N.

Figure 3.14 shows the traction coefficients for the same three commercial samples as those evaluated for Figure 3.13, but these were aerated for 150 seconds.

Elmlea Full Fat and J. Sainsbury's cream in Figure 3.14 just after 10 mm/s show the same traction coefficient, but Elmlea Light starts with a higher traction coefficient and then after as the ball speed increases all three aerated creams begin to show the same traction coefficient in the mixed regime.

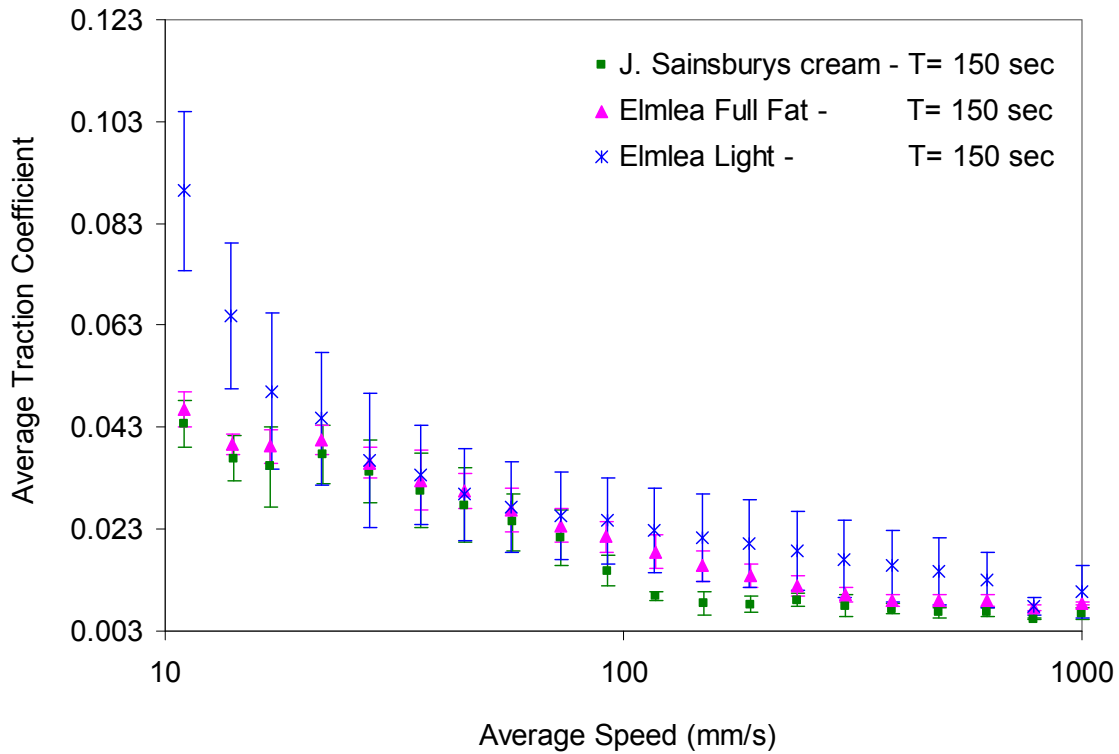


Figure 3.14 Thin Film Rheology on the aerated commercial mixes. Mixes aerated for 150 seconds. Stribeck curves for Ball on disc at 37°C, 50% SRR, 3 N

It is interesting to see in Figure 3.14 with the commercial samples that were aerated, that between the speeds just after 10 mm/s and 100 mm/s, the traction coefficients are the same for all three systems. The behaviour of the material is identical in all three cases and that the three samples are providing equal lubrication in that region. What one can conclude from this, is that through aeration, regardless of the oil levels within each of the creams, which have been discussed at length previously in this chapter, all the creams show the same behaviour. This is interesting for the fact that a “light” cream once aerated, is showing the same response as its “full fat” counterpart, but this response is achieved only through the addition of air.

It should be noted with regards to Figure 3.13 and Figure 3.14 that the

differences between an unaerated and an aerated sample appear not to be as large as expected, as the sample gets overheated to between 40 °C and 44 °C before the measurements start and the machine begins to record. The temperature control is poor, leading to a degree of de-aeration and melting before the measurement was taken. With better temperature control through the addition of a cooling-bath and maybe soft-soft contact the differences observed might be larger. Taking measurements at 1 N instead of 3 N might give a larger difference in the response that was observed as a lighter ball load at 1 N might have a more protective effect on the cream structure.

Differences like those observed between the aerated and unaerated samples evaluated with the tribometer in this section, are also seen later on in the chapter when evaluating the reformulated emulsions in section 3.3.3.

3.2.8 Oscillatory rheology with aerated samples at 10 °C

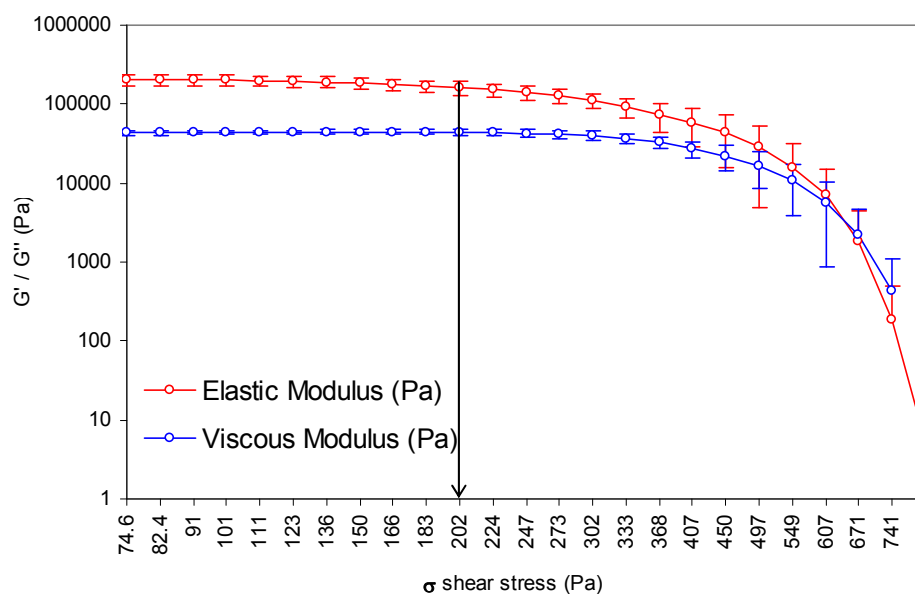


Figure 3.15: Elmlea Full Fat oscillatory rheology taken at 10 °C after 150 seconds whipping time

In Figure 3.15 with the Full Fat Elmlea, $G' > G''$ and so the material exhibits a slightly more elastic than viscous response. The Linear Viscoelastic Region, reaches up to 200 Pa. If in comparison one were to compare the graph for Elmlea Light (in Figure 3.16), there G' still remains larger than G'' , by nearly the same magnitudes, but this sample is only linear up to 50 Pa and therefore one can conclude that the light formulation is not as structured as its full fat counterpart.

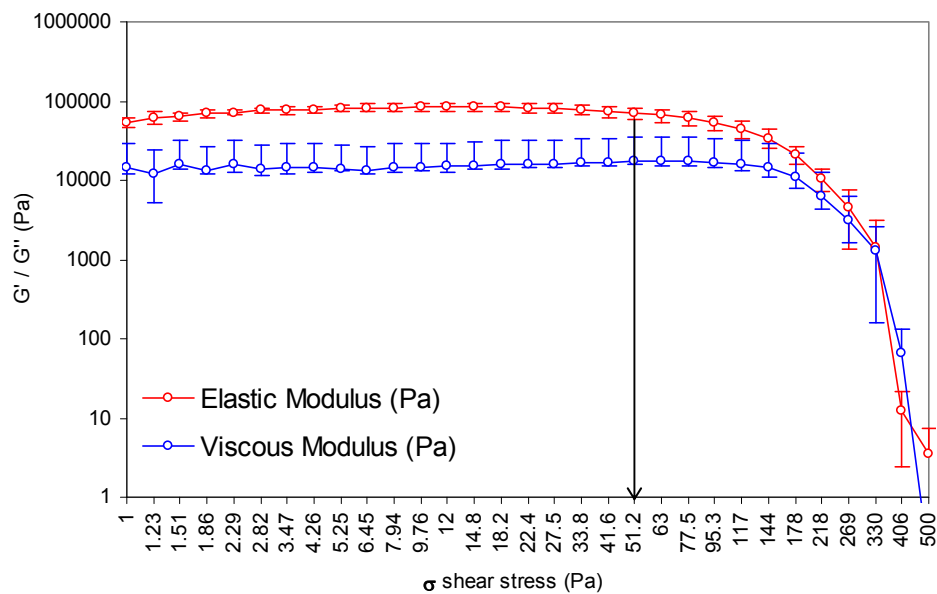


Figure 3.16: Elmlea Light oscillatory rheology taken at 10 °C after 150 seconds whipping time

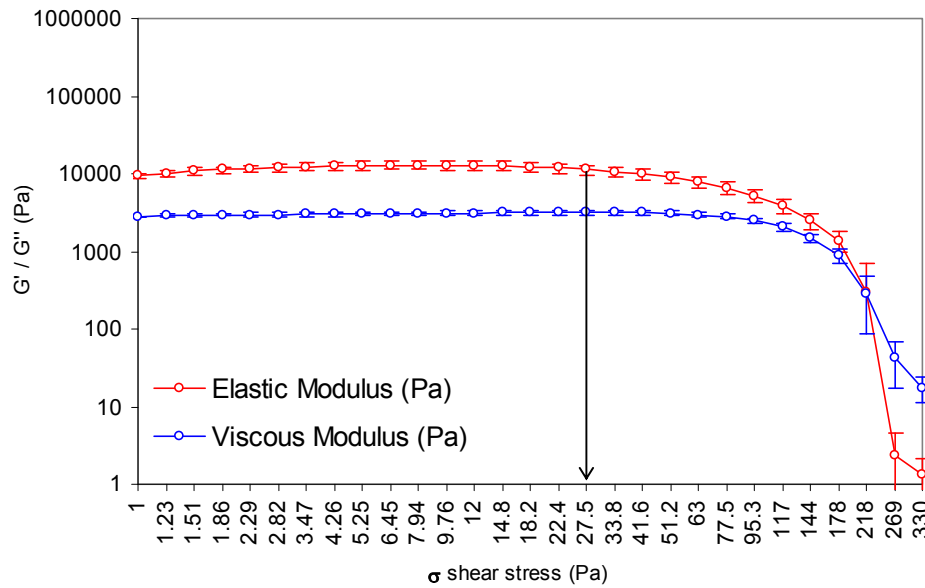


Figure 3.17: J. Sainsbury's whipping cream oscillatory rheology taken at 10 °C after 150 seconds whipping time.

Comparing now the J. Sainsbury's cream in Figure 3.17 with the Elmlea samples, here too G' remains larger than G'' , but now the linear viscoelastic region extends up to 27 Pa only. This again suggests less structure in this cream than that in the two Elmlea samples.

There is less structure in the J. Sainsbury's cream as it is solely relying on the partially coalesced fat phase to lend it the 'body' required. The Elmlea creams are also reliant on the partially coalesced fat but they also both contain stabilisers for added structure. The difference in total fat content between J. Sainsbury's cream and Elmlea Light is nearly double (with Elmlea Light containing 24.3% and J. Sainsbury's 47.5%), so in Elmlea's case the structure cannot purely be derived from the fat phase alone.

Another comparison that can be made between the samples is the crossover point of G' and G'' . Which for Elmlea Full Fat is just after 600 Pa, for Elmlea

Light it is 330 Pa and for the J. Sainsbury's cream it is 218 Pa.

3.2.9 Oscillatory rheology with aerated samples at 25 °C

In the following experiments oscillatory rheology at 25 °C was undertaken.

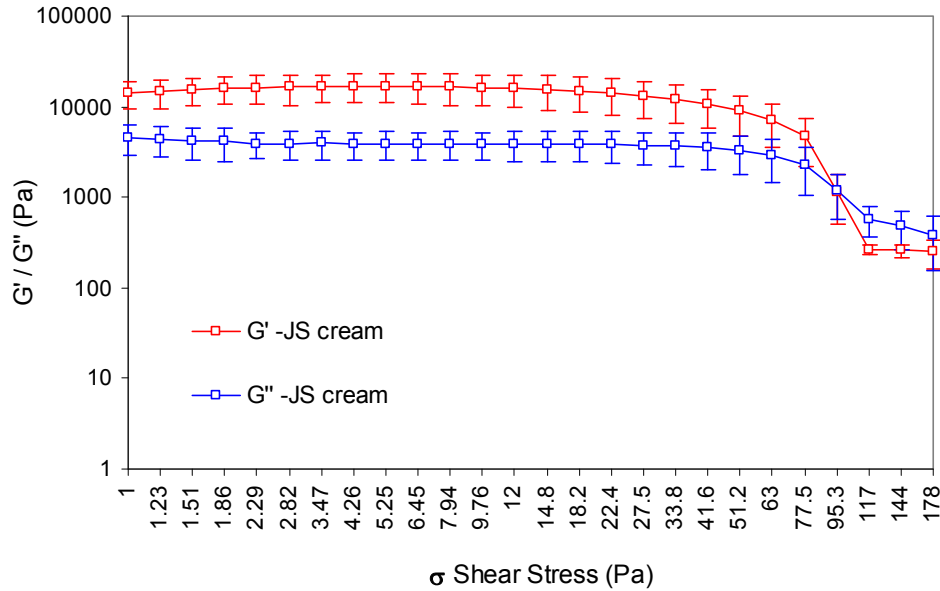


Figure 3.18: Oscillation rheology on triplicate measurements on aerated J. Sainsbury's cream at 25°C. Sample aerated for 150 seconds. Bohlin Rheometer, parallel plate geometry and a 2000 μm gap size.

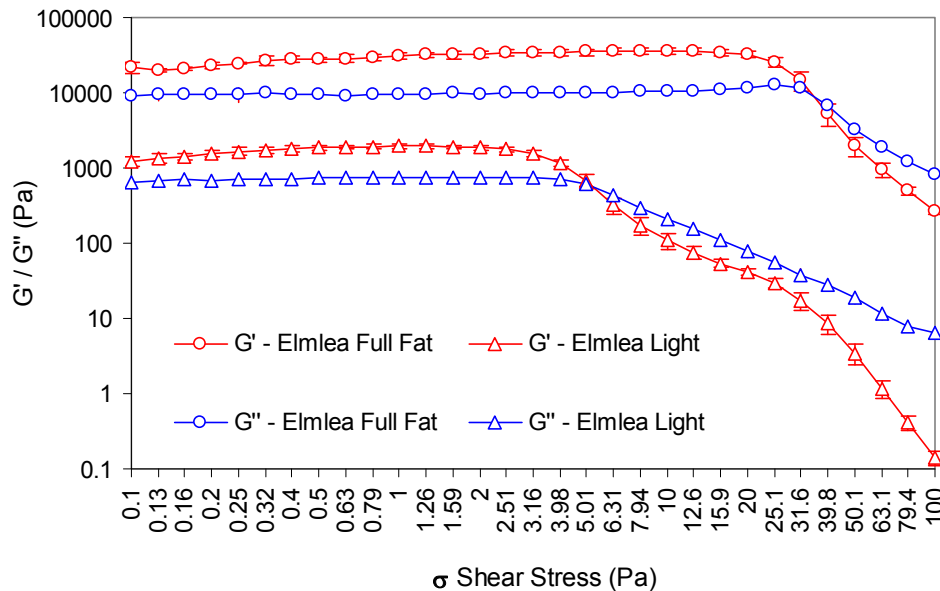


Figure 3.19: Oscillation rheology on triplicate measurements on aerated Elmlea creams at 25 °C. Sample aerated for 150 seconds. Bohlin Rheometer, parallel plate geometry and a 2000 μm gap size.

By plotting the Elmlea Full fat and the Elmlea Light oscillatory traces

on the same graph, it can be seen how very different the creams' structures are. For all three samples G' remains larger than G'' . The crossover points are indicative of the loss of structure that each of the creams undergoes at the respective shear stress. The crossover point for Elmlea light takes place at a shear stress of 5 Pa and the one for Elmlea full fat takes place between a shear stress of 31 and 40 Pa.

In contrast to the two Elmlea creams, the traces for J. Sainsbury's dairy cream crosses over at the much higher shear stress of 95 Pa.

For Full Fat and J. Sainsbury's cream G' is of similar order of magnitude, but for Elmlea Light G' is an order of magnitude less, suggesting the light version is less structured compared to the other two.

The crossover points for all three creams with the measurements at 25 °C are much lower than those that were taken at 10 °C. This suggests that the creams are less structured at 25 °C than they are at 10 °C.

3.2.10 Analysis of fat content by Differential Scanning Calorimetry

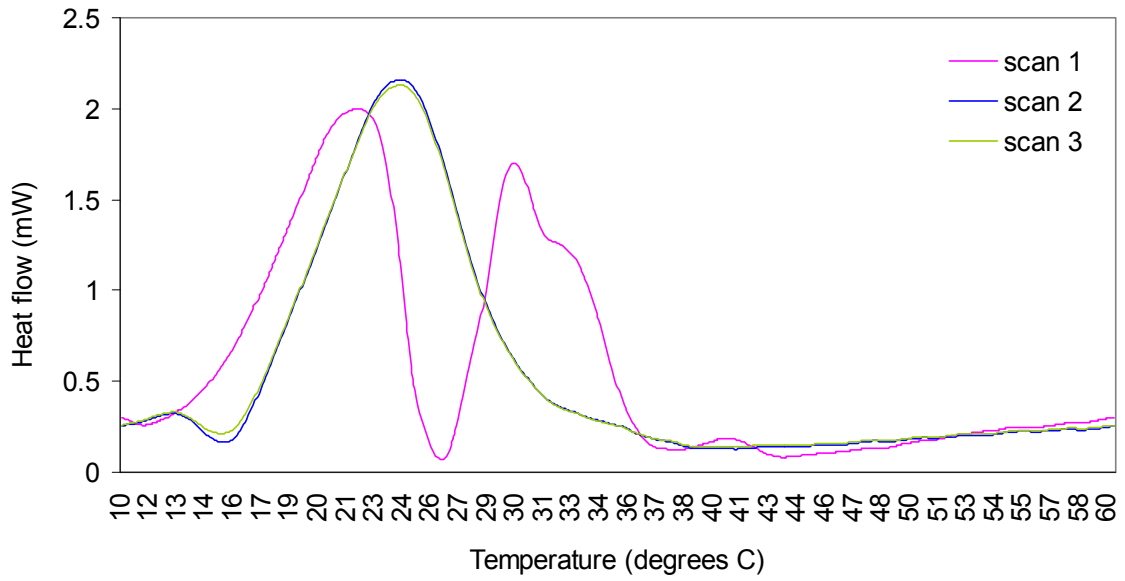


Figure 3.20: DSC measurement of Elmlea light cream at a sampling rate of 5 °C per minute. Traces include baseline subtraction.

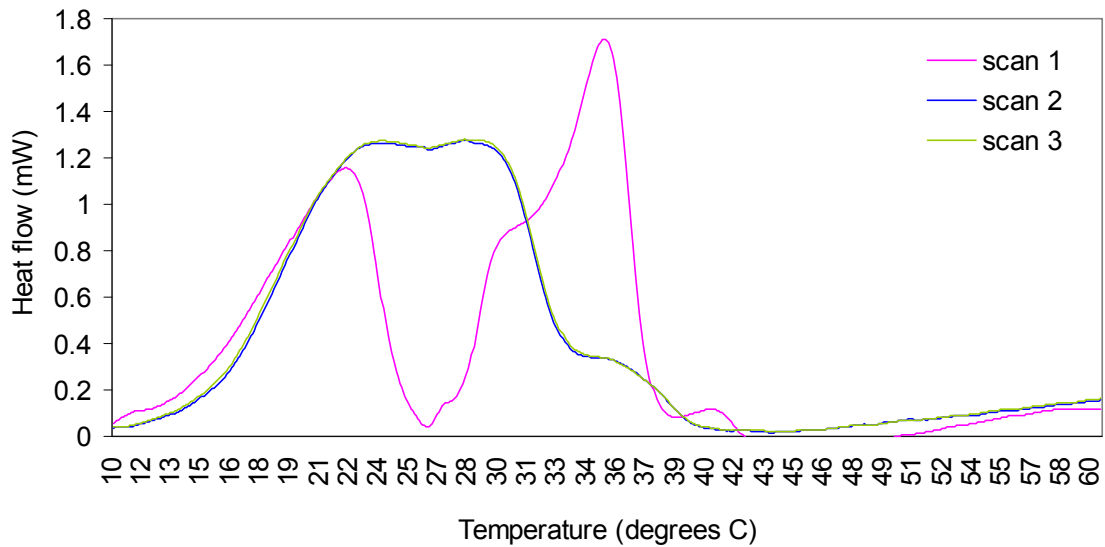


Figure 3.21: DSC measurement of Elmlea full fat cream at a sampling rate of 5 °C per minute. Traces include baseline subtraction.

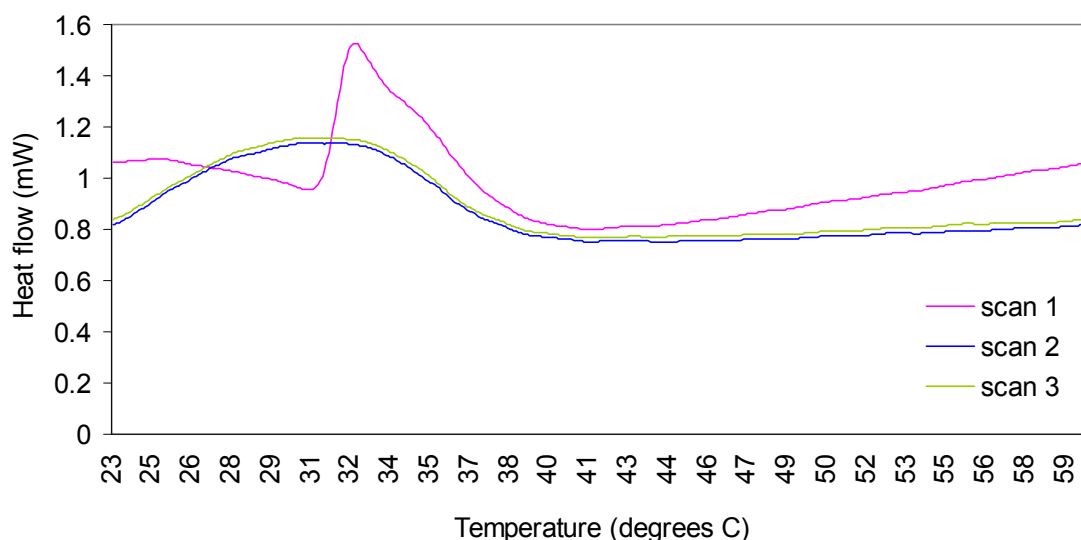


Figure 3.22: DSC measurement of J. Sainsbury's cream at a sampling rate of 5 °C per minute. Traces include baseline subtraction.

The commercial whipping creams were subjected to DSC analysis in order to understand the composition of the fat phase in the three different whipping creams. Figure 3.20 through to Figure 3.22 are the DSC traces of the 3 creams.

The 2 prominent peaks that appear in the Elmlea traces (Figure 3.20 and Figure 3.21), are almost certainly due to the tempering step that is added to the Elmlea formulation in order for it to be whippable within 4 minutes. The patent authors state that they found a new process which made unwhippable low-fat Non-dairy-creams (NDC's) whippable within a 4 minute time-frame. The process includes a tempering step at the end of the normal NDC manufacturing process. The NDC manufacturing process comprises the making of the emulsion of a water phase, containing thickener and optionally a butter milk component and a fat phase, containing fat and the emulsifier system. The resultant emulsion is further processed by heating, sterilisation, homogenisation and cooling to a temperature below 15 °C. The subsequent process contains the

tempering step which is carried out after the cooling period. It is performed by warming the emulsion to ambient temperature between 20 °C to 25 °C and it is kept at this temperature for several hours, after which it is then cooled to below 15 °C. The NDC after homogenisation is usually cooled to below 15 °C and preferably below 10 °C. For the tempering step, the emulsion is normally warmed to a temperature of 15 °C to 25 °C and is held at this temperature for 18 to 30 hours (Morrison et al., 1992). It is exactly between these two temperatures of the tempering step that the first peak appears for both formulations of Elmlea (the Light and Full Fat version), where it can be seen that the fat in the formulations melt.

Table 3.1 Peak analysis of the thermal behaviour of the commercial creams within the DSC

| Analysis to Figure 3.20 Elmlea Light | | | | |
|--|--------|------------|------------|----------|
| | | | Peak onset | Peak end |
| scan 1: | peak 1 | 2.64 J/min | 10 °C | 26.5 °C |
| | peak 2 | 1.93 J/min | 26.5 °C | 37 °C |
| scan 2 | | 3.73 J/min | 16 °C | 38 °C |
| scan 3 | | 3.73 J/min | 16 °C | 38 °C |
| Analysis to Figure 3.21 Elmlea Full Fat | | | | |
| | | | Peak onset | Peak end |
| scan 1: | peak 1 | 1.61 J/min | 10 °C | 26 °C |
| | peak 2 | 2.21 J/min | 26 °C | 39 °C |
| scan 2 | | 4.02 J/min | 10 °C | 40 °C |
| scan 3 | | 4.02 J/min | 10 °C | 40 °C |
| Analysis to Figure 3.22 J. Sainsbury's cream | | | | |
| | | | Peak onset | Peak end |
| scan 1: | peak 1 | 0.49 J/min | 31 °C | 41 °C |
| scan 2 | | 0.69 J/min | 23 °C | 38 °C |
| scan 3 | | 0.69 J/min | 23 °C | 38 °C |

Table 3.1 is a summary of the Peak Analysis. The DSC graphs were analysed and it can be seen that in the first scan within the Elmlea creams, two peaks predominate (which are present due to the tempering step), and by the second and third scan both peaks have fused together, due to the heating and cooling of the sample.

3.2.11 Slumping behaviour of the whipped creams

The slumping behaviour of all the commercial creams investigated in this section will be scrutinised at four different temperatures. This was done in order to understand the stability of the creams at the different temperatures and also to understand if the melting behaviour is formulation dependent. After the results have been tabulated with representative photos of the behaviour, they are then discussed at the end of this section.

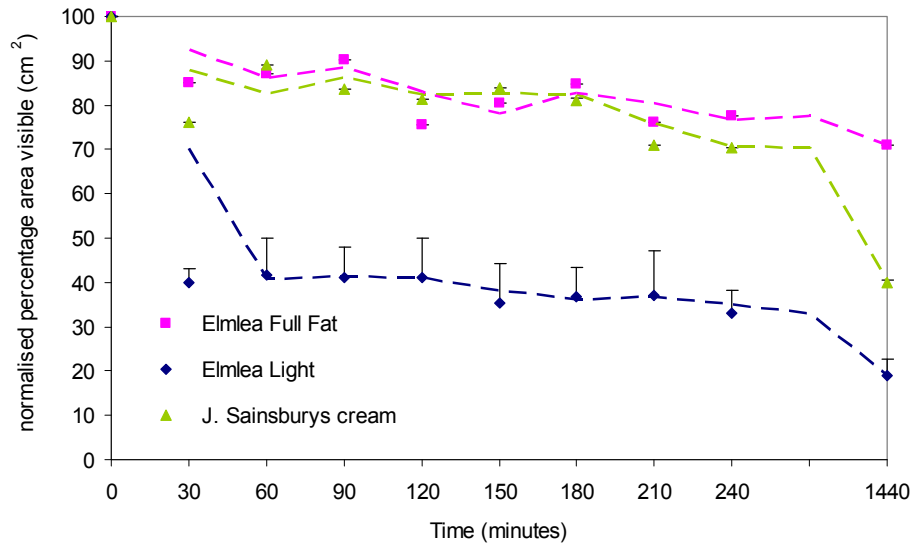


Figure 3.23: Loss of visible area of samples relaxing under gravity at 25 °C. The trendline is a moving average.

Table 3.2: Representative photos of cream samples relaxing under gravity at 25 °C.

| | 0 hours | 1 hour | 4 hours |
|-------------------------------------|---|--|---|
| <i>Elmlea Full Fat</i> 25°C |  |  |  |
| <i>Elmlea Light</i> 25°C |  |  |  |
| <i>J. Sainsbury's cream</i> 25°C |  |  |  |

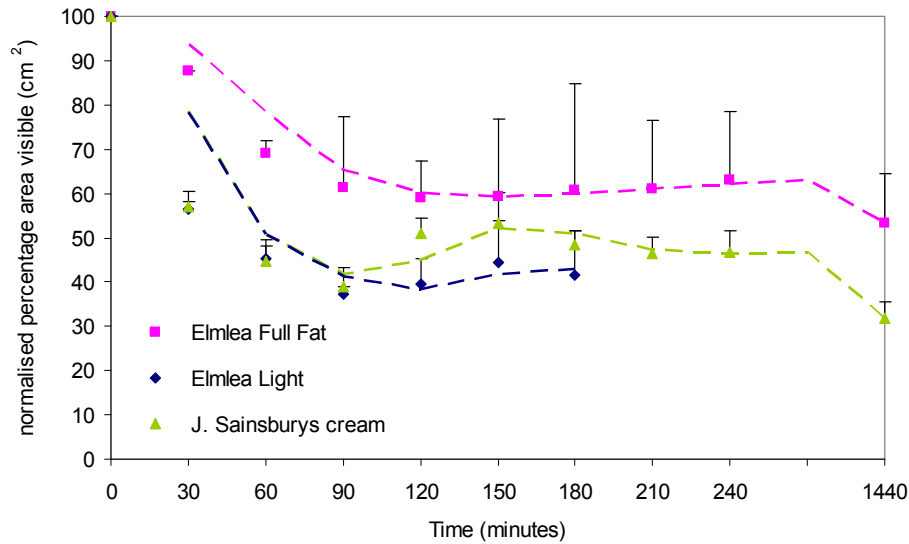


Figure 3.24: Loss of visible area of samples relaxing under gravity at 30 °C. The trendline is a moving average.

Table 3.3: Representative photos of cream samples relaxing under gravity at 30 °C.

| | 0 hours | 1 hour | 4 hours |
|-------------------------------------|---|--|---|
| <i>Elmlea Full Fat</i> 30°C |  |  |  |
| <i>Elmlea Light</i> 30°C |  |  |  |
| <i>J. Sainsbury's cream</i> 30°C |  |  |  |

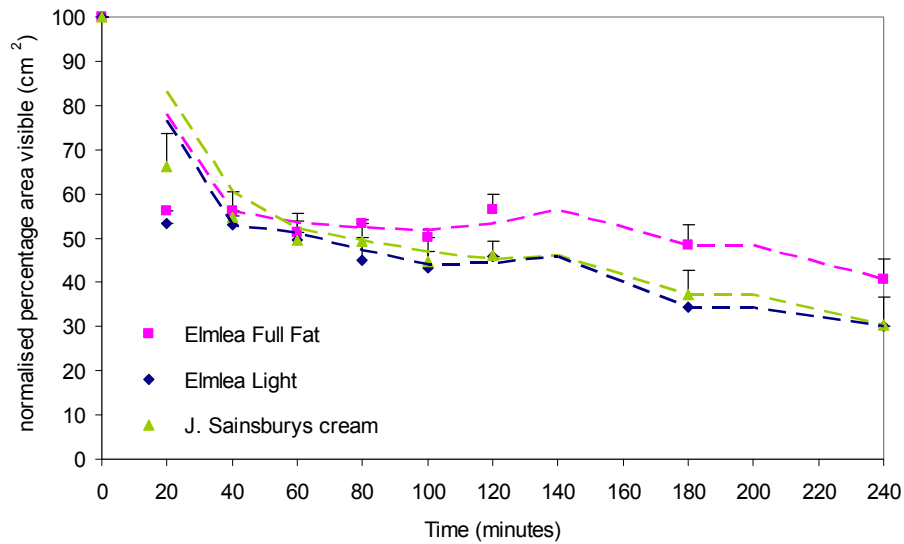


Figure 3.25: Loss of visible area of samples relaxing under gravity at 35 °C. The trendline is a moving average.

Table 3.4: Representative photos of cream samples relaxing under gravity at 35 °C.

| | 0 minutes | 20 minutes | 2 hours |
|-------------------------------------|-----------|------------|---------|
| <i>Elmlea Full Fat</i> 35°C | | | |
| <i>Elmlea Light</i> 35°C | | | |
| <i>J. Sainsbury's cream</i> 35°C | | | |

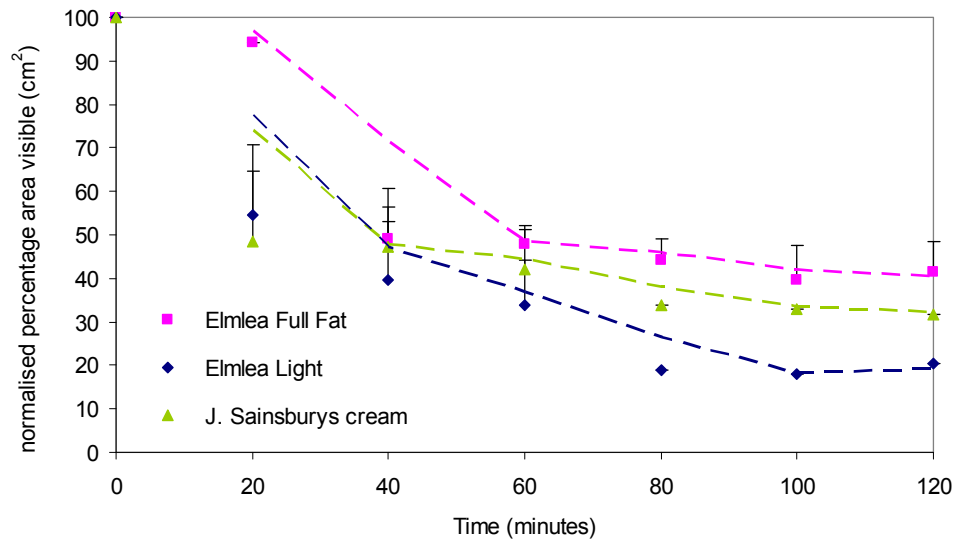


Figure 3.26 Loss of visible area of samples relaxing under gravity at 40 °C. The trendline is a moving average

Table 3.5: Representative photos of cream samples relaxing under gravity at 40 °C.

| | 0 minutes | 20 minutes | 2 hours |
|-------------------------------------|---|--|---|
| <i>Elmlea Full Fat</i> 40°C |  |  |  |
| <i>Elmlea Light</i> 40°C |  |  |  |
| <i>J. Sainsbury's cream</i> 40°C |  |  |  |

3.2.12 Micrographs of commercial samples

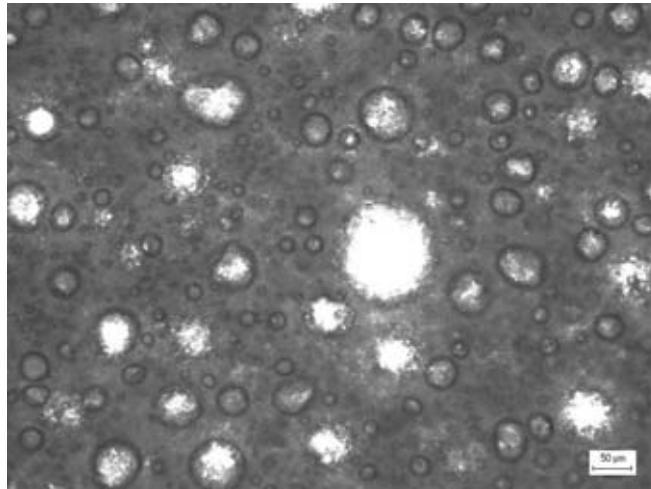


Figure 3.27 Full Fat Elmlea sample aerated for 150 seconds and imaged with a 10× Objective.

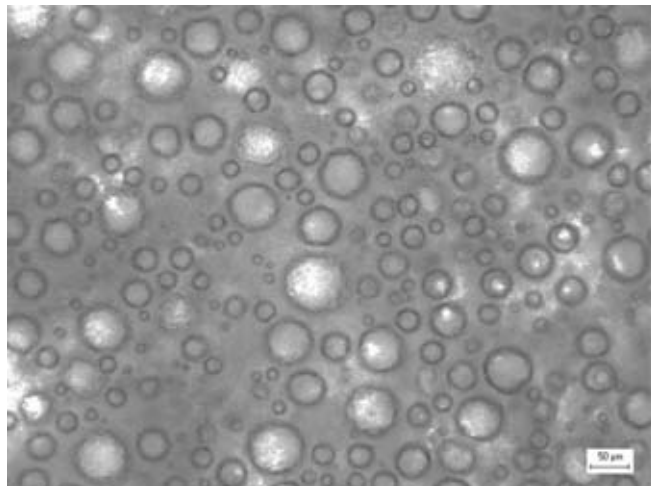


Figure 3.28 Elmlea Light sample aerated for 150 seconds and imaged with a 10× Objective.

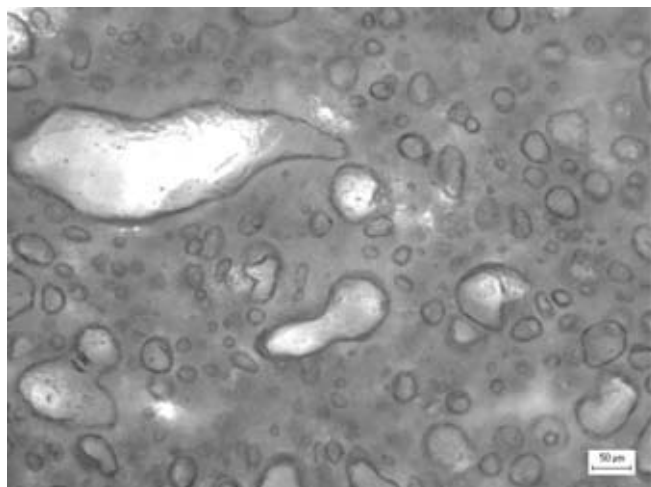


Figure 3.29 J. Sainsbury's cream sample aerated for 150 seconds and imaged with a 10× Objective.

Structures similar to the three micrographs in Figure 3.27 to Figure 3.29, were contained in the whipped creams that were subjected to the slumping process at the four different temperatures for the chosen experiments. They all had the same aeration times. The micrographs show the difference in bubble structure between the J. Sainsbury and the Elmlea creams.

In the slumping experiments, at 25 °C both the J. Sainsbury's cream and the Elmlea Full Fat sample did not slump at all throughout the experiment. This may have been in part due to the sample leaning somewhat on the ruler, but the sample was nevertheless still able to stand up. The data is not presented here, but other experiments have seen the same observation where the cream lent against the ruler, but nevertheless still slumped away into the tray. So, for the case above, it is safe to conclude that the results are due to sample stiffness and the ability to stand up. The Elmlea Light sample at 25 °C slumped completely after 30 minutes.

At 30 °C all three samples completely slumped away after a period of 40 minutes, with a little further settling in the 20 minute observational slots after this.

When the creams are observed at 35 °C, both Elmlea Full Fat and Elmlea Light slumped after 20 minutes. At this stage the J. Sainsbury's cream had not yet completely slumped, but by the 40 minute time-point the dairy cream had

reached the same level of slumping as that experienced by the other two creams.

At a slumping temperature of 40°C both the J. Sainsbury's dairy cream and Elmlea Light have slumped after 20 minutes, leaving only the Elmlea Full Fat which also slumps but only after 40 minutes have elapsed.

Except for 25 °C it could otherwise be seen that regardless of the temperature J. Sainsbury's cream slumped consistently after 40 minutes.

Within the slumping experiments the first temperature that was trialled was 25 °C, with later experiments in 5 °C increments to 30 °C, 35 °C and with a maximum slumping temperature of 40 °C. Future work might test for slumping below the tempering temperature of 20 °C and chart the creams' behaviour in this regime. It might be technically somewhat more challenging (due to the added care required in the handling and imaging) than was the case with the experiments undertaken for this work, but possibly quite interesting to see the difference in behaviour. Handling at lower temperatures would be challenging as condensation on the camera lens would need to be eliminated and adequate sample cooling would also need to be guaranteed. Technically, the work would not be a trivial exercise.

The above work with the Elmlea and the dairy cream was work towards building a mechanistic understanding of optimum whipping conditions, cream behaviour, microstructural composition, melting, bubble sizing, thin film and bulk rheological properties. These attributes were studied based on the Elmlea formulation and in addition using a dairy whipping cream for comparison purposes. The work and knowledge-base then helped towards creating emulsions with a varying oil ratio of hard palm oil to liquid rape-seed oil. The total oil concentration was kept constant at 34%. The results obtained will be discussed in the following pages.

3.2.13 Closing remarks

Due to the fact that Elmlea Full Fat and Elmlea light both have different fat ratios, different buttermilk levels, and that in the case of the Elmlea light it has the addition of 1 more stabiliser, it is difficult to conclude which reaction within the whipping dynamics is just purely due to the fat level alone. It is therefore suggested that a cream be reformulated with a continuous phase that has the same level of ingredients each time, but in which just the ratio of the hard to liquid oil varies.

The viscosity of a sample is perhaps the most important parameter as it will have a bearing on its tribology and hence on its mouthfeel too. Viscosity will also dictate to some extent how fast the sample will slump in given conditions. The importance of the slumping experiments becomes all too clear when the creams are whipped and are being prepared for serving. It would be unacceptable to have a cream that slumped straight after whipping and the

importance of temperature on the slumping behaviour becomes apparent in the hotter summer months too. In addition to its interest at UK latitudes, it might also have an effect and be of importance if it is to be used in hotter climates abroad.

At 25 °C, 30 °C and 40 °C Elmlea Full Fat showed the best stand-up behaviour and was the cream that slumped the slowest. In terms of slumping behaviour Elmlea Full Fat is clearly the most robust of the three commercial cream samples analysed.

3.3 *Analysis of reformulated whipping cream with a vegetable oil base. Elmlea patent.*

3.3.1 Overrun Assessment of six reformulated creams

Six different emulsions were created by varying the hard (palm oil) to liquid (rape seed) oil ratios. These mixes were then subsequently aerated and their behavioural response charted as overrun against time. For a complete description of the formulation and preparation method, refer to Chapter 2, Part I.

Whipping of the re-formulated systems can be divided into four distinct regions (see Figure 3.30 and Table 3.6). These four regions are formed during whipping if one excludes the initial phase before the cream gets properly whipped which is during the first few minutes. The behaviour of the cream has been arbitrarily split up into convenient phases to allow these to be discussed. The tie-lines were chosen according to the cream's prevalent Overrun behaviour. The respective whipping behaviour can then be described around these tie-lines. The description of the observations is anecdotal evidence of what happened during the whipping process. In addition some interpretation is made as to what might be taking place microstructurally within the cream. Later on in the chapter (see Section 3.4) the microstructural interpretation is confirmed with the SEM micrographs gathered.

Phase I can then be characterised by the vegetable oil emulsion forming

microstructures similar to those of whipped cream. This is due to the partially coalesced fat phase within the system, which then reaches a maximum at the maximum Overrun. The fat phase can only sustain bubble entrapment as long as the partially coalesced fat is still present on the bubble interface. Once this is removed from the interface through further whipping, the system moves into a second phase, termed phase II and which coincides with the over-whipping stage. Mixes 1 and 2 show very little evidence of overwhipping. Their bulk microstructure shows very little 'grainy-ness' unlike that exhibited by Mixes 3 to 6, which are substantially grainy in Phase II. Mixes 1 and 2 could be said to go straight back into a similar behaviour which is prevalent in Phase III. In the initial phase, regardless of cream formulation, all six of the mixes aerate at the same rate and have similar slopes, the reaction of the different formulations at this stage varied only by the maximum overrun that each of them was able to sustain; those with less hard oil having a higher final overrun (Mix 1) than those with more hard oil in their formulation (Mix 6).

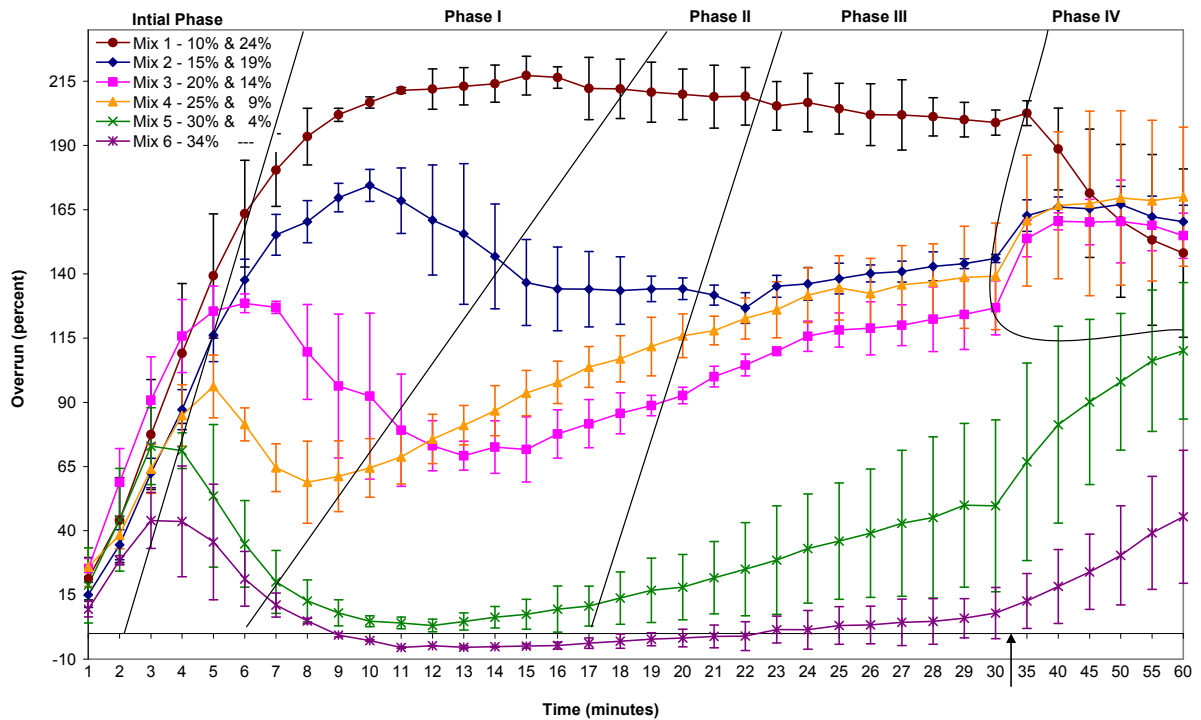


Figure 3.30: Overrun characterisation of six different mix emulsions with varying hard palm oil and liquid rape-seed oil concentration. Always making up a 34% total oil phase, e.g. Mix1 – 10% and 24%, is 10% hard oil and 24% liquid oil. The mix overrun was measured every minute, for 30 minutes and then every 5 minutes, to make one hour aeration. The arrow demarcates the skip from 1 minute to 5 minute aeration. Results of Mix 1 to 4 are triplicates and Mix 5 and 6 are duplicates.

The structures which are formed during Phase I (in contrast to those later formed in Phase IV) seemingly create more fragile creams, these are much whiter and resemble whipped cream much more. Those in Phase IV seem to have a much more oily appearance. These visual observations have been gathered empirically and experimental tests might later suggest a different behaviour.

The structures present in Phase II, which is dependent on which of the mixes is being aerated, varies in appearance from something coarse grained, to a mix containing structures with completely flocculated particles. Therefore the appearance of each of the resultant structures is mix dependent.

In phase III the whole of the bulk cream formulation is being sheared and re-whipped. Most of the flocculated particles have disappeared from the cream during this phase. The interfacial species within the system is still able to aerate the bulk ingredients. But it must be stressed that it cannot at this stage re-create the initial structures which were formed initially by the partially coalesced fat. The ratio of hard fat to liquid oil is influential during aeration at this stage, as it will have a bearing on how quickly the cream is able to re-whip. A cream with a high hard fat content in general took longer than one with a low content of hard fat. The first model system (Mix 1) with only 10 percent hard oil, never went through the “re-whipping” phase, and its air phase volume remained constant throughout the whipping process. Whereas the formulation with no liquid oil at all (Mix 6) and with 34 percent hard oil, during the re-whipping phase actually completely de-emulsified and even went into negative Overrun values. The presence of negative values is actually possible, since the initial starting emulsion will have consisted of a dispersion of oils and a small proportion of air introduced during the homogenisation process. This mix, mix 6 which was substantially more viscous than the other mixes, will have had perhaps more gas dispersed and entrapped within its matrix. This entrapped gas during re-whipping will have escaped and hence produced a negative Overrun value, relative to the initial mixes’ weight.

In Phase IV the cream formulations have re-whipped. An interesting point to note at this stage is that the mixes 1 to 4, all end in similar Overrun values after 1 hour of whipping. It can only be deduced that Mixes 5 and 6 may at

some point have reached these values too, but they certainly did not do this within the hour. The hard oil phase was influential in this case in not allowing them to achieve the same level of Overrun at the end, as was the case with the other creams.

That they all reach the same Overrun values is possibly due to the rate limiting ability of the emulsifiers to be interfacially active and sustain renewed bubble formation, albeit with a different mechanism of stabilisation. The bubble surface is stabilised initially through partially coalesced fat, but at this stage it is then stabilised through the proteins and emulsifiers in the mix with the air then contained in the congealed oil phase of the mix.

Table 3.6 Cream behaviour during the main stages of whipping with a description of the phenomena taking place.

| PHASE [<i>defining characteristic</i>] | DESCRIPTION |
|--|---|
| Initial phase [<i>under-whipped</i>] | Whipping and entrapment of bubbles within a partially coalesced fat phase |
| Phase I [<i>whipped</i>] | Whipping taking place with the achievement of the highest Overrun possible, for the formulation under scrutiny. Overwhipping starting to take place. |
| Phase II [<i>over-whipped / churned</i>] | Overwhipping has already occurred; the partially coalesced fat phase has been stripped from the bubble interface. The bubbles are swimming around the matrix 'naked' and in a mass of congealed hard and liquid oil. Bubble stability is being conferred by the bulk protein and emulsifier in the system. The hard oil forming part of the bubbles' structural stability. |
| Phase III [<i>re-whipping</i>] | By and by the system is being re-whipped with the interfacial species (protein / emulsifier) present and still active within the system. This is working itself around the matrix to help re-aerate the system. This is easier and faster in the system with a higher liquid oil content and less hard oil (Mixes 1 to 4). Testament to this fact are Mixes 5 & 6 which do not enter Phase IV. They may do after a long whipping time, but do not achieve this at least after 60 minutes total whipping. |
| Phase IV [<i>re-whipped</i>] | The final stage exists with a seemingly strong and stable whipped cream (which is now much more yellow and oily), very different from the starting structures. Evidence of the fact that we are dealing with a completely different cream is that the first four formulations, although with different oil ratios, all re-whip to a similar Overrun! (See: Mixes 1 to 4). Bubble size data shows little difference throughout the entire aeration process, average bubble size at the beginning is very similar to that at the end. |

The descriptions outlined in Table 3.6 are consistent with the observations made through SEM microscopy. The images collected will be discussed at length at the end of this chapter, in Section 3.4.

3.3.2 Bubble sizing and characterisation of reformulated mixes

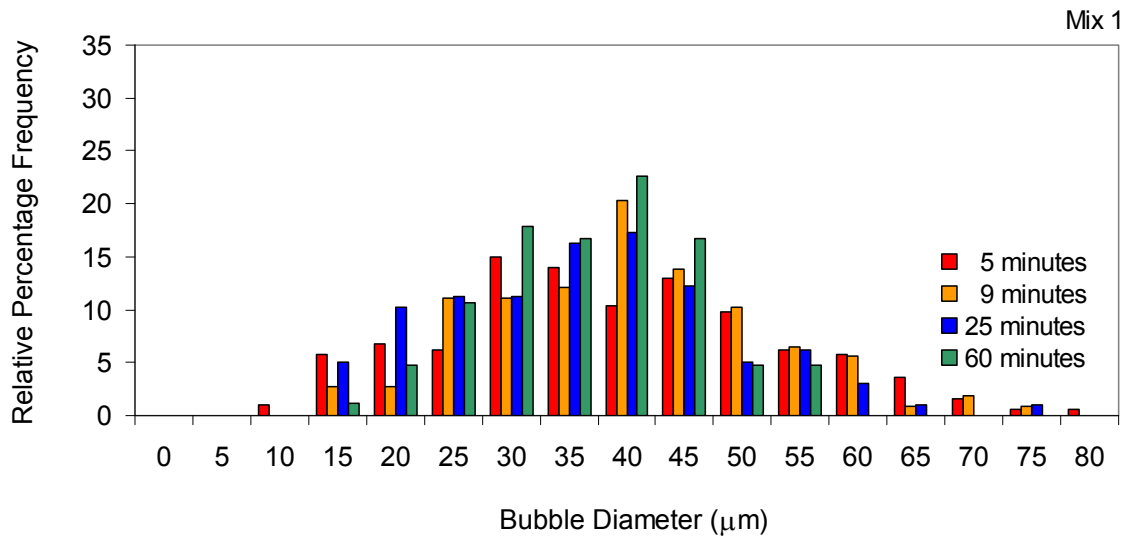


Figure 3.31: Bar graph of Mix 1 with the highest proportion of liquid oil, illustrates the normalised bubble size distribution as a function of whipping time. Hard oil and liquid oil are 10 and 24 percent respectively.

Figure 3.31 is interesting for the fact that the results are somewhat expected, as the Overrun value (as assessed in section 3.3.1) of this mix, hardly varied at all throughout the hours' aeration. The air incorporation into the mix remained static after 11 minutes, which is the time-point where the mix attains its highest Overrun value. The sampling time points for each of the micrographs (5, 9, 25 and 60 minutes) were chosen after studying the Overrun behaviour for that particular mix. In general the time points chosen were the following; usually a timepoint before maximum Overrun was achieved, a timepoint of maximum Overrun, a timepoint in the “overwhipped” regime (not applicable in the case of Mix 1), and a time in the re-whipped regime. The timepoints will hence be

mix dependent and will differ for all the mixes studied. For this reason a uniform sampling time could not have been chosen, unlike the work with the commercial samples, where 150 seconds was taken.

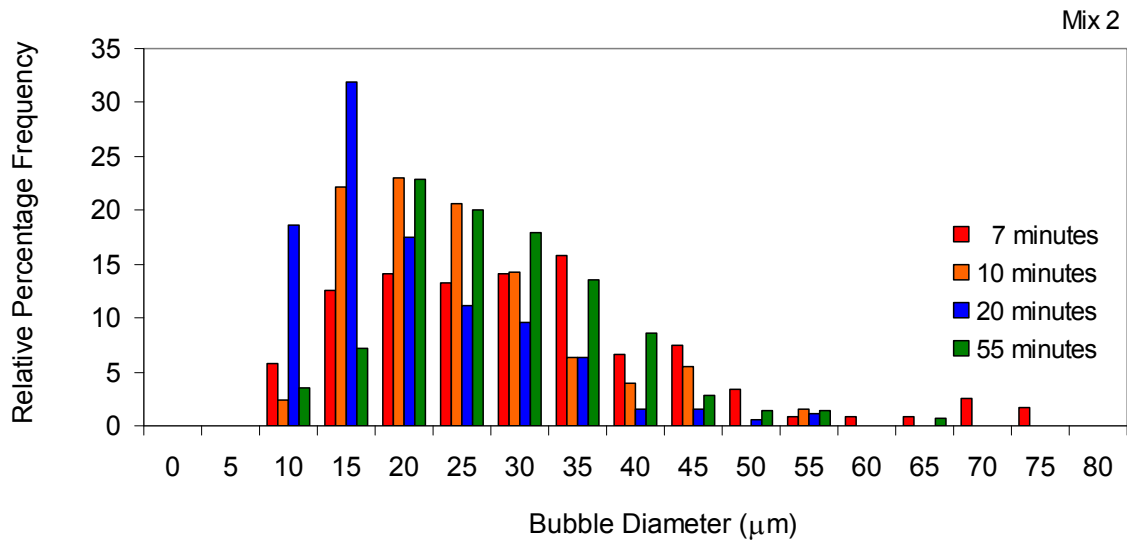


Figure 3.32: Bar graph of Mix 2 with the next highest proportion of liquid oil, illustrating the normalised bubble size distribution as a function of whipping time. Hard oil and liquid oil are 15 and 19 percent respectively.

Further bubble analysis as a function of whipping time of all the other creams is included for comparison in appendix 3. With ever increasing levels of hydrogenated oil and as the creams go getting more viscous, the proportion of bubbles of smaller and smaller size seems to get larger. Interestingly though (as it will be seen in Figure 3.39) the average bubble size will remain constant, irrespective of the mix being whipped, or the timescale.

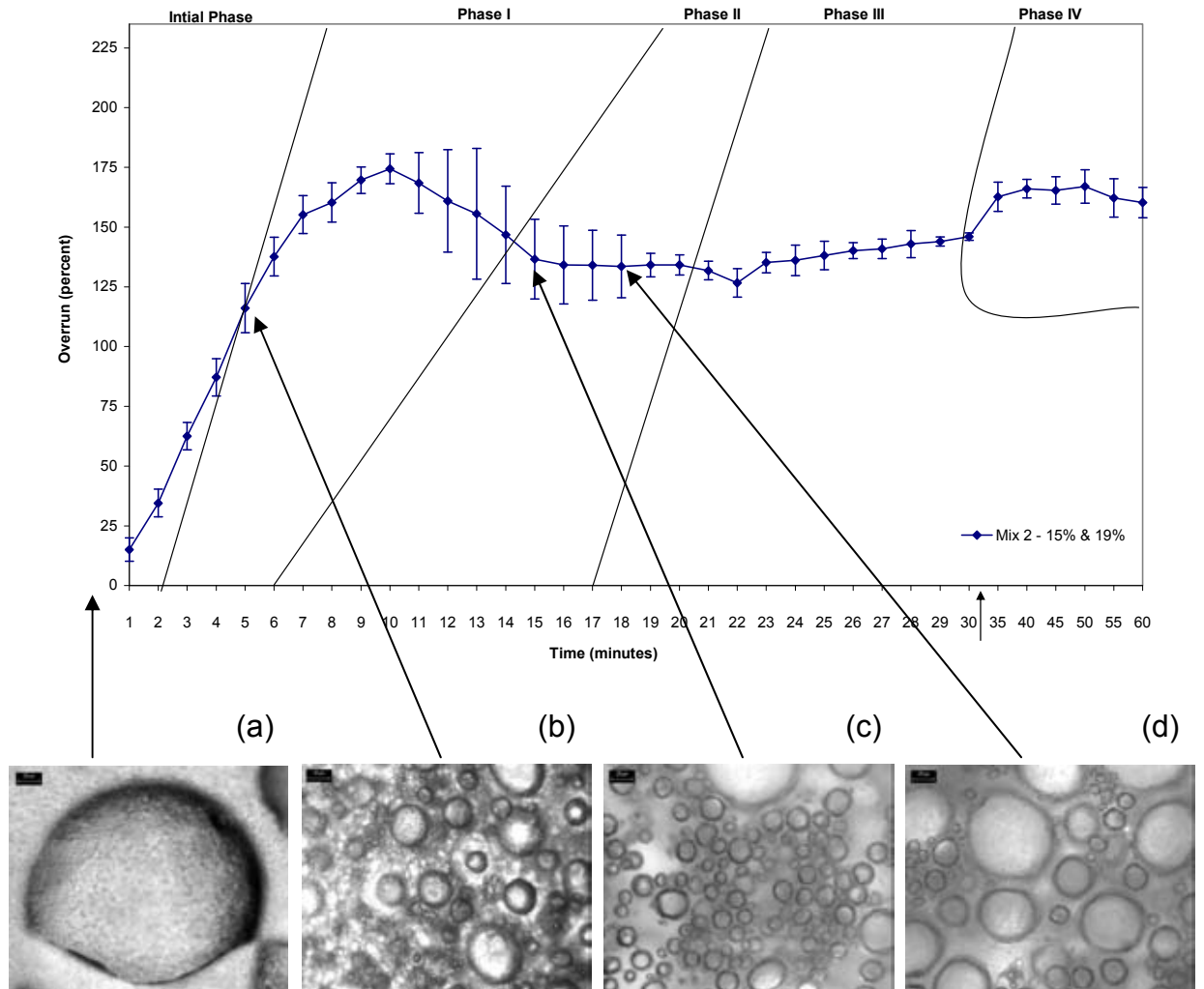


Figure 3.33 Whipping graph of Mix 2 and representative images of the aeration process at the selected imaging points. Scale bar is 25 μm .

Figure 3.33 gives a visual representation of the microstructural evolution of the bubbles within a whipping cream as a function of Overrun and of time. It can be clearly seen that the bubbles in Figure 3.33b and Figure 3.33c are indeed very different from each other. The bubbles in 'b' are stabilised by partially coalesced fat on the interface giving it a somewhat rough appearance whilst those in 'c' through continued whipping have already lost this from the bubbles' surface and give the bubbles a smoother appearance.

There was no point in using Mix 1 within a bubble evolution graph, seeing as its Overrun did not change throughout the aeration process. Mix 2 was chosen for graphical representation as it formed part of the histogram in Figure 3.32 and also showed some variation in Overrun evolution. Mix 3 and Mix 6 are scrutinised at length throughout the remainder of the chapter.

For the Overrun assessment performed in section 3.3.1, Mixes 1 through 6 were assessed. In all the further tests that follow, due to only subtle changes in physical behaviour between each of the neighbouring mixes, it was not possible to assess all 6 of the creams, so only 3 were selected, namely mixes 1, 3 and 6. 1 and 6 were chosen as they were mixes with very different thicknesses and Mix 3 was a mix with a formulation space between these two.

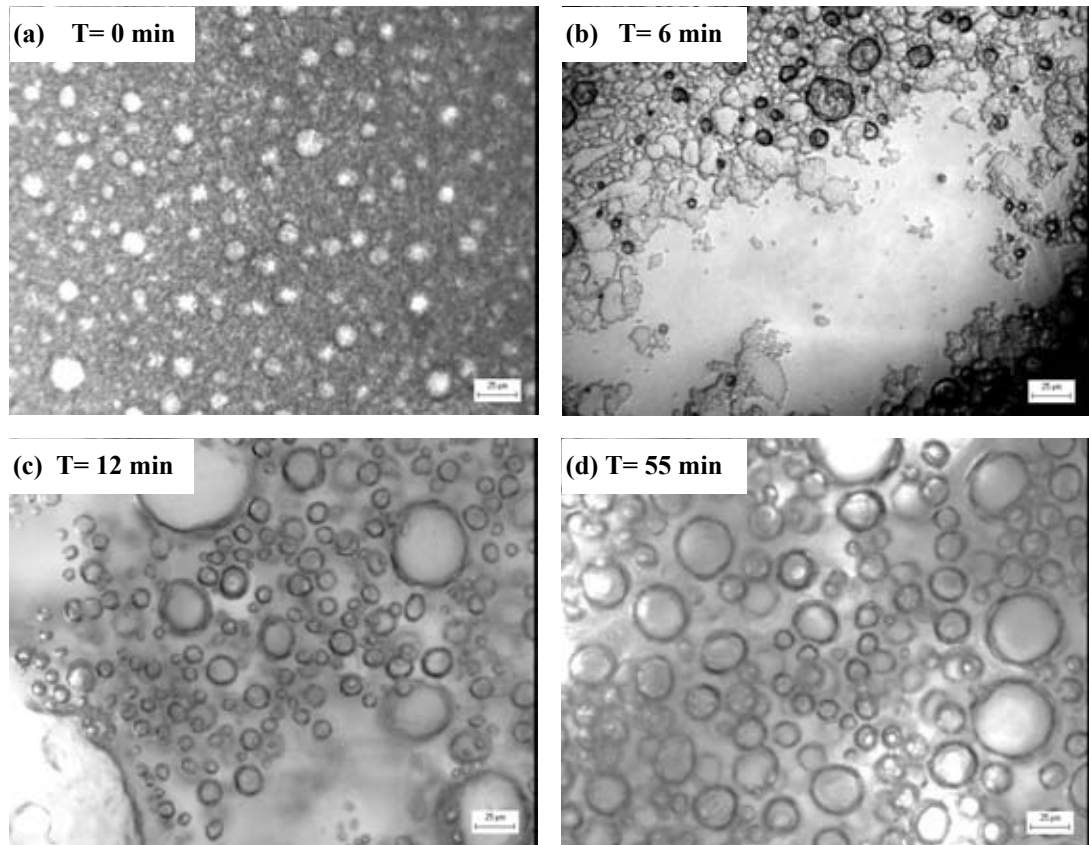


Figure 3.34 Representative micrographs of mix 3 (20% hard oil and 14% liquid oil) and the whipping behaviour at the different phases. Taken at the start (Initial phase) image (a), 2 images in the middle (one from Phase I, b, & one from II, c) and at the end of the whipping curve (Phase IV), image d. They were imaged with a Polyvar and a 25× Objective. Scale bar = 25 µm

Similar to work with Mix 2 (Figure 3.33), whipped cream micrographs and bubble interfaces from Mix 3 are shown in Figure 3.34. The evolution of the cream as a function of whipping time is similar to that of Mix 2. The loss of the partially coalesced fat from the bubble interface can be seen from micrograph 3.34b when compared to that in micrograph 3.34c, which is only with a difference of a further 6 minutes whipping time.

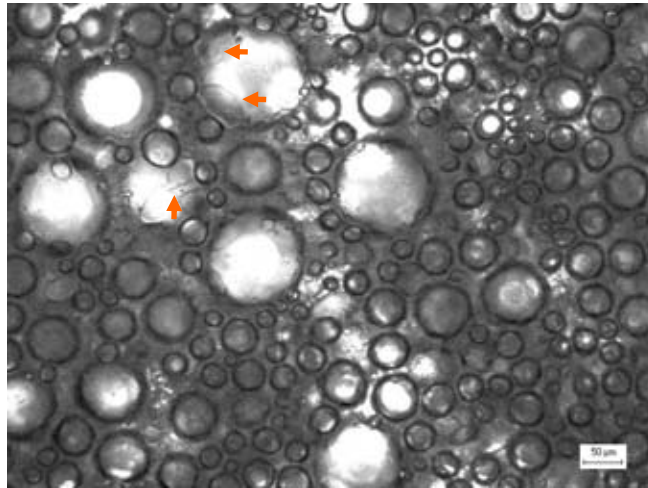


Figure 3.35 Micrograph of Mix 1 aerated for 11 minutes, reaching an Overrun of 168%. The image was taken with a 10× Objective. Visible liquid oil pooled at the bubble interface (arrows) can be seen. Scale bar = 50 μm.

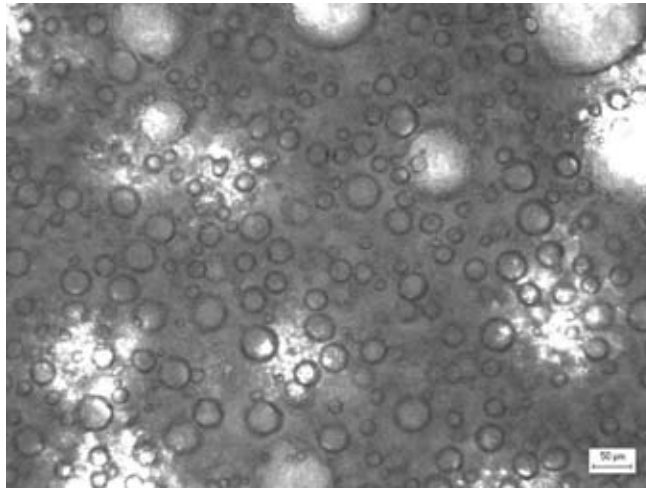


Figure 3.36 Micrograph of Mix 3 aerated for 7 minutes, reaching an Overrun of 91.7%. The image was taken with a 10× Objective. Scale bar = 50 μm.

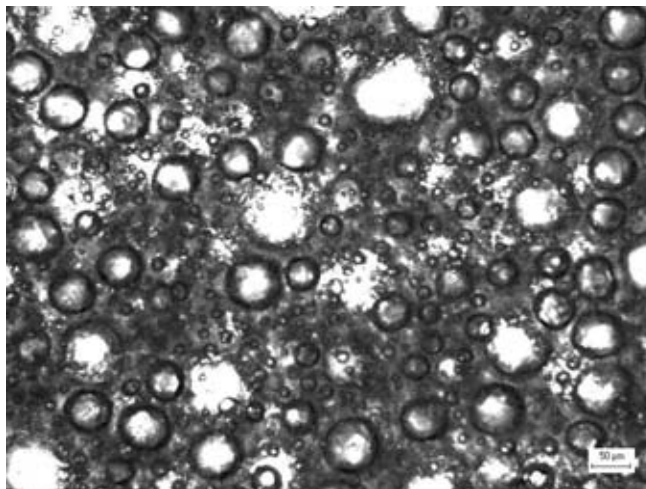


Figure 3.37 Micrograph of Mix 6 aerated for 4 minutes, reaching an Overrun of 77.7%. The image was taken with a 10× Objective. Scale bar = 50 μm.

The same structures as those seen in Figure 3.35 are seen again with mix 1 in the SEM micrographs, (Figure 3.72 and Figure 3.73) showing the same type of ‘lenses’ present on the bubble interface.

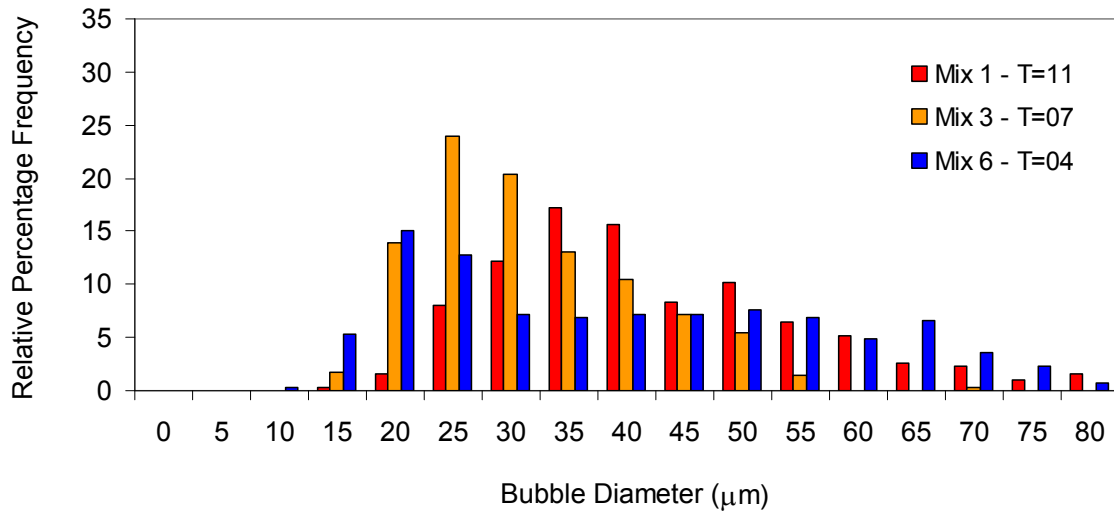


Figure 3.38: Comparison bar graph of three mixes, illustrating the normalised bubble size distribution as a function of formulation at the optimum whip time, in minutes. Optimum whip is the highest Overrun achievable of each mix.

Mix 6 has a higher proportion of smaller bubbles, of its overall bubble count (those in the 20 µm category) relative to the other two mixes. But in addition it also has the highest proportion of larger bubbles of those in the category 60 µm+.

Of the bubbles sized, Mix 3 follows with the second highest proportion of small bubbles, with this mix having the highest percentage in the 25 µm category. It has no bubbles larger than 55 µm.

Finally Mix 1 shows the highest count of bubbles in the 35 µm category, but like Mix 6 also has bubbles in the ‘large’ category of 70 µm and beyond.

It might be argued that the bubble size distribution encountered is directly linked to the proportion of hard oil to soft oil present in the mix. This is perhaps being caused by a higher concentration of the soft oil allowing the larger bubbles to develop at the optimum whipping time chosen, without being hindered by a high amount of hard oil. In addition, mix 6 has to counter the effect of the hard oil and can thus only achieve a smaller bubble distribution, which in turn is coupled to less Overrun.

Figure 3.38 is the bubble size range ‘snap-shot’ present at the time of optimum whipping conditions reflected in peak overrun values. In contrast however, Figure 3.39 is the average bubble size measurement for all the mixes at the selected timepoints taken throughout the entire whipping process.

In Figure 3.39 however, the average bubble size hardly changes throughout the entire whipping process within one mix (albeit with large standard error bars). Most mixes also show little difference between them with regards to the average bubble size present. The largest difference seen is that between Mix 1 and Mix 6, with all the other mixes being more similar to mix 6 than to mix 1. This is why Mix 6 and Mix 1 are plotted separately again in Figure 3.40.

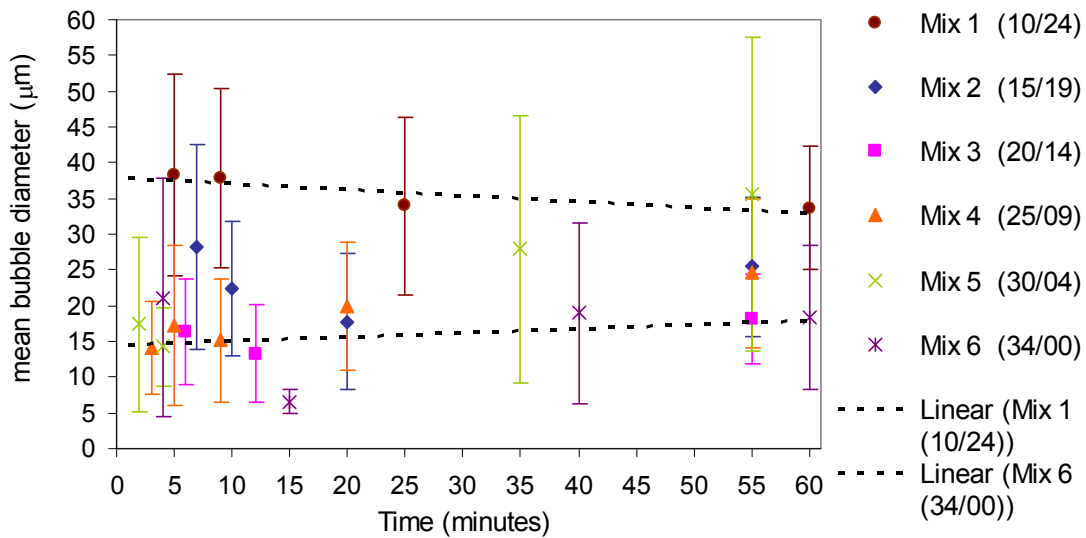


Figure 3.39 Average bubble size taken at the different time points within the entire whipping process. The ratio of hard oil to liquid oil in percent is included in the parenthesis (e.g. 34/00). The first is the hard oil the second the liquid oil

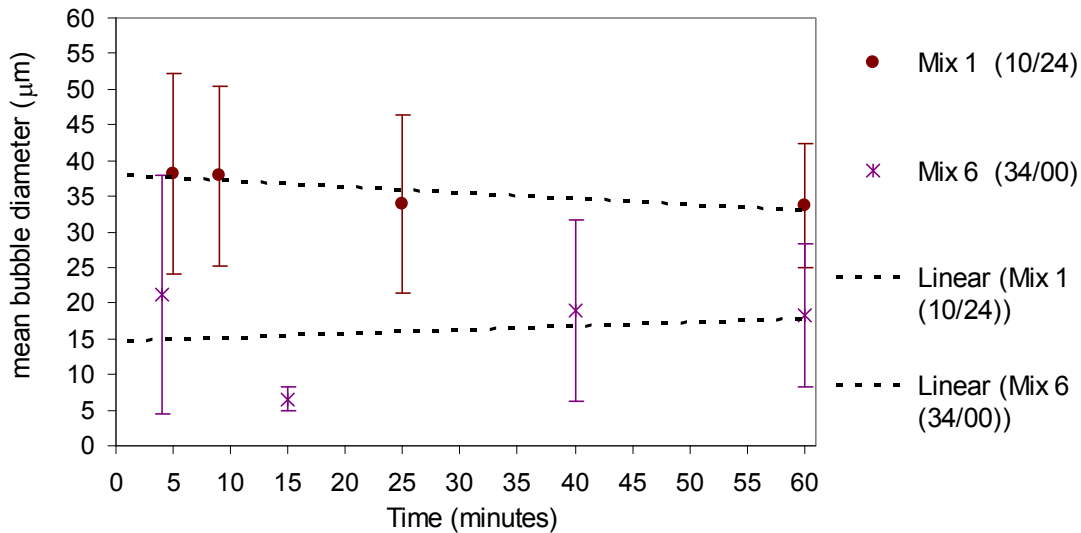


Figure 3.40 Average bubble size taken at the different time points, for Mix 1 and 6.

The bubble size data shows that as the ratio of oil changes, an increase in hard oil in the mix, has the consequence of reducing the mean bubble size (although the overall mean bubble size within a mix remains constant throughout the entire whipping process). This is perhaps an explanation why at the time-points of >50 minutes the two final formulations (Mixes 5 and 6) are never able to reach the final phase IV in the whipping curve.

And with the other formulations, that do reach an equilibrium stage in phase IV, nearly all with the same Overrun values, independent of formulation, it can be said that they all maintain the same bubble size throughout (albeit with large errors), which is actually interesting. One would perhaps expect the average bubble size range to change throughout the aeration process, especially at the end. But each formulation maintains its mean bubble size throughout the entire whipping process. This suggests that the only major change taking place within each mix is the difference in bubble interface species dominating each given instance.

3.3.3 Bulk rheology of the reformulated mixes

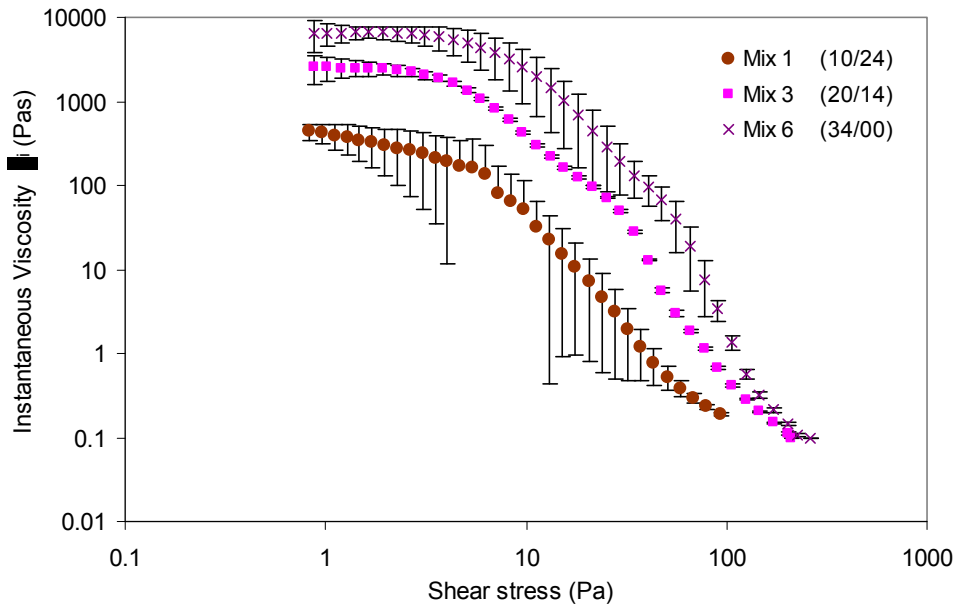


Figure 3.41 Un aerated mix Instantaneous viscosity on triplicate measurements at 25°C with a Bohlin Rheometer, parallel plate geometry and a 1000 μm gap size.

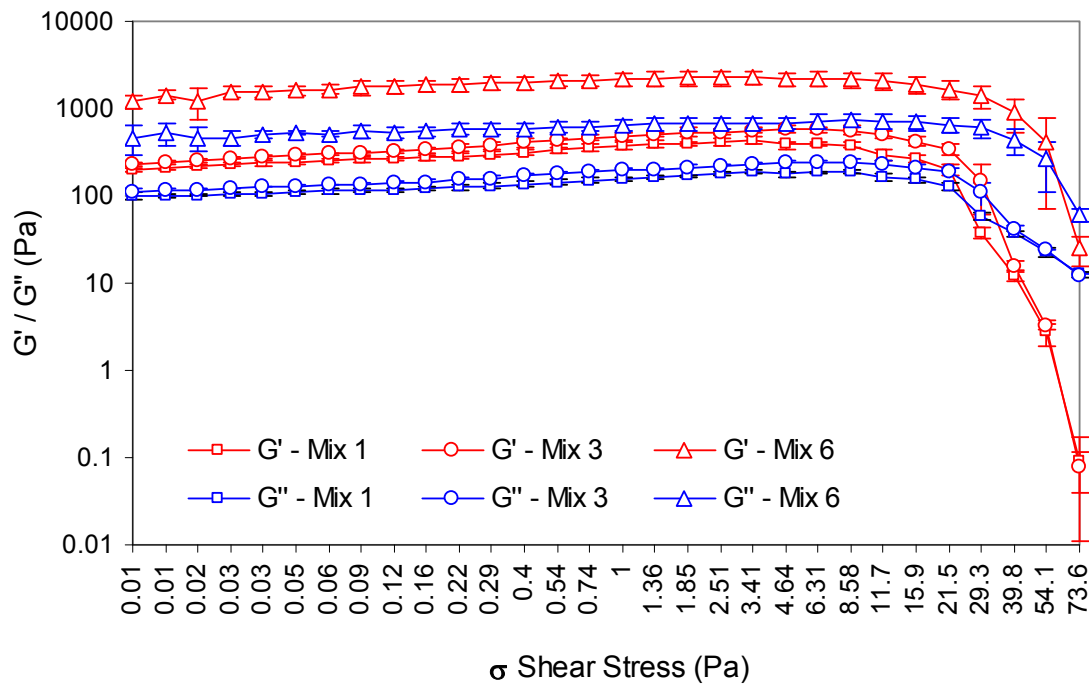


Figure 3.42 Un aerated mix Oscillation rheology on triplicate measurements at 25°C with a Bohlin Rheometer, parallel plate geometry and a 1000 μm gap size.

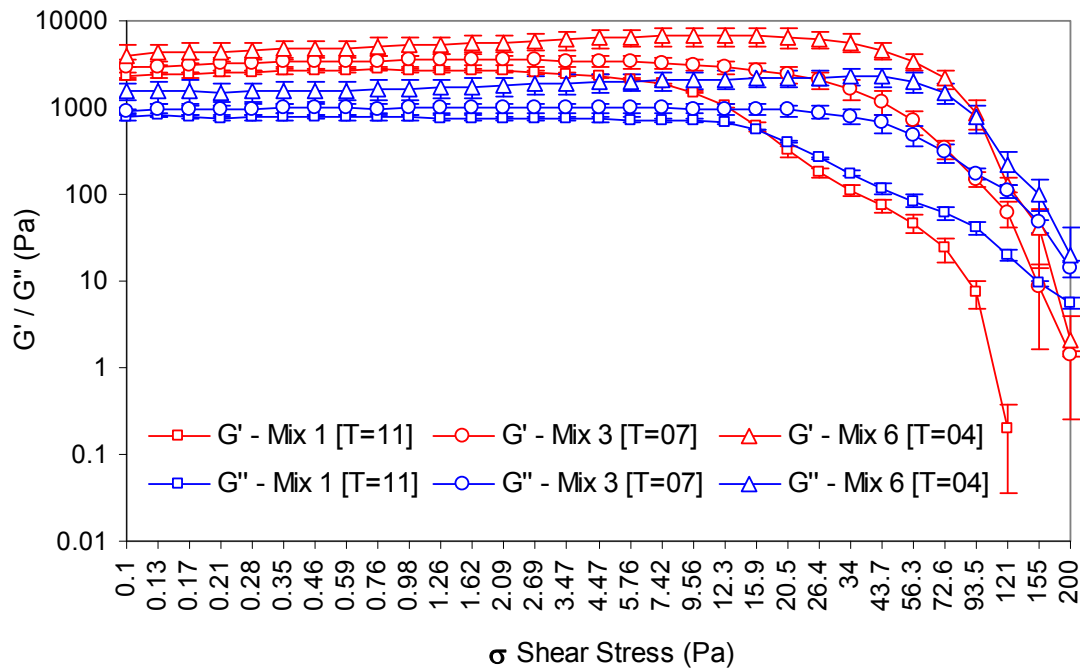


Figure 3.43 Aerated mix Oscillation rheology on triplicate measurements at 25°C with a Bohlin Rheometer, parallel plate geometry and a 1000 μm gap size. Total whipping time is indicated in square brackets.

Figure 3.43 reveals that the continuous phase of all three aerated mixes shows the same structural behaviour to oscillatory movements and the G' and G'' response at low shear stresses is similar in all three cases. It is only at the larger shear stresses that the complex network of fat particles and bubbles thickening the mix, have an effect on the whipped cream. Each of the three creams exhibit a different cross-over point (Mix 1 – 16 Pa, Mix 3 – 73 Pa and Mix 6 – 94 Pa). The mix with the crossover point at the weakest shear stress is the mix with the highest level of liquid oil which is Mix 1, then followed by Mix 3 at a higher shear stress and finally Mix 6. Further to the argument that the continuous phase of the mix is very similar in each of the mixes is Figure 3.42 where the crossover point of the unaerated mixes is very similar. Both mixes 1 and 3 are nearly identical, with only mix 6 differing somewhat in its crossover point. This is to be expected as Mix 6 is the mix without any liquid

oil and is the thickest mix. The differences seen in the crossover point between the traces in Figure 3.42 and Figure 3.43 are directly attributable to the effect of aeration on the structure of the emulsions. The aeration having as a consequence a considerable stiffening of the mixes. This effect can also be seen if one compares the response of G' in the aerated and unaerated mixes. The difference is nearly one order of magnitude for mixes 1 and 3. The response of G' for mix 6 is nearly the same in both the aerated and unaerated mixes. Whipping of the creams with less hydrogenated oil leads these to stiffen, and hence show a difference in response, but Mix 6 with the most hydrogenated oil either aerated and unaerated shows no difference.

3.3.4 Thin film rheology of the reformulated mixes

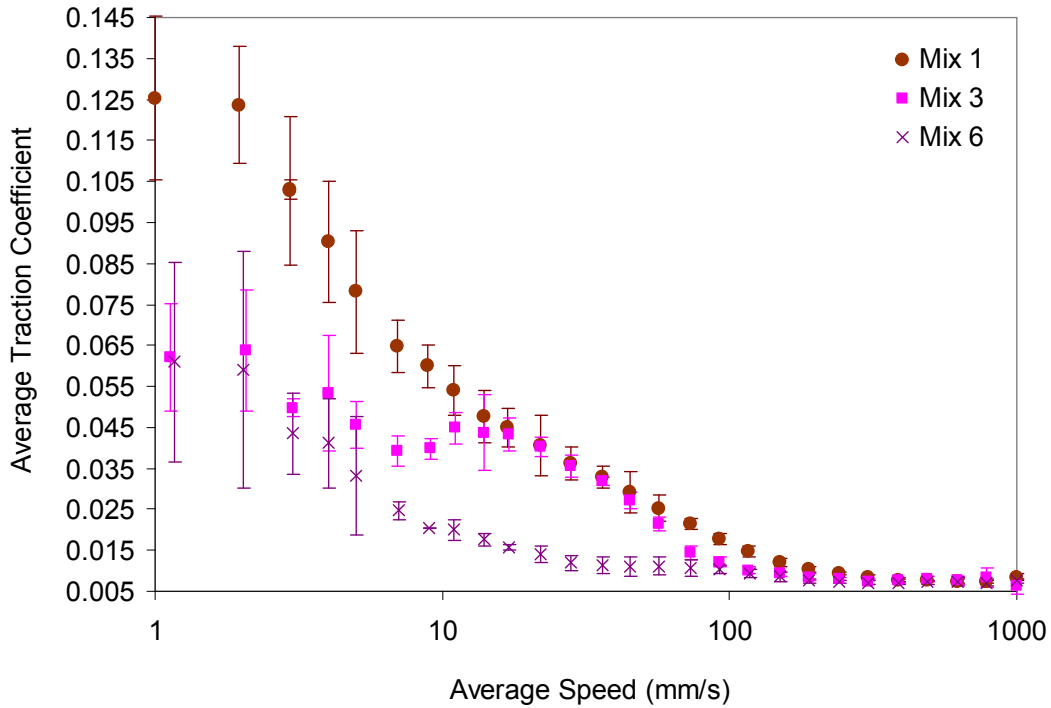


Figure 3.44 Thin Film Rheology on the unaerated reformulated mixes. Stribeck curves for Ball on disc at 37°C, 50% SRR and 3N ball loading.

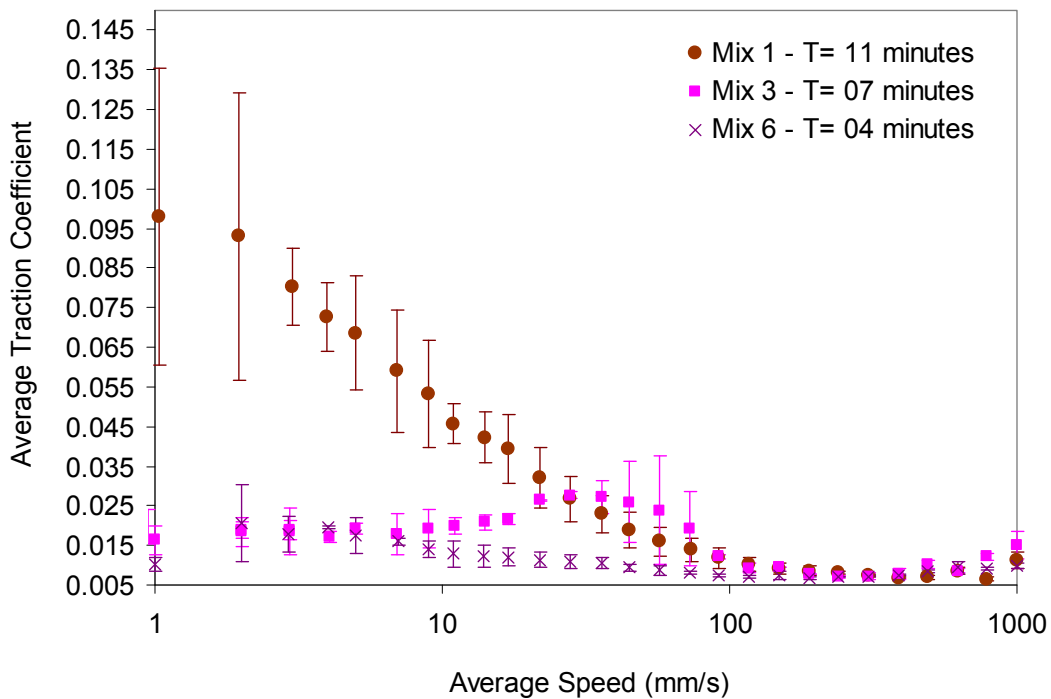


Figure 3.45: Effect of Aeration and the Thin Film Rheological response on the reformulated mixes. The aeration time for each mix was different. The mixes were aerated to the point of maximum overrun. Stribeck curves for Ball on disc at 37°C, 50% SRR and 3N loading. Overrun of the samples was: Mix 1 = 168%, Mix 3 = 91.7% and Mix 6 = 77.7%.

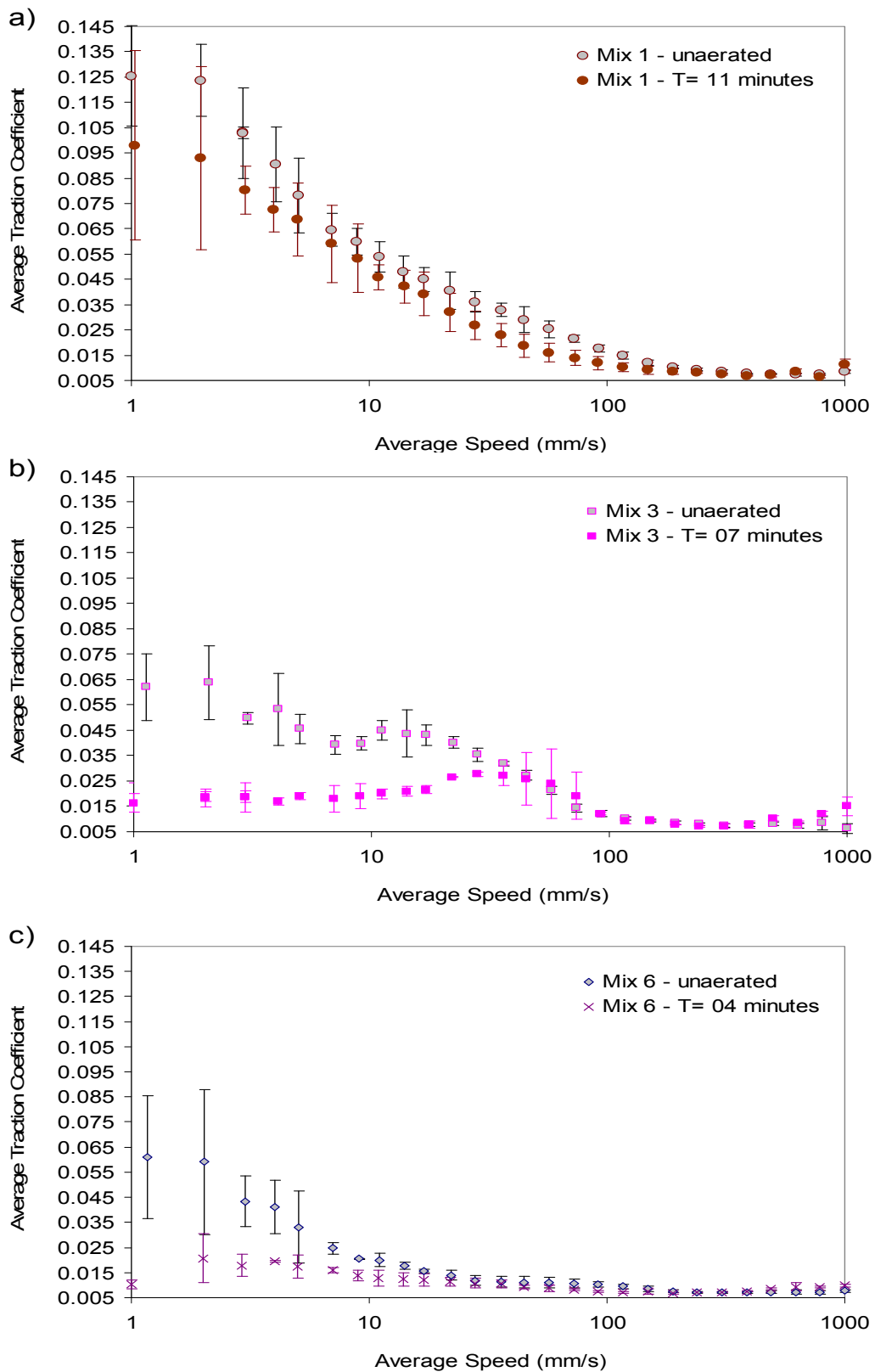


Figure 3.46: a,b,c) Re-plotted data from Figure 3.44 and Figure 3.45 to allow the comparison of the aerated and unaerated mixes side by side.

As the level of hard oil in the aerated sample increases, the respective traction coefficient on the tribometer decreases, when compared to the

unaerated sample. Comparing Figure 3.44 & Figure 3.45 it can be seen that the difference in initial traction response between both the aerated and unaerated samples of Mix 6 is very different from that of Mix 1. Graphs of the same cream type, but aerated and unaerated have been included together for comparison purposes in Figure 3.46. The difference in response between the unaerated sample of Mix 1 and its aerated counterpart is negligible. This goes to show that the cream is quite fluid and that the addition of aeration to the mix has a negligible effect on its thin film behaviour. This can be explained by the fact that the softer unaerated mix and its aerated counterpart will both exert little if not the same resistance to deformation within the tribometer. It may also be argued that the continuous phase with a high liquid oil content in Mix 1 shows the same traction coefficients, and those coefficient behaviours are almost certainly due to mix viscosity. The addition of air does not change the mix behaviour at all. At 37 °C the mix with the higher liquid oil does not have as much hard oil to melt as the mix with 34 percent hard oil and no liquid oil (Mix 6).

In the same instance the tribometer also sees this resistance to deformation by the fact that its ball load varies throughout the run (see: Figure 3.47). The deflection of the ball to the thicker aerated sample is much higher than it is with the thinner aerated sample. The load measured when the thinner aerated sample is present, is much less by the mere fact that the sample does not deflect the ball as much at the higher speeds due to its more fluid nature. Visual observations have even seen that the sample in the mixed regime which it

experiences during the higher speeds actually skirts around the ball geometry and does not get entrained between the ball and the silicon mat at all. The thicker sample is not able to do this, but must pass between the ball and the mat.

These observations are also consistent with those seen by de Vicente et al., (2006), where the authors quote that in general, the friction coefficient falls with increasing concentration of polymer in solution over the whole speed range. In this case at lower speed ranges below 10 mm/s the ball load response from the tribometer is less predictable than those at the higher speeds where the response is more predictable, and for this reason the readings that fall below a speed of around 10 mm/s are less reliable and should be treated with caution. In general it can be said that the actual ball loading exerted on the silicon sheet by the tribometer is less for a thinner sample than it is for a thicker one.

The behaviour of the mixes on the tribometer and the mix viscosities as elucidated by the Rheometer are both consistent. Mix 1 with a lower viscosity shows a higher traction coefficient and Mix 6 with a high viscosity shows the lower traction coefficient.

In addition, although the ball load results that have been shown in Figure 3.47 indicate differences in ball load in the order of 0.01 N, it must be stressed that the load cell is only a 10 Newton load cell and can only measure with an accuracy of 10% (i.e. detect a 0.1 N difference only). It is therefore important

that the ball load results be used with caution as a diagnostic feature of sample thickness or response. The results are triplicate (error bars have been omitted for clarity).

It must also be noted at this stage (as mentioned in the Materials and Methods section, Chapter 2, Part I) that the silicon mat must be used no more than 3 times. Failing to do this would greatly affect the quality and reproducibility of the results obtained. If this frequency is exceeded, the quality of the results suffers, with a large increase in the size of the error bars a direct consequence, and an erratic response. An example of this can be seen with Figure 3.12 and the rather large error bars present. Those results were gathered while setting up the machine, and later, strict adherence to changing of the rubber mat after a triplicate experiment was carried out was instituted. Those results were only included to show the difference in response to two very different samples.

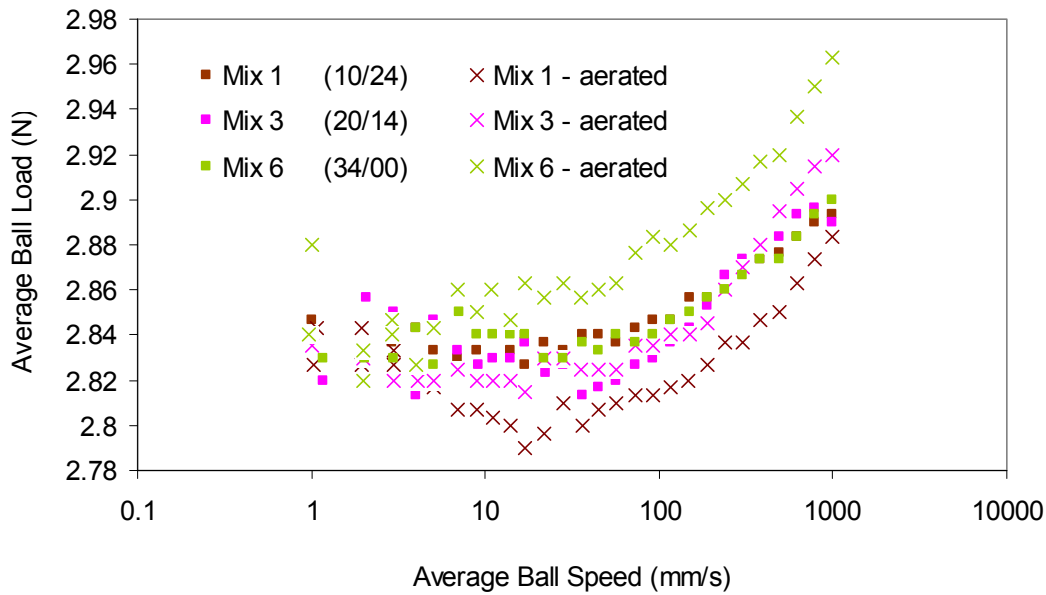


Figure 3.47: Average Ball Load on the disc (in N), with samples of different thickness. Either aerated or unaerated. The results are based on triplicate read-outs. Error bars have been omitted for clarity purposes.

3.3.5 Fat particle sizing with a Mastersizer

The three reformulated emulsions chosen for rigorous analysis were subjected to particle sizing with the Mastersizer. The three mixes exhibit an average particle size around 10 μm see figures Figure 3.48 to Figure 3.50. Mix 3 and Mix 6 both show a monomodal distribution, with the only one showing a bimodal distribution being Mix 1. This behaviour can perhaps be attributed to the higher proportion of liquid oil in Mix 1, perhaps dispersing as smaller droplets. Mix 3 and Mix 6 probably did not have enough free liquid oil to freely disperse as droplets in the Mastersizer; or indeed Mix 3 or Mix 6 did not exhibit as much phase separation as Mix 1 did. This is perhaps what contributed to the bimodality seen in Mix 1. Further discussion of phase separation with a visual example taken from the micrographs of the unaerated mixes will be covered in section 3.4.1.

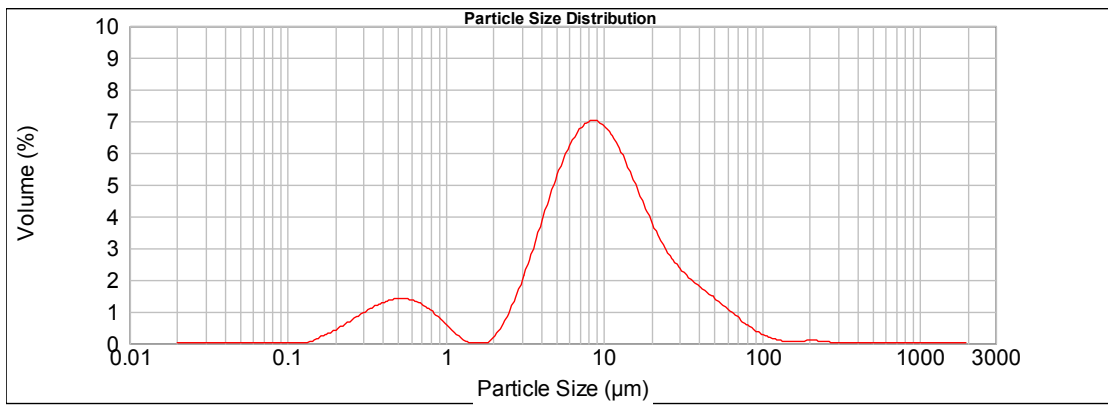


Figure 3.48 Mix 1 Emulsion particle analysis.

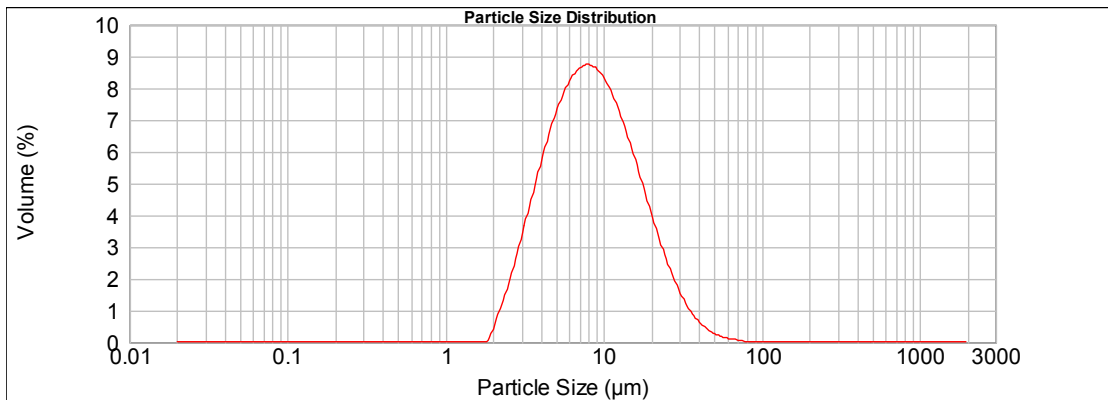


Figure 3.49 Mix 6 Emulsion particle analysis

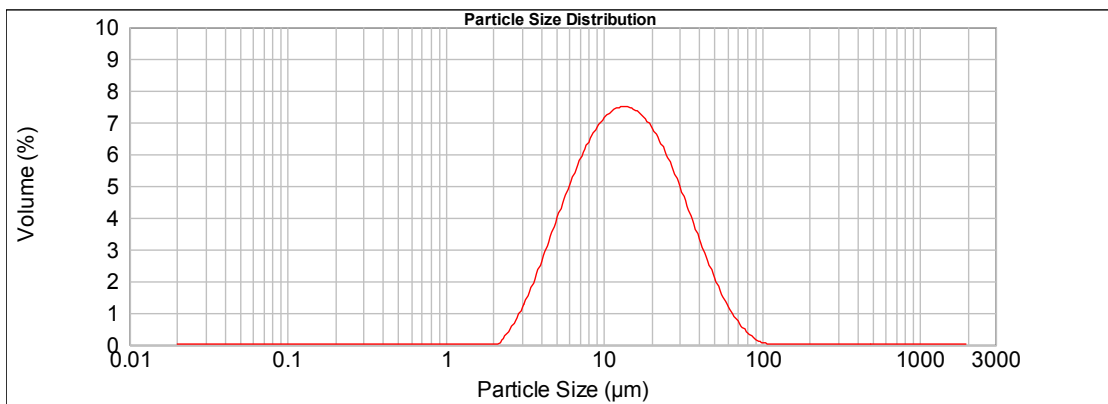


Figure 3.50 Mix 3 Emulsion particle analysis

3.3.6 Slumping behaviour of the reformulated cream

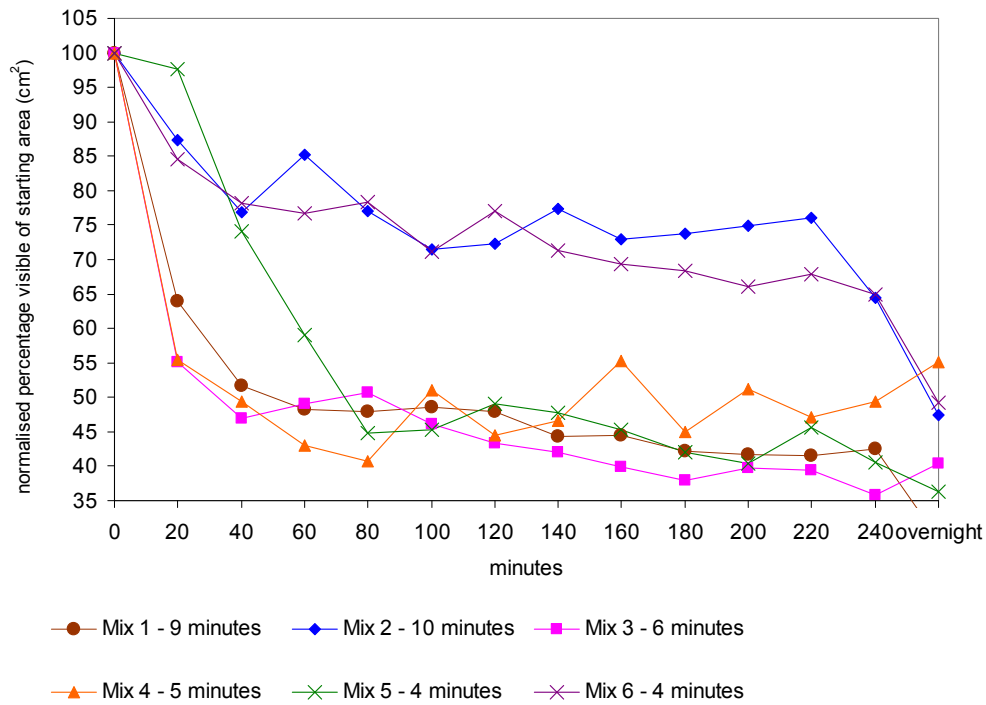


Figure 3.51: Slumping at 25 °C of self made whipped vegetable oil emulsions, optimally whipped. Whipping time indicated next to each mix.

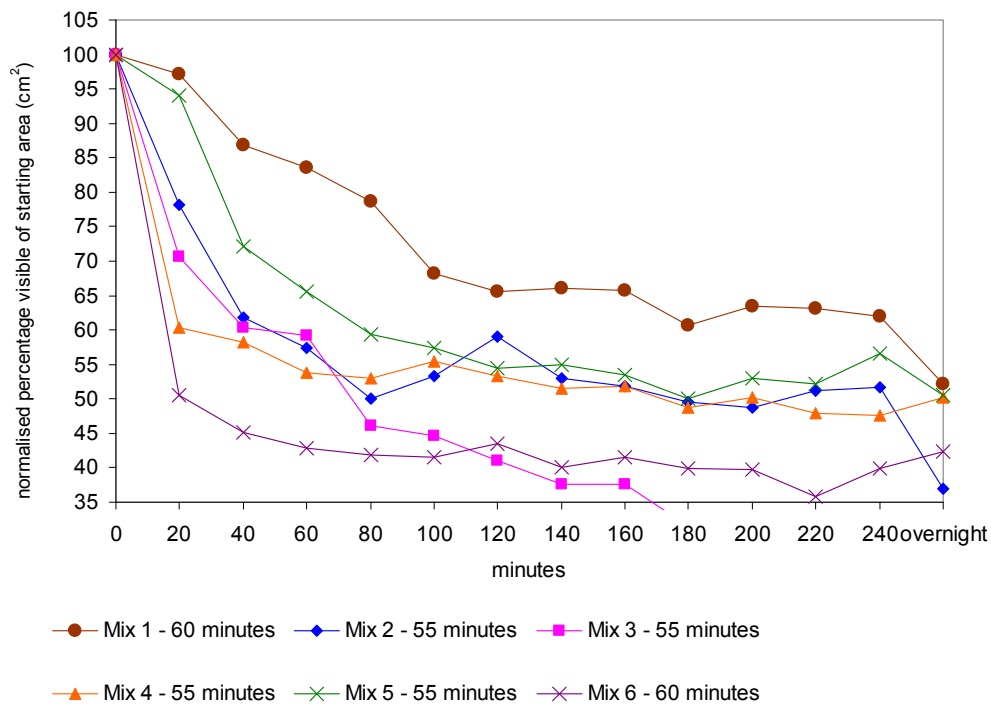


Figure 3.52: Slumping at 25 °C of self made whipped vegetable oil emulsions, overwhipped. Overwhipped samples were taken either at 55 minutes or 60 minutes.

Figure 3.51 charts all six of the reformulated optimally whipped creams

slumping at 25 °C. Tests were performed with the “peak” whipped samples and also their overwhipped counterparts were analysed and these results are in Figure 3.52.

After 80 minutes it is safe to say that all formulations have slumped.

With the exception of two Mixes (numbers 6 and 2) the optimum whipped sample of each of the creams is always the first mix to slump away. The overwhipped sample, independent of which mix is analysed, always slumps away last, which can be seen in Figure 3.52.

This observation might be explained microstructurally by the fact that during whipping, build up of a complex but fragile structure is taking place. This delicate structure gets lost through overwhipping. The loss of this structure is then evident in the meltdown traces. In general the optimally whipped samples show a faster meltdown than the overwhipped counterparts which slump the slowest. The partially coalesced fat network is seemingly less robust at standing up under the pressure of its own weight than the re-formed fat phase which forms part of the overwhipped samples. These are overall more resilient to the slumping pressures. Evidence of the spatial distribution of the fat layer in the optimal whipped creams and the overwhipped structures can also later be seen in the SEM micrographs in section 3.4.

It was uncertain what the exact process behaviour was for the fat phase

during overwhipping and re-whipping, and how the fat got transformed. The slumping experiments were work towards understanding this process and being able to shed light on this aspect. It is telling that the microstructures after slumping must be different indeed. The structure of the target whipped cream was in each case very smooth, and the structure of the overwhipped sample was open, slightly oily, wet and grainy. This was especially more evident after overnight ageing. This can be seen in Figure 3.53. The grainy-ness discussed earlier and the loss of structure of the overwhipped sample is evident in this photo. This graininess was most evident with the cream with no liquid oil in it, Mix 6. The increased loss of water is also evident when compared to the peak whipped sample. Both creams have been exposed to the same temperature and humidity for the same time period.

The oil phase behaviour at the bubble interface of all the whipping creams that were studied in this chapter were analysed through a selection of SEM micrographs also. This is discussed in section 3.4.



Figure 3.53 Mix 6, 34% hard oil only and no liquid oil (34/00) with overnight ageing at 25°C. The overwhipped sample (left) aerated for 60 minutes and the peak whipped cream (right) aerated for 4 minutes.

3.4 SEM images of all the whipping creams studied

The following section will highlight some SEM work that was undertaken to build an understanding of the stabilisation mechanism of dairy whipping cream, its non-dairy alternative and reformulated mixes which have a similar continuous phase to non-dairy creams like Elmlea. With the SEM work the oil phase should be imaged and especially its behaviour at the air bubble interface elucidated. The reformulated mixes were created in order to test the softening limit of the cream. This was achieved by progressively adding more and more liquid oil to the mix, but keeping the total oil content at 34 percent. The limit was found with mix number 1. After achieving a maximum Overrun of around 200 percent, the cream retains that Overrun value throughout the entirety of the whipping process. Whereas all the other mixes reach a maximum Overrun which is dependent on the amount of liquid oil in the mix. Therefore they either overwhip quickly (if they are purely composed of hard oil), or the overwhipping sets in progressively slowly with each increase of liquid oil

contained in the mix.

The first micrographs presented in Figure 3.54 through to Figure 3.65 are the unaerated mixes. The structures that were imaged and which are present within these mixes are later discussed after the twelfth micrograph.

Images captured for this section are the unaerated mixes, which are included at the start of the section. These were gathered in order to have a microstructural reference image of the creams' composition. For the images in the mid section, the creams were whipped to peak Overrun and their structure captured. For the commercial samples the time-point of peak overrun was taken as the overrun at 150 seconds (or 210 seconds for the Elmlea light, but this is still within the bounds of sample variability). For the reformulated mixes, peak overrun was achieved after eleven minutes for Mix one (10 percent hard oil, 24 percent liquid oil), after seven minutes for Mix three (20% and 14%) and 4 minutes for mix six (34 percent hard oil and no soft oil). In addition, an "overwhipped" structure was gathered for each of the three reformulated mixes. Here the overwhipped structures were gathered after 30 minutes whipping for each of the creams respectively. The structures were all formed and gathered by stopping and starting the mix, as this was what was carried out for the Overrun determination initially, and for consistency purposes this protocol was retained for the entirety of this work.

In this SEM work the commercial samples and the reformulated mixes were all

included in this section together and not in separate sections as all the other work has been. The results were presented here together in order to be able to compare some of the imaged structures and also discuss some of the differences seen.

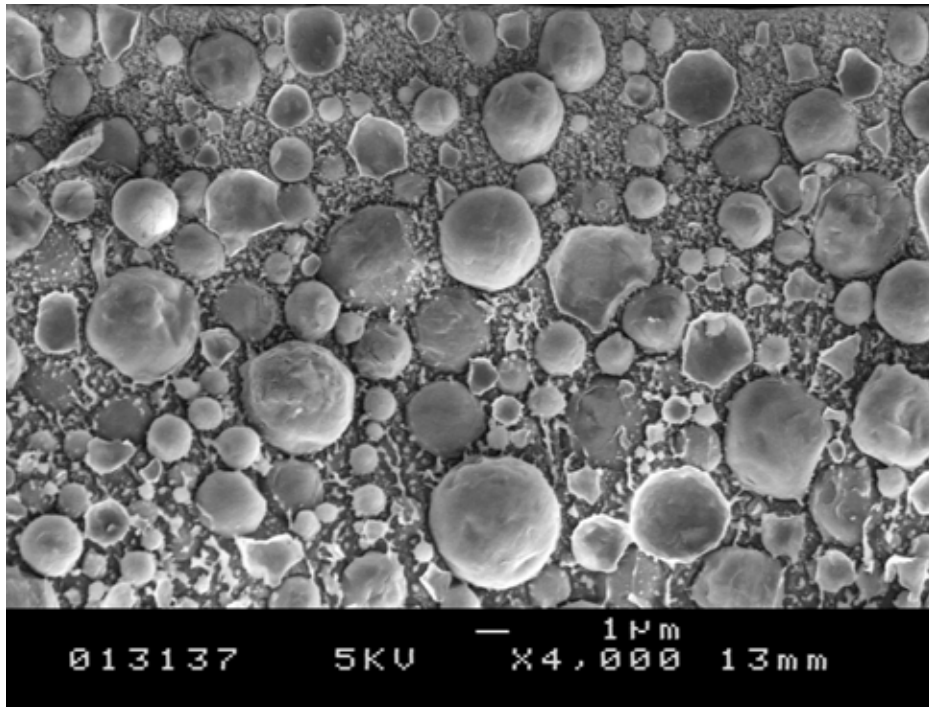


Figure 3.54 J. Sainsbury's un-aerated

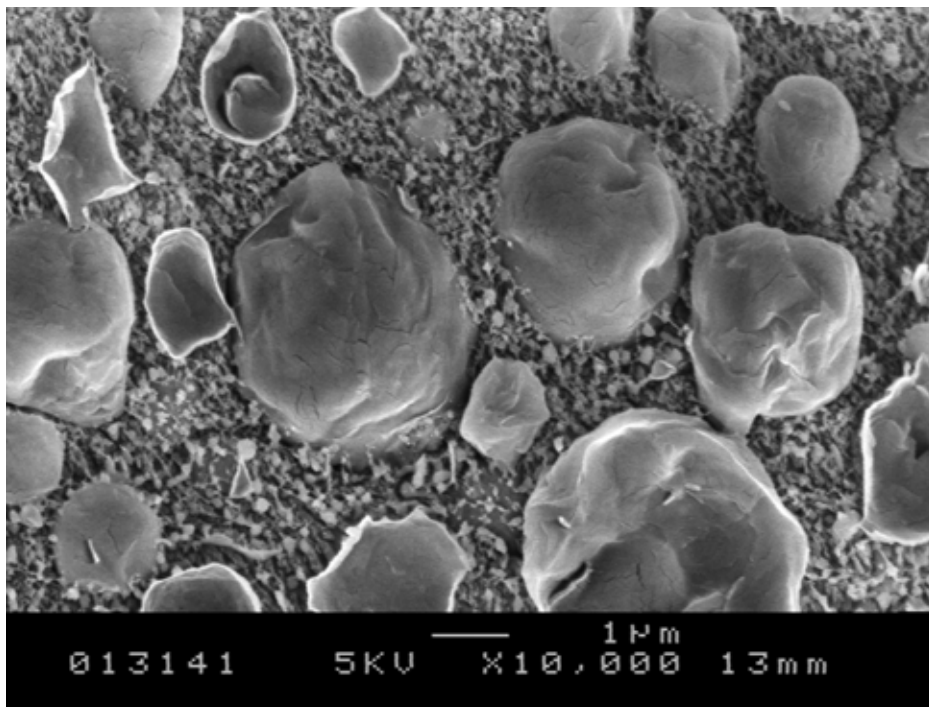


Figure 3.55 J. Sainsbury's un-aerated

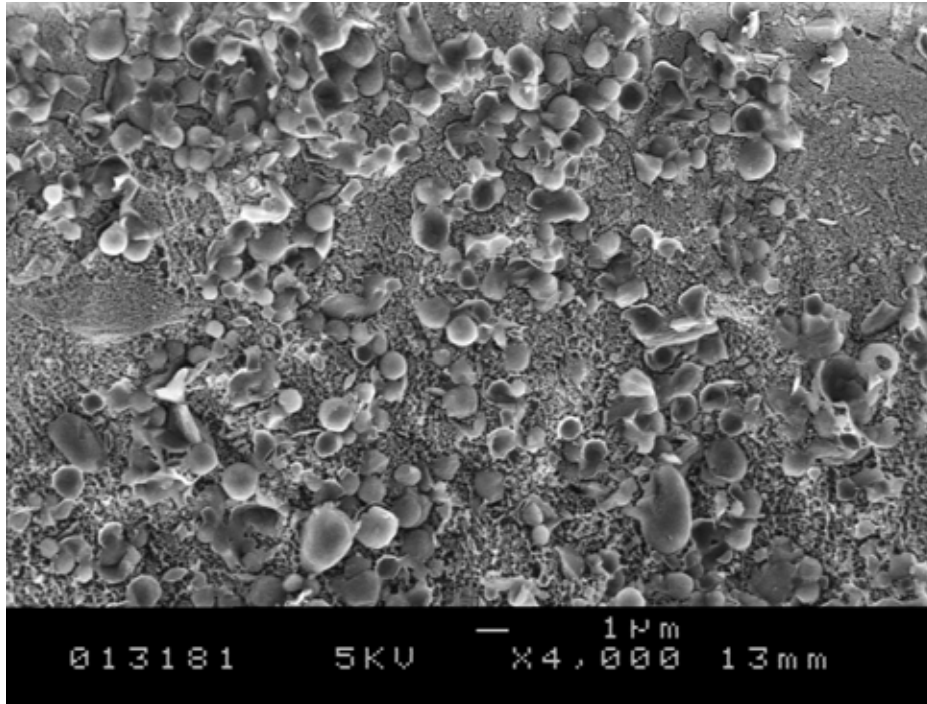


Figure 3.56 Elmlea Full Fat un aerated

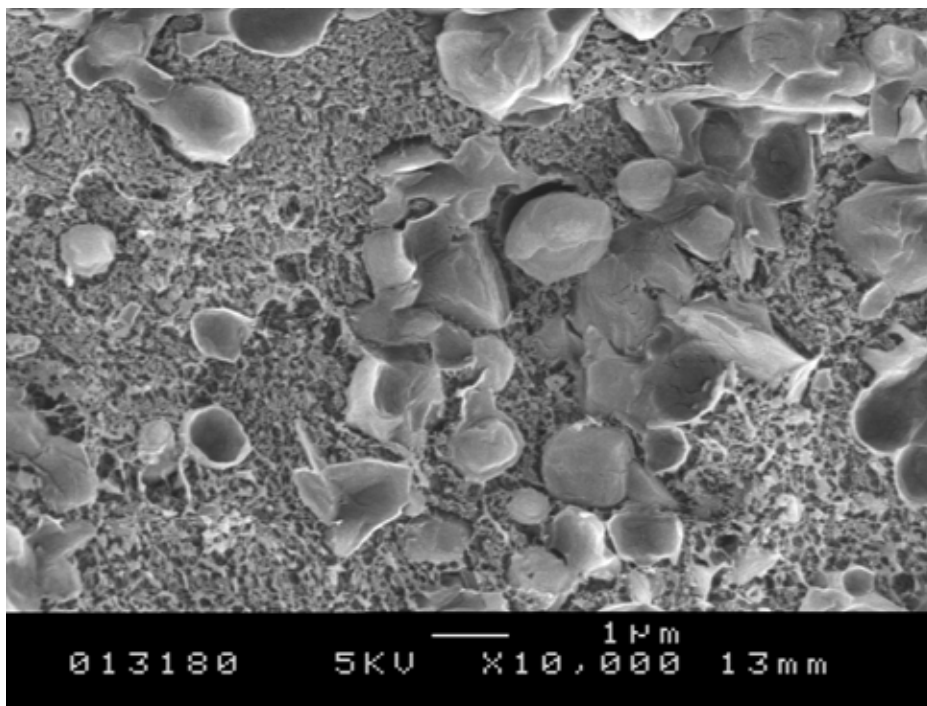


Figure 3.57 Elmlea Full Fat un aerated

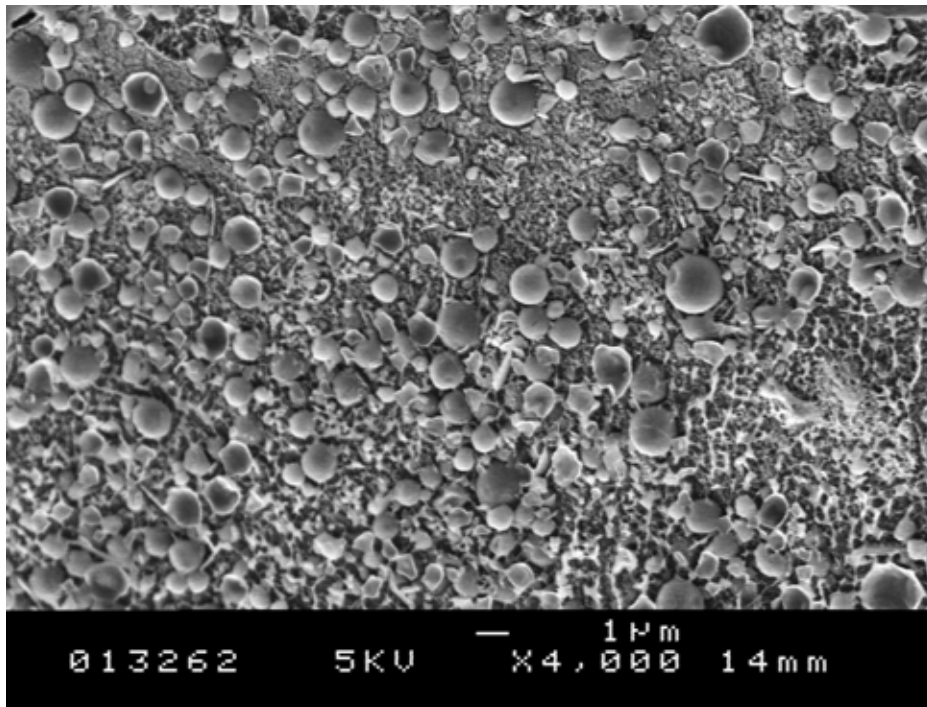


Figure 3.58 Elmlea Light un aerated

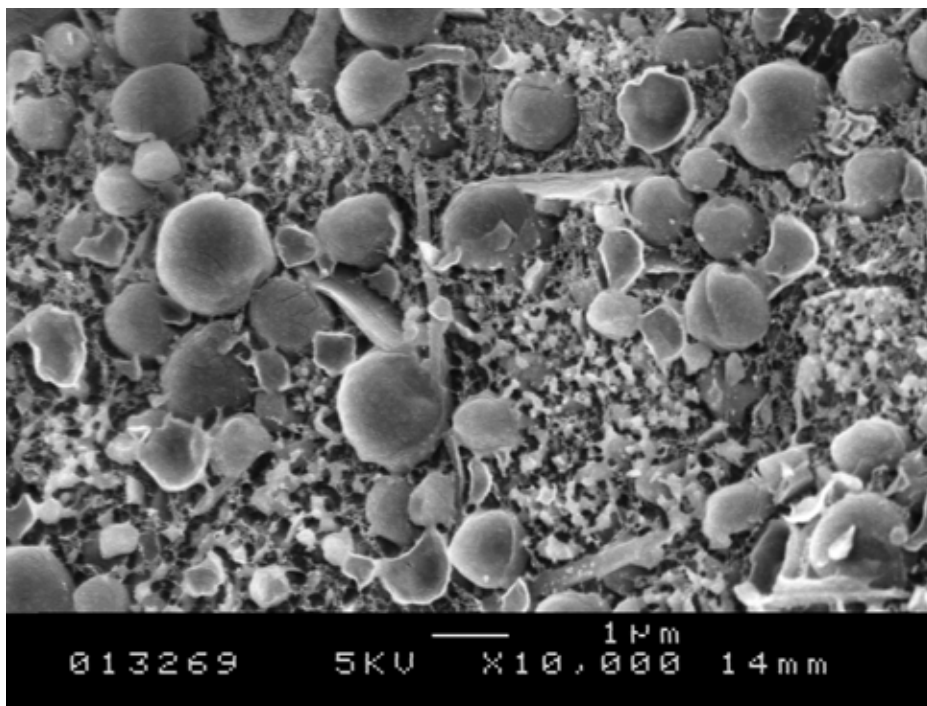


Figure 3.59 Elmlea Light un aerated

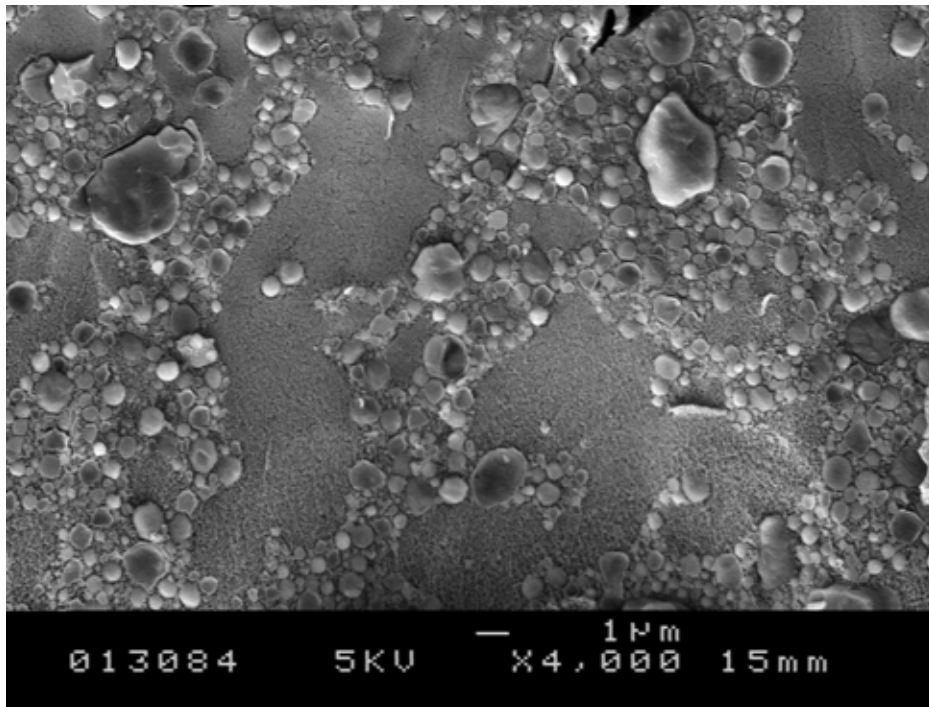


Figure 3.60 Mix 1 un-aerated

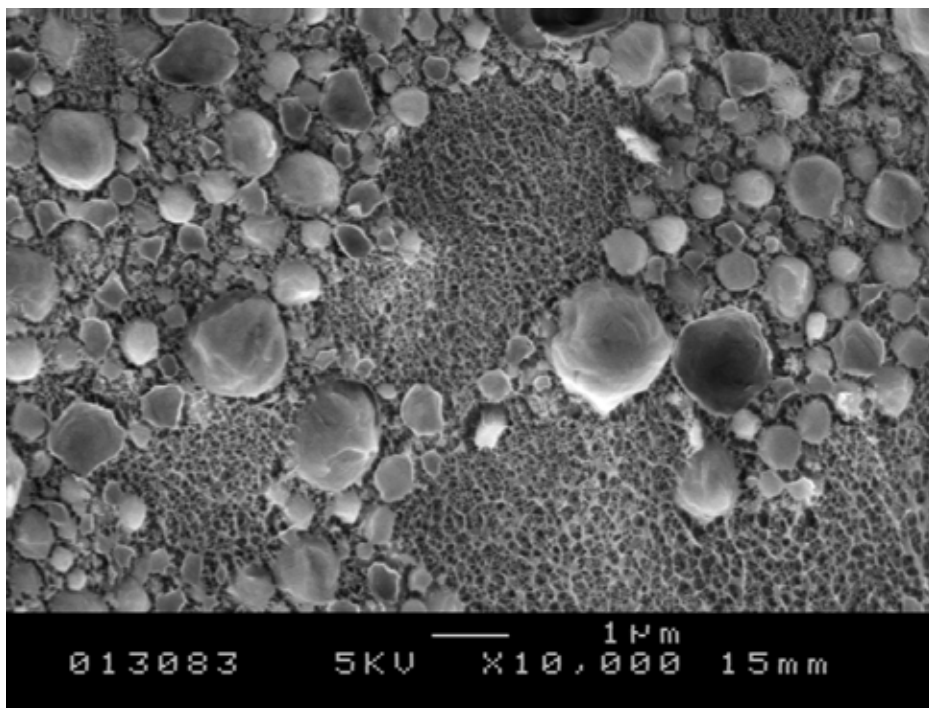


Figure 3.61 Mix 1 un-aerated

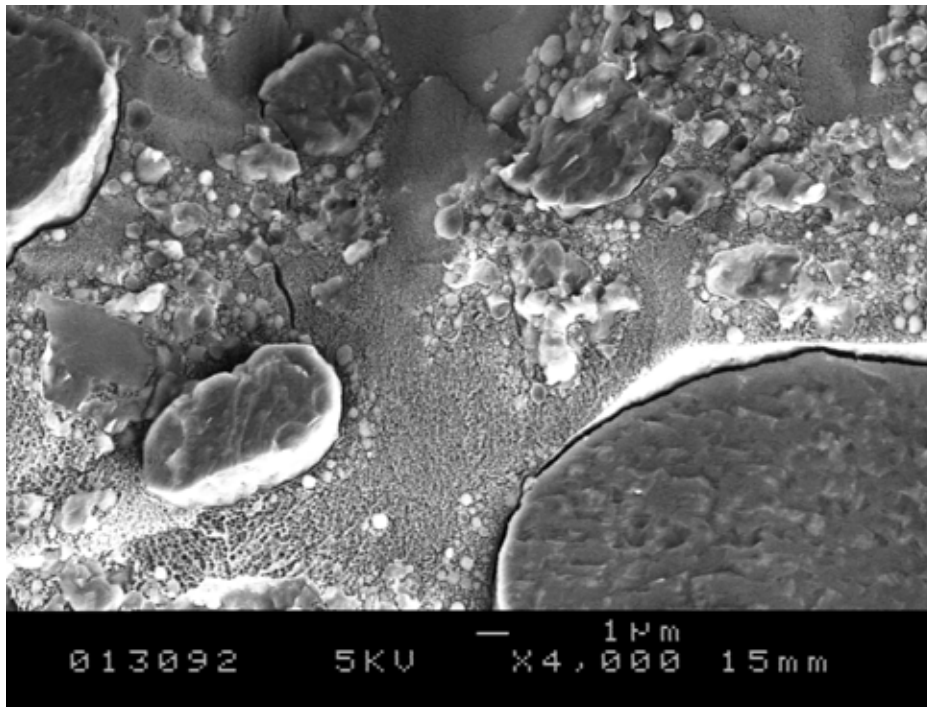


Figure 3.62 Mix 3 unaerated

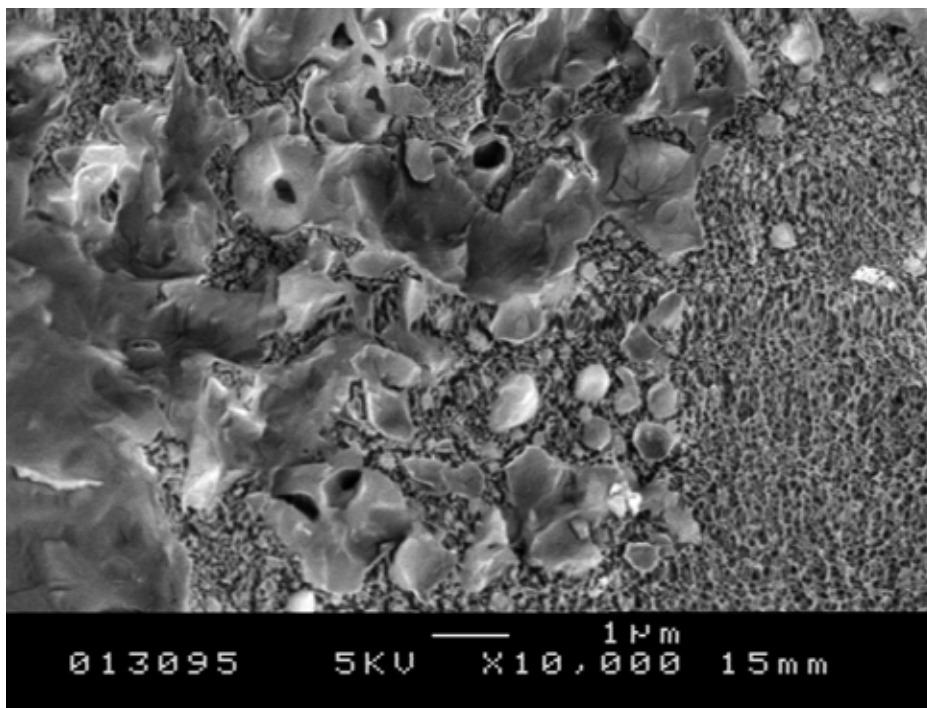


Figure 3.63 Mix 3 unaerated

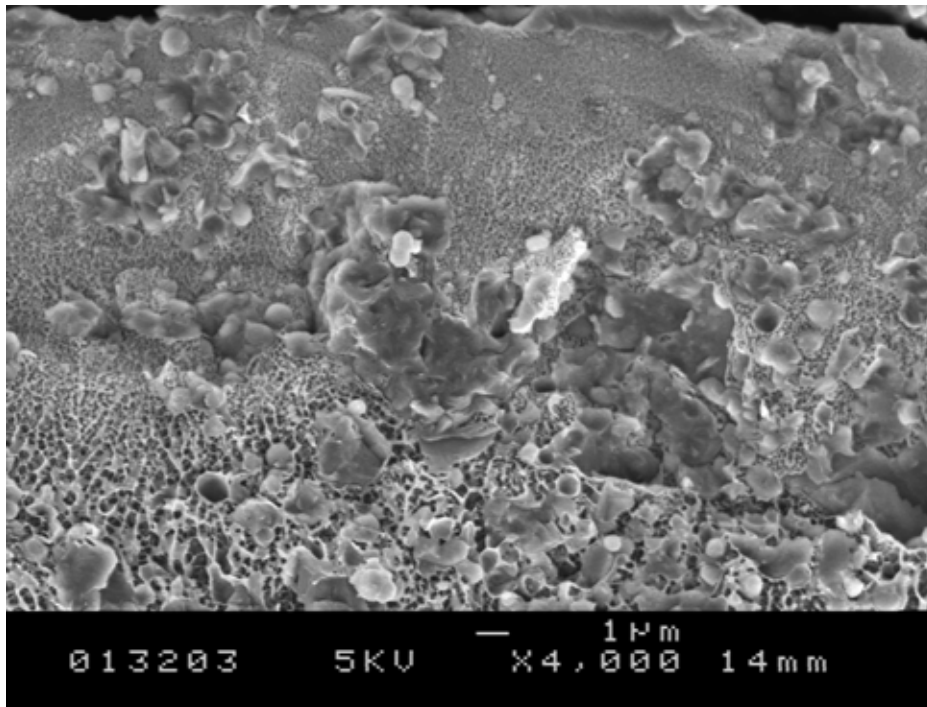


Figure 3.64 Mix 6 un-aerated

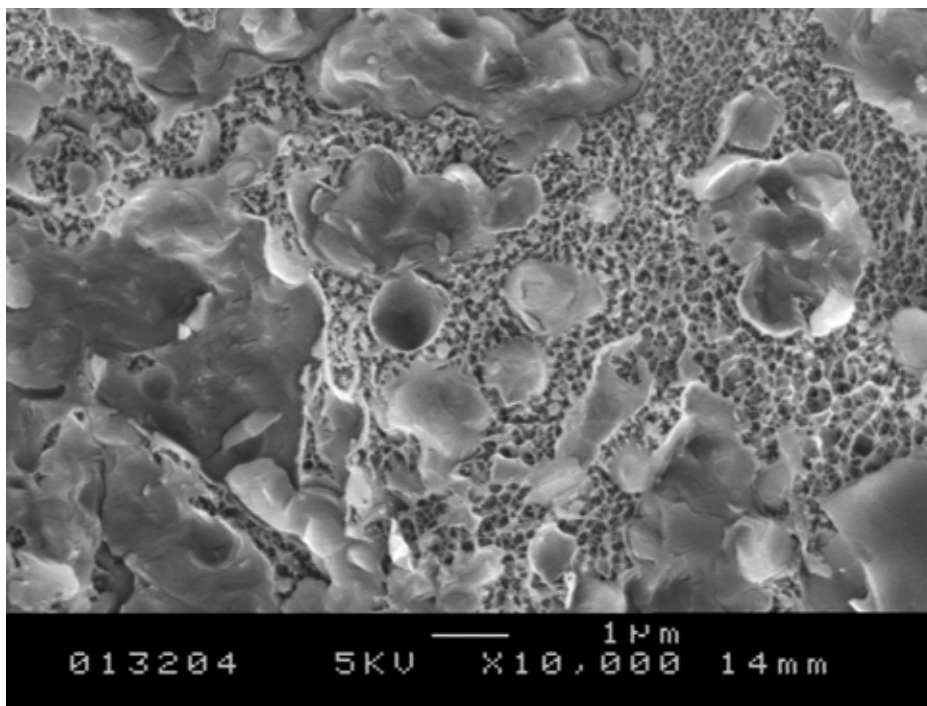


Figure 3.65 Mix 6 un-aerated

3.4.1 Comments on unaerated micrographs of all the whipping creams

The micrographs of all the unaerated mixes presented in Figure 3.54 through to Figure 3.65 were not concerned with the structural layout of the oil globules. The micrographs were merely gathered for comparison purposes and in order to have a reference point to compare the aerated mix with.

The only preliminary remark that can be made at this stage regarding the microstructure of the creams, and without having any aerated structures to compare the creams to, is that both Elmlea Light and Elmlea Full Fat contain platelet structures in the matrix. These are sheet-like or needle like protrusions that are formed between the round oil globules and an example of this can be seen in Figure 3.59. There are no platelet structures associated with any of the reformulated mixes, see for example Figure 3.61, where the oil globules are all spherical. The SEM's of the commercial samples are presented first in Figure 3.54 to Figure 3.59 and the unaerated reformulated mixes are then presented last in Figure 3.60 to Figure 3.65.

If one observes the fat particles within the commercially available whipped creams in Figure 3.54 which is the J. Sainsbury's cream, Figure 3.56, Elmlea Full Fat and Figure 3.58 which is Elmlea Light; it can be seen that the largest fat particles are contained in the J. Sainsbury's cream, with a size ranging from 2 to about 6 μm , this is then followed by Elmlea Full Fat with particles of about 1 or 2 μm and Elmlea Light having the smallest particles at 1 μm and smaller.

The reformulated mixes exhibit large islands of aqueous material and this can typically be seen in the micrographs of Figure 3.60 and Figure 3.61. It is believed that this takes place largely due to phase separation of the emulsion, with a concentration of the water around the Xanthan and the subsequent exclusion and separation of the oil droplets from the main part of the mix. It can be speculated that this phase separation is the one responsible for the bimodality seen for Mix 1 in the mastersizer measurements in section 3.3.5, Figure 3.48. This behaviour is much less prevalent in the Elmlea mixes or indeed in the dairy whipping cream formulation. The aqueous phase within the micrographs can be characterised by the presence of porous honey-comb structures. These structures are visible in all the micrographs, and they are left behind after the ice has been sublimed during sample preparation. A good example of this honeycomb structure can be seen in Figure 3.65, which is present between the oil particles. The fat droplets in the commercial samples seem to be more evenly distributed than those in the reformulated mixes. The structure of the commercial samples seems more homogeneous.

The next section contains micrographs that are of ‘peak aerated commercial creams’ and these run from Figure 3.66 through to Figure 3.71. Starting with J. Sainsbury’s cream, then Elmlea Full Fat and the final one is Elmlea Light. In general the moment of peak aeration can be characterised as the moment of highest achievable Overrun. The structures present in the creams are then discussed after the Elmlea light micrograph.

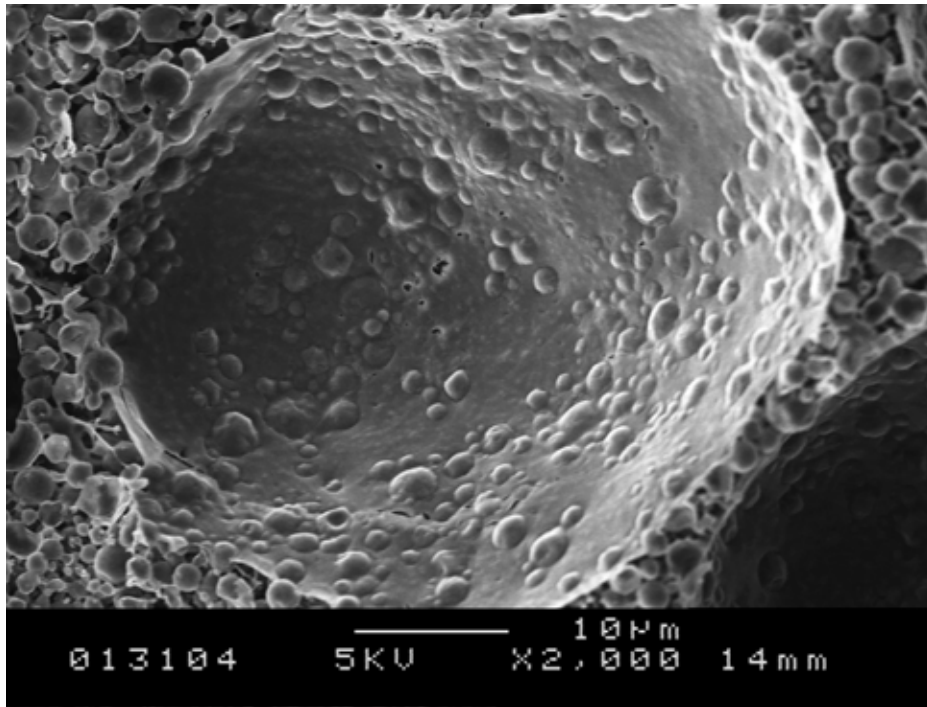


Figure 3.66 J. Sainsbury's aerated for 150 seconds

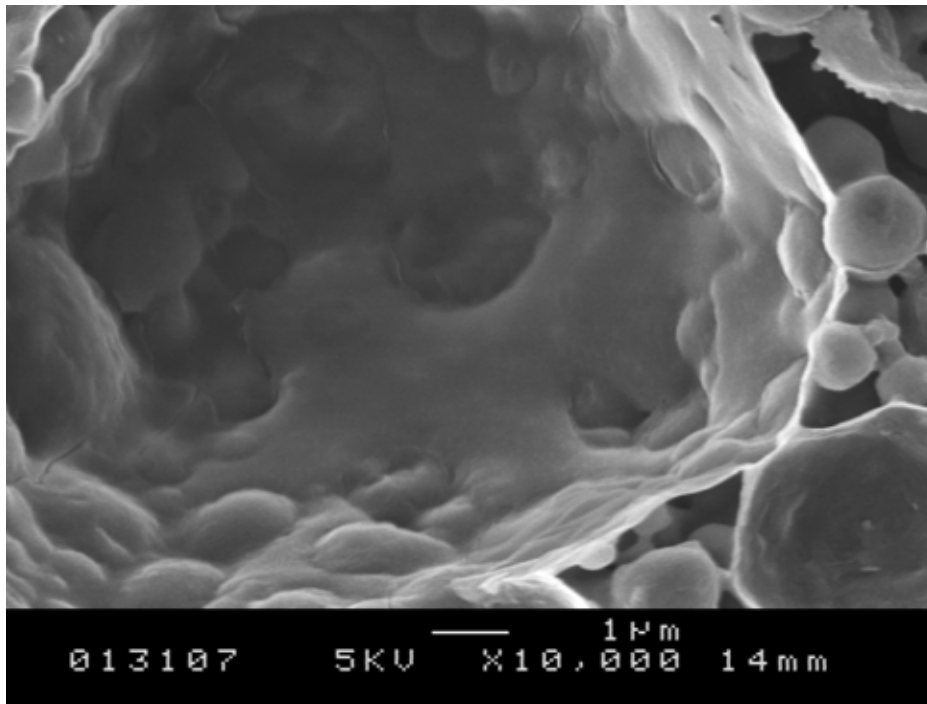


Figure 3.67 J. Sainsbury's aerated for 150 seconds

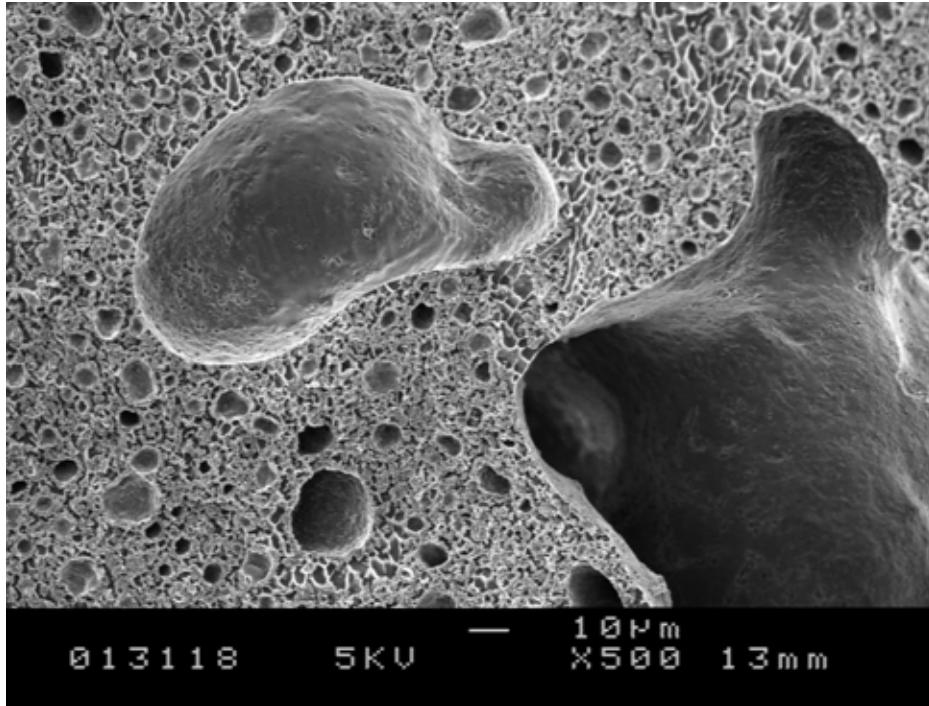


Figure 3.68 Elmlea Full Fat aerated for 150 seconds

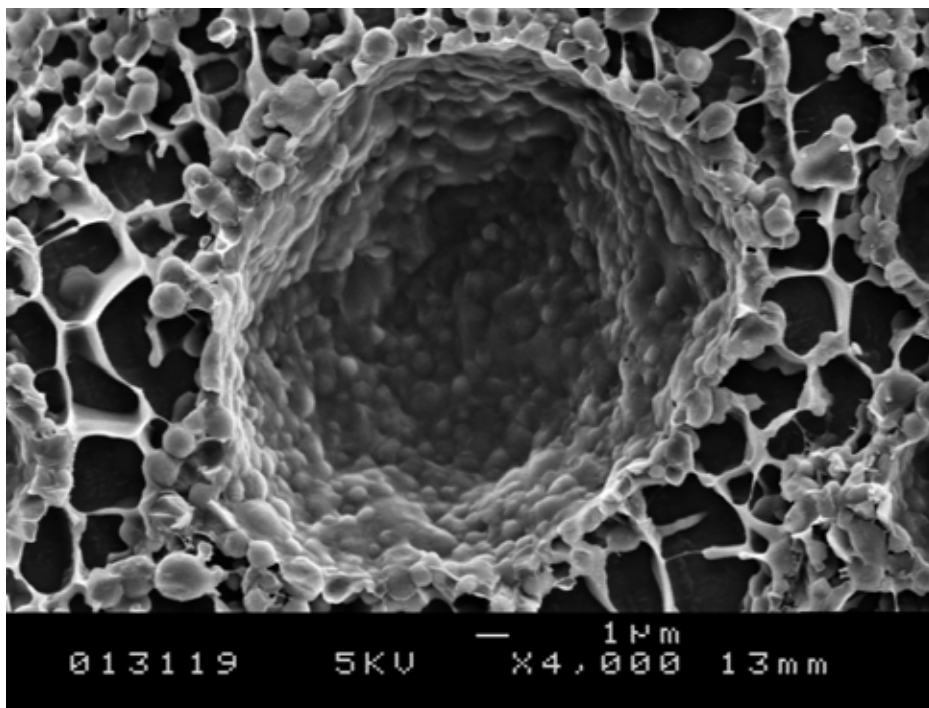


Figure 3.69 Elmlea Full Fat aerated for 150 seconds

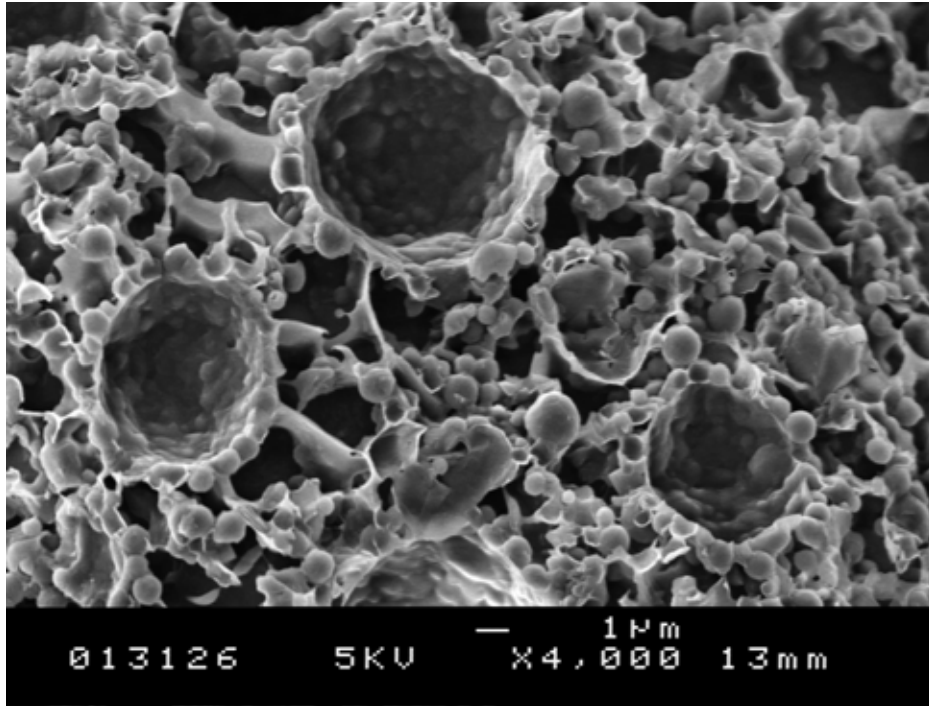


Figure 3.70 Elmlea Full Fat aerated for 150 seconds

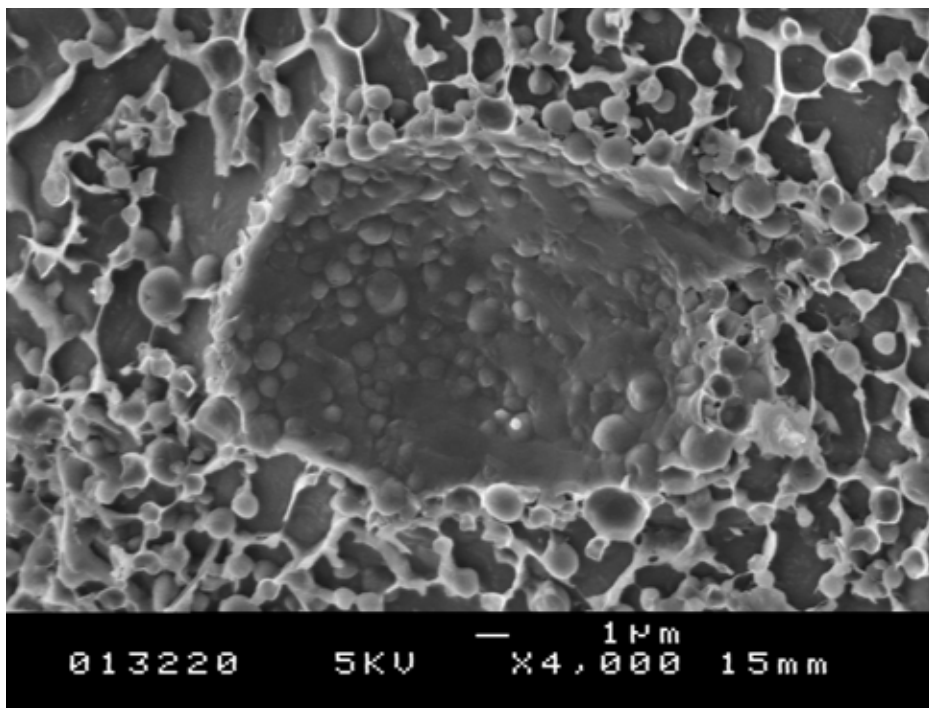


Figure 3.71 Elmlea Light aerated for 210 seconds

3.4.2 Comments on micrographs of the aerated commercial samples

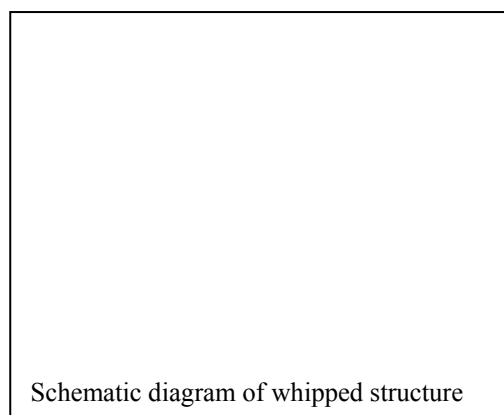
The micrograph for the aerated J. Sainsbury's dairy whipping cream is shown in Figure 3.66 and Figure 3.67. The first micrograph in each of the sets presented on each page is always a low magnification image, followed by a high magnification micrograph which was mostly gathered from a sub-section within the low magnification image. The whipped cream shows the typical fat globule coverage of a bubble surface, consistent with that of a whipped cream structure. The high magnification image shows the exact anchorage point of the fat globules on the bubble interface.

The Elmlea Full Fat micrographs in Figure 3.68, Figure 3.69 and Figure 3.70 show the fat distribution and the bubble stabilisation of the interface with the fat particles which follows a similar mechanism to the dairy whipped cream. Possibly the only difference is the presence of an aqueous phase between each of the air bubbles. These aqueous phases within the matrix can be distinguished by the presence of voids which have formed a honey-comb structure.

The final microstructure is of Elmlea Light shown in Figure 3.71. Seemingly the fat particles are not as close packed on the bubble interface on this cream as they are with the Elmlea Full Fat cream. Between the fat particles on the interface it seems as if liquid oil has also pooled on it. This behaviour is not seen with the Full Fat variety, but this might be due to the higher level of

liquid oil in the Light variety compared to that in the full fat cream.

Figure 3.72 to Figure 3.75 are of mix 1 and will be discussed first (the mix with 10 percent hard oil and 24 liquid oil), this is then followed by mix 3 (20% hard oil & 14% liquid oil) presented in Figure 3.76 to Figure 3.79 and finally mix 6 (with only 34% hard oil) which will be the last to be discussed and is presented in Figure 3.80 to Figure 3.83. For each of the mixes a peak whipped sample was gathered and an overwhipped sample was also gathered. Following the definition above, 'peak whip' will be taken as the time-point of highest Overrun within the 'stop-start' whipping curve. Again the micrographs are presented consecutively, first the peak whipped images, with a low magnification and later a high one, and then the overwhipped ones, again with a low magnification and high magnification image (except for Mix 3 which presents a peak whipped micrograph next to an overwhipped one, this was done in order to be able to compare the structures side by side).



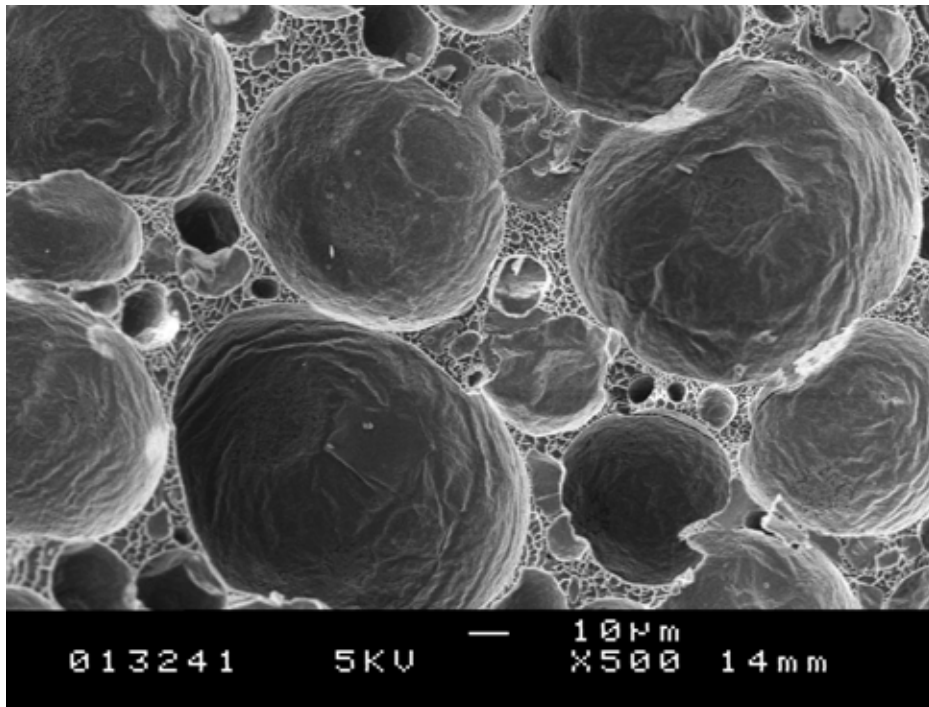


Figure 3.72 Mix 1, peak whip, aerated for 11 minutes

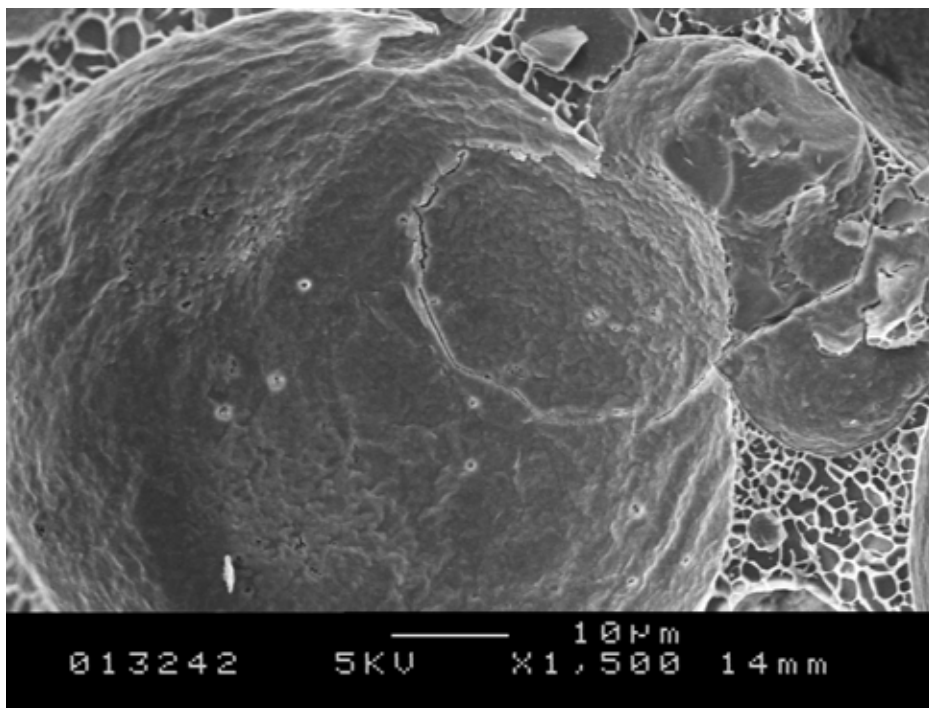


Figure 3.73 Mix 1, peak whip, aerated for 11 minutes

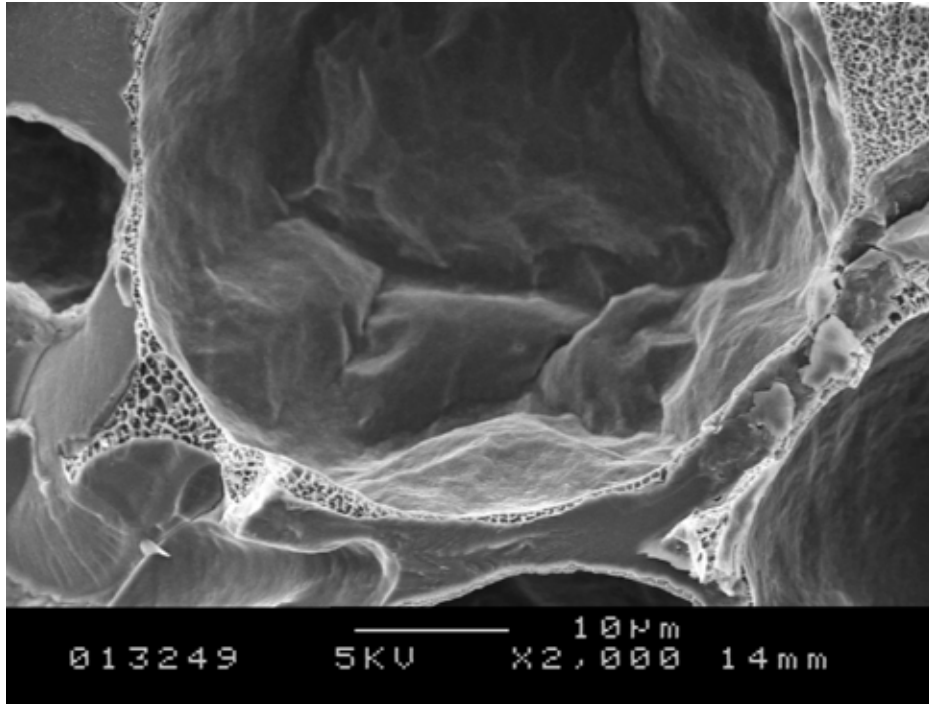


Figure 3.74 Mix 1, overwhipped, aerated for 30 minutes

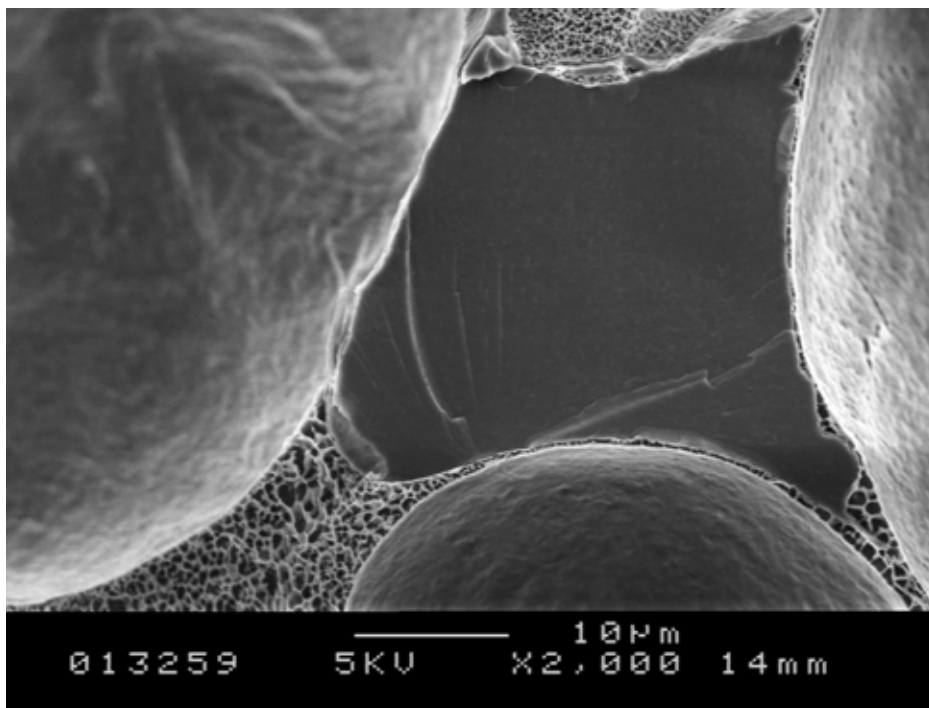


Figure 3.75 Mix 1, overwhipped, aerated for 30 minutes

3.4.3 Comments on Mix 1 micrographs

An interesting point to note is the composition of the bubble interface with this mix. The bubbles are very rough and crumpled in texture. In Figure 3.73 the oil layer is partially in the matrix and also partially covering the bubble, forming a cap-like structure. This behaviour was also captured in the micrograph obtained with light microscopy where the liquid oil was also pooled on the bubble interface in a similar fashion, which can be seen in Figure 3.35.

In the peak whipped samples (the first two images) the oil is distributed in the matrix in discrete pockets. But in the overwhipped samples (the final two images) the oil has pooled in larger blocks. In Figure 3.74, with a block size of about 20 μm and in the final image, Figure 3.75, a block size of nearly 30 μm (the dark structure in the middle). Another interesting feature is that between these blocks a very thin aqueous layer has formed between the oil and the bubble interface. Evidence of this is a small void between the oil particle and the bubble surface. The characteristic structure and evidence of the presence of water through honeycomb-like hatchings is evident. This is particularly visible in Figure 3.75.

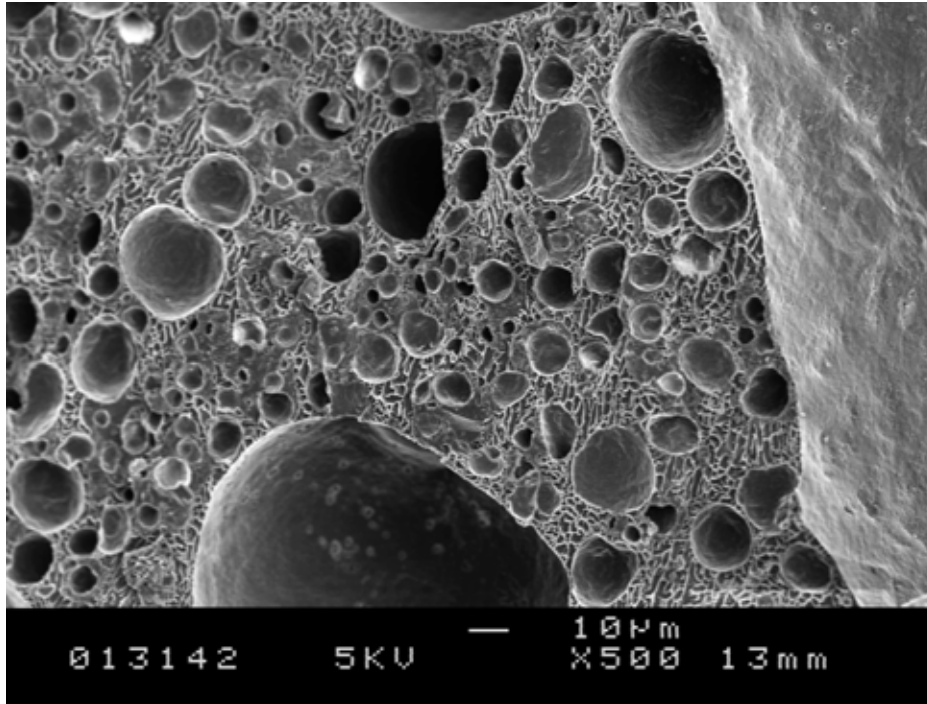


Figure 3.76 Mix 3, peak whip, aerated for 7 minutes

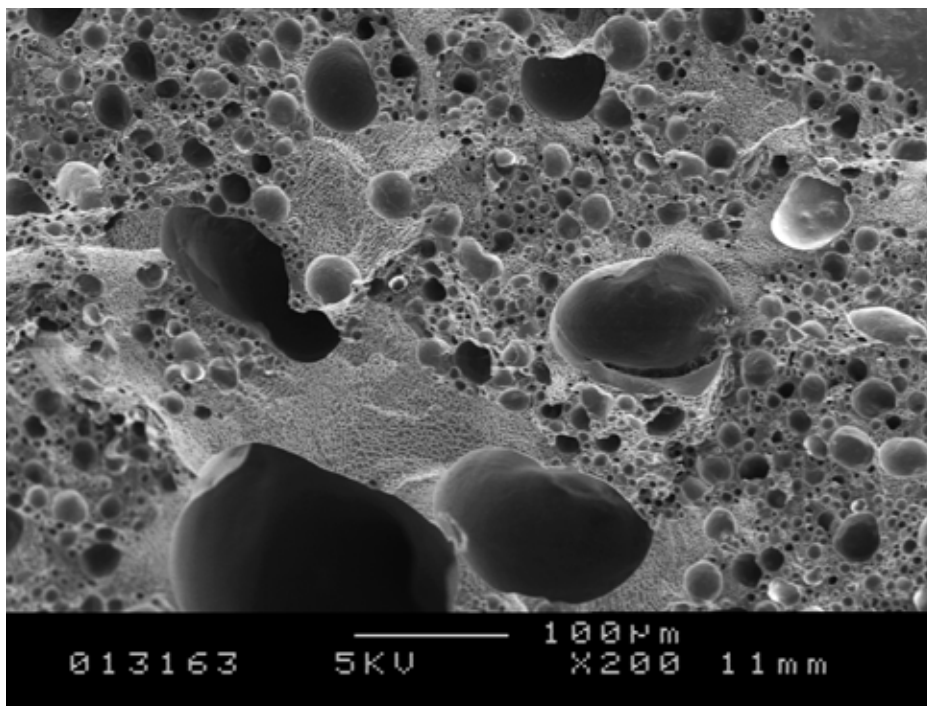


Figure 3.77 Mix 3, overwhipped, aerated for 30 minutes

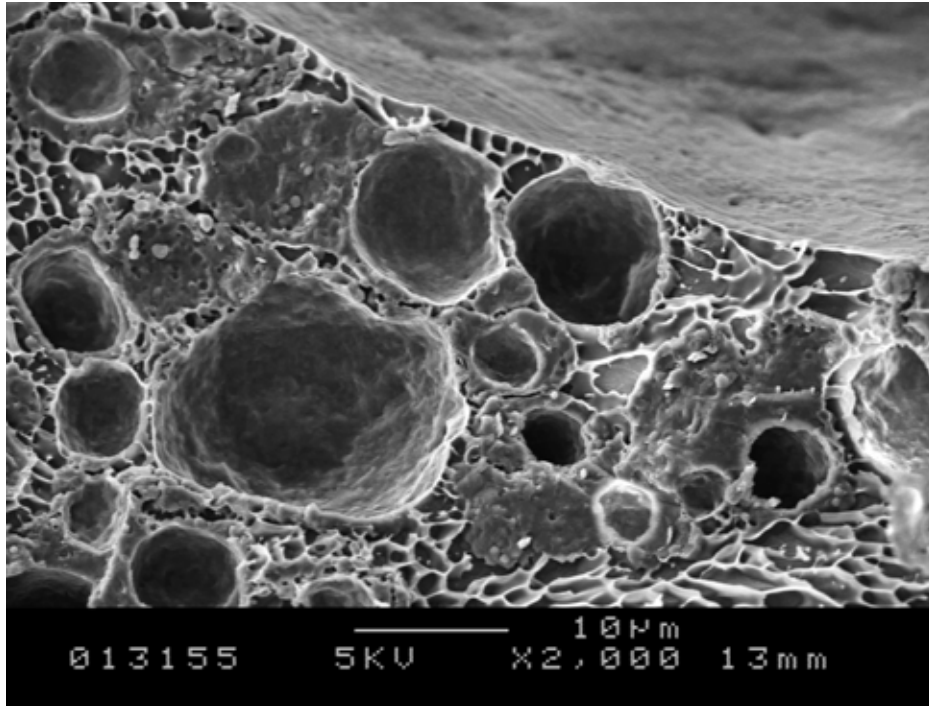


Figure 3.78 Mix 3, peak whip, aerated for 7 minutes

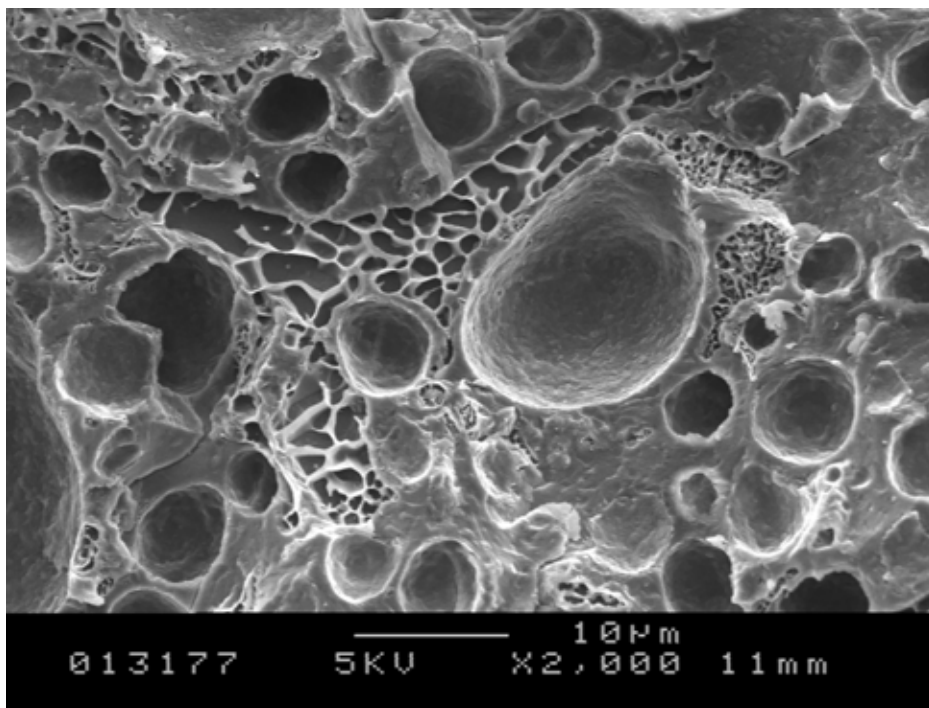


Figure 3.79 Mix 3, overwhipped, aerated for 30 minutes

3.4.4 Comments on Mix 3 micrographs

Mix 3 is the only reformulated mix where the peak whipped and the overwhipped micrographs have been placed side by side. This was done in order to be able to compare the structures of each of the two whipped cream structures. In the other mixes this type of comparison was not possible, and there the low magnification and high magnification images of each whipping regime were the ones placed next to each other.

Visually the oil layer in the peak whipped sample in Figure 3.76 but especially visible in Figure 3.78, seems rougher and more brittle than that in the overwhipped regime, visible in Figure 3.79. In the overwhipped regime the oil structure seems a lot smoother. The oil and aqueous phases seem well mixed in the peak whipped structures, with an even distribution of each of the structures throughout the image. The aqueous phase in the overwhipped samples shows a patchy distribution of the aerated and congealed fat particle droplets. The oil phase seems fairly aggregated. Aqueous zones are again evident and present where the honeycomb structure has been left behind after freeze fracture of the sample, sublimation and coating, which took place before the imaging began. The oil sections in the image are those that mainly contain the majority of the bubbles. The next micrographs that follow are those of Mix 6, which are captured in Figure 3.80 through to Figure 3.83. Mix 6 is the mix that contains 34 percent hard oil and no liquid oil.

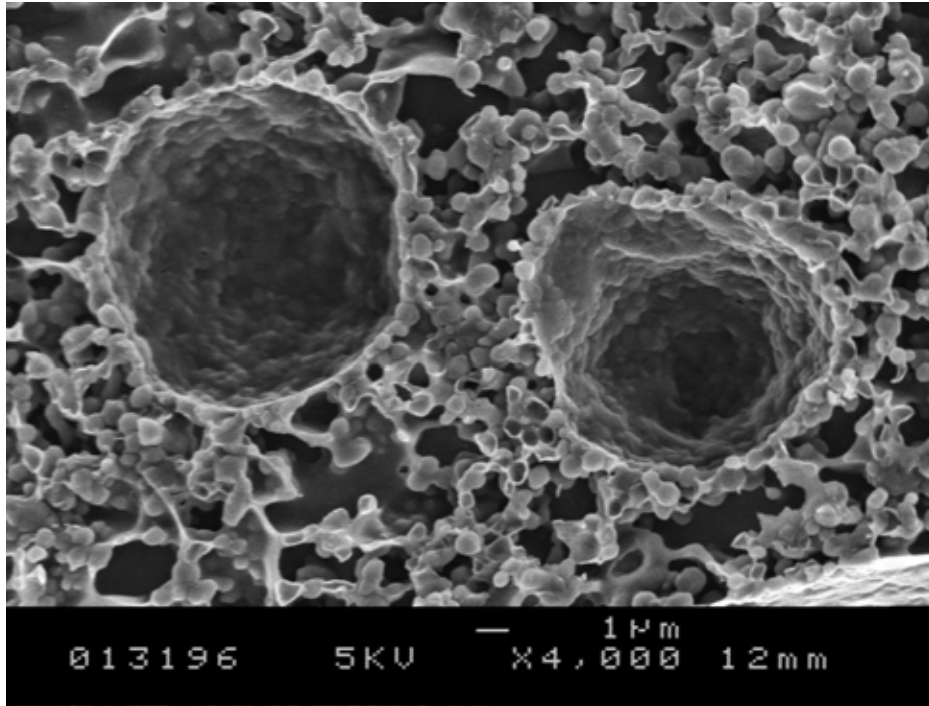


Figure 3.80 Mix 6, peak whip, aerated for 4 minutes

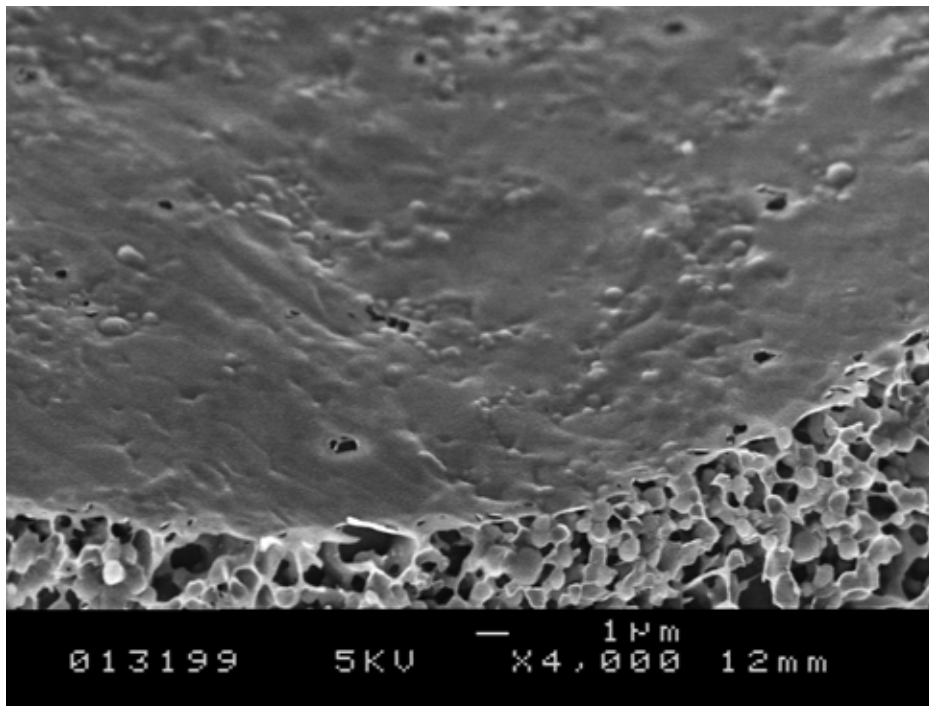


Figure 3.81 Mix 6, peak whip, aerated for 4 minutes

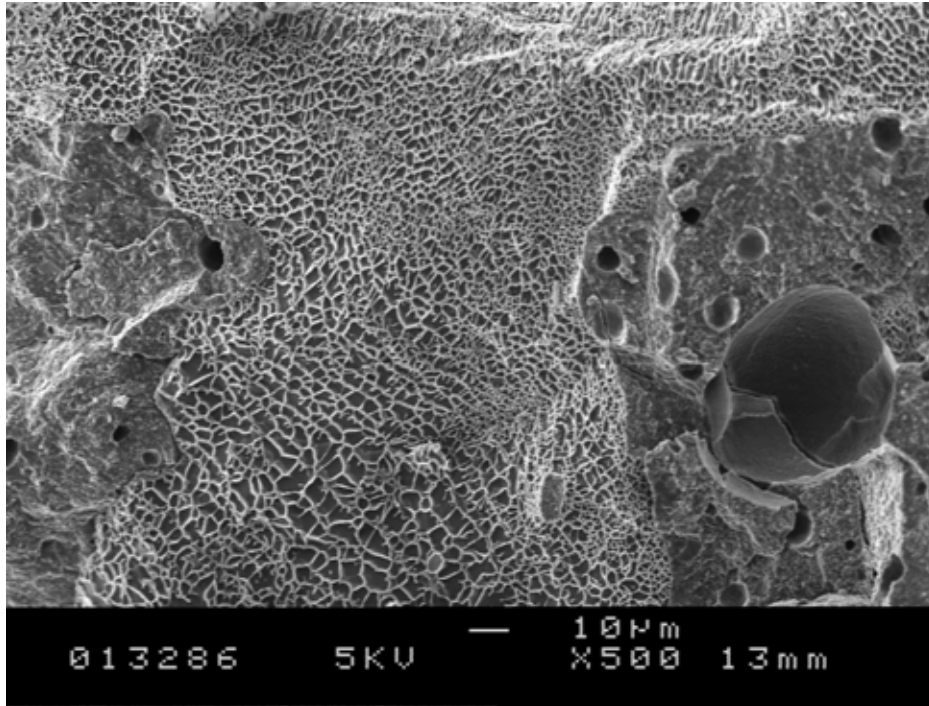


Figure 3.82 Mix 6, overwhipped, aerated for 30 minutes

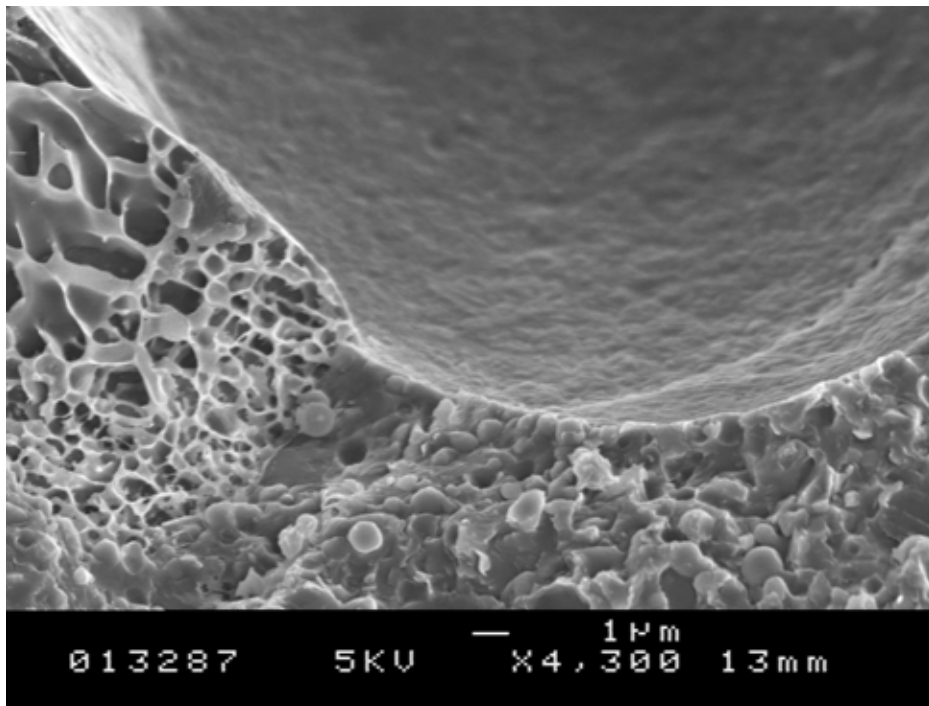


Figure 3.83 Mix 6, overwhipped, aerated for 30 minutes

3.4.5 Comments on Mix 6 micrographs

The peak whipped structures of Mix 6 are the only ones that have a similar fat particle association and distribution on the bubble interface as that of the Elmlea or the dairy creams. It is seemingly the only reformulated cream that has actual particles adhered on the bubble interface, as evident in the micrographs in Figure 3.80 and Figure 3.81. Mixes 3 and 1 have fat in the vicinity of the bubbles but they do not form part of the interface as with Mix 6. It is therefore not possible to call any of the reformulated mixes “Elmlea-like”, as the fat does not behave on the interface anything like it does on the Elmlea creams. Only Mix 6 seems to approximate to a degree the Elmlea behaviour, especially if one compares Figure 3.69 and Figure 3.80, the images are indeed not very different one from the other.

The final two images, Figure 3.82 and Figure 3.83, of the overwhipped structure show the aggregation behaviour of the oil around the air particles (in Figure 3.82 the whole dark square at the bottom right, is aggregated oil, which is surrounded by the typical water honey-comb structures). The final image shows how a bubble is both stabilised by the aggregated oil (present on the bottom right of the image), but is also surrounded by an aqueous layer (on the bottom left). Where the bubble meets the aqueous phase it is covered by a very thin interfacial active species. The bubble is fragile in the extreme, due to a very thin interface which was dissected during sample preparation and can be seen on the top left.

The interface of the peak whipped structure is also very thin (Figure 3.81), evidence of this are the thin artefacts (visible as black holes) that have been left behind on the bubble interface when the water sublimed off during sample preparation. This is particularly visible on the high magnification image.

The high magnification image also shows how thin the bubble interface really is and also shows the aggregation of the oil droplets forming an interlinked network, bead-like, around the bubble.

As a final remark to the reformulated mixes, it can be said that the ratio of liquid oil to hard oil is evidently affecting the aerating properties of the cream (which can be seen with the Overrun values obtained in Figure 3.30). This is unlike the Full Fat Elmlea and the Light versions of the commercial creams, where the fat particles are attached to the bubble surface and create a rigid network around it (e.g. in Figure 3.69 and Figure 3.71). The fat phase in the reformulated mixes behaves very differently and is seemingly just instrumental in creating the bulk thickness of the continuous phase (seen in Figure 3.75 and Figure 3.79). This in turn then dictates how the active emulsifier and foaming species, which are both contained at the same concentration level in each of the six emulsions, will perform in the mix. The only cream that has fat particles associated to the bubble interfaces is Mix 6, visible in Figure 3.80.

3.5 *General discussion*

For the slumping experiments, rendering what is essentially a 3-D object

into 2-D might add some experimental error to the results, but it can be argued that this method is a good way of turning “qualitative” data into a “quantitative” measure. The errors that arise through using this technique could perhaps have been the underestimation of the area measured, for example because the standing cream either leant towards or away from the angle it was photographed at, obscuring some of the surface area and placing it out of view.

Another sampling artefact might have been that the camera may not have been placed in the exact same position each time. However by ensuring that each of the pictures taken are similar and the scale bar appears the same size, this sampling artefact is eliminated.

For the initial analyses of the fat phase of the commercial samples, where these were boiled and spun down, then later allowing the sample to congeal at ambient temperature will have introduced an unwanted ‘tempering’ step to the isolated fat. Analysis of the cream without isolation of the fat phase gives a completely different melting and crystallisation profile. This analysis was then used throughout the remainder of the study, i.e. for the DSC traces in Figure 3.20, Figure 3.21 and Figure 3.22 (and also the traces contained within Appendix 4).

For all further assessments of the fat phase, only Elmlea creams that had not been heat treated were used. The DSC traces of the separately isolated oils have not been included.

Bell et al. (2007) mention that small viscosity measurements are commonly used to monitor changes in fat rheology due to crystallisation, but that the application of shear can destroy some of the delicate interactions present in fat systems. The aim of their study was to compare the rheology during crystallisation of three fats differing in composition but with similar melting profiles, and to study any effects of the crystallization on subsequent melting of the fats after solidification. Similar work was undertaken in this study, but using a commercially available cream and reformulated mixes. The system studied keeps the same base level mix of stabilisers, emulsifiers and proteins, but the ratio of hard oil to liquid oil is changed, and the total oil phase always remains at 34%. The viscosity of Mix 1 was much less than that of Mix 3 and this one in turn was less than that of Mix 6, as might have been predicted just through empirical assessment. Rheology with the reformulated mixes was carried out only at 25 °C. 10 °C was not selected as only 25 °C was of interest, as this was also the temperature at which the cream slumping was carried out at.

Narine and Marangoni (1999) outline the levels of structure which are present in a typical fat network. These are defined by the authors according to the way the fat crystallizes from the melt. They mention that growth of a fat crystal network can be visualized in the following way: Firstly, that the triglycerides present in the sample crystallize from the melt into particular polymorphic/polytypic states. These crystals then grow into larger

microstructural elements ($\sim 6 \mu\text{m}$) which then aggregate via mass- and heat-transfer limited processes into larger microstructures ($\sim 100 \mu\text{m}$). The aggregation process continues until a continuous three-dimensional network is formed by the collection of microstructures. Trapped within this solid network structure is the liquid phase of the fat (Narine and Marangoni, 1999). These partially coalesced phases are those responsible of forming a structure during the whipping process, which initially is in charge of creating and sustaining the highest Overrun level of each mix, which then through further re-whipping gets expelled from the bubble interface and leads to the cream collapsing.

In relation to a cream's rheological response, Narine and Marangoni (1999) mention that the microstructures are nearest level of structure in size after the macroscopic network. This is because there have been no other structural building blocks identified in fat crystal networks that are larger than the microstructural level. Consequently, the level of structure that is immediately stressed when the network is stressed (such as when rheological measurements are performed) is the microstructural level. Heertje (1993) has shown that parallel plate compression of a fat crystal network results in a breakage of the links between microstructures, whilst the microstructures themselves remained intact. Of course, catastrophic breakage of the entire structure would result in complete breakage of levels of structure below the microstructures (such as the links between microstructural elements as well as the crunching of actual microstructural elements). However, for compression and shear measurements that involve only small deformations within the elastic limit of the network, it

seems likely that only the links between microstructures are stressed when the network is stressed. It follows, therefore, that the rheological behavior of the network at small deformations (small strain levels) is a reflection of the microstructural more than any other structural level in the network. It must be realised, however, that the microstructural organization is due to the manner in which the other levels of structure are arranged, therefore implicating all levels of structure in the determination of the mechanical strength of the network. However, Narine and Marangoni (1999) are of the opinion that it is essential to assign more importance to consideration of the microstructural level than has been the case in the past. Narine and Marangoni (1999) argue that as it could be appreciated from the above argument, a consideration of the polymorphic nature and lipid composition of the network in isolation ignores the crucial role of the microstructural level in influencing the mechanical strength of the network.

In addition to the rheological response of the microstructural network in a cream, it would be interesting to test the reaction of the whipped cream to a difference in pressure, or it's rearrangement to a pressure cycling regime. Work of this nature would feed into work discussed in following chapters of this thesis.

According to Narine and Humphrey (2004) the addition of fully hydrogenated fat will increase the Solid Fat Content of the sample since more of the sample is then solid at 20 °C due to the addition of the higher melting fat

as well as the formation of successively higher melting compounds.

The results indicate that increasing the levels of hydrogenated oil has a direct impact on the aeration and rheological response. Increasing the level of hydrogenated oil prevents the cream from obtaining high Overrun levels.

The use of a Kenwood Chef as described in the original patent (Morrison et al., patent number US 005149557 A) was used for aerating the emulsions throughout this study. No claims are made on the packaging of the commercially available products with regards to optimum whipping times. No suggestions are given. Through experimentation two and a half minutes were seen to be long enough to reach at least something in the order of the highest overrun. For fresh double whipping cream, this was a time that if further whipping would have taken place, would have led quite easily to over-whipping. With fresh double cream and the Elmlea, any less than one minute did not build up enough structure and led to an aerated liquid, but not a stiff mix.

The patent also describes that Elmlea has in general been formulated to whip in less than 6 minutes, but in addition has also been treated and tempered to be whippable within a 4 minute time-frame. The Elmlea quite easily whips within a 4 minute time-frame. In general, for the Elmlea Full Fat and Light by 4 minutes, overwhipping already begins to take place.

For the Elmlea, directly after homogenisation and manufacture the cream is chilled to below 15 °C straight away if possible. It is then warmed and held at 15 to 20 °C for several hours. It is then cooled again. The tempering step comprises holding the cream at 15 to 25 °C for a further 18 to 30 hours, after it has been manufactured (Morrison et al., 1992). An interesting point to note is that these two ‘boundary’ temperatures, 15 and 25 °C, are exactly those two temperatures at which the first peak appears in the DSC analysis of both the Light and Full fat versions of the Elmlea cream. These must be directly attributable to the tempering step.

The Elmlea whipped cream exhibited interesting behaviour after 4 minutes whipping, after this time-period the maximum overrun value has been achieved on the full fat variety. If one observes the standard deviation of the mean after the 4 minute time-period, it decreases substantially in the next value, at 270 seconds (together with the overrun measured) after which, progressively, overwhipping sets in. Overwhipping in addition to a diminishing Overrun brings with it an increase in the error bars.

For the Light version of the Elmlea double whipping cream, the maximum Overrun sets in 30 seconds prior to the 4 minute guide time (at 210 seconds). After this time, overwhipping takes place and in addition a more marked increase in the error bars can be seen. These error bars are larger than those on the full fat cream.

All the experiments that were carried out on the commercially available products used double cream and the Elmlea “light” version of the double cream. This was the only Elmlea whipping variety commercially available in the Birmingham area. It was later seen that Elmlea also has a (non-double) whipping variety, but no further tests (bar Overrun measurements), were carried out on this one. This one was not available in Birmingham though.

In order to create homogeneous whipping conditions over the entire volume of the cream to be whipped, it is recommended that a planetary mixer be used. Although the whipping conditions are created to a large extent, even through the use of a planetary mixer a completely homogenous cream mixture is not created, as there are always pockets where the whisk does not reach (especially on the side walls and the bowl bottom) once the cream begins to stiffen and whip. This does not pose such a problem when the mix is initially liquid and can slip back into the centre to be folded in again. It was thus ensured that when samples were extracted for analysis, that only those parts of the middle and the whipped sample were taken out of the bowl, and the slightly softer and un-whipped sample was left behind around the bottom and the edges. If the sample was to be whipped again (in the stop-start mode), then it was ensured that the softer foam was folded back into the centre to be re-whipped again, to create as far as possible a homogenous mixture.

In the reformulated mixes, softening a cream by only replacing the hard oil fraction by a difference of 5 percent with liquid oil has a dramatic effect on the

resultant microstructure. The softening 'limit' was reached with mix number one where the hard to soft oil ratio was 10 to 24 percent. Once the maximum Overrun was achieved, it remained at this level for the duration of the aeration event (except in Phase IV), where increasingly de-aeration began to take place.

Mix number six, with 34 percent hard oil, hardly aerated at all. Subsequently after maximum overrun was obtained, which took place after a very short time, overwhipping set in almost straight away, bringing with it a clear change in microstructural behaviour. Mix 6 was one of the few mixes where a distinct graininess was visible during phase II and part of phase III. In all the other creams the overwhipping stage was less dramatically punctuated by a change in microstructure, where the changes were mostly quite subtle. If slight graininess of the mix took place this would not have been as marked as in Mix 6.

Curiously from the SEM images, Mix 6 was really the only cream that showed any microstructural similarities to those of the Elmlea cream, with the fat droplets aggregated at the air interface of the bubble. All the other reformulated creams hardly had any oil associated with their interfaces. The interfaces were mainly smooth and the oil layers and globules of partially coalesced fat were very often in the matrix phase. In some formulations the oil was clustered around the interface in crescent or lens shaped structures, but these did not resemble anything like the structures present in the Elmlea or the dairy cream.

3.6 *Concluding remarks*

Through the use of multiple techniques the entirety of a whipped creams' behaviour has been categorised. The comparative reformulated structures manufactured from an initially hard oil emulsion which was progressively softened with varying levels of liquid oil, allowed the limit of 'softening' of an emulsion to be quantified. This limit was reached with a cream containing 10 percent hard oil and 24 percent liquid oil. The un-softened emulsion contained 34 percent hard oil. It was seen that the commercially available Elmlea whipping creams have very different Overrun profiles to that of a dairy whipped cream like J. Sainsbury's which begins to overwhip after only just 150 seconds. This behaviour of Elmlea, where overwhipping sets in very slowly is due to the fact that both the light and full fat versions have been 'softened' with liquid oil.

The interesting finding is the behaviour of the Elmlea creams within the tribometer, where through aeration a Light formulation acts more like its unaerated Full Fat counterpart.

In addition with the reformulated creams it was also shown that the optimal whipped and re-whipped structures were different in their melting behaviour. The re-whipped structures melted slower than those of the peak whipped creams, which generally melted first. This behaviour correlates with the structures seen in the SEM micrographs. The peak whipped structures are fragile distributions of partially coalesced fat particles on or near an air

interface, which are also present within the creams' matrix. In contrast overwhipped samples are large lumps of oil which have been aerated but which are largely congealed. They are unable to re-form the partially coalesced structures that were created initially and thus exist as a conglomerate once overwhipped.

CHAPTER 4

Model foam and its pressure stability

4.1 *Introduction*

This chapter describes development of an experimental methodology to study the effect of pressure change on the stability and coalescence of bubbles in a foam, where the foam was subjected to an increase in pressure, subsequently followed by a decrease. These pressure changes either took place once only, or different cycles were carried out to simulate repeated exposure to pressure fluctuations. The particular concept in the experimental design was the direct and 3D imaging power offered by confocal microscopy to visualise microstructures even in fairly turbid systems. This capacity therefore allows the study of more complicated foam mixes in-situ.

A foam was chosen which showed resistance to coalescence and creaming over a period of a few days in quiescent conditions, formulated using a lipogel emulsifier (Krog, 1997). In the current model mix formulation, PGE (a poly-glycerol-ester of fatty acids) was used together with whey protein in a solution of corn syrup. The foam was analogous in formulation to the whipped cream prepared for the work carried out in Chapter 3. This statement holds true as the whipped creams contained an emulsifier and a protein too, similar to the model mix foam, which will be used in the following chapters. The difference in the whipped cream system to the one used throughout Chapters 4 and 5 is that the

continuous phase in this case will be corn syrup and for the whipped creams it was Palm- and Rape-seed oil. The PGE together with the viscosity of the Corn syrup, in the model foam mix, conferred the long range stability required, in order for the foam not to collapse immediately after preparation. However, when the foam was subjected to a pressure increase from ambient conditions followed by a pressure decrease back to ambient then coalescence could be observed. It can generally be said that a disturbance of any nature caused coalescence within the foam. Through a better understanding of foam stability within such process steps as mentioned in Murray et al., (2002a), it is ultimately hoped to be able to formulate systems that allow better control of the foam structure in dynamic processes.

Various experiments were carried out to test the stability of the model foam, they could be categorised primarily into tests performed under quiescent conditions, and tests undertaken under dynamic conditions.

Examples of quiescent conditions were where the sample was left to cream, without any further intervention other than observation; this was included in section 4.2.2. To contrast this, and build on the knowledge base, rheological tests were then performed on samples where the test sample was left on the bench to disproportionate for 5 hours. For the purposes of this work this procedure was still considered a ‘quiescent’ test as no extraneous pressure or shear changes were applied to the sample, this too is presented in section 4.2.2.

A variation of this disproportionation test was also performed. To counter-act ageing of the foam, the master batch method was used. In the master batch method, sample inversion takes place every 15 minutes for 5 hours. After this the sample was then analysed rheologically.

Examples of dynamic conditions were many and varied. A video was captured of the release of the last few bar from the pressure chamber, this was discussed in 4.2.1. Further analysis of dynamic conditions included: pressurisation of the foam on a micro scale. This took place in the pressure cell. In addition bulk pressurisation of a ‘macro’ sample in a large pressure tank also took place. These results are presented in section 4.2.5. Some further tests where the sample is subjected to multiple pressure cycles is discussed in 4.2.6 and finally, where a sample is subjected to a high pressure cycle and low pressure cycle is discussed in 4.2.7

4.2 Results and Discussion

4.2.1 Dynamic video sequence and bubble imaging

Through a very slow release in pressure it was possible to capture a dynamic video using the current CSLM setup.

For the capture of a dynamic video sequence the pressure was released slowly and continually from 3 bar to 1 bar, this cannot therefore be directly compared to a pressure release rate experienced during a normal experimental

run. It was performed slow enough in order to catch the bubble dynamics with the confocal setup. But it did visually confirm the mode of coalescence taking place within the system. The release rate for the video capture was in a different ball-park to that used during a normal pressure cycle. No accurate numbers are available for the rate of release, but the entire duration to release the pressure from 3 bar absolute to 1 bar absolute took 90 seconds. This compares with just a matter of a few seconds per bar in a normal pressure release, like that undertaken during release within a single pressure cycle (for example in Figure 4.9)

Under pressure, and subsequent pressure release, some of the bubbles in the aerated mix coalesce in a very short space of time and over a very small pressure difference window. As the actual coalescence events themselves take place relatively slowly due to the viscous nature of the system they can be captured in near 'real time' sequences using the current CSLM setup.

Results with the CSLM are promising as visually it is possible to infer parts of the foam failure mechanism through direct observation of distortion and rupture of the films which are characteristic of two touching bubbles. Evidence of this can be seen in Figure 4.1 which represents images taken from a dynamic video sequence of a foam sample during depressurisation.

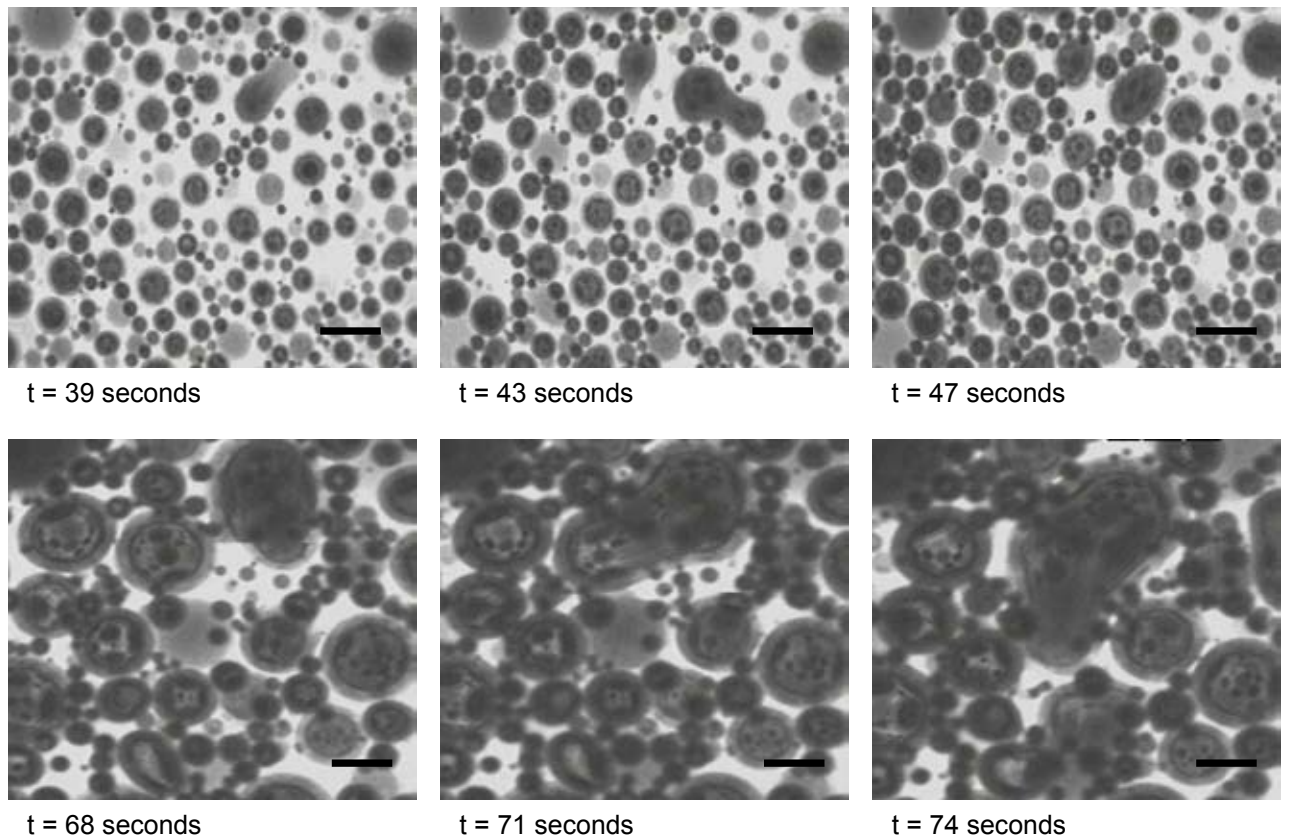


Figure 4.1: Captured coalescence events and time evolution from the first observed coalescence event captured within a dynamic video sequence. The video sequence was obtained during depressurisation from 3 bar absolute pressure to 1 bar absolute. Total run time of the video was 90 seconds. Scale bar is 200 μm .

Initially, in the dynamic video, before the final bars in pressure are released (Figure 4.1) at $T= 39$ seconds the small bubbles are spaced quite far apart. But coalescence is slowly starting to take place. With the pressure being released further, at $T= 43$ seconds, the coalescence events are taking place much more frequently now. Progressively as the bubbles get bigger, the distance from bubble to bubble grows smaller, which then also has as a consequence a more favourable environment for coalescence to continue.

Direct high resolution imaging of the foam clearly showed the benefits of the confocal imaging wherein the 3D foam structure and its connectivity could be partially observed (Figure 4.2). With some bubbles it was even possible to tell how many other bubbles were in its proximity. This key feature was of interest as it could help to generate an understanding of the mechanism of coalescence and foam structure ‘failure’. Another interesting feature that was observed was that in effect the bubbles being imaged were spherical in nature.

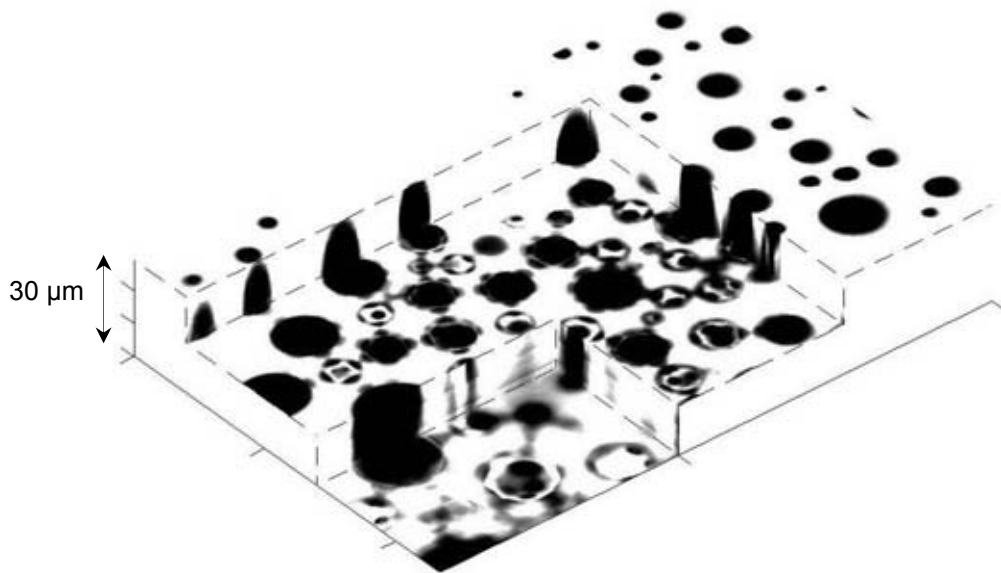


Figure 4.2: 3-D sectional slice at 40× magnification of a foam with an air phase volume $\phi = 0.6$. Each step in the reconstruct is 15 μm . 30 images were taken for the reconstruct. Displacement between images was 1 μm . Image dimensions were 768 × 512 pixels (each pixel 0.46 μm in size).

For this reconstruction a series of 30 micrographs were gathered from a typical fresh foam that had not undergone a pressure treatment. In the reconstruct the top most plane was the one that was imaged first and was the one closest to the coverslip (but at least 5 μm or more below it). Each subsequent image was taken within a distance of 1 μm away from the next, with the “floor” of the reconstruct 30 μm away from the first image taken.

4.2.2 Quiescent foam stability and drainage

The initial experiment was direct visual observation for creaming. This was carried out over a time period of 48 hours at ambient temperature. Various formulations were tested. It was observed that no visible creaming took place and no foam collapse took place for the formulation containing 70% corn syrup, 0.2% PGE and 3% whey powder that had been added to the mix once it had cooled down (labeled ‘whey separate’). The same was true even if the same ingredients (the PGE and the whey) were heated up separately and then added together before aeration. But on the other hand if the two ingredients were heated to 60°C together, this had disastrous consequences for the foam stability. This can be seen in Figure 4.4 (in the legend it’s the second sample, the dashed lines). In comparison, mixes were made, keeping the corn syrup as a base ingredient, but only aerating either PGE or the whey powder on their own. PGE had quite good stability, but still creamed before the end of the 2 days. The mix with whey on its own was nearly as poor as the one with whey and PGE heated together. Another whey powder, Bi-Pro (Davigo, Switzerland)

with a protein content of 95% w/w was also used. A mix was created with this sample to give the same protein loading as that contained in the standard mix which was used throughout the study. The whey powder used for the standard mix had a protein content of 12% w/w but only made up 3% w/w of the total mix (i.e. giving a 0.36% w/w total protein). Bi-Pro was added at this concentration to the mix which was studied in the creaming experiment. Its long range stability was not very good.

In addition to the creaming experiments a whipping experiment was also undertaken which is given in Figure 4.3, where two different Hobart mixers are compared with each other. The A200 Hobart aerated 2 litres of mix at 360 rpm and the N50 Hobart aerated 500 ml of mix at 580 rpm. The N50 Hobart was the one that was used throughout this study, as it was not feasible to use the large Hobart for some of the experiments in the following sections.

The whipping curves are nearly identical up until the 25 minute mark, after which they begin to diverge. The mix was hardly ever aerated to those higher overruns, for most experiments the foam was aerated for 25 minutes (or the time was adjusted accordingly dependent on the Overrun required).

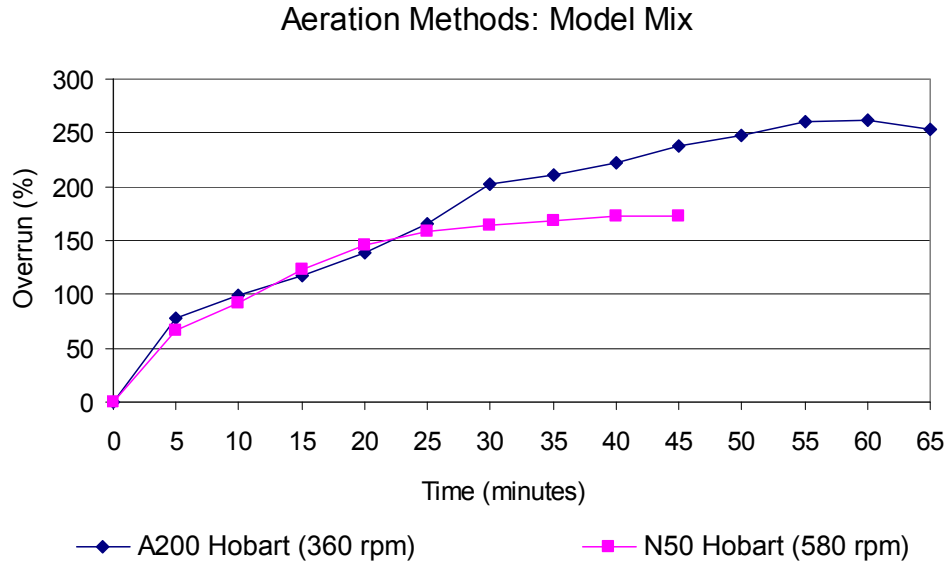


Figure 4.3: Achievement of different Overrun levels through the use of different sized Hobart mixers with different maximum speeds (in brackets).

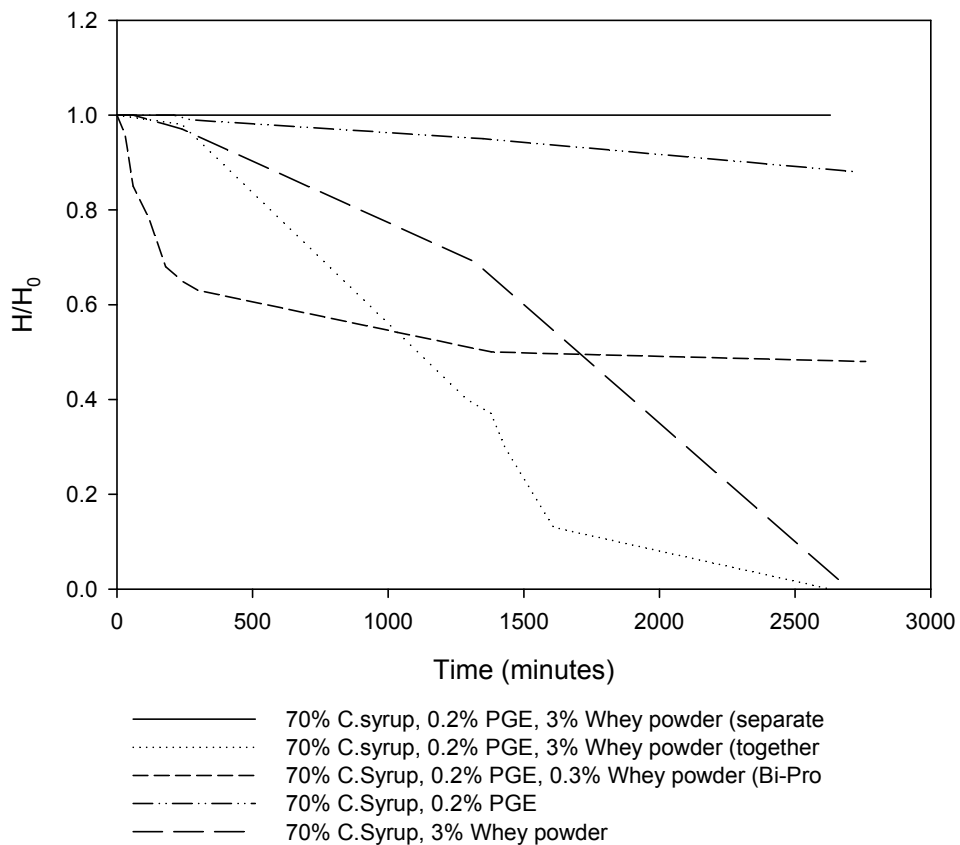


Figure 4.4: Foam creaming and collapse of the formulations over time. $H_0 = 100\text{ml}$. H_0 the initial level of the foam before the creaming experiment began, and H is the top level of the foam minus the serum level collected at the bottom of the measuring cylinder.

A further test of the quiescent properties of the foam explored the rheological characterisation of it to measure the moduli G' (the storage modulus) and G'' (the loss modulus) with time. In one experiment the foam was created and placed within the vane inserts of the rheometer. All the samples were covered with cling film and left on the bench until required. The samples were analysed every 30 minutes for a total of 5 hours. For each new 30 minute timepoint a fresh undisturbed sample was used. These samples would assess drainage and creaming phenomena taking place in the foam (Figure 4.5). In a further experiment the samples were taken from a bulk master batch. This typically showed little evolution of G' and G'' over time (Figure 4.7). Also the zero shear behaviour of the foam can be seen to have $G' > G''$ at all times and therefore has a relatively elastic gel like response and a microstructure resistant to change.

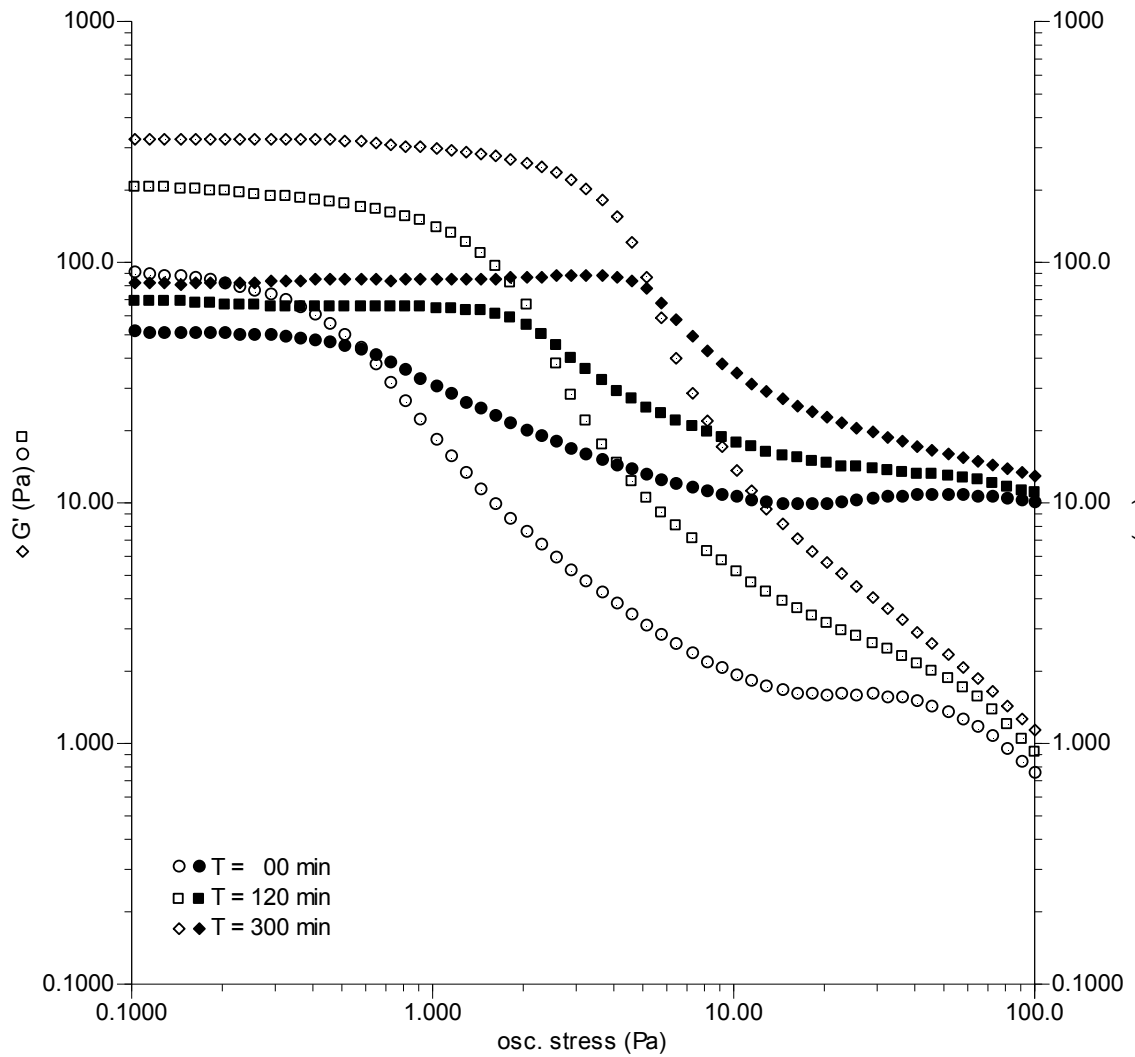


Figure 4.5: Drainage evidence. The sample once aerated was placed in multiple vane inserts which were sampled every 30 minutes up to a maximum of 5 hours. The results were gathered through oscillatory rheology at 1 Hz. Only the results for the start of the experiment, 2 hours and 5 hours are shown for clarity.

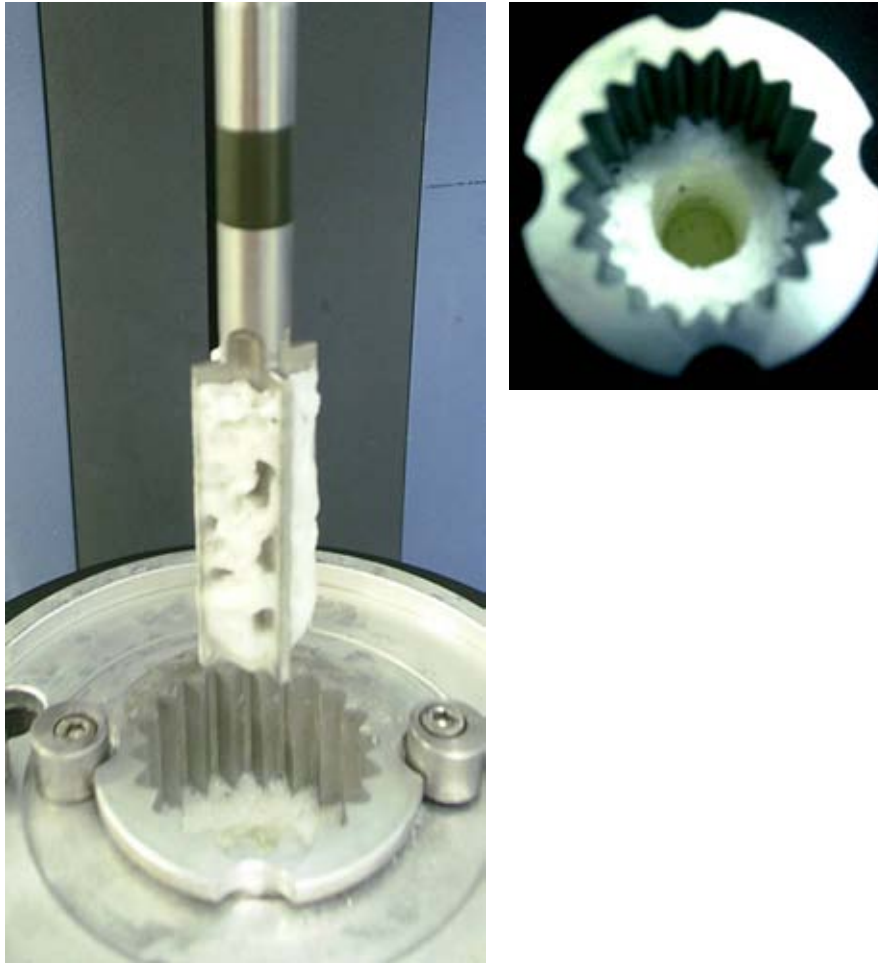


Figure 4.6: Vane Rheometer cup and geometry after carrying out an experiment with a “dry” foam from Figure 4.5. The coarsened structure of the foam can clearly be seen where it has left holes on the shaft of the vane. The foam is so dry that even the well that the vane created within the cup remains after the insert has been taken out.

Table 4.1: Cross-over point of G' and G'' at given oscillatory stresses for the 3 samples assessed in Figure 4.5

| Time | Osc. Stress Cross-over point (G' / G'') |
|-------------|--|
| 0 Minutes | 0.6 Pa |
| 120 Minutes | 2 Pa |
| 300 Minutes | 6 Pa |

In Figure 4.5 the Linear Viscoelastic region increases with time which reflects a build up of structure through the creation of a drier foam over time.

The G' and G'' cross-over point (Table 4.1) increases by one order of

magnitude over the 5 hour period which also reflects the structural change within the foam.

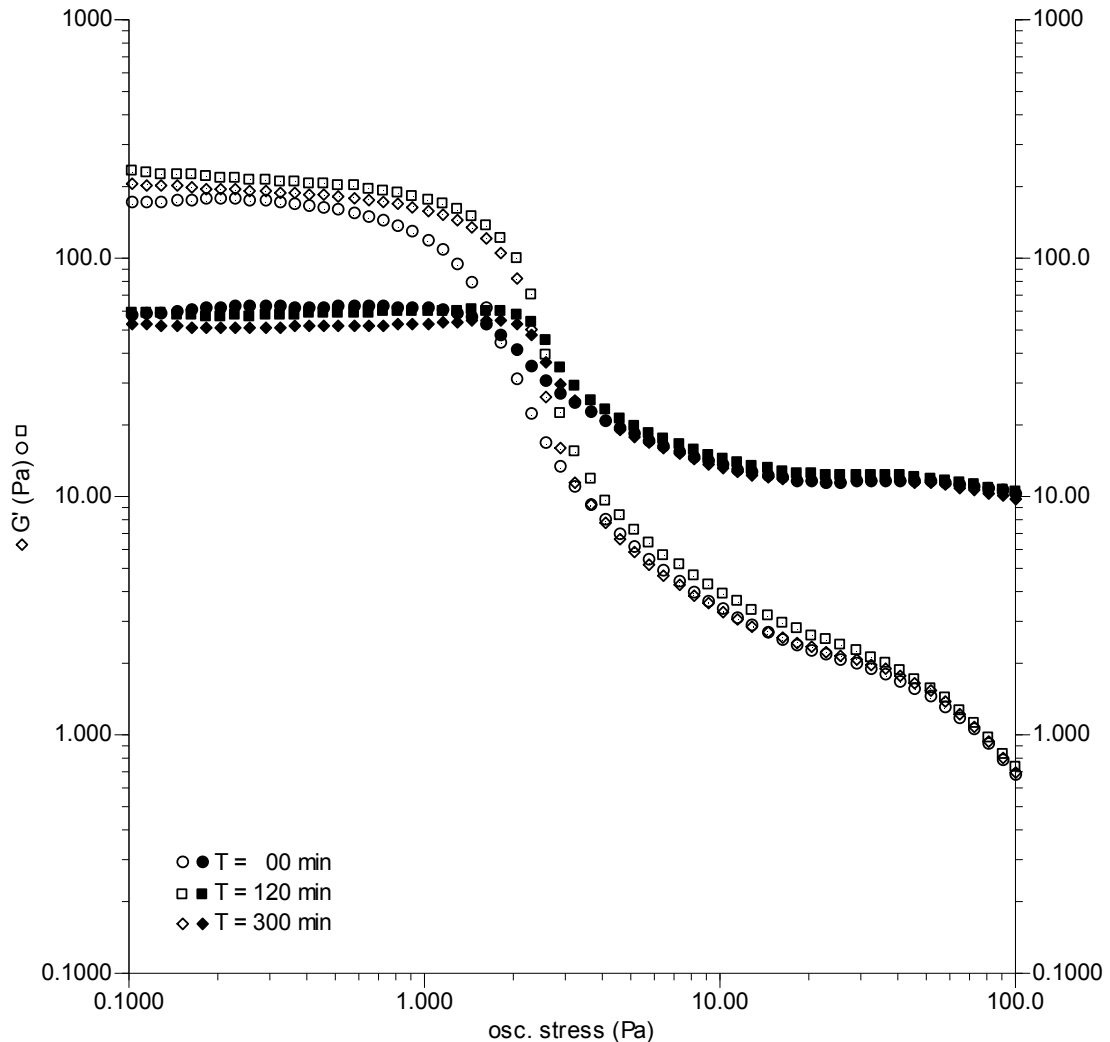


Figure 4.7: The samples for this experiment were taken from a bulk master batch. This was held in three 500 ml Nalgene bottles and inverted every 15 minutes for a maximum of 5 hours. Samples were assessed every 30 minutes. The results were taken straight after the foam was made, 2 hours and 5 hours after aeration and assessed with oscillatory rheology at 1 Hz.

The data sets in Figure 4.7 are closer together in comparison to those in Figure 4.5 as the sample is more liquid and the vane moved through the foam without creating the structures seen in Figure 4.6

4.2.3 Single pressure cycle

The following sections describe dynamic experiments that were carried out to test the sample's robustness to pressure change. The sample was subjected to either a single pressure cycle or to multiple cycles at different target pressures. Samples varying in the amount of air that had been whipped into the mix were also investigated.

The response of the model foam to pressure treatment can be seen from the confocal micrographs in Figure 4.8. The first micrograph was captured before pressurising the chamber. The second is of the foam fully pressurised to 11 bar. Some intermediate micrographs of the system while it was being de-pressurised are shown. The final micrograph is of the foam at the end of the experiment, once all the coalescence events have taken place and the pressure chamber has been fully de-pressurised. No micrographs are shown of the upward pressurisation stage (*i.e.* from 2 bar to 10 bar absolute). No coalescence took place on the pressurisation side and most of the micrographs were similar to those of the depressurisation side of the experiment (except those where coalescence took place). For the model foam, coalescence was observed strongly only on the depressurisation cycle and only at pressures around 2 bar absolute, but not before.

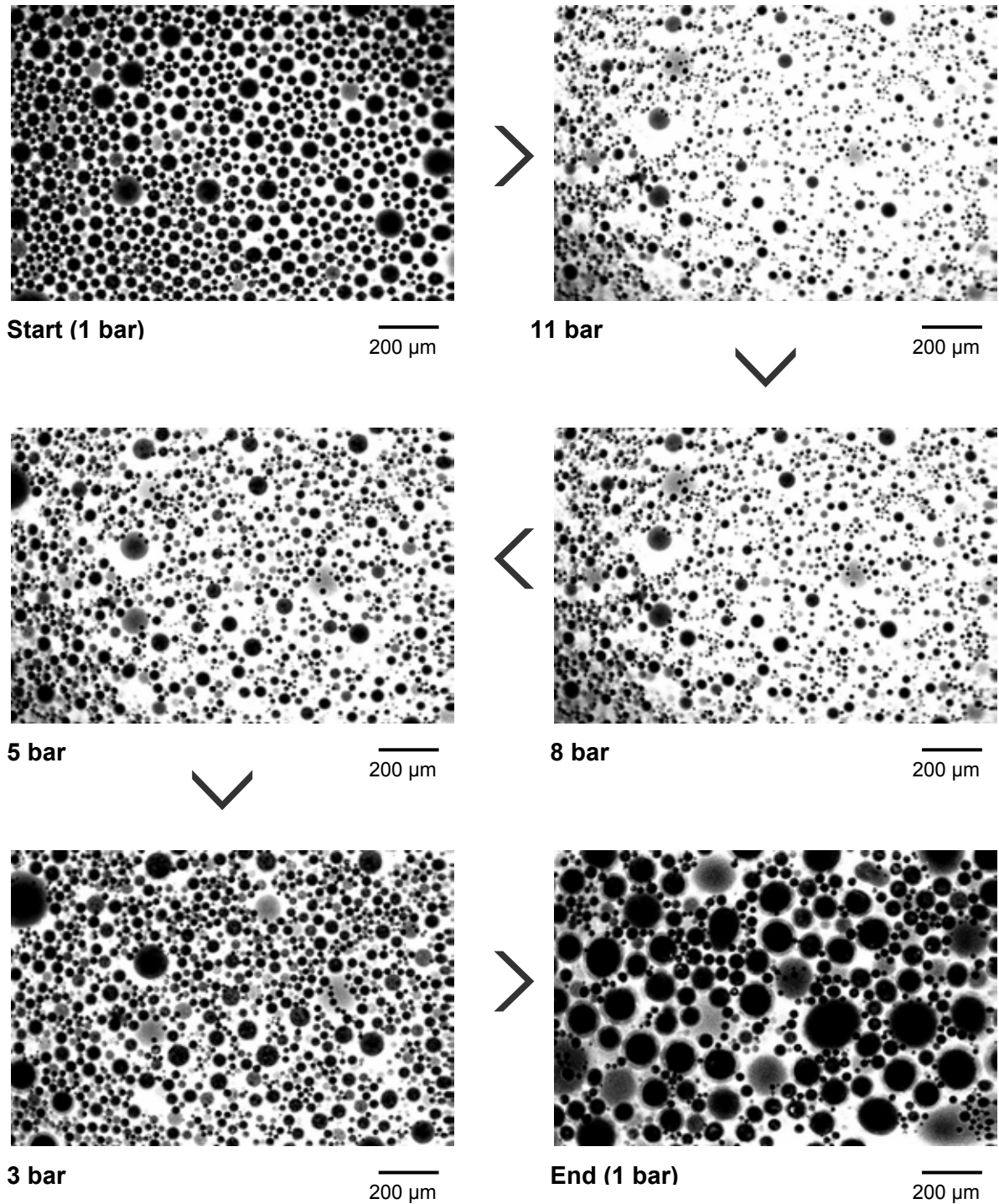


Figure 4.8: Confocal Scanning Laser Micrographs showing the pressure response of the model foam. The foam was pressurised to 11 bar absolute and the pressure gradually released in 1 bar steps. A confocal image was captured on each bar released, representative images are shown here. Experiment {A} as shown in Figure 2.16.

The effect of pressurisation on bubble size in the model foam that is subjected to a cycle (as described in Figure 2.16) from 1 to 11 and back to 1 bar

absolute (Route {A}, in Figure 2.16) is shown in micrographs in Figure 4.8. The data corresponding to the captured images was analysed in three different ways, to highlight the factors influencing the coalescence phenomena. The results obtained were: bubble density per unit area, change in bubble surface area with pressure and pressure corrected mean bubble volume. The bubble size data was corrected by using the Universal gas law by multiplying the pressure by the bubble volume obtained at that pressure. This would enable coalescence events to be visualised as a departure from linearity on a size versus pressure graph.

Volume V is seen at pressure p and therefore the pressure correction can be written as:

$$V_c = V \times (p / p_c) \quad (\text{equation 4.1})$$

where V_c is the volume the system would have at pressure p_c so V_c is plotted by applying equation 4.1.

Figure 4.9 shows the corrected mean bubble volume response at the different pressures. As the bubble volume remains constant the foam shows resistance to coalescence while the pressure is reduced from 11 bar until a pressure of about 2 bar absolute. This is because there is no evidence of any coalescence taking place. Three repeats of the same experiment (at constant air phase volume fraction $\phi = 0.6$) showed very little variation from a linear pressure \times volume trace and hence were averaged to a single trace (Figure 4.9).

Similarly, bubble density is invariant with pressure until 2 bar pressure is reached. This observation rules out any significant amount of coalescence before 2 bar on the depressurisation cycle. Hence a pressure of 2 bar absolute is seen in the system studied as the critical pressure where most coalescence events begin to take place, producing a loss of 50% in bubble density and about a mean volume size increase of nearly $\times 7$. Conceivably the observed reaction to these pressure changes is very much formulation dependent and a model mix with a different formulation might react differently. But in this case the onset and occurrence of coalescence at around the 2 bar pressure point was highly reproducible (see: Figure 4.10).

From these initial observations it is clearly possible to seek to explore further how the system responds to pressure and/or variations in formulation. Of principle interest in this work, however, is the response of the system to a large range of air phase volumes and the effects of pressure change. One would predict that ultimately, air phase volume would become a factor that determines the amount of coalescence that occurs, as with a higher air phase volume the bubbles are at a higher packing density, which means that nearest neighbours are on average in closer or more intimate contact with each other. In addition, rates of total pressure change will probably affect coalescence behaviour, due to local dynamic stresses imposed on the interface and the ability of the stabilising molecules to quickly reach newly forming interfaces on the bubble surface.

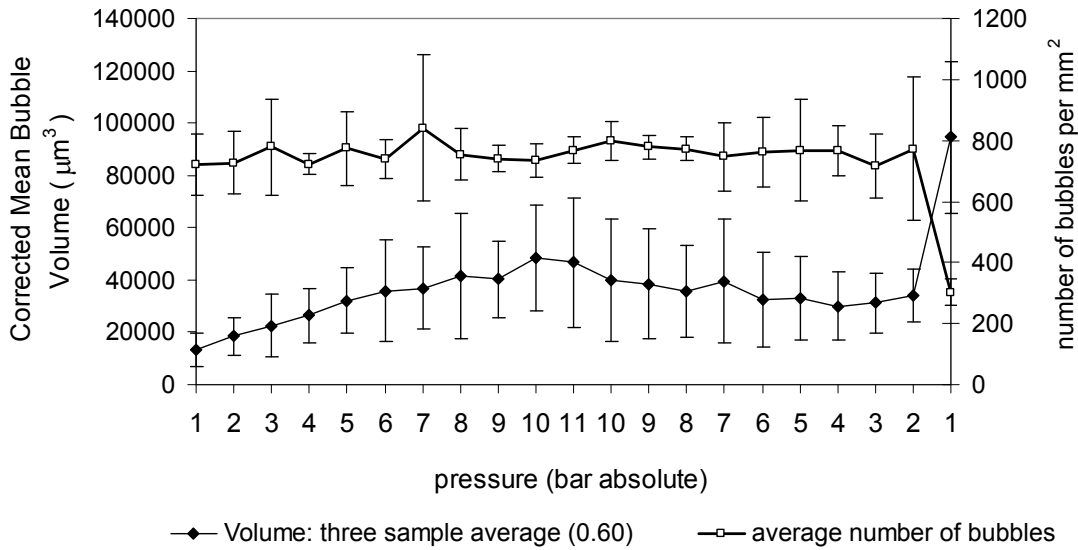


Figure 4.9: Single pressure cycle experiment, pressurising to 11 bar and de-pressurising to ambient pressure, carried out on three different samples with the same air phase volume, ϕ (in brackets). The graph above is an average of three experiments and shows the volumetric dependence of the optimised model foam corrected for universal gas law, where $p \times V = \text{const}$. Experiment {A}.

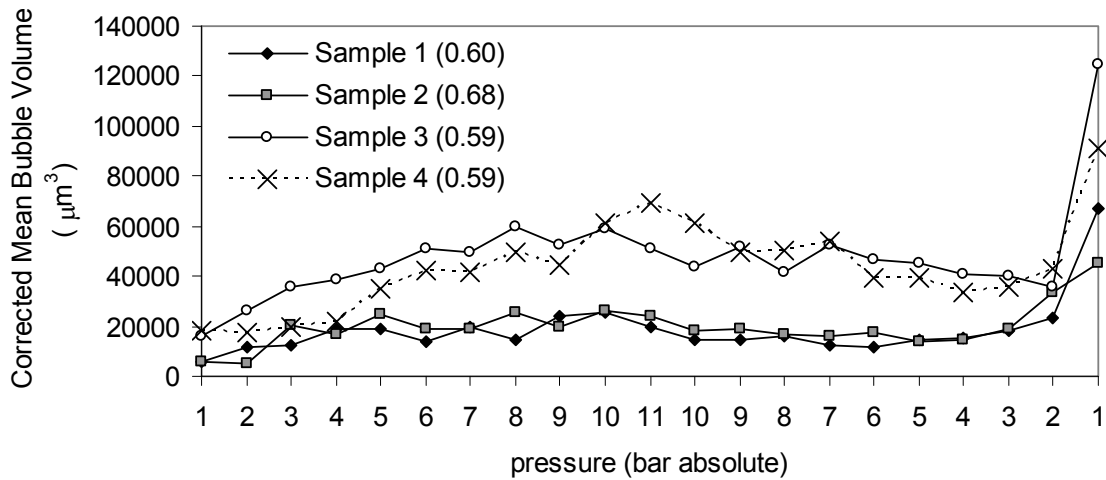


Figure 4.10: Single pressure cycle experiment, pressurising to 11 bar and de-pressurising to ambient pressure, carried out on four different samples with different final air phase volume, ϕ (in brackets). All four traces show a reproducible onset of coalescence at the 2 bar pressure point. The trace is a volumetric dependence of the optimised model foam corrected for universal gas law, where $p \times V = \text{const}$. Experiment {A}.

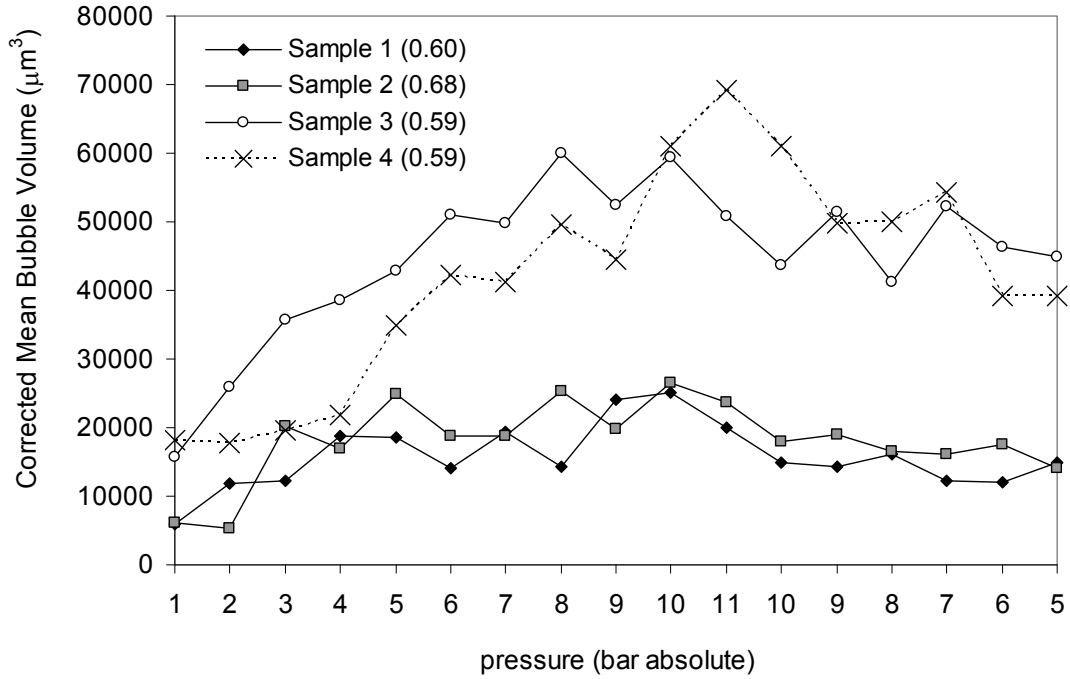


Figure 4.11: Sub-sampling Figure 4.10 to deduce the actual shape of the first part of the graph (without the coalescence).

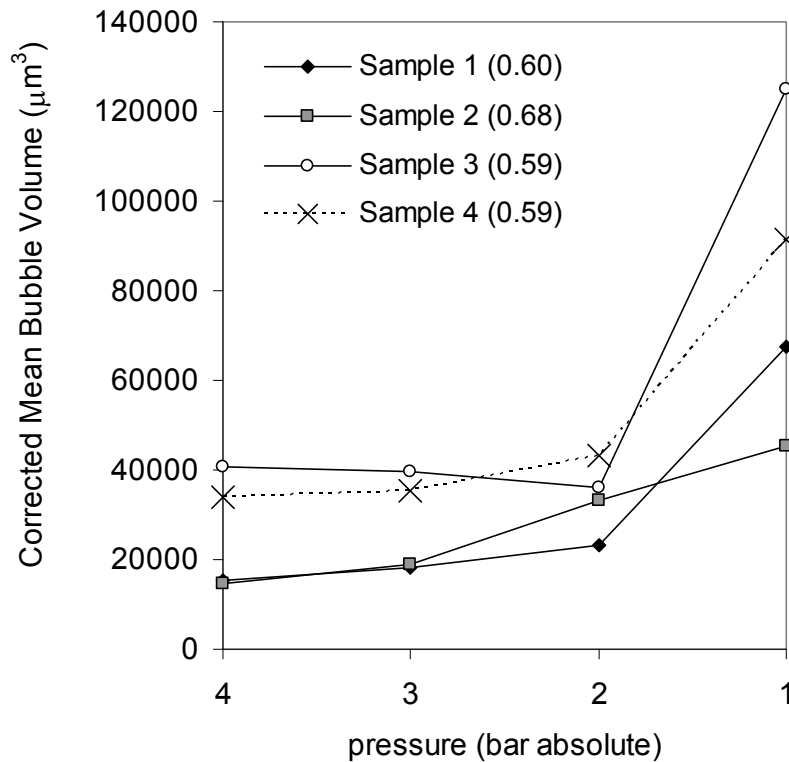


Figure 4.12 The coalescence section of the sub-sampled graph Figure 4.10

One reason why the four traces in Figure 4.10 are slightly different, might be due to the fact that Sample 1 and Sample 2 have a higher air phase volume and that this might bring with it a higher packing of the bubbles, making the foam slightly thicker. It is possible that the shape of the graph is due in part to a restructuring of the foam during an increase in pressure, especially with samples 3 and 4, as a slight maximum in foam volume is present at the highest pressure. This phenomenon is predominant throughout the pressure work at 11 bar. The mean bubble volume reduces somewhat after the pressure is released, and it does this until the pressure of 2 bar, where then coalescence takes over. A similar observation can be seen with Figure 4.13

4.2.4 5-bar consecutive pressure cycles from 1 to 6 bar {C}.

Analysing the effect of air phase volume.

Experiments were carried out at a range of air phase volumes $0.62 < \phi < 0.35$ and the foams that were measured for this pressure cycling regime show several consistent trends (results are shown in Figure 4.13). The initial mean bubble volume, in the first pressure cycle, is fairly uniform in all the samples, i.e. begins at the same mean starting volume. In addition all the samples display the same type of sensitivity to coalescence, that is when the last bar pressure is released. All samples showed coalescence and structural rearrangements at the absolute pressure sampling points of 2 bar and 1 bar absolute on the depressurisation stroke with final rearrangements again at 2 bar pressurisation. Initially, the higher air phase volume sample is the most structurally robust and shows the least deviation with regard to volume change and structural rearrangements during pressure cycling. Therefore the $p \times V$ behaviour of the mean volume, in the graph, is the flattest. The lowest air phase volume sample ($\phi = 0.35$) appeared to show more structural rearrangements leading to a pseudo creaming process which then degraded the $p \times V$ mean volume trace and led the resultant mean Volume of this sample to be higher than all the rest during pressurisation. For all samples, by the end of the third pressure cycling experiment, the foam had mostly lost its structure. Evidence of this is a drastic loss in the measured mean bubble volume upon pressure release.

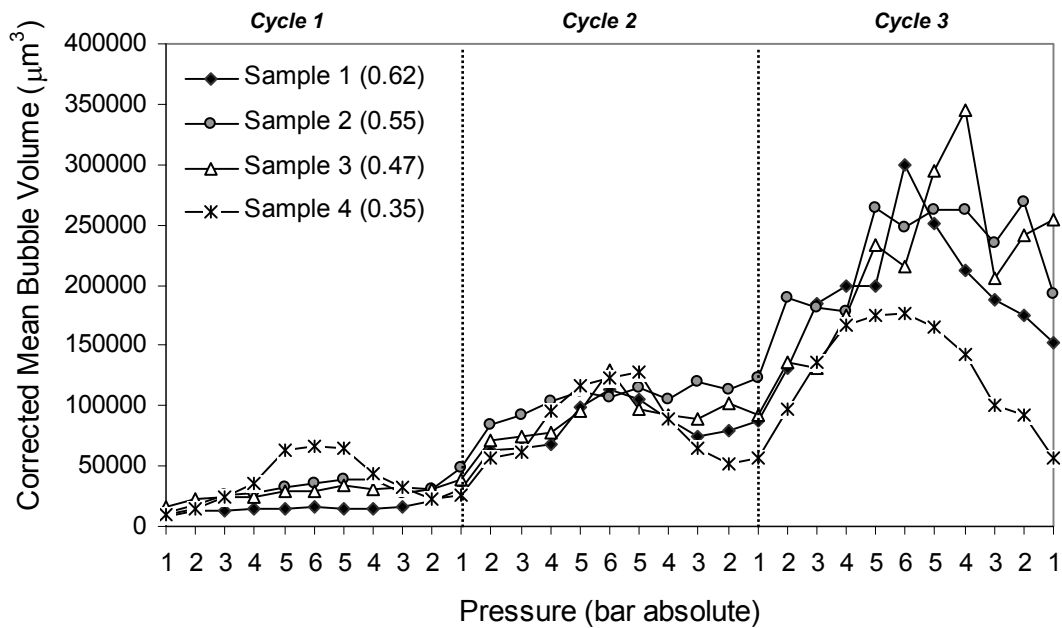


Figure 4.13: The graph summarises the results obtained for 12 samples pressurised from 1 bar absolute to 6 bar absolute. Each trace comprises 3 averaged experiments per air phase volume ϕ (in brackets). Each fresh sample was subjected to three full cycles with a maximum Δp of 5 bar from the start pressure. The curves show the volumetric dependence of the optimised model foam corrected for universal gas law, where $p \times V = \text{const}$. There's almost complete structure collapse by the end of the third cycle. Experiments {C}. For clarity purposes error bars were omitted.

An alternative examination of the same data but using the bubble density curves (Figure 4.14) show more clearly a dependence of ϕ on coalescence. As expected the bubble density is highest for the highest air phase volume and a significant reduction ($\sim 50\%$) in bubble density, occurs at the transition pressure regime, from the first to the second cycle (2 bar to 1 bar to 2 bar absolute), where the rate of surface area change is also highest. In the second pressure cycle a further significant reduction ($\sim 25\%$) in bubble density occurs. It might be expected that a similar but less dramatic behaviour with decreasing air phase volume take place. This was observed with similar trends for samples

with $\phi = 0.55$ and $\phi = 0.47$. However this was only observed to be somewhat the case for sample $\phi = 0.35$. In this case structural re-arrangements within the foam took place which were obvious and this sample exhibited partial creaming during the pressure cycle experiment, which in turn makes concise analysis of observed trends for this sample difficult. Each added cycle brought with it a subsequent destruction of the sample.

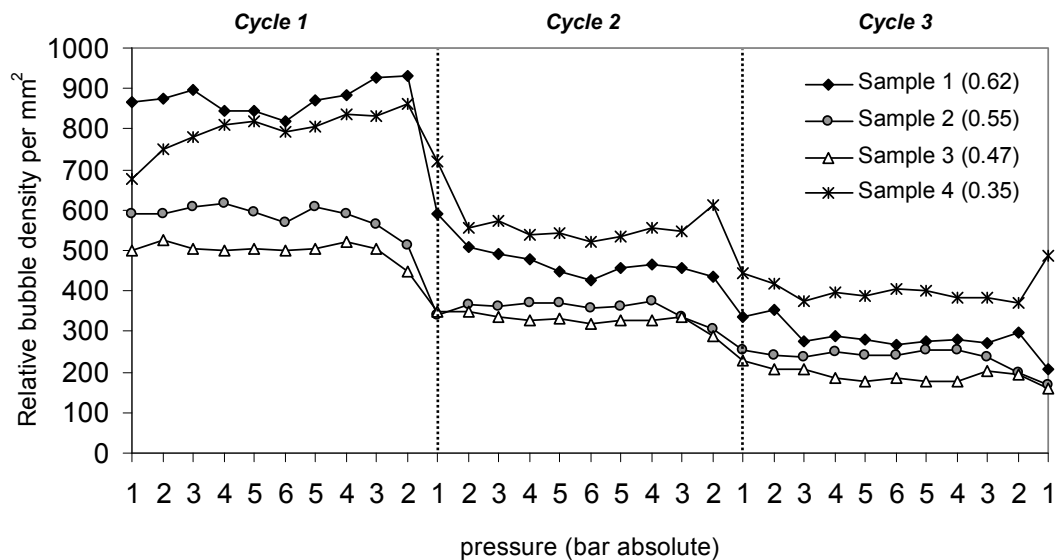


Figure 4.14: The results show the number of bubbles counted per mm^2 of image. Each sample was analysed in triplicate. The counting corresponds to experiments described in Figure 7a. (Experiments {C}) In sample 4 partial creaming could be observed. Error bars have been omitted for clarity purposes.

The image analysis script in Matlab included an added code that returned the result of calculated (theoretical) versus expected area fraction. The calculated area fraction was returned by the imaging script (Luengo Hendriks et al., 2006). It was derived and computed from a manually inputted Overrun value which was calculated after each sample was aerated, prior to image analysis. Confirmation of creaming is provided by summation of individual

bubble areas to give an a priori indication of total air phase volume ϕ expected versus that which was measured. Hence it can be noted from the data that at the lowest ϕ the discrepancy was high between the expected and the actual measured results (Figure 4.15 compared to Figure 4.16). This is probably an indication of a partial creaming effect causing bias with regard to further analysis. Future work in this context would need to deal with this issue in more detail.

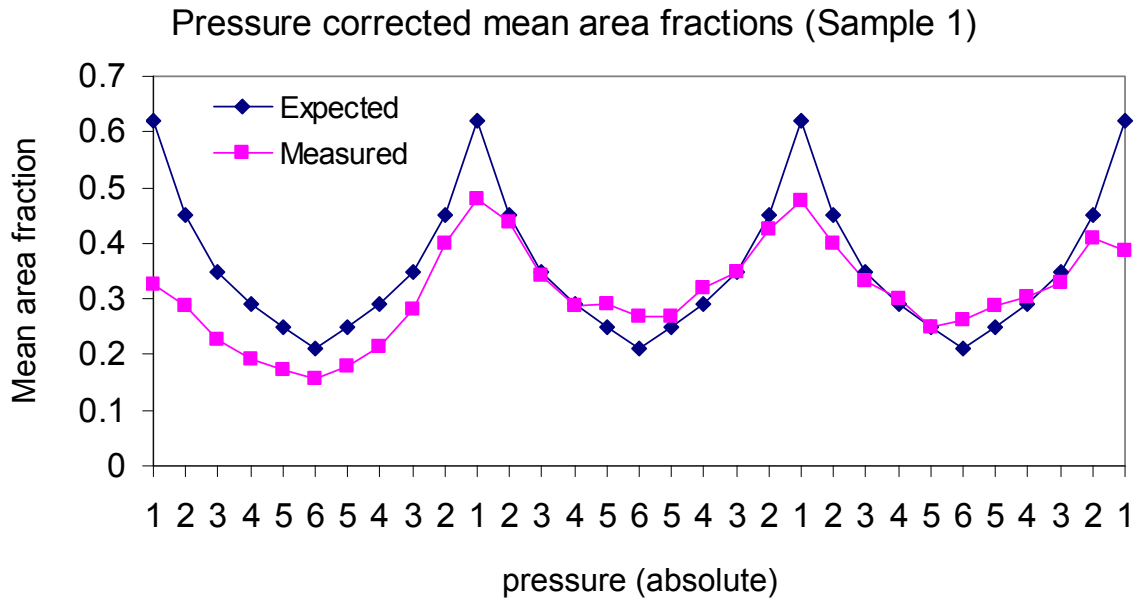


Figure 4.15: Mean area fraction for actual measured results versus those that might be expected. The results are those for Sample one, in Figure 4.14, the sample with the highest air phase volume, ϕ (0.62).

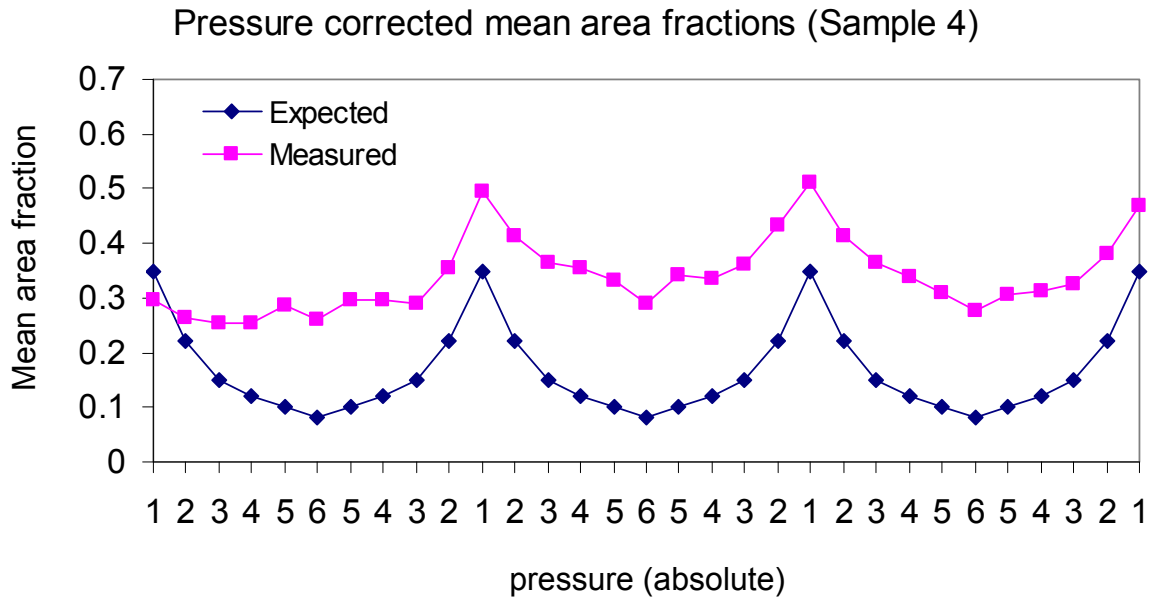


Figure 4.16: Mean area fraction for actual measured results versus those that might be expected. The results are those for Sample four, in Figure 4.14, the sample with the lowest air phase volume, ϕ (0.35).

4.2.5 Bulk pressurisation: single cycle and three cycles

The rheological characterisation of the model foam is presented in Figure 4.17. It was performed after pressurisation of the foam had taken place inside the pressure tank, with a release of each bar pressure over 30 seconds. Each foam sample was then placed in the rheometer. The samples were taken from a bulk master batch. In this case the traces at 1 and 2 bar are different from those at 3 bar up to 6 bar absolute. The transition zone from 1 and 2 bar and 3 bar up to 6 bar is the precise pressure regime where coalescence phenomena were measured and observed with the Linkam pressure cell confocal setup. It is reasonable to infer that the two traces at 1 and 2 bar are different to those at the higher pressure, due to the lack of coalescence.

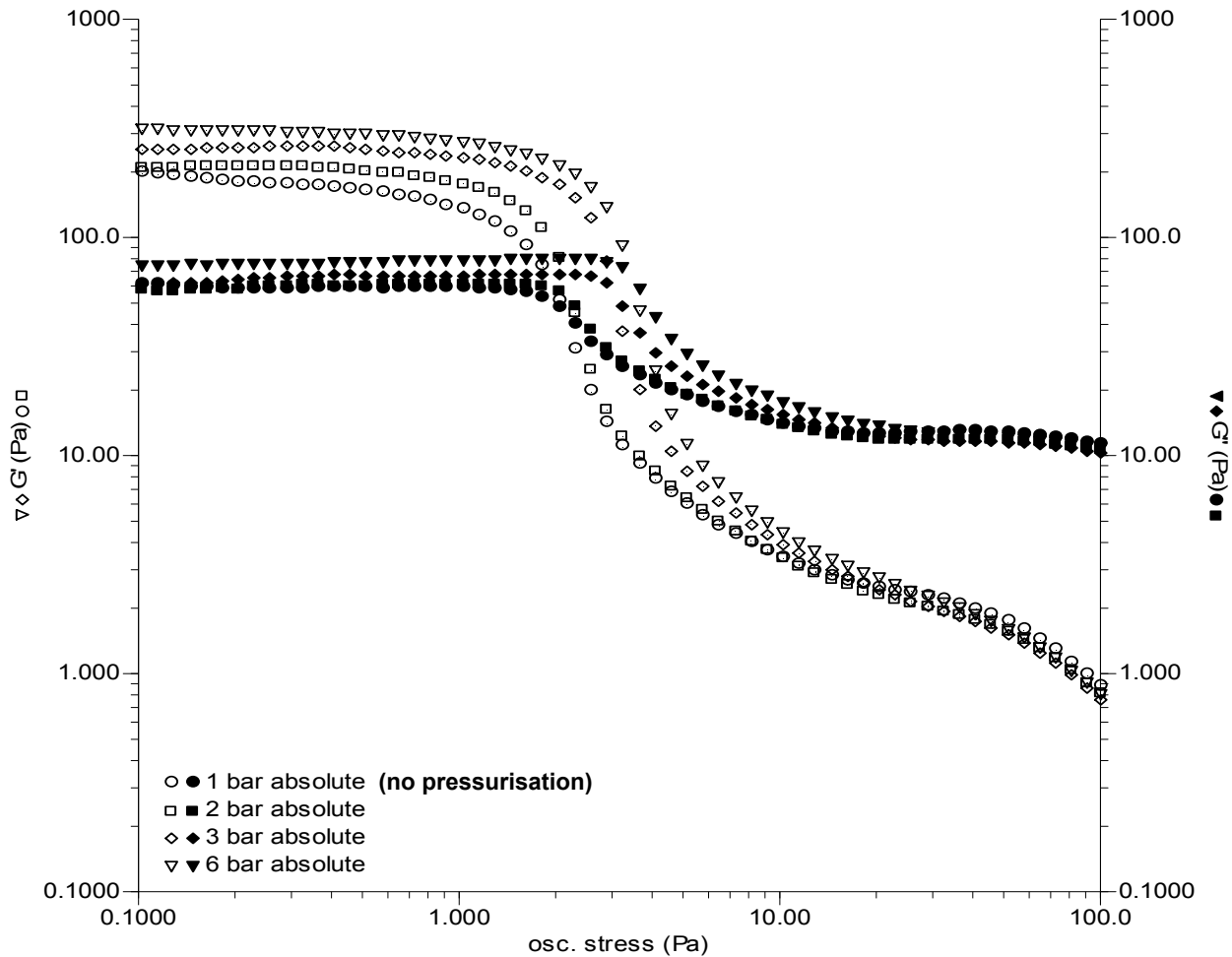


Figure 4.17: Vane rheology measurements taken at 22°C of the model foam, $\phi = 0.60$. Experiments were performed after bulk pressurisation and release to a maximum of 6 bar absolute pressure.

It is clear from this data (i.e. G' and G'' both increased), seen in Figure 4.17 and Figure 4.18, that there is a greater degree of coalescence when the difference in overall pressure change experienced by the foam increases. This may not be noticeable until the system is depressurised to about 3 bar absolute from where a significant increase in bubble surface area occurs (see Figure 4.20).

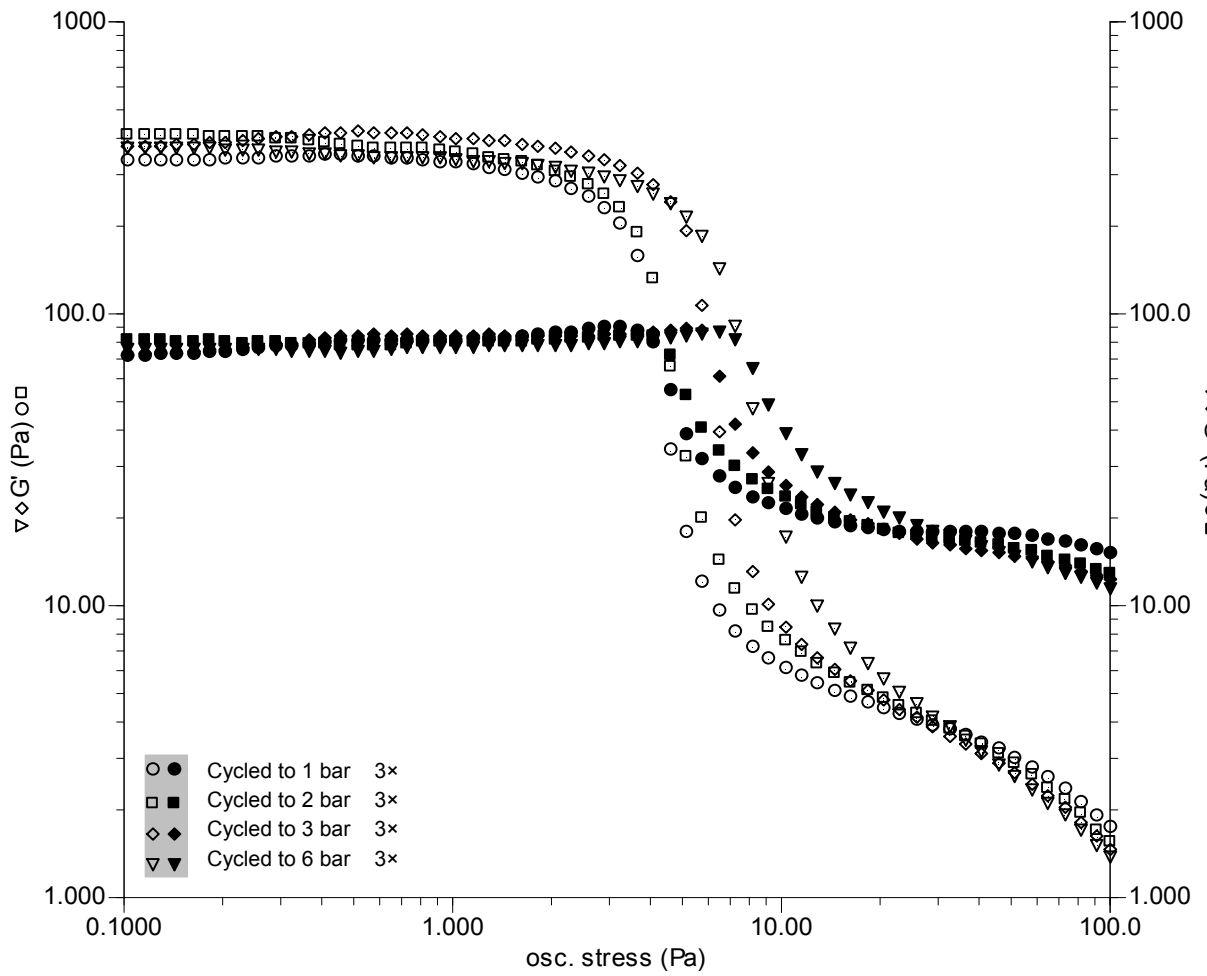


Figure 4.18: Vane rheology measurements taken at 22°C of the model foam, $\phi = 0.66$. Experiments were performed after bulk pressurisation and release to a maximum of 6 bar absolute pressure. The foam was cycled 3 times to the specified pressure.

4.2.6 5-bar pressure cycles. A comparison of 6 to 11 bar {B} with 1 to 6 bar {C}.

In this case, triplicate experiments of 5 bar pressure cycles were compared. One experiment was carried out at elevated pressures, that is between 6 bar and 11 bar absolute and the other at lower pressures that is 1 bar to 6 bar absolute. Key summary data is presented in Figure 4.19 and Figure 4.20. Results at the higher pressure are considerably different to the experiment at lower pressures, from 1 bar to 6 bar absolute. At the higher pressure (experiment {B} of Figure 2.16), evidence for microstructural rearrangements and coalescence events which were observed at the lower pressure cycle {C} (figure 2.16) were very much weaker, with much lower levels of coalescence taking place and little additional structural breakdown or rearrangements taking place. The mean bubble volume graph does not depart from linearity, which would therefore suggest that no coalescence is taking place. In Figure 4.19 direct comparison is made between two samples. Both samples have a relatively high air phase volume $\phi > 0.6$. The corrected mean bubble volume data and the bubble density data, in the case of the high pressure cycle, suggest very little coalescence takes place during this experiment. The initial bubble density for both experimental samples was around 1000 per mm^2 . But after three pressure cycles this density had fallen to around 200 per mm^2 for the 1 to 6 bar cycled sample, but remained at about 1000 per mm^2 for the high pressure cycled one. Similarly the corrected mean bubble volume for the 6 – 11 bar cycled experiment had

increased by less than a factor of two by the end of the third cycle. On the other hand, the 1 to 6 bar cycled sample had increased 10 fold. It could be said that its microstructure had essentially collapsed at this stage.

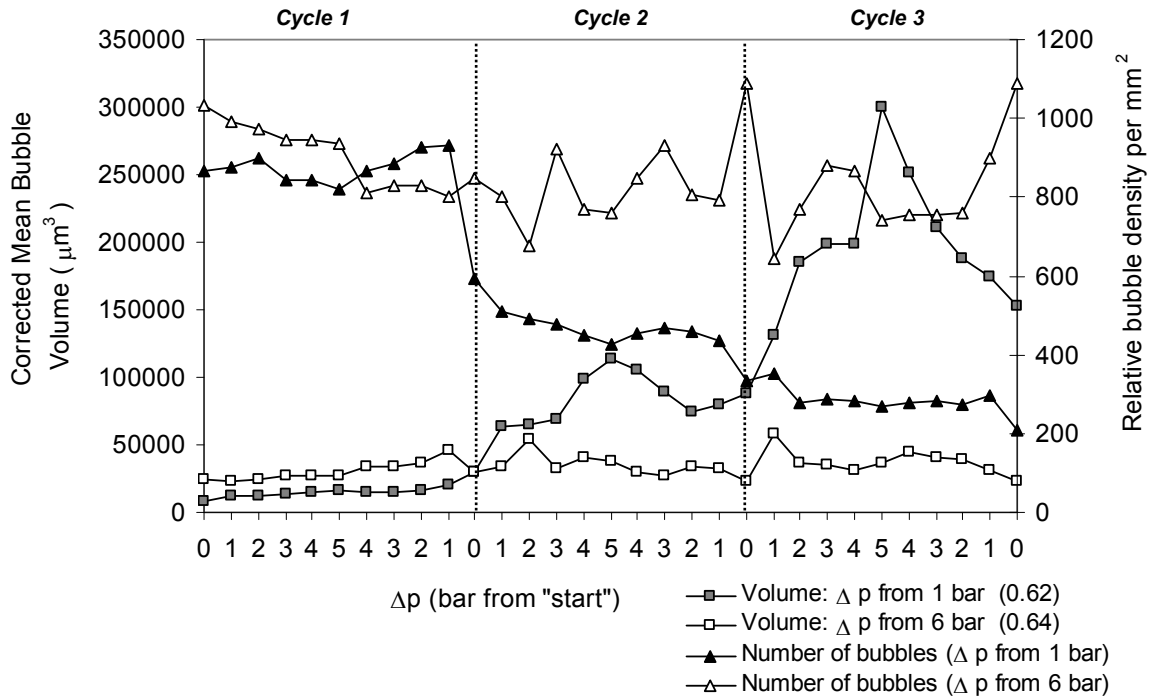


Figure 4.19: The experiments described are matched for their air phase volume ϕ (in brackets). Each sample was subjected to three full cycles with a maximum Δp of 5 bar from the start pressure (i.e. from 6 bar absolute for Experiment {B} and from 1 bar absolute for Experiment {C}). The curves show the volumetric dependence of the optimised model foam corrected for universal gas law, where $p \times V = \text{const.}$ and the evolution of bubble density per mm^2 of the captured images.

The most obvious explanation for these effects again resides in the complex interplay of coalescence due to film drainage and the change of the surface area of the bubbles due to pressure. To explore this, the mean bubble surface area change with pressure was examined during the 1 - 6 bar pressure cycle and the 6 -11 bar pressure cycle. The results obtained are compared in Figure 4.20. This Figure shows the dramatic increase in the new surface area required when the low pressures are reached in the 1 – 6 bar pressure cycle and coalescence is

observed between the experiments. At this stage however it is impossible to tell more precisely if the limiting factor in the foam instability is the rate of new surface formation and with this, the rate of diffusion and re-arrangement at the interface of the stabilising protein layer, or the stresses inherent in the film, overcoming drainage. The direct observation by confocal optics highlights this (evidenced in Figure 4.1), as film failure could be observed to be mostly through connected bubbles and their respective thin films. More detailed analysis could follow and this work would benefit from a systematic study of the effects that the rate of de-pressurisation has on the system. This study could also further benefit from a higher imaging rate of the confocal system used.

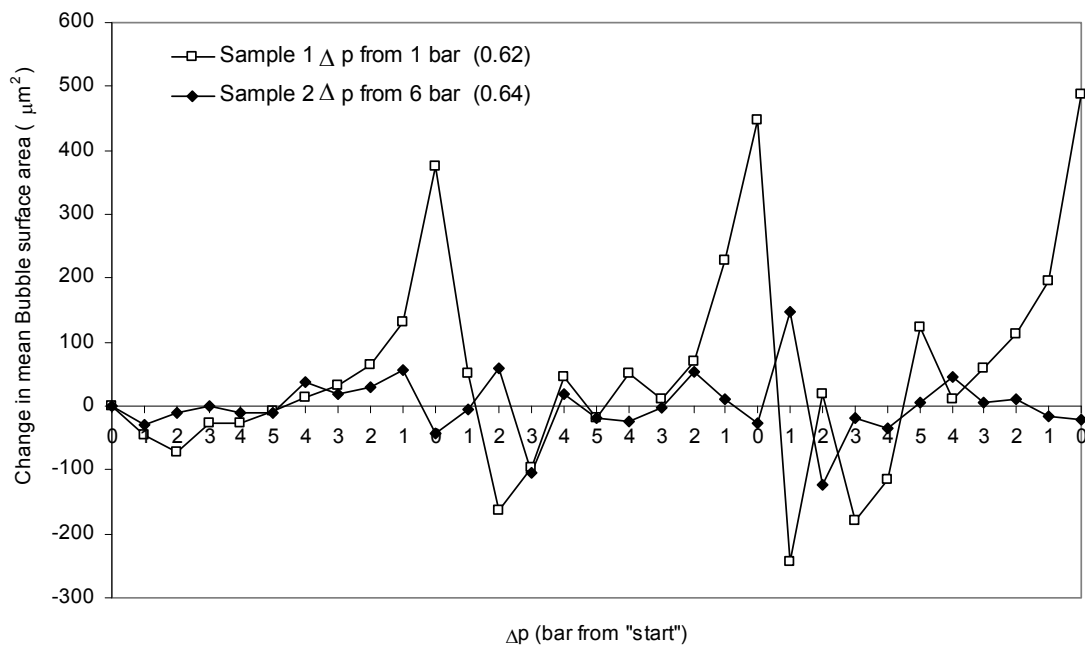


Figure 4.20: In contrast to Figure 4.19, this graph shows the average surface area change for the bubbles at each given pressure. The plots are not pressure corrected as is the case for those in Figure 4.19 which are. The samples were matched for their air phase volume ϕ (in brackets). Each sample was subjected to three full cycles with a maximum Δp of 5 bar from the start pressure (i.e. from 6 bar absolute for Experiment {B} and from 1 bar absolute for Experiment {C}).

4.2.7 Comparison of pressure cycling events from 1 to 11 bar {A} and from 1 to 6 bar {C}

The effect of the absolute change in pressure on the model foam can be observed from data already described above. Hence from Figure 4.10 to Figure 4.14, samples exist with air phase volumes, ϕ of 0.35 to 0.62.

The measured mean volume at the end of the single 10 bar pressure cycle increased approximately seven times over that of the initial measured mean volume. Compared to the results for the first cycle, in Table 4.2, this is the highest increase in measured mean volume for a pressure release event. This is further evidence for a dependence of overall bubble size increase on the total Δp that a system experiences. In addition from the data in Table 4.2 it can be seen that the samples with a higher ϕ (samples 1 & 2) achieve a higher increase in mean Volume at the end of each cycle when compared to those with a lower ϕ (Samples 3 & 4).

Table 4.2: Increase in Measured Mean Bubble Volume relative to starting mean bubble volume during three consecutive pressure cycles.

| | ϕ | After cycle 1 | After cycle 2 | After cycle 3 |
|-----------------|--------|---------------|---------------|---------------|
| <i>Sample 1</i> | 0.62 | 4.0 | 11.5 | 20.1 |
| <i>Sample 2</i> | 0.55 | 4.3 | 10.8 | 17.0 |
| <i>Sample 3</i> | 0.44 | 2.5 | 5.8 | 15.8 |
| <i>Sample 4</i> | 0.35 | 2.5 | 5.7 | 5.5 |

It is clear from the data gathered for the sections outlined above that there is a greater degree of coalescence when the difference in overall pressure change experienced by the foam increases, even though this may not be

noticeable until the system is de-pressurised to about 3 bar absolute from where a significant increase in bubble surface area occurs (Figure 4.20). Murray et al. (2002b) analysed the surface tension response of proteins undergoing a pressure change. In this case although the coalescence is at least induced by the surface area change associated with the pressure change, it can be postulated that there could also be other important parameters involved. The nature of the adsorbed stabilising layer which is coating the bubbles is likely to play a key role in their stability when subjected to pressure changes. For example, an adsorbed species that confers flexibility to the surface and can diffuse and adsorb rapidly may be expected to provide a greater degree of stability in the event of a pressure change. Conversely, an adsorbed species that results in a rigid surface, or one which does not respond rapidly to a pressure (surface area) change, may be expected to be less stable in such an event. Such results have been noted by Murray et al. (2002b), where long after the equilibrium surface tension was reached within their experiments, aggregation and/or cross-linking occurred within the Whey Protein Isolate films. This leads to a more solid like structure (in comparison to that in pure β -lactoglobulin or caseinate) and in addition this made the resultant films more liable to rupture under the higher rates and extents of deformation (Murray et al., 2002b).

In the case of PGE and whey protein adsorbed at the bubble surface as studied here, clearly it is not possible for this combination to completely

stabilise the bubbles in the final pressure change from 3 to 1 bar. A surface stabilised purely by PGE would be more stable than the PGE and whey combination. Mixed interfaces of two different types of stabilising agents because of competition at the interface (protein and small molecule emulsifier) are known to show a lesser stabilising capacity than the individual molecules by themselves. Damodaran (2004) mentions that the displacement of protein by surfactant is believed to follow an orogenic displacement mechanism. Orogenic effects can be described as causing distinctive structural phenomena, and particularly said of faulting or folding mechanisms (for a further description of orogenic displacement and some sample micrographs, see section 1.2.9.5). However, there is clearly much scope for further formulation effects of this nature to be studied with the experimental setup used here.

A further possible reason for the more coarse structure resulting when de-pressurising from 11 bar absolute to 1 bar absolute is related to the solubility of the gas. If smaller bubbles completely vanish on pressurisation due to the increase in solubility of the air, then on de-pressurisation the gas may not form new bubbles but simply diffuse into bubbles already present, leading to an overall increase in measured bubble size.

However, a separate experiment on an un-aerated mix that was pressurised and subsequently de-pressurised, revealed that no new bubble formation took place. In addition it might thus be speculated that the mix is so viscous for there

to be little solubilisation from the surrounding air into the mix in the timescales used in the experiments.

A future experiment might explore the solubility of different gases and how this may affect foam coalescence / disproportionation behaviour.

Film distortion and rupture are clear in the ‘snapshots’ of coalescing bubbles which were taken during the capture of a dynamic video sequence, Figure 4.1. Access to higher speed imaging rates with the CSLM should allow fuller understanding of these rupture events and a possible approach to 3D imaging of a foam during the failure process.

4.3 Concluding remarks

The development of an experimental methodology to study the effect of pressure change on the resistance of bubbles to coalescence in foam, was described, where the foam was subjected to dynamic pressure cycling effects. The novel concept was the direct and potential 3D imaging power offered by confocal microscopy to visualise microstructures under pressure even in fairly turbid systems typical of the food industry. This method should also be capable of explaining rate, surface composition, interface and displacement effects through more refined versions of the fluorescence imaging methods described here.

The data shows that pressure changes in aerated systems can have a particularly dramatic effect on foam microstructure through significant coalescence of air bubbles. Larger pressure differences of 10 bar have a greater effect on the resultant bubble size distribution than smaller 5 bar cycles, although in both cases most of the coalescence takes place over a small pressure range at the end of the pressure drop where rates of surface area change are highest.

Although the major effects on the microstructure are measurable, there is still plenty to be understood with respect to bubble rearrangement in the pressure cell (*i.e.* through the use of tracer particles) and how this may affect the captured images, coalescence and the resulting data. Further understanding is needed to be able to comprehend the effect of air phase volume, solubility, interfacial composition and rheology, in order to be more predictive in terms of elucidating the effects of pressure on aerated systems.

It could be argued that a refinement of the methodology would be achieved through the use of an inverted confocal microscope which performs the imaging from below, instead of imaging from above. It might also be argued that the pseudo-creaming effect, seen particularly with the lowest air phase volume, could be mitigated against, as the bubbles floating on the surface would not be imaged, and instead the foam structure would be captured from below. Yet it could also be argued that the drained liquid from the foam at the

bottom of the crucible, might be too thick to enable correct imaging, and this would then rule this out as a viable method altogether.

The foams studied here were all ambient stable foams. The study of model food foams containing ice particles, would add a separate level of complexity to the understanding of the dynamics taking place.

Pressure induced changes have a considerable impact on foam rheology and flow during processing. It will ultimately also have an impact on the microstructure, stability and texture of the finished aerated product. However, this methodology offers new routes to follow these changes and add a new insight into the dynamics of foam behaviour under increasingly complicated situations.

CHAPTER 5

Effect of pressure release, foam structure and gas solubility

5.1 *Introduction*

Bubbles by their very nature are transient structures and as such in foams they are generally more deformable than emulsion droplets, and this makes them more susceptible to coalescence. The volume of a bubble undergoing a pressure change during processing must increase or decrease in inverse proportion to the pressure (Murray et al., 2002a), and in so doing, change the surface coverage of its stabilising surfactant at the same time. The gas bubbles in many foamed products, in addition, are large enough so that they can be much more easily deformed than emulsion droplets by hydrodynamic forces commonly operating during processing environments (Murray et al., 2005).

Bubbles can also be quite unstable due to dissolution of the gas into the continuous phase, leading to coarsening (disproportionation) of the bubble size distribution. However, coalescence can often be much more rapid than coarsening, especially if the bubbles are subjected to a mechanical disturbance. The literature suggests that coalescence could be considerably accelerated by a rapid drop in pressure, with catastrophic bursting of bubbles taking place over the time scale of the pressure drop. Experimental analysis will test this statement and what effect a rapid or slow pressure release has on the foam. Instances of foam processing where there can be a significantly high rate of

bubble expansion due to a pressure drop are the exit of foam from a mixing or aeration chamber and the extrusion of an aerated product from a nozzle, taking place in dispensing and filling (Murray et al., 2005).

Problems also occur when ice cream is shipped from low to high altitudes or vice versa. Shrinkage of the ice cream causes a great economic loss to the manufacturer, as was also noted in greater detail in Chapter 1, section 1.1.1. Cole in 1940 in (Dubey and White, 1997) observed that the changes in atmospheric pressure that occur when ice cream is shipped from one altitude to another might contribute to shrinkage. Atmospheric pressure changes could then cause ice cream to either shrink and pull away from the sides of the container or actually push out of the containers (Dubey and White, 1997).

The experiments that were carried out in the first part of this chapter attempted to mimic the pressure drop that a sample experiences when it is dispensed from an ice-cream freezer. Not only was it the intention of this experiment to replicate the pressure drop, but it was also undertaken at different release rates to try and gauge which of them was the least harmful to the foam microstructure.

The second part studied bubble interactions in a static condition. This was done by looking at foam disproportionation using different gases. The foam was left to disproportionate for 5 hours and it was imaged every 30 minutes. The foam was either pressurised to 11 bar, 6 bar or left at ambient pressure. In

the final part, the stability of the foam which was subjected to different shear regimes was also investigated.

There is little external literature available relating to the subject of coalescence and its associated relationship to pressure release rates. This chapter aims not only to tackle but also try and address some of these issues.

5.2 Release Rate and disproportionation

The release rate experiments were carried out using the master batch method, by inverting the sample every 15 minutes. The full description of the Method can be found in Section 2.14. In order to use this method a fresh sample was aerated at the start of each new day. Each release rate was assessed on a separate day. The four different release rates which were assessed were 2 minutes, 30 seconds, 10 seconds and 1 second. The Overrun level was matched as near as possible between the samples. For each pressure release ‘step’ (i.e. Δp of 6 bar, Δp of 5 bar, etc) a fresh sample of the master batch was loaded into the pressure cell and the previous sample discarded. The whole step was carried out without stopping, meaning that all of the gas was evacuated from the cell and the valve only closed again once it was empty.

The experiments for disproportionation were carried out over 5 hours, which consisted in direct confocal imaging of the foam every 30 minutes. The sample was left to disproportionate under 3 different pressures, at 1 bar

absolute (ambient) pressure, at 6 bar absolute and 11 bar absolute. Experiments were carried out in air, argon, nitrous oxide (N₂O), carbon dioxide (CO₂) and helium. The experiments would assess the disproportionation potential of these five different gases, each with a very different solubility measured in water at 25 °C. It is given by the Henry's law constants ($\times 10^{-4}$ M/atm) see Table 5.1 (Sander, 1999). Henry's law is described thus: at a constant temperature, the amount of a given gas dissolved in a given type and volume of liquid is directly proportional to the partial pressure of that gas in equilibrium with that liquid. For a more thorough description of the method used to manufacture and aerate the model mixes with the different gases, refer to the materials and methods chapter 2 part II (contained in sections 2.13, 2.15.9 and 2.15.10).

Table 5.1: Henry's law constants, taken at 25 °C in water (Source: Sander, 1999)

| Gas | <i>Air</i> | <i>CO₂</i> | <i>N₂O</i> | <i>Helium</i> | <i>Argon</i> |
|---|------------|-----------------------|-----------------------|---------------|--------------|
| Henry's Constant ($\times 10^{-4}$ M/atm) | 13.0 | 340.0 | 250.0 | 3.75 | 14.0 |

Disproportionation would be expected to be more rapid with the more soluble gases, i.e. CO₂ and N₂O than with air, and slower with helium.

5.3 *Pressure release*

The aim of the experiments in this section was to pressurise the foam to different target pressures (incorporating the range of pressures usually found in an ice-cream freezer) and to depressurise at a range of different rates. So not only would the difference in pressure be analysed, but also the release rate. It was therefore essential to have samples with the same Overrun, in order to have reproducible foam conditions between the samples. Each different release rate

was assessed on a separate day. The master batch method was used throughout the release rate experiments.

5.4 Results

5.4.1 Pressure Analysis

5.4.1.1 Release rate

The results in Figure 5.1 for the different release rates were obtained by manually releasing the pressure, of the Linkam pressure chamber, containing the model foam, at different rates. Each full data point for a given Δp is a fresh sample. Each bar in pressure that is released, is released at the rate indicated in the legend, until all the pressure has been released fully (i.e. for 5 bar, release from 5 bar to 4 bar took place over the unit of time indicated, from 4 bar to 3, again over the same time unit, etc). The release rates were 2 minutes, 30 seconds, 10 seconds and 1 second respectively.

The pressure release at 1 second per bar released, was the condition that showed the least difference between the steps, when compared to all the pressure steps that were tested.

The release rate that showed the most difference between all the steps was the 2 minute release. It can therefore be argued that abrupt and fast changes seem to have a protective effect on the foam microstructure. Whereas changes

taking place over long time-scales seem to have a detrimental impact on the foams' structure.

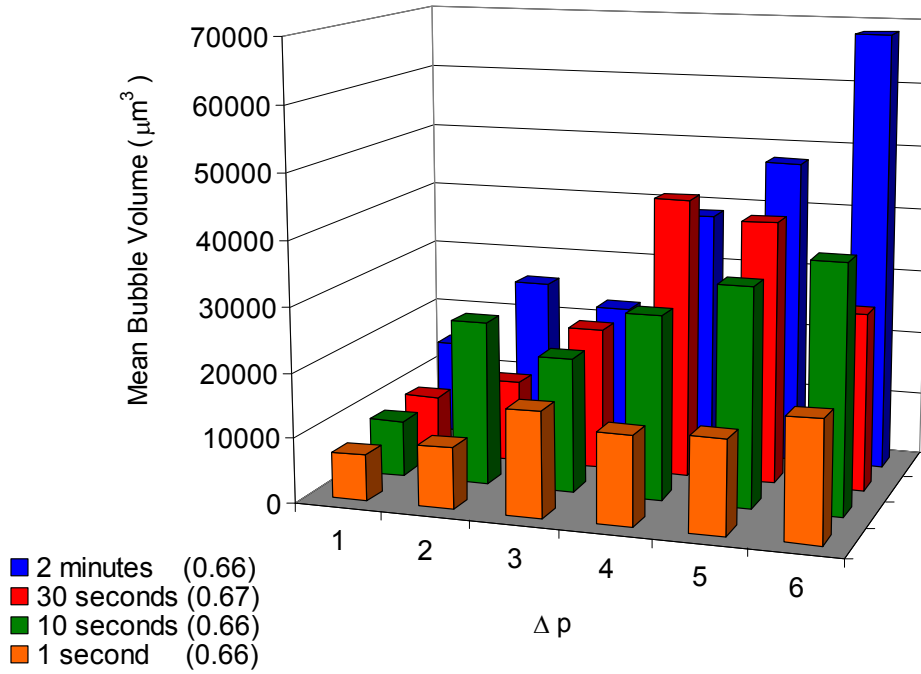


Figure 5.1: Different pressure release rates: Effect on bubble Volume. Each column at each Δp is a fresh sample. The target pressure is pumped into the cell for each Δp which is then released using different release rates. The time indicated in the legend is the time taken to release the air per bar (e.g. two minutes, is two minutes per bar released).

The graph in Figure 5.2 was compiled from micrographs that were taken once the release events had taken place and after a set time was allowed to elapse. Once the pressure had been released an image was taken. This is represented in the data reproduced in Figure 5.1. After a period of time another image was taken. During this waiting period, coalescence events were still taking place and a consequent increase in mean bubble volume will have taken place, this data fed into the results in Figure 5.2.

The results in Figure 5.2 were obtained by imaging the foam after waiting a few minutes once the pressure release had taken place. For the two minute release rate, 4 minutes were allowed to elapse before the image was taken, for the 10 second and 30 second release rates, 2 minutes were allowed to elapse. 2 minutes proved to be more than long enough to allow all the coalescence events to take place. On the other hand as the 2 minute release rate was extremely slow, the coalescence events resulting from the given pressure release, were slow too. In this release rate, after 4 minutes “waiting”, all the coalescence events had finished taking place. For the 1 second release rate, the coalescence that had occurred prior to imaging did not continue after the first image had been taken, and hence only one image was taken.

Similar to the findings in Figure 5.1 the release with the fastest rate (in this case the 10 second release) in Figure 5.2, showed a somewhat protective effect on the foam microstructure, as little extra coalescence took place, even after waiting. This can also be seen in Figure 5.4. The two minute release (the slowest release rate) showed the most continued coalescence, even once the release event had taken place.

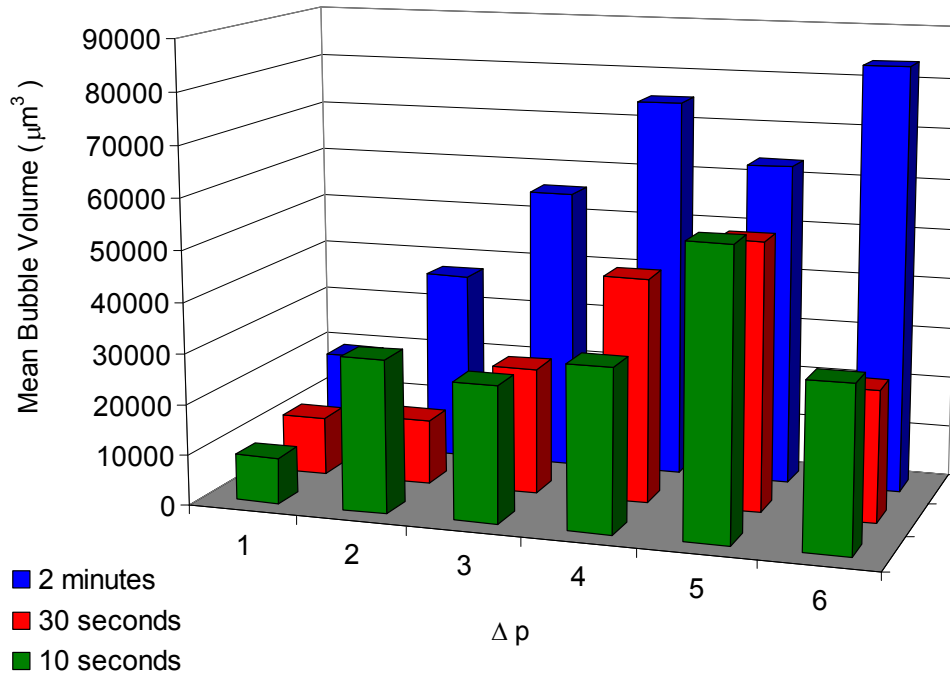


Figure 5.2: Second image, taken after a waiting period after full pressure release of 4 minutes for the 2 minute release rate data and 2 minutes for the 30 second and 10 second release rate data. Coalescence events continued for a long time after the whole pressure had been released, this second image was taken to see how much the volume had changed over that extra time period.

The largest difference, in Figure 5.3, seen on both charts, the one of increase in mean bubble volume and bubble numbers count, between the starting and final condition, was seen at the 6 bar pressure drop. The other five treatments did not show as much difference.

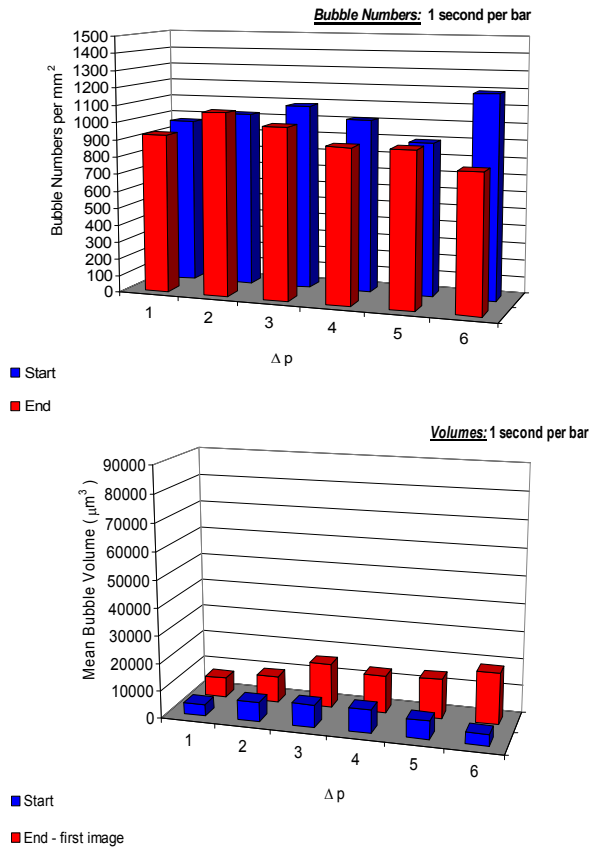


Figure 5.3: 1 second per bar pressure release. Comparison of total bubble numbers from the field of view before and after the pressure release event has taken place and a comparison of the change in measured mean bubble volume, before and after the pressure release event.

The difference seen above in Figure 5.3, between the different pressurisation levels and its effect on the resultant microstructure became even more pronounced in Figure 5.4 with a pressure release rate of 10 seconds per bar. The slightly anomalous results seen in the increase in bubble numbers between the initial and final images seen at the pressure release step of 1 Δp might be explained by the fact that it is only a small pressure release. It is believed that the disturbance is only so minor that not much coalescence really takes place and therefore the bubble numbers do not decrease and the volume does not increase substantially. The increase in bubble numbers could be due to

bubble buoyancy, with the slight disturbance at the interface allowing more bubbles to rise from under the surface that was imaged.

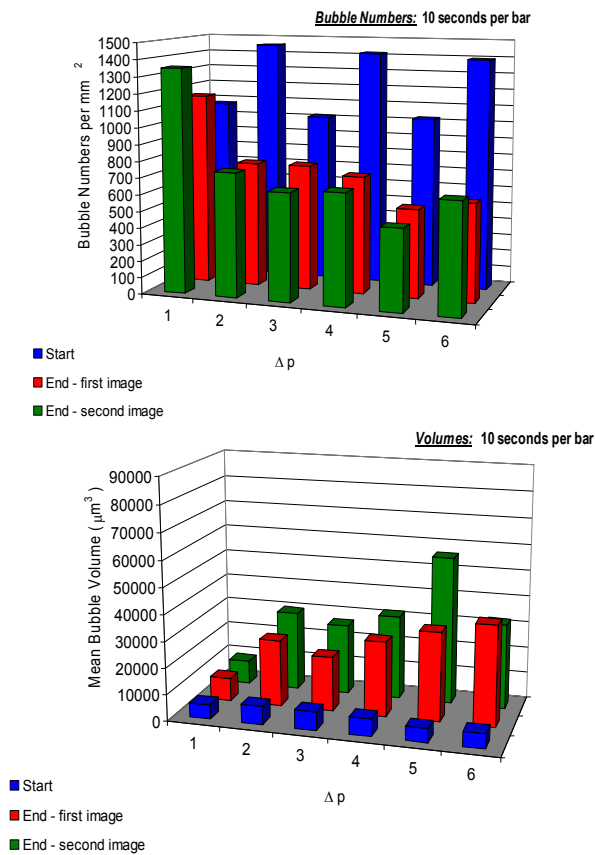


Figure 5.4: 10 seconds per bar pressure release. Comparison of total bubble numbers from the field of view before and after the pressure release event has taken place and a comparison of the change in measured mean bubble volume, before and after the pressure release event. A third measurement was included which involved leaving the sample to rest.

There seems to be an effect seen in each of the different pressure steps when one considers the different target pressures. The effect the release has on bubble numbers before and after is greatest at the $6\Delta p$ stage, with the effect decreasing until $1\Delta p$ which has the least effect on the final bubble numbers. The same could be said for the effect with the Corrected Mean Bubble volume graph. The two pressures experiencing the least change before and after the intervention (inclusive after waiting) are the $1\Delta p$ and $2\Delta p$ pressure changes.

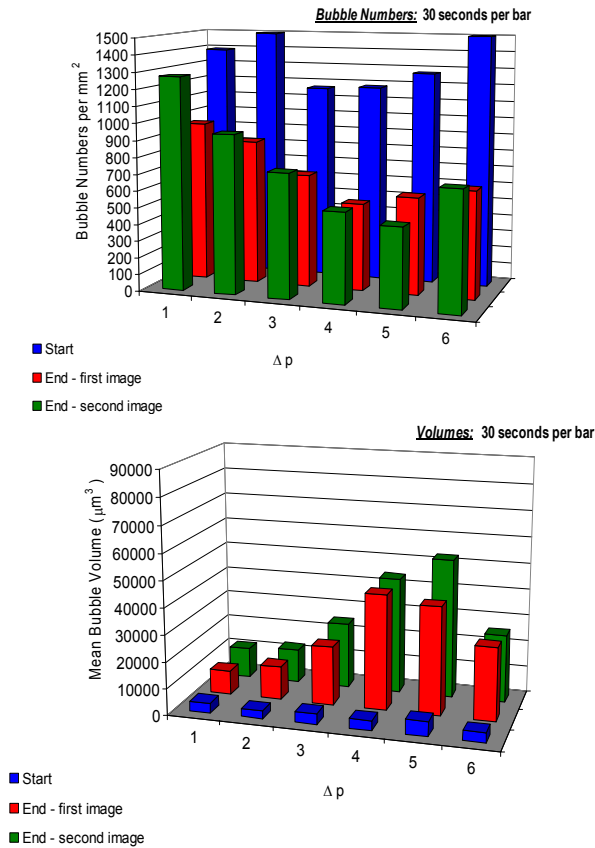


Figure 5.5: 30 seconds per bar pressure release. Comparison of total bubble numbers from the field of view before and after the pressure release event has taken place and a comparison of the change in measured mean bubble volume, before and after the pressure release event.

In Figure 5.6 there is a reduction in bubble numbers in each of the pressure steps, except for $1\Delta p$. From Δp_6 to Δp_2 after the first image was taken the bubble numbers are all somewhat different. After the rest period all the bubble numbers in the 5 pressure steps have equalised and are all the same, except for the bubble numbers seen in Δp_1 . The behaviour seen within the Bubble Volume graph is interesting. The pressure step of Δp_1 gave a Volume increase after the first release step, but additional waiting did not have a further change in Volume as a consequence. All the other pressure steps elicited a dramatic increase in bubble volume after the pressure was released. The addition of the waiting period also further increased the mean Volume measured.

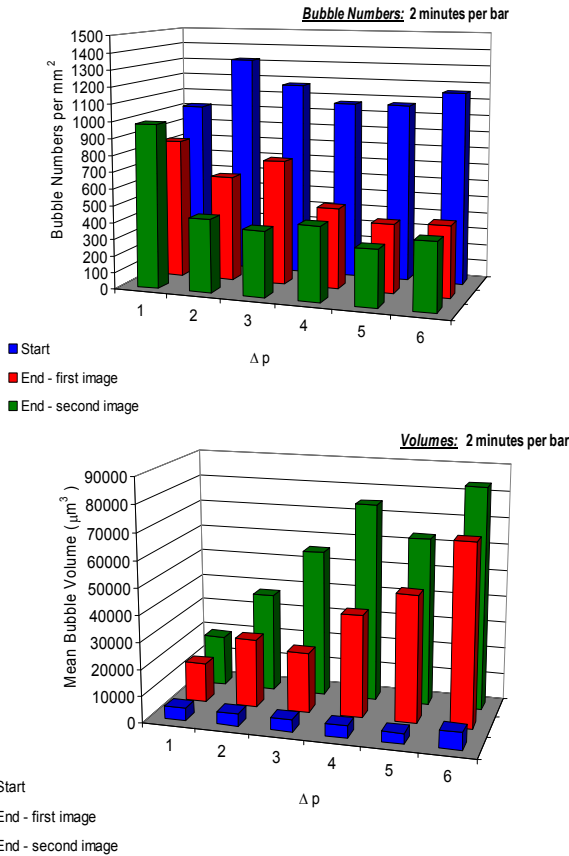


Figure 5.6: 2 minutes per bar pressure release. Comparison of total bubble numbers from the field of view before and after the pressure release event has taken place and a comparison of the change in measured mean bubble volume, before and after the pressure release event.

The overall trend in Figure 5.4, Figure 5.5 and Figure 5.6 is that a dramatic reduction in bubble numbers takes place at the pressure release step of Δp 6 and Δp 5, leaving only a small number of bubbles when compared to the number of starting bubbles. Those left contribute to the large increase in measured mean bubble volume, as they are substantially larger than the starting bubbles.

The following figure, Figure 5.7, is a quotient between the starting Corrected Mean Bubble Volume (which was a micrograph of the foam before the pressure release experiment had taken place). This was then divided by the

end mean bubble volume after release had taken place (data from Figure 5.1). The result of this quotient gave the results in Figure 5.7.

By plotting the experiments in this way, each of the release rate experiments can be compared with one another and the results obtained are then relative to the starting conditions of the corrected mean volume of each treatment. By doing this the results are in effect ‘normalised’ to compensate for any differences experienced in the starting conditions.

The data with the largest difference between the initial and final mean bubble volume was the experiment with a slow 2 minute release. The sample that showed the least difference was the one with a 1 second release rate. This is again further evidence of the protective effect that quick release rates have on the bubble microstructure and on bubble numbers.

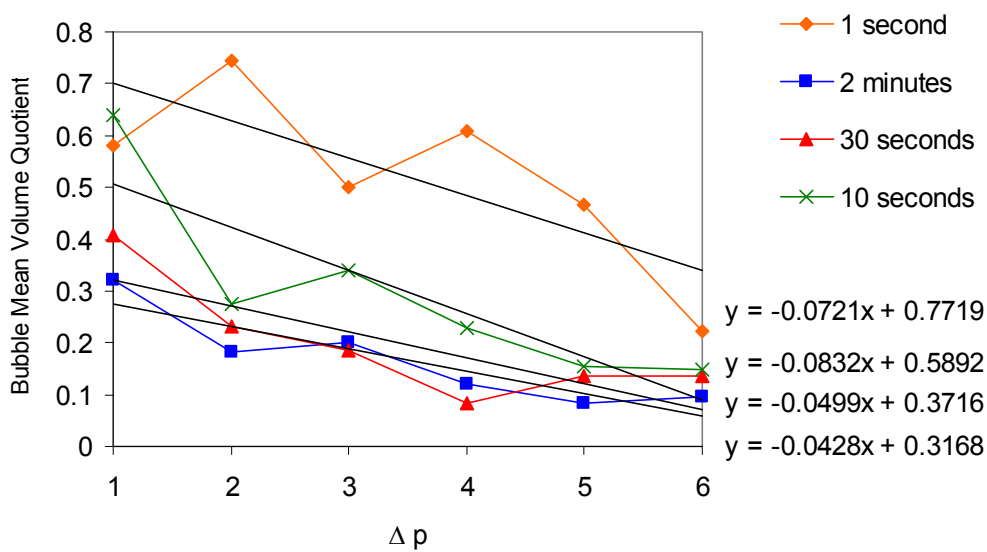


Figure 5.7: In this figure the results for the starting mean bubble volume were divided by the mean bubble volume at the end, once the foam had undergone the pressure release regime.

The initial bubble number of the field of view being analysed, before the sample was depressurised, was divided by the resultant bubble number after the release rate experiment was carried out. The results are presented in Figure 5.8. This graph was plotted to see which of the four treatments had the greatest loss of bubbles. This could then be compared to the one which had the least. By the fact that results are expressed as a quotient which was dependent on the initial starting conditions of the foam, this change in relative bubble numbers could be visualised. Again, like above, the results are thus normalised and can then be analysed independently of the starting conditions of each sample.

The foam sample which shows the least change and the least loss of bubbles was the foam with a 1 second release rate, in contrast, the sample with the most loss and a large decrease in bubble numbers was the one with a 2 minute release rate.

This graph is testament to the fact that a slow pressure release has a more detrimental effect on foam bubbles and foam bubble numbers than a quick pressure release. From this it can be deduced that a quick release rate has a protective effect on bubble density and thus on the foam microstructure itself.

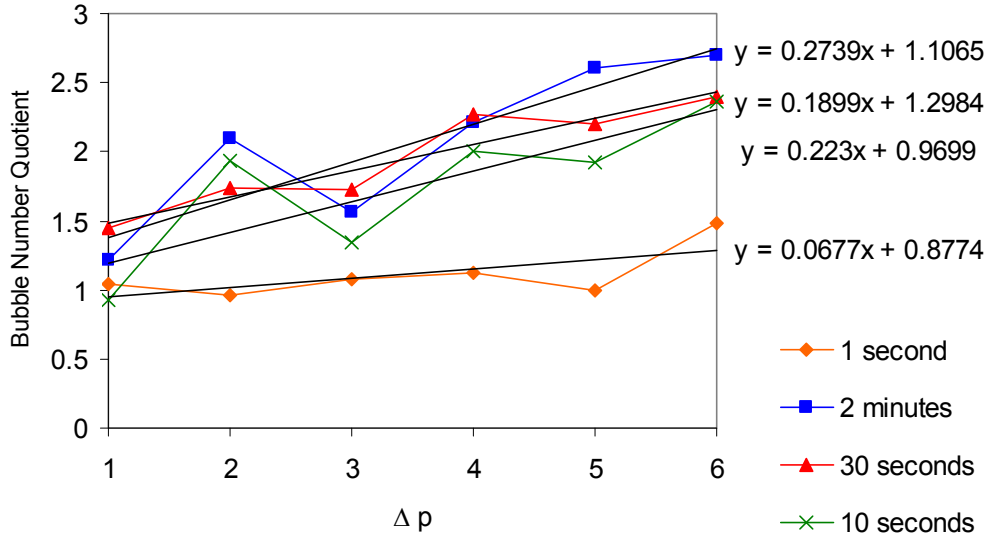


Figure 5.8: In this figure the number of Bubbles counted at the beginning of the experiment in one field of view, was divided by the number of bubbles that were left once the pressure release event had taken place.

5.4.2 Disproportionation of foam microstructures under: Air, Nitrous Oxide, Carbon Dioxide, Helium and Argon.

The disproportionation experiments with the different gases is a scouting exercise in order to try and find a suitable replacement for Nitrous Oxide (N₂O) which is frequently used as carrier gas within aerosolised canister systems. A nitrous oxide alternative is sought, in order that a better carrier might be found which could maintain the original shape of the extruded foam for longer and might resist disproportionation. Nitrous oxide is the second most soluble carrier gas after Carbon Dioxide, so a less soluble gas which might not diffuse through the foam quickly and which might prevent excessive disproportionation, might be useful. The least soluble of the five gases chosen is Helium (see: Table 5.1 in section 5.2).

5.4.2.1 *Disproportionation with Air*

For the disproportionation experiments, the cooled and prepared pre-mix, which was made following the description in the Methods and Materials section (2.13, 2.15.3, 2.15.5, 2.15.7 & 2.15.8), was then aerated with the target gas. In this case it was air. This meant that the mixing bowl did not need covering or aerating with gas, but for the sake of reproducibility it was. In addition the mix was purged with air and the bowl aerated with air from an airline, to keep all the conditions the same. For all the gases, the mixer was covered with a big plastic bag. The pre-mix was purged with the gas for 5 minutes using a metallic rod and frit attachment. The foam was subsequently aerated in the mixer until a target Overrun of about 180 percent was reached. In the results, the air phase volume that was finally obtained is indicated next to the description of each sample in the legend. The foam sample was then loaded into the sample chamber of the pressure cell and the cell was then sealed. The sample was imaged every 30 minutes for a total of 5 hours. The results in Figure 5.9 of the disproportionation behaviour of a foam with air, show little disproportionation at a pressure of 1 bar absolute, but evidence of increased disproportionation at 6 bar absolute and also nearly equal disproportionation at 11 bar.

Bubble numbers, for the bubble numbers graphs, are counted automatically by the script in Matlab. The numbers it gives are representative of the field of view in question. Bubble loss (Figure 5.10) is minimal at 1 bar and 6 bar and only slightly increased at 11 bar absolute.

The oscillatory rheology trace for the disproportionation behaviour with air as an aeration agent, Figure 5.11, shows only a marginal difference between the G' values at 0 hours and 5 hours, an indication that few bulk microstructural changes have thus taken place within the foam. The foam was analysed for this experiment straight after aeration, and for the 5 hour reading the sample was placed in a 500 ml Nalgene Bottle and inverted every 15 minutes according to the Master batch protocol.

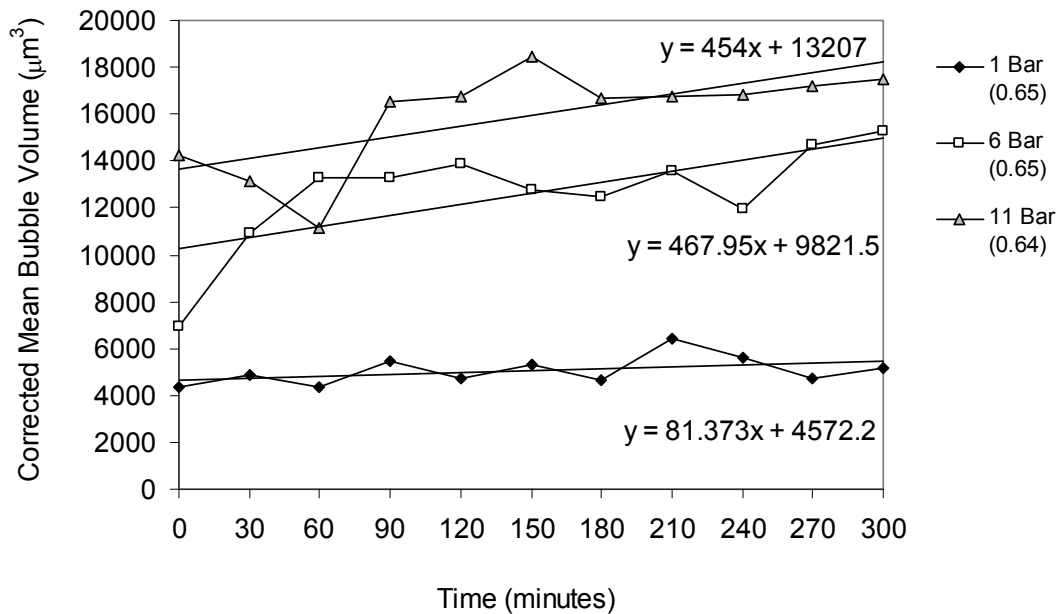


Figure 5.9: Air: CSLM imaging in *air* of disproportionation behaviour for 5 hours of the model mix sample under 3 different pressure regimes. Imaging took place at $\frac{1}{2}$ hour intervals. Initial air phase volume of the mix shown in brackets (ϕ). The volumetric dependence of the foam was corrected using the universal gas law, where $p \times V = \text{const}$.

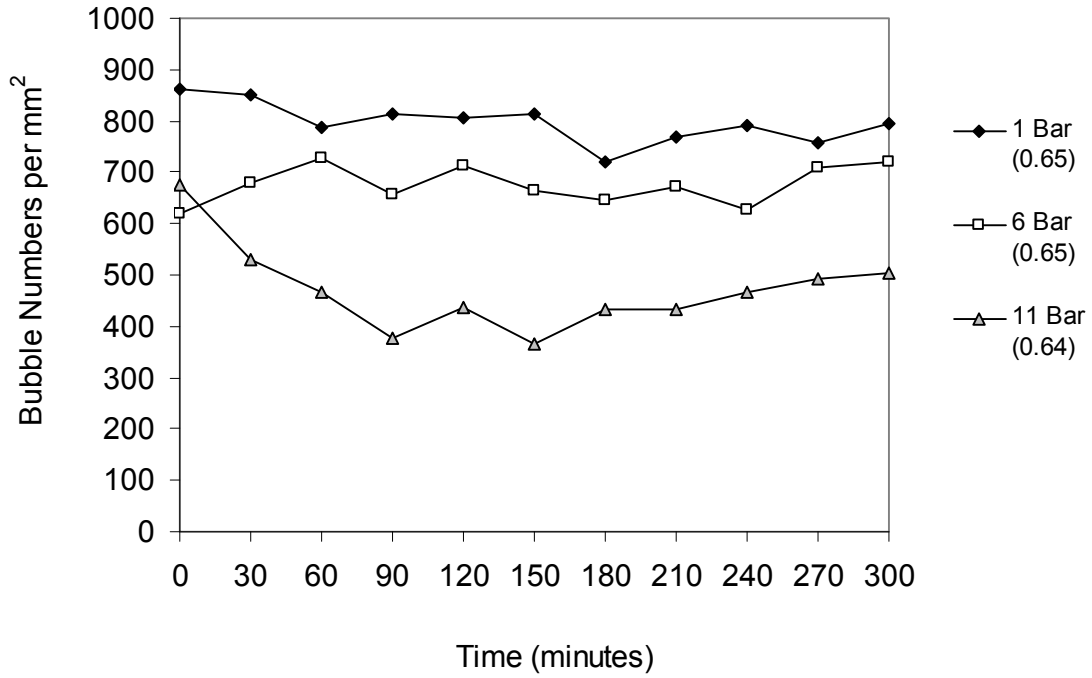


Figure 5.10: Bubble Count per mm² of image captured for a 5 hour experiment in Air

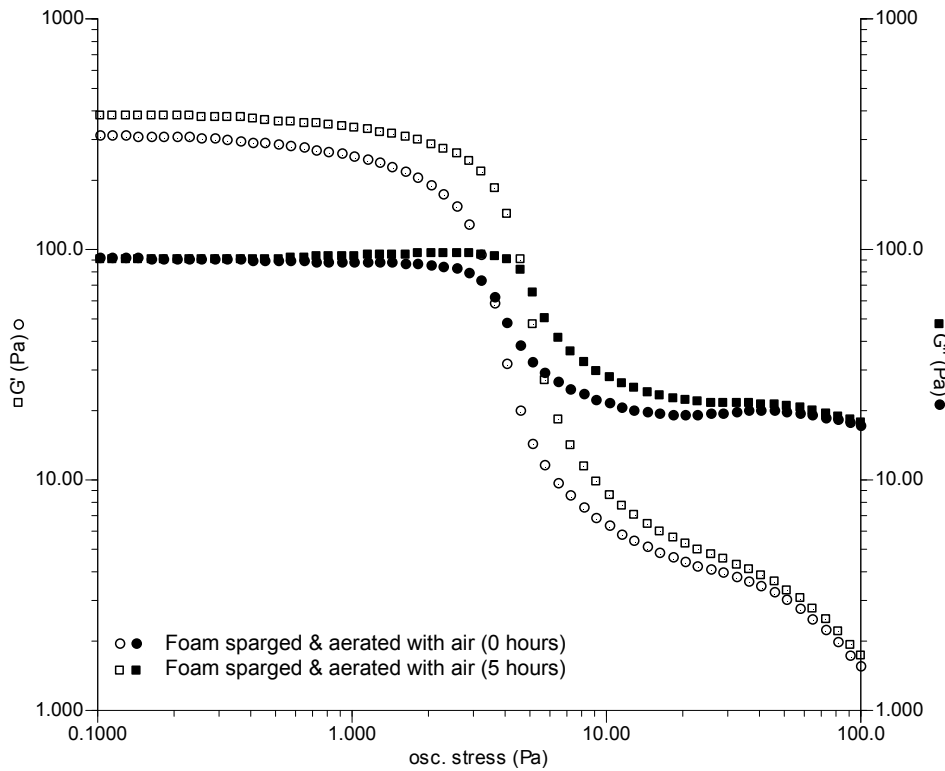


Figure 5.11: Sample aerated with air. Oscillatory vane rheology measurement on a fresh sample and a master batch sample after 5 hours disproportionation.

5.4.2.2 *Disproportionation with Nitrous Oxide (N₂O).*

The samples that were made with different gases, from here-on, all the rest, were aerated in the mixer, under continuous release of the gas (at 7 to 10 litres per minute). The mixers' grating was covered with foil and the whole mixer was covered with a polythene bag to contain the gases while aeration was taking place.

For the results in Figure 5.13, the sample was aerated with Nitrous Oxide, in it the 1 bar trace loses a certain number of bubbles from the foam sample, but at 6 bar there is a more marked loss of bubbles. The sample at 11 bar experiences a slight loss of bubbles. This result is consistent with the observations made in Figure 5.12, where 1 and 6 bar experienced a big rise in Mean Bubble Volume, and 11 bar did too. It must therefore be assumed that the loss of bubbles in this case (Figure 5.13) meant that most of them fused together to create a bigger bubble. Furthermore it must also be assumed that the loss of bubbles is not due to bubbles bursting and being released to the environment, which could have happened but which would be difficult to prove.

Microstructurally the sample does not change much at all. Both traces in Figure 5.14 remain the same, despite a difference of 5 hours in their measurement. No change takes place, due possibly to the fact that the sample is very liquid and the system remains fluid, with no real loss of bulk

microstructural properties, but nevertheless a continued drive towards disproportionation.

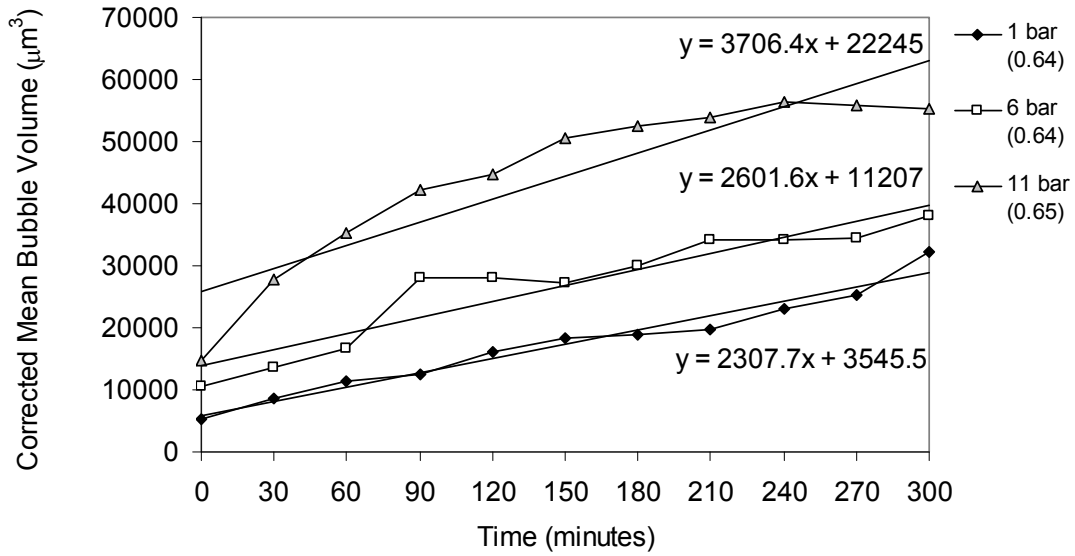


Figure 5.12: Nitrous Oxide: CSLM imaging in *Nitrous oxide (N₂O)* of disproportionation behaviour for 5 hours of the model mix sample under 3 different pressure regimes. Imaging took place at ½ hour intervals. Initial air phase volume of the mix shown in brackets (φ). The volumetric dependence of the foam was corrected using the universal gas law, where $p \times V = \text{const}$.

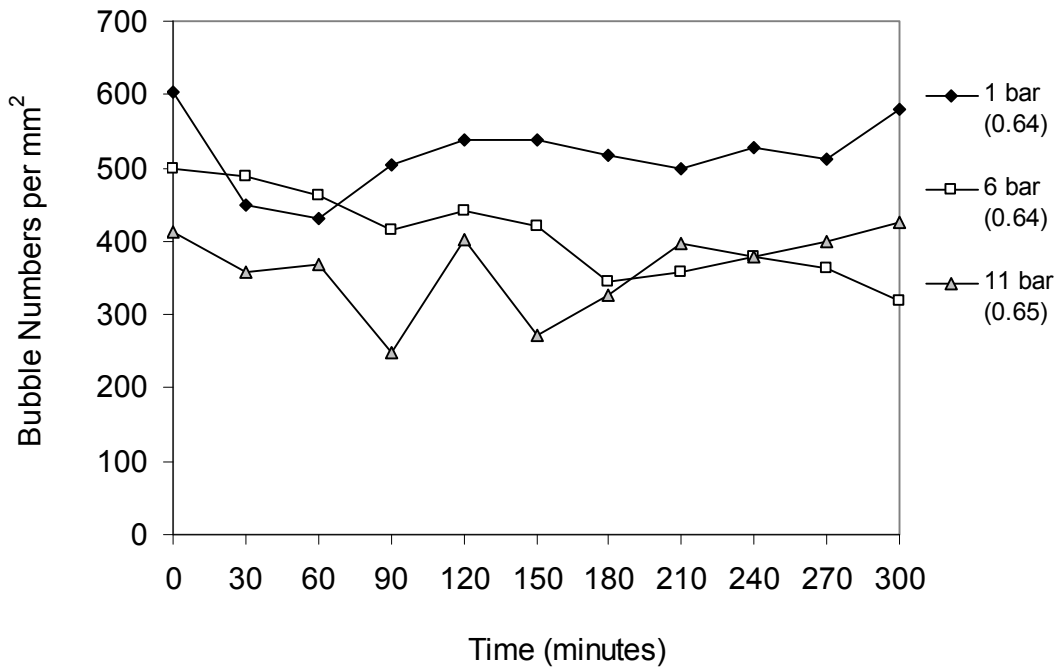


Figure 5.13: Bubble Count per mm² of image captured for a 5 hour experiment in Nitrous Oxide

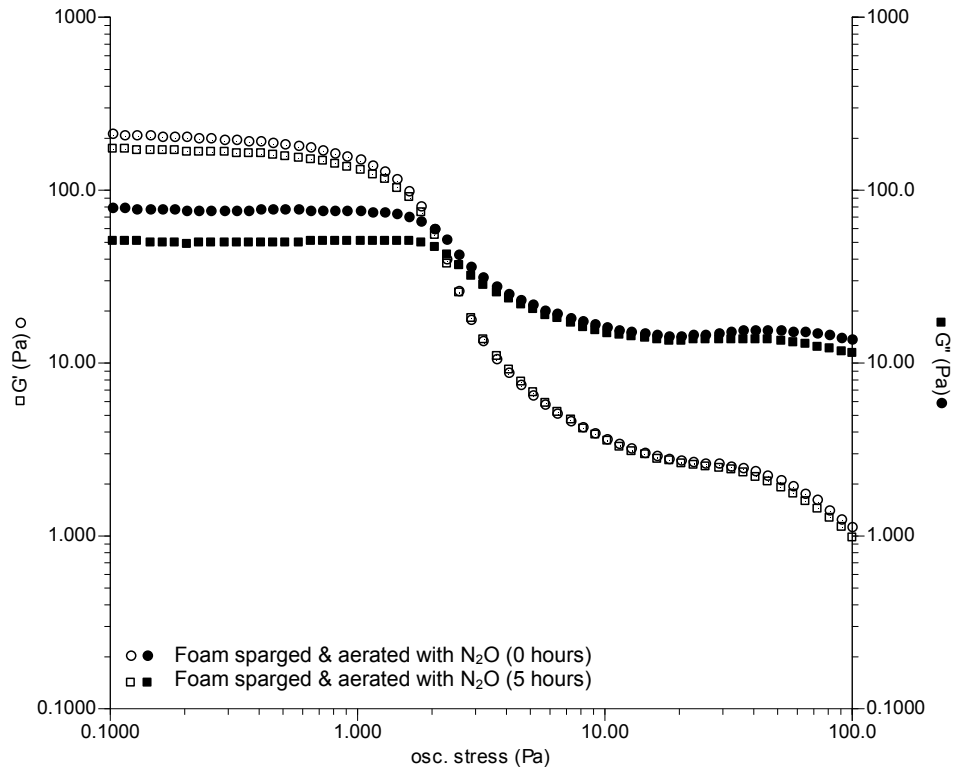


Figure 5.14: Sample aerated with nitrous oxide. Oscillatory vane rheology measurement on a fresh sample and a master batch sample after 5 hours disproportionation.

5.4.2.3 *Disproportionation with Helium*

There is very little evidence of microstructural change taking place in the foam sample aerated with Helium. The Helium results later formed part of the results in Figure 5.15 at 1 bar and 6 bar. In contrast a marked increase in mean Volume takes place at 11 bar. This result is mirrored in the bubble count graph in Figure 5.16, where for 1 bar and the first 30 minutes there is a drastic change in bubble numbers but thereafter only a marginal loss. Yet a drastic loss of bubbles is seen for the 11 bar regime.

Bulk changes due to disproportionation do not take place, which can be seen from the rheology traces in Figure 5.17. The helium sample was the only one of the five gases that was purged with the gas in question for 15 minutes.

All the other gases that were used were only purged through the sample for 5 minutes. The longer purging time was performed in order to give Helium sufficient time to diffuse into the sample, as it is a gas with a very low solubility.

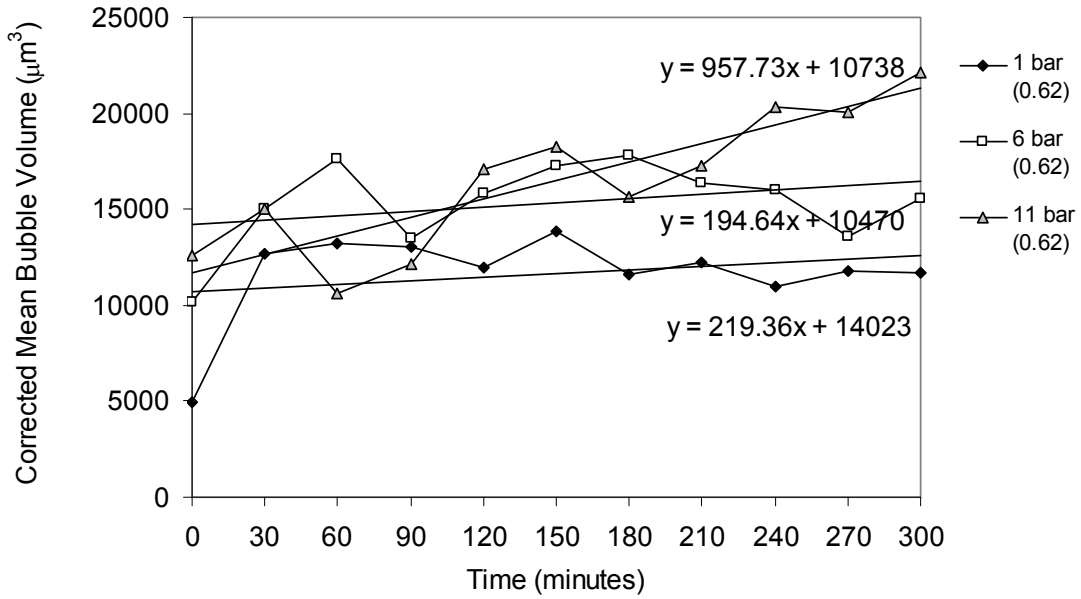


Figure 5.15: **Helium**: CSLM imaging in *Helium* of disproportionation behaviour for 5 hours of the model mix sample under 3 different pressure regimes. Imaging took place at ½ hour intervals. Initial air phase volume of the mix shown in brackets (ϕ). The volumetric dependence of the foam was corrected using the universal gas law, where $p \times V = \text{const}$.

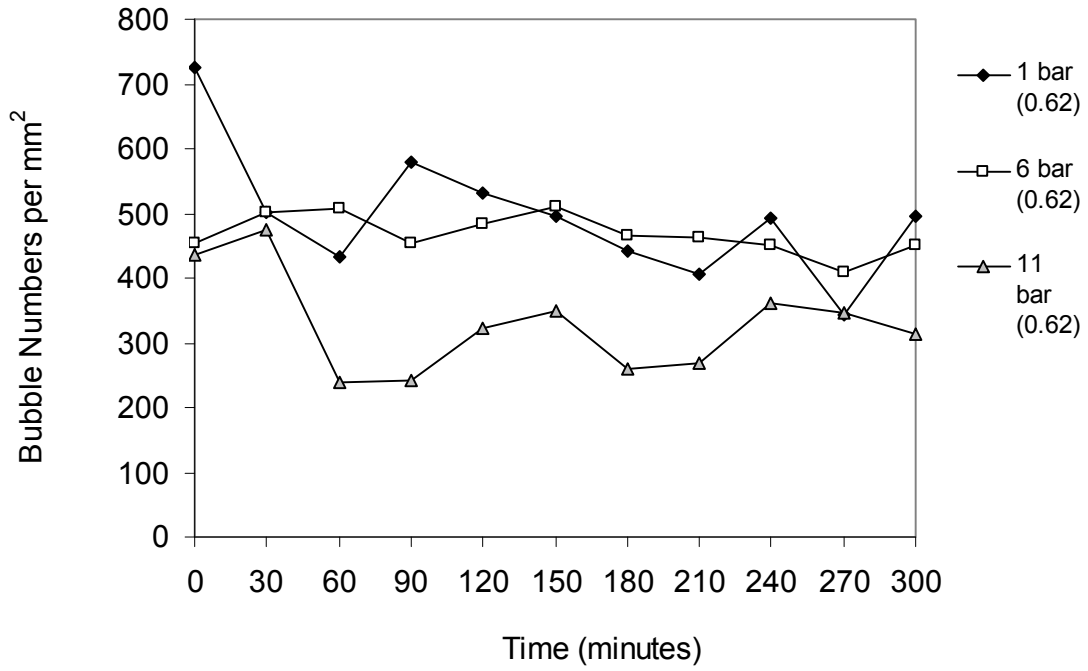


Figure 5.16: Bubble Count per mm² of image captured for a 5 hour experiment in Helium

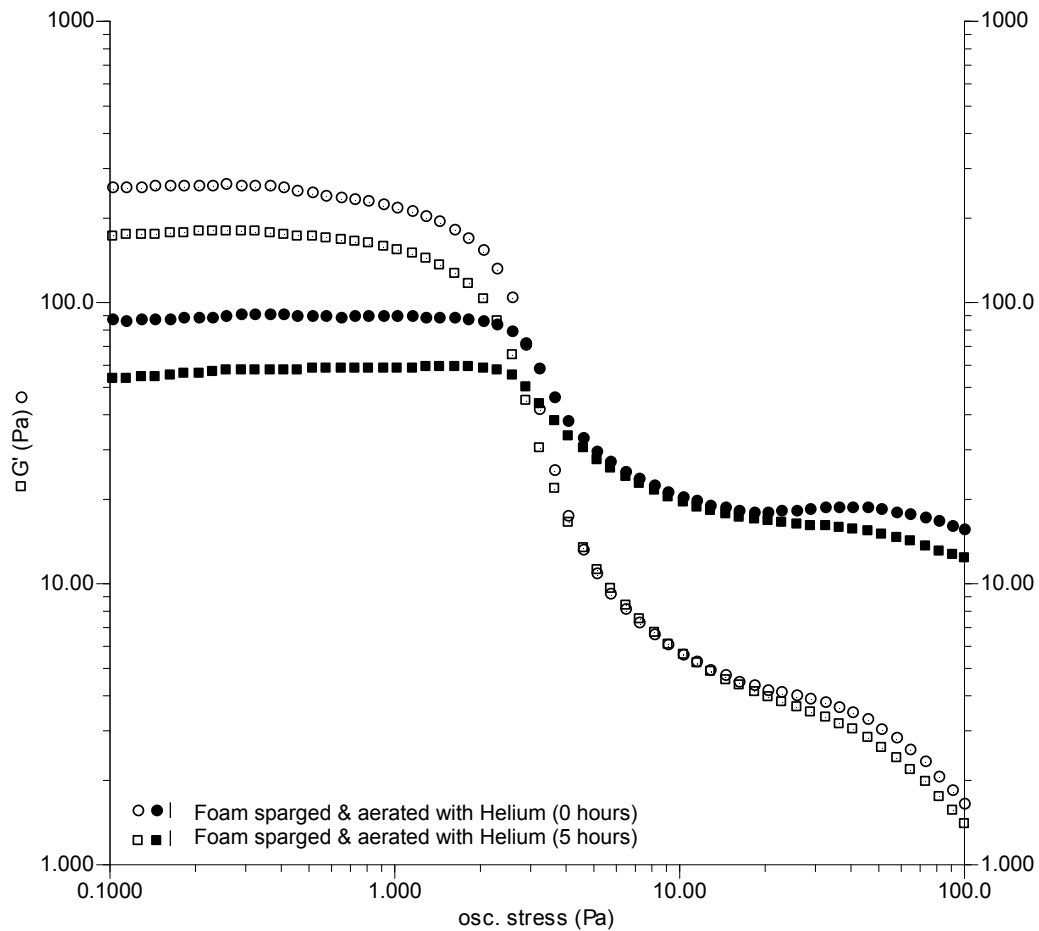


Figure 5.17: Sample aerated with Helium. Oscillatory vane rheology measurement on a fresh sample and a master batch sample after 5 hours disproportionation.

5.4.2.4 Disproportionation with Argon

In the Argon samples, there is little change at 1 bar absolute and only a little more change in the Measured Mean Volume at 6 and 11 bar. The result for these last two pressures is nearly identical. The lack of change is also seen in the evolution of bubble numbers over time. Very little change is also seen in the bulk microstructural changes when rheological analysis is applied to the sample. This is interesting, as the solubility of Argon is nearly double that of air. But yet the trends with Argon, as the aerating gas (with regards to a change in Mean Volume, Loss of Bubbles and rheological stability) are not very different from those where air was used.

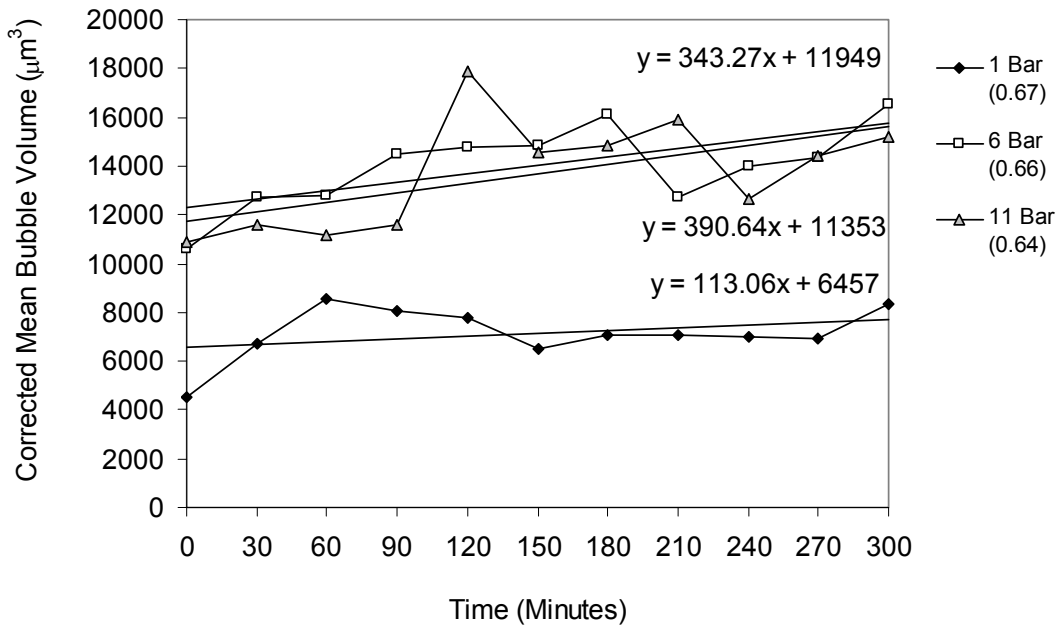


Figure 5.18: Argon: CSLM imaging in *Argon* of disproportionation behaviour for 5 hours of the model mix sample under 3 different pressure regimes. Imaging took place at ½ hour intervals. Initial air phase volume of the mix shown in brackets (ϕ). The volumetric dependence of the foam was corrected using the universal gas law, where $p \times V = \text{const.}$

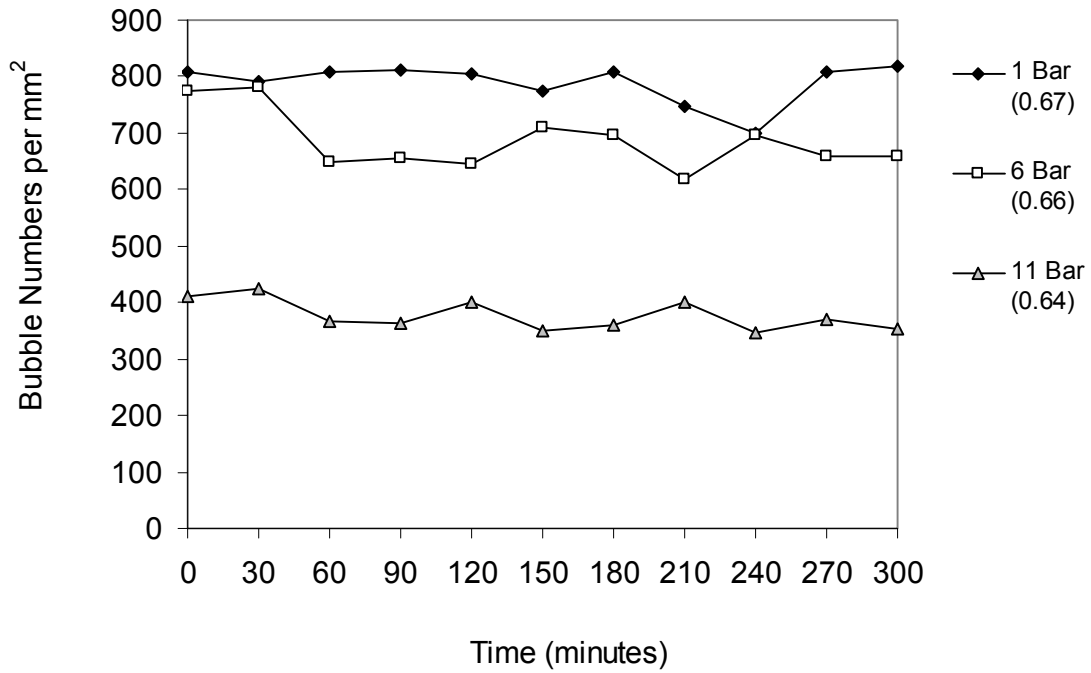


Figure 5.19: Bubble Count per mm² of image captured for a 5 hour experiment in Argon

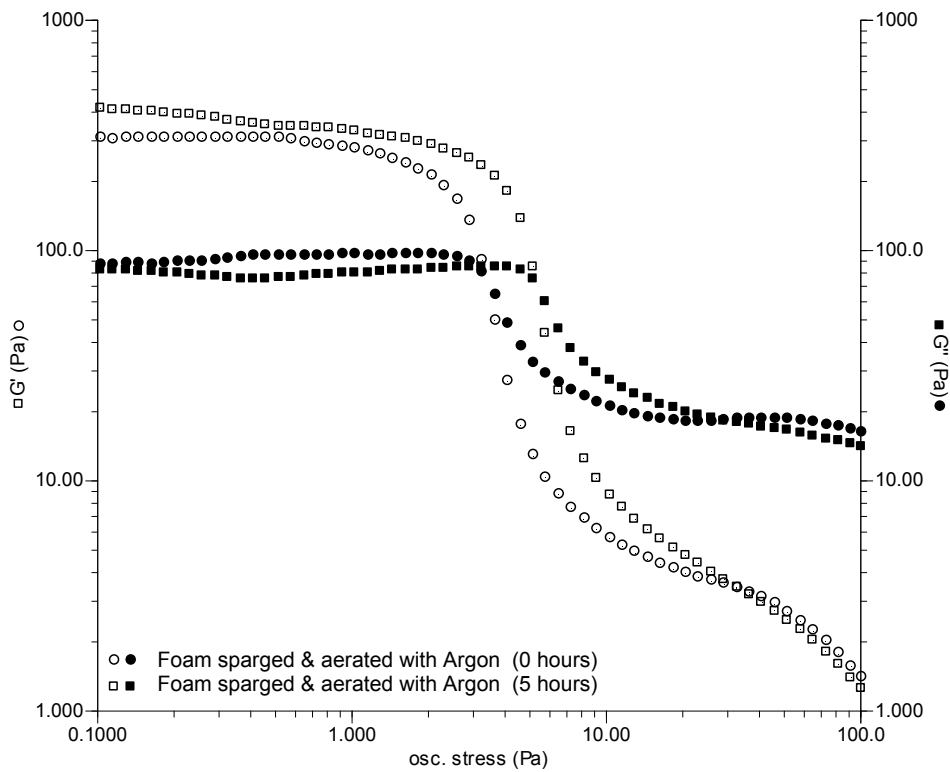


Figure 5.20: Sample aerated with Argon. Oscillatory vane rheology measurement on a fresh sample and the same sample after 5 hours disproportionation.

5.4.2.5 Disproportionation with Carbon Dioxide (CO₂)

It might be argued that a negative value for the slope of the 1 bar pressure graph Figure 5.21 not be a true representation of the disproportionation behaviour of the carbon dioxide sample. After 5 hours at the end of the experiment, the sample had microstructurally degraded and hardly any bubbles were left, Figure 5.21. The trend is thus a true representation of the actual events that were witnessed. This coincides with a dramatic loss of bubbles in Figure 5.22. A large bulk microstructural change was not seen in the sample, as the rheology traces (Figure 5.23) at 0 hours and 5 hours were similar.

Exposing the sample to overnight ageing during constant agitation (to prevent creaming or serum separation), followed by a disproportionation run for 5 hours at atmospheric pressure, produced the results seen in Figure 5.24. The mix was agitated using a Heidolph Reax2 agitator (Hadleigh, Essex, UK), which continuously inverted the sample and was set to the lowest setting. This experiment was undertaken in order to test a sample that had been aerated using the gas with the highest solubility, of the five being analysed in this study.

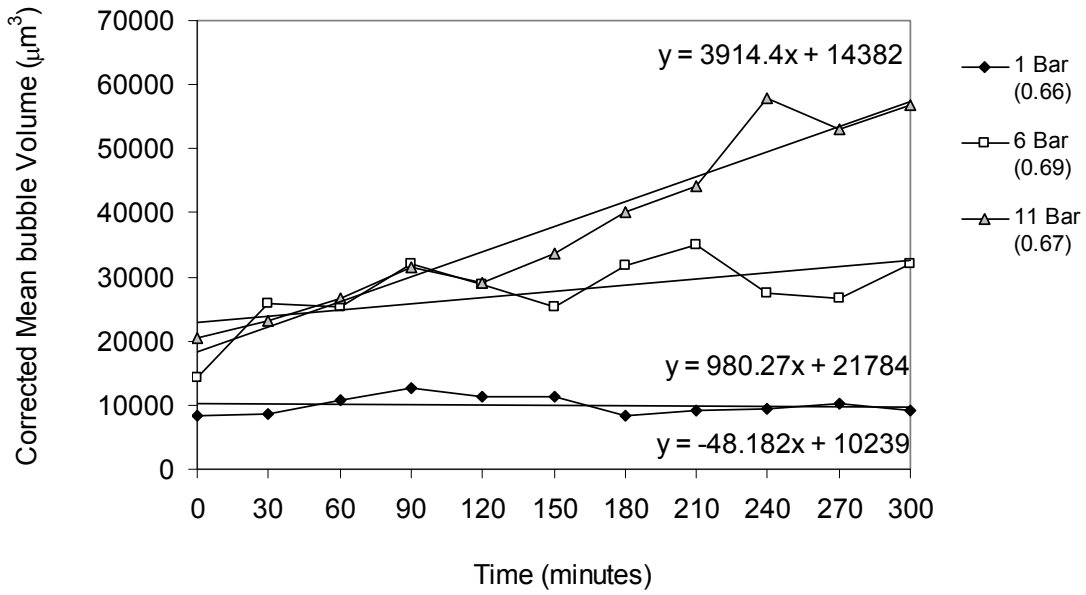


Figure 5.21: **Carbon Dioxide:** CSLM imaging in *Carbon Dioxide* of disproportionation behaviour for 5 hours of the model mix sample under 3 different pressure regimes. Imaging took place at $\frac{1}{2}$ hour intervals. Initial air phase volume of the mix shown in brackets (ϕ). The volumetric dependence of the foam was corrected using the universal gas law, where $p \times V = \text{const}$.

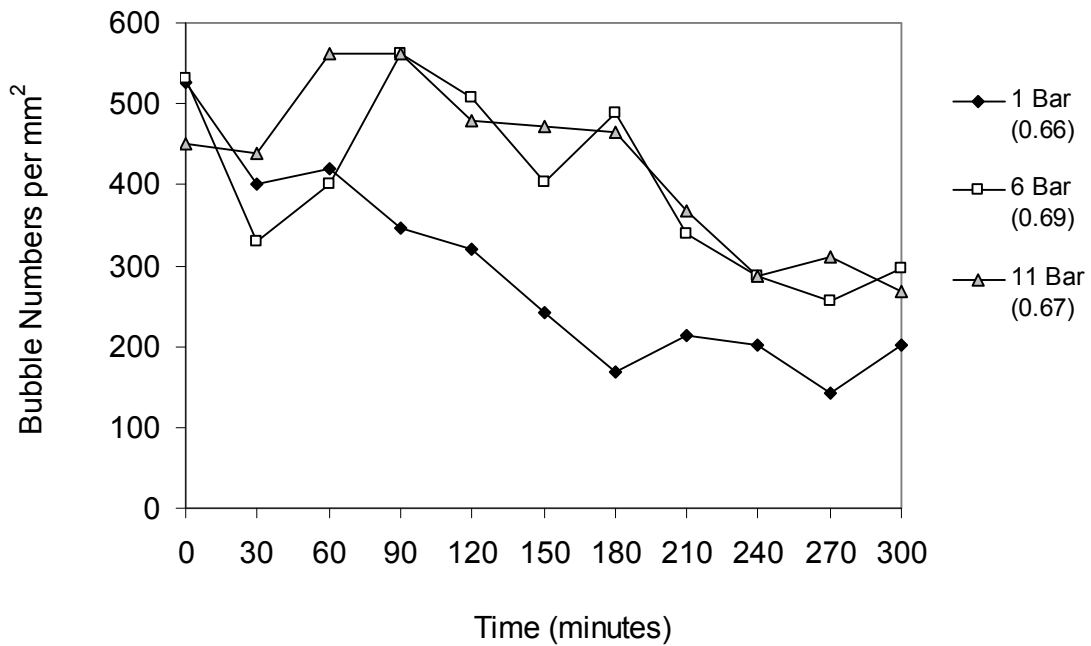


Figure 5.22: Bubble Count per mm^2 of image captured for a 5 hour experiment in *Carbon Dioxide*

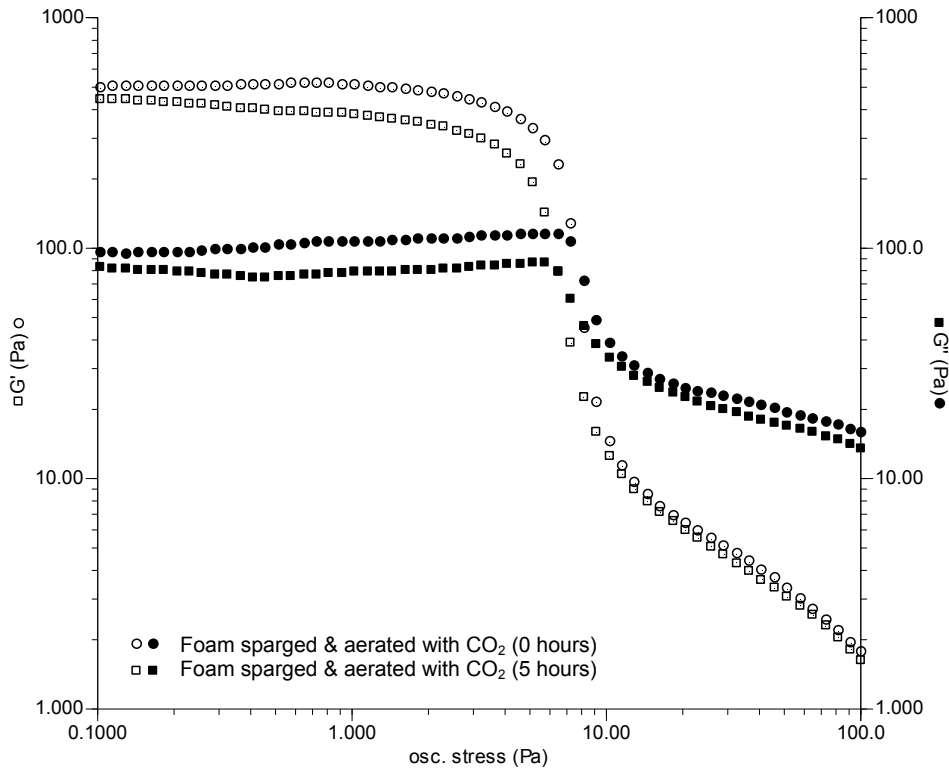


Figure 5.23: Sample aerated with Carbon Dioxide. Oscillatory vane rheology measurement on a fresh sample and the same sample after 5 hours disproportionation.

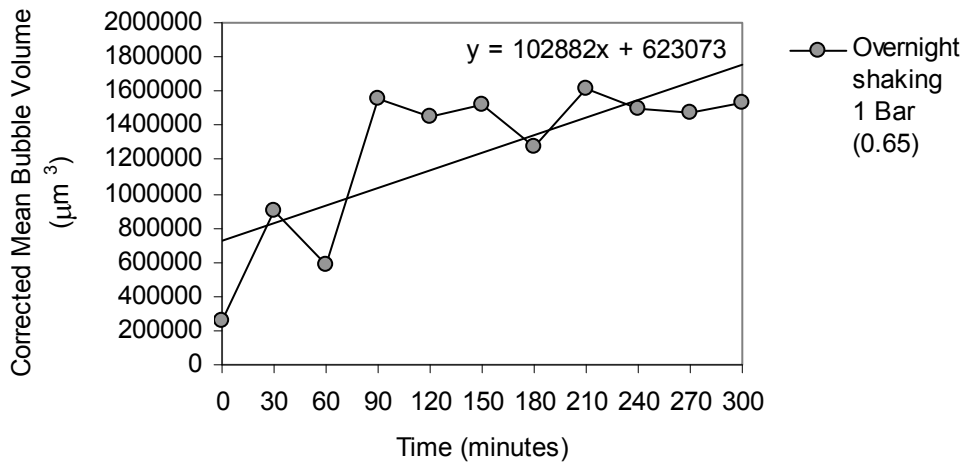
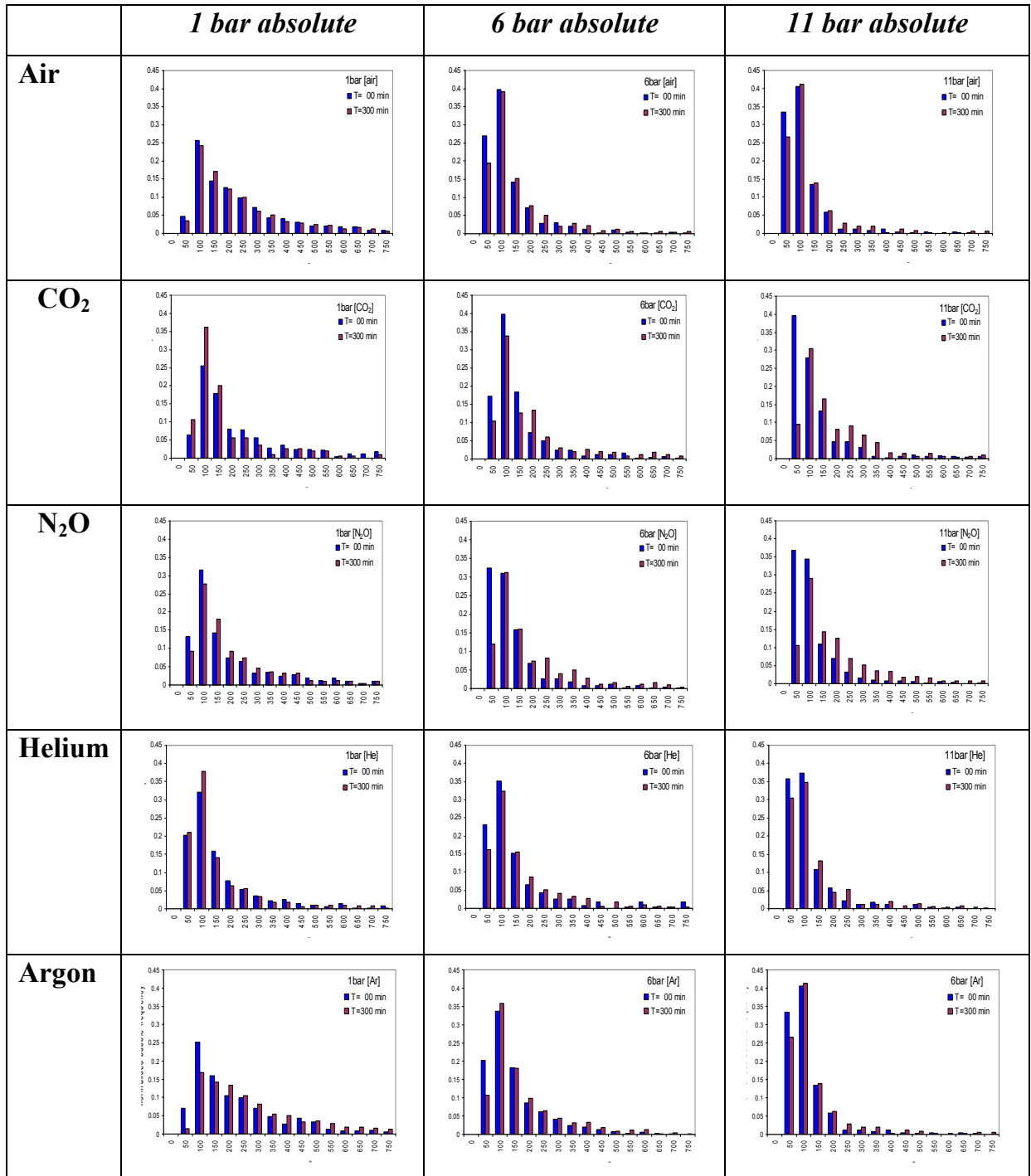


Figure 5.24: Carbon Dioxide: The sample was shaken overnight for 17 hours. Subsequent imaging a day later took place at ½ hour intervals, up to a total of 5 hours. The sample was at ambient pressure. Initial air phase volume of the mix is shown in brackets (ϕ). The volumetric dependence of the foam was corrected using the universal gas law, where $p \times V = \text{const.}$

Table 5.2: Disproportionation histograms for the foams with five different gases. They were studied at three different pressures and the data represented is the initial foam condition and its evolution after 5 hours. The graphs are plots of normalised bubble frequency against bubble size, measured in mean bubble surface area.



For all gases at the highest pressure, as would be expected, there is a higher incidence of smaller bubbles, especially in the size range of $50 \mu\text{m}^2$ to $150 \mu\text{m}^2$.

From the graphs in Table 5.2, foams containing carbon dioxide and nitrous oxide experience the most disproportionation.

5.4.3 Aeration times, solubilities and textures of the foams with the different gases

During aeration with the different gases, it was assumed that the beating time of the sample, would be uniform, and would not differ between gases. It was assumed that for example to reach a desired Overrun, the beating times would be the same, regardless which gas was used. After extensive knowledge was acquired through aeration with air, a target Overrun of 180% was nearly always achieved after about 20 to 25 minutes. It was seen while using different gases that this time differed widely. The different times that it took the foam to reach the target Overrun of about 180%, with all the other gases, could roughly be categorised into the following sequence **Argon < CO₂ < Helium < Air < N₂O** (this could only take place after extensive experimentation with the other gases had begun). This sequence was arrived at through empirical assessment.

The different solubilities taken from Table 5.1 can be categorised from least to most, in this sequence: **Helium < Air < Argon < N₂O < CO₂**.

The information in Table 5.3 was included as a comparison between the different aeration gases. This was added to compare the influence the different

gases had on the resultant foam texture. It can be seen that quite marked changes between the gases were in evidence. Foams made with Nitrous Oxide and Helium were both strikingly different in handling and appearance. The texture of the foam with Argon gas was not very different to that of air, but on the other hand its' aeration time (see above) was markedly different from most of the other gases. It was the gas that aerated the mixture the quickest of them all.

Table 5.3: Visual assessment of Aeration textures

| | |
|-----------------------|--|
| Air | Very smooth / creamy |
| Argon | Very smooth / lumpy (but not as lumpy as CO ₂) |
| CO₂ | Very thick / lumpy |
| Helium | Bitty / Gloopy with a chunky consistency |
| N₂O | Very liquid / extremely free-flowing |

Most of the rheological traces hardly show a difference between the initial reading and the one taken after a disproportionation time of 5 hours. This might be due to 2 reasons: either bulk rheological measurements are not able to discriminate between very subtle changes that are taking place in the microstructure due to disproportionation. The other reason might be that the bulk master batch method might prevent severe disproportionation events from taking place. It was originally devised to prevent creaming or serum deposition, but it might have unwittingly affected disproportionation and bubble-bubble interactions as well.

5.4.4 Shear Analysis

5.4.4.1 *Vane rheometry*

Two main experiments were carried out with the rheometer. In one experiment the sample was sheared where the shear profile started slowly and then throughout the experiment was progressively ramped in a linear fashion to the full and final speed of either 50, 100, 150 or 200 s⁻¹. The rheometer performed this ramp automatically. Once it was finished, the sample was taken out and placed in a small plastic Petri dish and imaged. In the second experiment the sample was sheared continuously for the time period specified, but unlike in the previous experiment, no ramp was conducted, the sample was sheared at the one set speed, without variation.

In Figure 5.25 the sample was exposed to the linear shear. This figure is interesting for the fact that the sample showing the largest and the most marked Volume increase was the sample sheared at 100 s⁻¹, this was then followed by 150 s⁻¹ as a sample with only a moderate increase in Mean Volume, and the sample with the least change being the sample that was sheared at the higher shear rate of 200 s⁻¹. A reason why this might be the case could possibly be correlated to the results obtained within the release rate experiments. One hypothesis which could be valid for both phenomena is that small disturbances in the sample are more detrimental to the foam microstructure than are large and fast changes, seen either with shear or pressure changes.

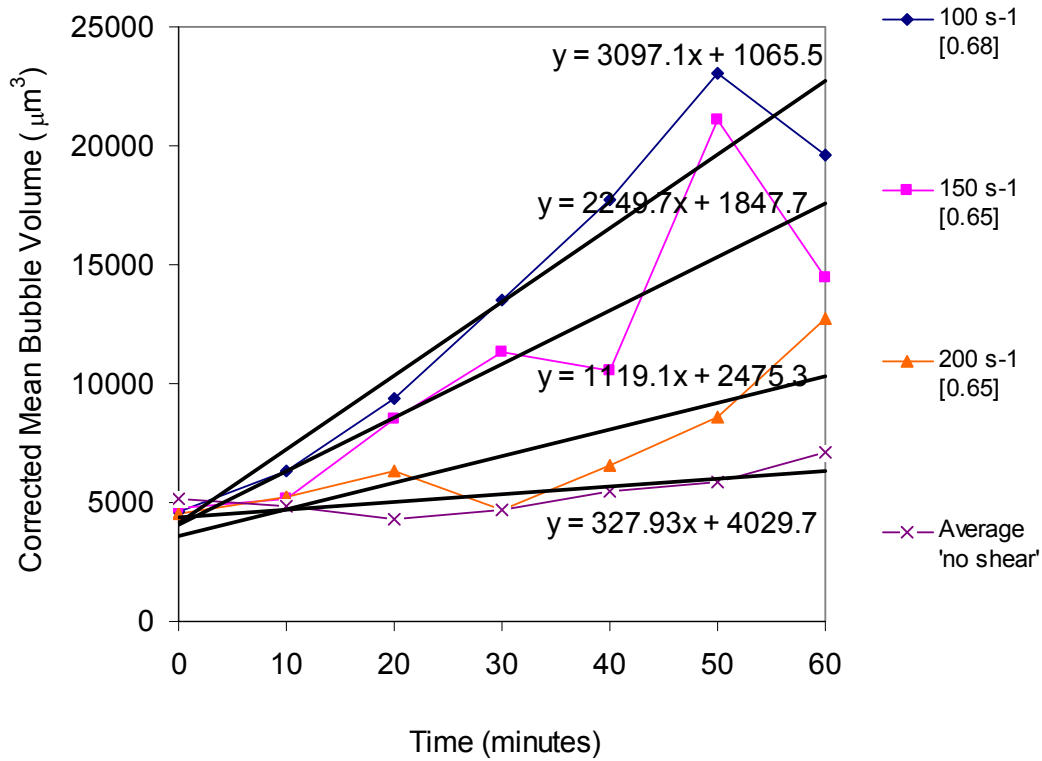


Figure 5.25: Shear rate and time evolution of foam sample on a linear shear regime. Air phase volume (ϕ) of the sample is given in square brackets.

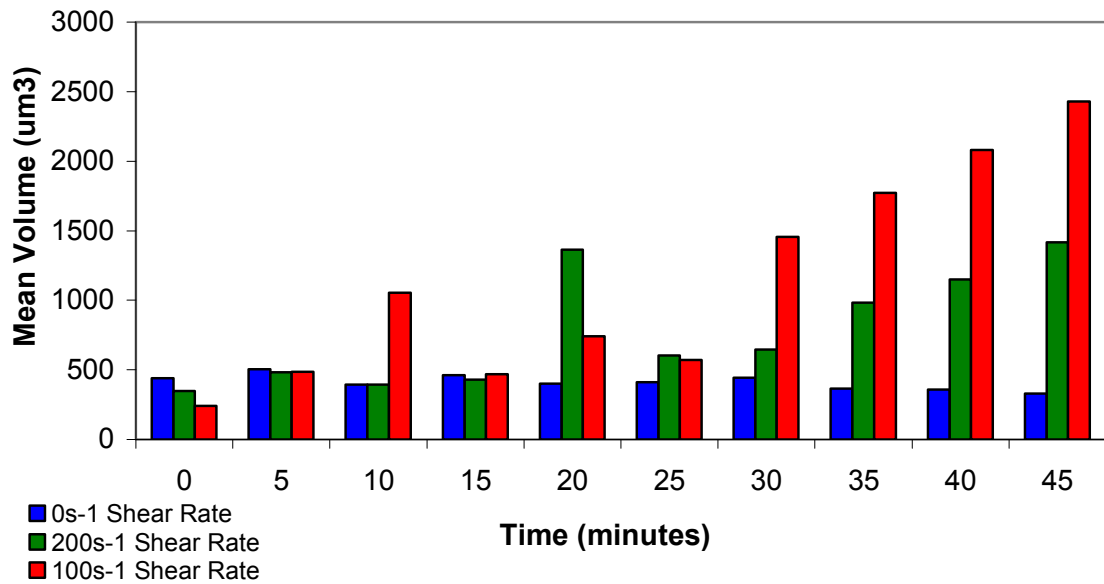


Figure 5.26 Linkam shear stage data at two different speeds

The graph in Figure 5.26 corroborates the data from Figure 5.25. The same behaviour of the foam is taking place with a larger increase in mean volume at

100 s⁻¹ when compared to the faster shear rate of 200 s⁻¹. The large ‘temporary’ increase in mean bubble volume at minute 10 and minute 20 for the shear rates of 100 s⁻¹ and 200 s⁻¹ respectively, are possibly due to the imaging of large transient bubbles in the field of view. This proved to be an inherent problem with the bubble sizing technique with the Linkam setup. A more thorough discussion with regards to imaging problems within the Linkam shear stage is carried out in section 5.4.4.2.

In Figure 5.27 the sample was sheared using the same linear shear mode described above for the vane rheometer.

The terms ‘forwards’ and ‘backwards’ in Figure 5.27 are defined as follows: In the forwards experiment, the first shear point to be analysed and imaged was the one that took place after 10 minutes shear. It was then followed by the 20 minute shear point and then the 30 minute one. The final shear point to be imaged was the one that had been sheared for 60 minutes. These shear times employed were constant shear, but with a linear acceleration of the vane rheometer. This implied that once the sample had been loaded into the vane insert it was sheared for the full time without stopping. It is important that the sample was sheared at 100 s⁻¹, as seen in Figure 5.28. It was this shear rate that did not lead to catastrophic loss of bubbles and sample liquefaction. In the ‘backwards’ experiment, the first sample to be imaged was the one that had been sheared for 60 minutes, this was then followed by the one that had been sheared for 50 minutes until the last image to be taken was the one that had

only been sheared for 10 minutes. As it can be seen, both samples are not the same, and due to this discernible difference in the two traces, it might be argued that even though the samples have been exposed to the ‘master batch’ method to avoid any creaming and syrup separation from taking place, that their shear properties are indeed different. Nevertheless there was still some microstructural rearrangement taking place that was not perceivable with the naked eye, but which was still measurable with our system. This might be due to some interfacial rearrangements taking place on the bubble surface. One speculation might be a form of protein relaxation, with a loosening of the mechanically denatured whey protein covering the bubble surface. This would perhaps create a slightly wetter foam, not dissimilar to the starting foam microstructurally, but one which was far more susceptible to shear.

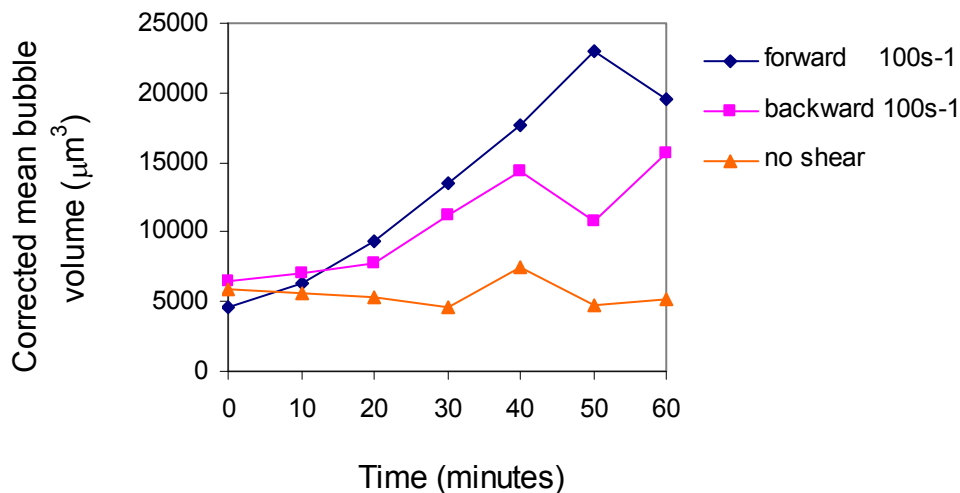


Figure 5.27: Dependence of sheared foam sample on sampling time-point and shearing time

For the linear shear regime, the output and evolution of shear stress against time was measured and charted. In the linear regime, the shear rate increased

over the set time period, to reach its maximum, shortly before the end. In the representative graph (Figure 5.28) the four different shear rates (50 s^{-1} , 100 s^{-1} , 150 s^{-1} and 200 s^{-1}) were used on a foam sample and it was sheared for 10 minutes. Similar traces were obtained for all further shear times and shear rates. The foam sample that makes up the 200 s^{-1} trace, degrades and breaks down after 6 minutes and about 180 Pa. Whereas the sample sheared at 150 s^{-1} , degrades after 8 minutes and 175 Pa. The samples sheared at 100 s^{-1} and 50 s^{-1} , do not degrade at all during the 10 minute time-frame of the experiment.

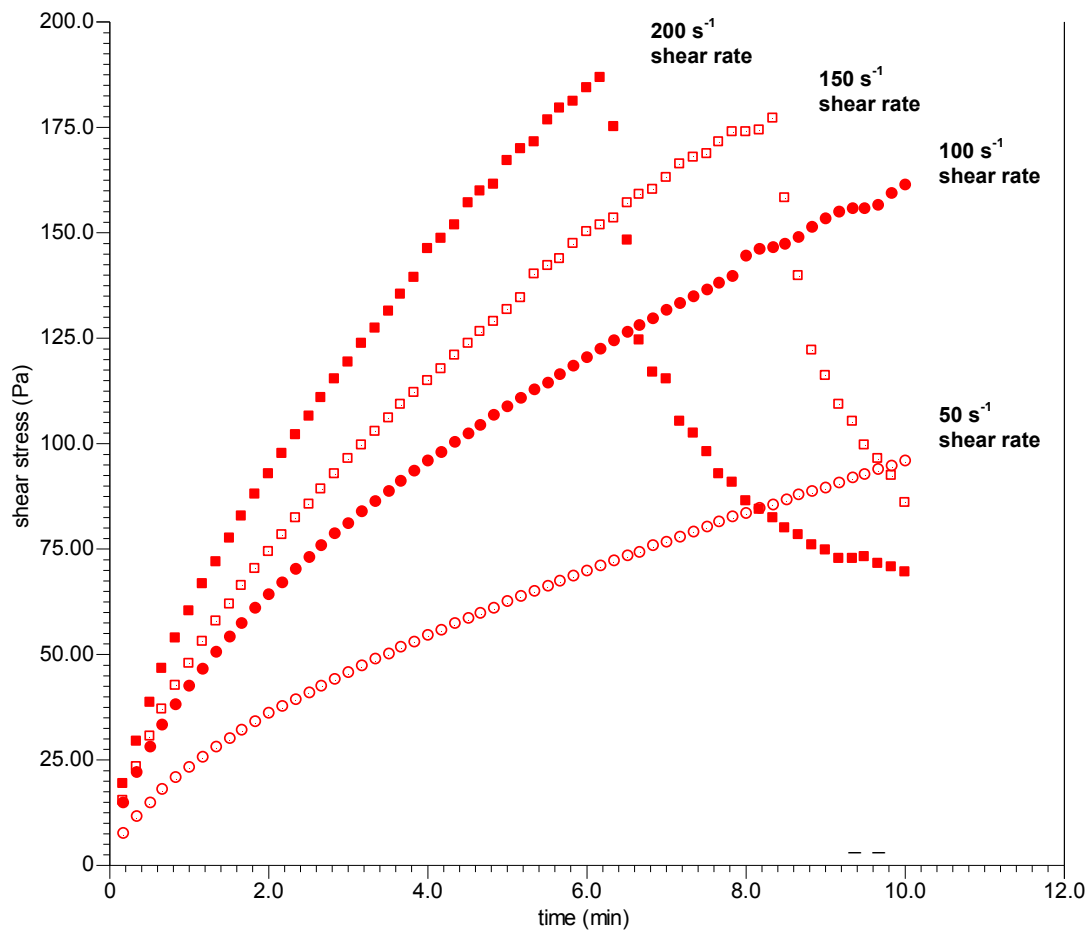


Figure 5.28: Shear rheometry, (sheared using a linear ramp) of a foam sample for 10 minutes using four different shear rates 50 s^{-1} , 100 s^{-1} , 150 s^{-1} and 200 s^{-1} .

In Figure 5.29 continuous shear was used, this meant that the sample was sheared at the target rate, for the entire time period. It was not linearly “ramped” like in the previous experiments. This meant that the sample was sheared for the whole time at the same constant shear rate. It is interesting to note that the sample starts at about the same initial shear stress before it breaks down, this is the same as the shear stress in Figure 5.28, before that one breaks down as well but not before around 175 Pa is reached.

Figure 5.28 is interesting as it shows the exact point of breakdown as a function of the shear rate which was used. But on the other hand Figure 5.29 gives an indication as to the time which it takes the structure to break-down, but the exact time-point of break-down is not clear cut. The only problem with the linear shear ramp is that it is not known what shear rate is being applied to the sample at any given time, only the target shear rate is known, which is applied roughly before the end of the run, after 10 minutes have elapsed.

In Figure 5.29 structural rearrangement of the sample took place for 50s^{-1} at around 2 minutes, it is fair to say that no sample breakdown took place in that sample.

For 150 s^{-1} and 200 s^{-1} it can be said that sample breakdown took place at around 5 or 6 minutes. But the exact time point of sample break-down is not clearly defined. Although it does confer with the results above, those samples broke down too at around the same time.

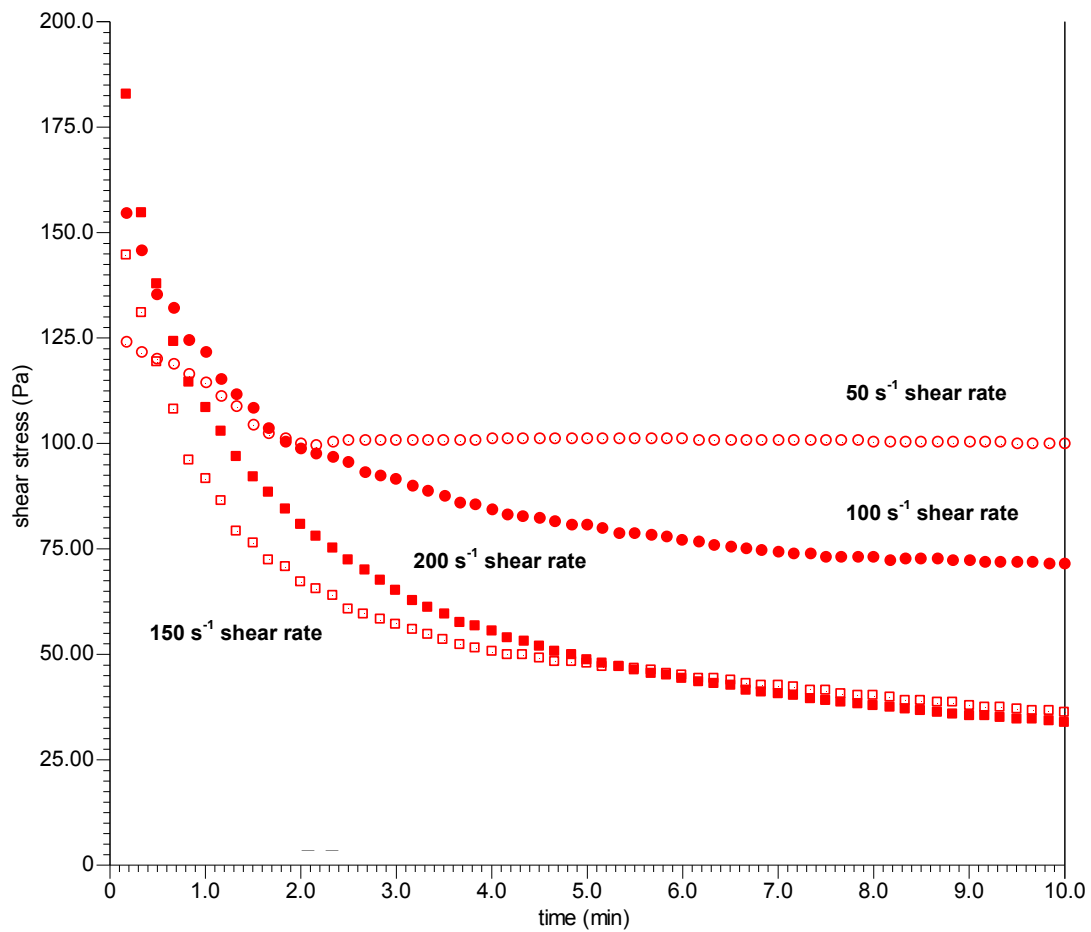


Figure 5.29: Shear rheometry of a foam sample for 10 minutes using four different shear rates 50 s^{-1} , 100 s^{-1} , 150 s^{-1} and 200 s^{-1} . Sheared using continuous shear at the set shear rate.

The samples in Figure 5.30 were exposed to the continuous shear regime, for the time and shear rate which are given on the x-axis and legend respectively. For each time point a new sample was loaded into the vane inserts. For each time point the sample was sheared for the time indicated. So for 10 minutes, the sample was sheared for a total of 10 minutes without interruption. The trends that were obtained through this experiment show a Mean Bubble Volume increase with time, which in addition, is dependent on the shear rate that the sample was exposed to.

For the trends in Figure 5.30, the 30 minute time-point seems crucial as this is where the increase in mean bubble volume begins to take place, regardless of the shear rate that the sample is exposed to. The regime that shows the biggest increase over time is the 50 s^{-1} shear rate. The trend is composed of an average of 4 readings, which helped in the elaboration of more robust data. All the other readings are an average of 2 readings (except for the “zero shear” trend which is an un-sheared control. 2 readings were taken of the un-sheared control for each sample analysed. But each control is paired with data of sheared samples and therefore the reading is composed of an average of all the readings. Which makes a total of 8 readings).

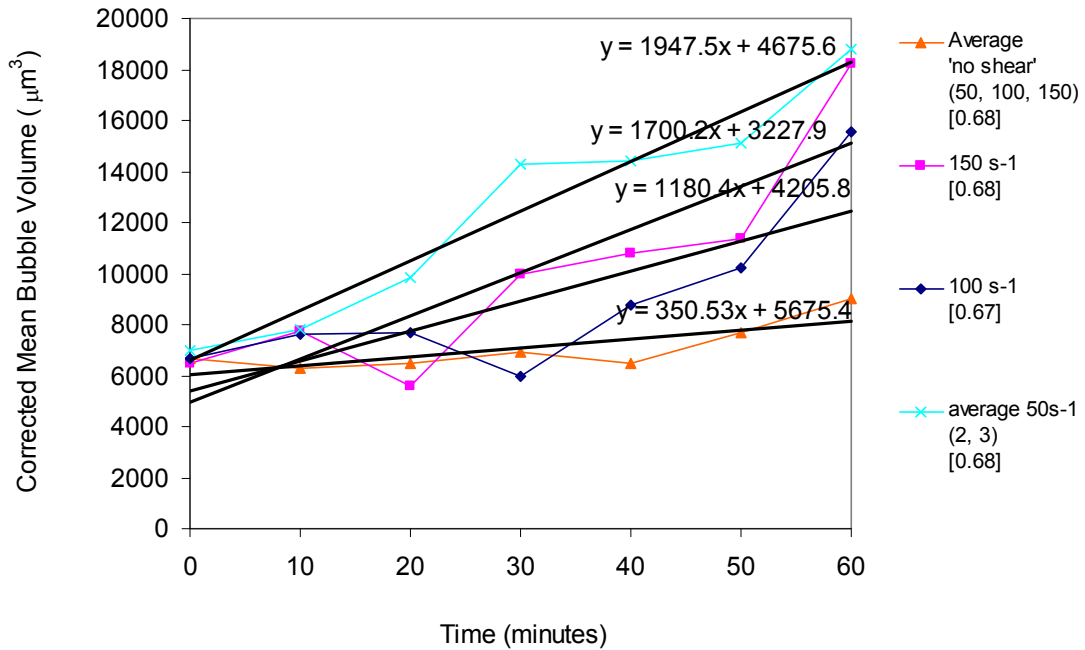


Figure 5.30: Shear rate and time evolution of foam sample on a continuous shear regime. Air phase volume (ϕ) of the sample is given in square brackets.

5.4.4.2 Linkam shear stage

For the shear break down experiment below, the sample was sheared until break-down was achieved or until 60 minutes had passed, whichever was the sooner. If no breakdown had occurred by the 60 minute time point, the experiment was terminated at that point and 60 minutes taken as the reference time. Three readings were taken for each shear rate and from that the average was created. ‘Breakdown’ was taken as the time period when a whole bubble covered the entire field of view as in Figure 5.31b. Due to non uniform shear fields associated with the use of the Linkam shear cell, these overarching bubbles were sometimes created but not imaged, as they did not cross the pin-hole aperture. Experiments had to be adapted to cope with the limitations of the equipment and the set-up. Nevertheless after much experimentation, some meaningful and satisfactory results were obtained.

Breakdown, following the definition above, took longer with a shear rate of 50 s^{-1} , averaging about 30 minutes, than it did at 200 s^{-1} , where it averaged about 10 minutes. This experiment hoped to elucidate the shear stability properties of the model microstructure. A better way was later found with the vane rheometer which was more accurate (Figure 5.28). Nevertheless the shear “break-ability” of the sample seems to follow the same trends. There the 200 s^{-1} shear-rate sample broke down the fastest, and the 50 s^{-1} and 100 s^{-1} sheared samples did not break down at all after 10 minutes shear.

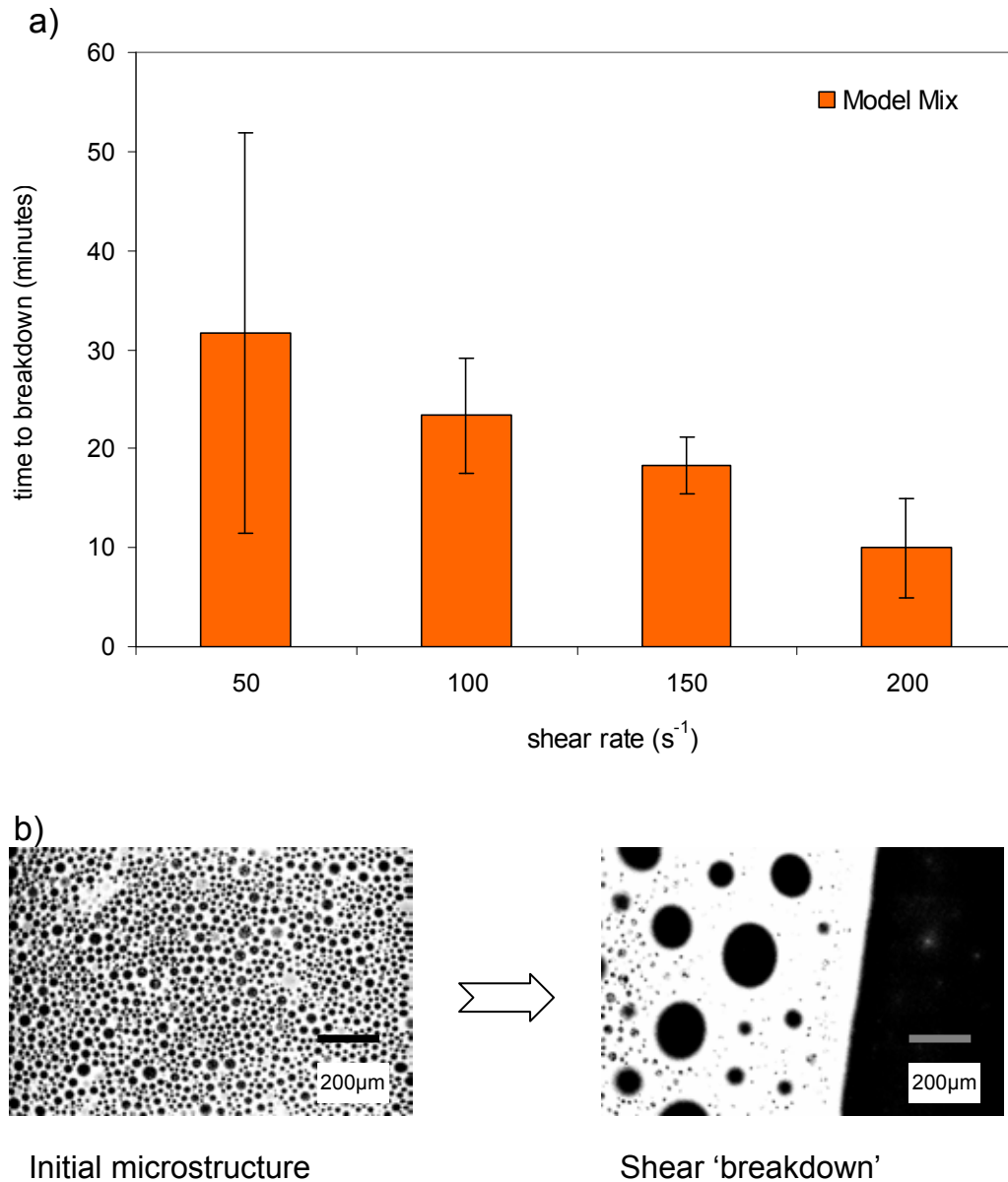


Figure 5.31: a) shear breakdown of the model mix as seen under the Linkam shear stage. The graph is shear rate against 'breakdown time' b) Representative images of the initial foam microstructure and the image which was taken at the time which was considered as the point of shear "breakdown".

Reproducibility of the results, for bubble size measurements, obtained with the Linkam shear stage were highlighted as a real issue. No bubble sizing with the Linkam setup was performed, hence for the breakdown experiment it involved setting an arbitrary and qualitative decision when the experiment was to be terminated. This method had to be adapted after rigorous quantitative

experimentation with bubble sizing had been carried out, which mostly yielded meaningless results. The main problem with the setup, was the sample's trajectory across the glass plate which was unpredictable and also only restricted to a pin-hole sized aperture for imaging. It thus meant that obtaining reproducible results was virtually impossible. It was deduced that reproducibility relied on sample homogeneity, with bubbles equally dispersed throughout the mix, which was unobtainable. Frequently events took place in "black spots" of the equipment that were only imaged much later, or perhaps not at all. Very often a thorough mixing of the sample on the glass plates never took place. The qualitative method (which assessed only bubble breakdown) proved to be the only way to obtain any decent and meaningful data with the Linkam set-up. Nevertheless, and despite these multiple drawbacks, the general trend of the data is not entirely dissimilar to that of the rheo-shear experiments with the Vane Rheometer (see Figure 5.28). In fact, if the two data points in Figure 5.31a are analysed (these being the 100 s^{-1} and 150 s^{-1}) they show the smallest error bars of the four data sets. These two shear rates lie between the 'critical' shear rate that has been discovered that exists for the sample. It is at the shear rate of 125 s^{-1} that the sample completely de-aerates. At the time it was unknown that 125 s^{-1} was significant for the foam structure and breakdown. Otherwise this shear rate would have been investigated further. The figure 125 s^{-1} was arrived at through observation of the foams' behaviour during shear in the vane rheometer. This was the exact shear rate where foam breakdown took place. No experimental evidence was gathered for this shear rate.

5.5 Discussion

An observation while carrying out the release rate experiments for Figure 5.1, indicated that upon rapid release, the resultant coalescence events also took place rapidly too, but if the pressure was released slowly then the resultant coalescence events also proceeded slowly too.

The results seem to indicate that a rapid release when compared to a slow release rate might have a more protective effect against coalescence, as slow release seems to have a more detrimental effect on the final foam structure.

The model system composed of Corn syrup with protein and emulsifier suspended in it, due to its viscosity, will prevent the protein layers from recovering the bubble surface once this has been lost due to a pressure change effect. In comparison to work by Murray and others, who are working with dilute protein systems, where this might readily take place and with great ease. There, bubble rearrangement and recovering under the Gibbs-Marangoni effect, was sometimes seen.

Murray et al. (2002b) mention that at the end of the rapid expansion, in their system, it was not expected that the surface load on the bubble would be any lower than before the cycle, when the bubbles were perfectly stable. And that it was therefore highly significant that there was any coalescence at all under such conditions. They speculate that inhomogeneities develop in the protein

layer during the expansion, which cannot be healed by rearrangement within the film or by new protein adsorbing to the surface and, in that way, interfacial regions must develop which were unstable to coalescence. They speculate further that any delayed coalescence within their system, was also probably a manifestation of the relatively long time scale of relaxation processes within the film compared to the time scale of the expansion. Their explanation was substantiated by Brewster angle microscopy of films with a WPI sample subjected to similar compression-expansion cycles, which showed long length scale inhomogeneities which could take minutes or even hours to disappear. Although they mention that the compression/expansion cycle used in their experiment was somewhat arbitrary, bubbles in food foams could be expected to be subjected to a range of compression and expansion cycles during their processing lifetime. They mentioned that those effects would not be without practical significance (Murray et al., 2002).

Murray et al., (2005) mention further that the volume of a bubble undergoing a pressure change during processing must increase or decrease in inverse proportion to the pressure, changing the surface coverage of stabilising surfactant. In addition, the gas bubbles in many foamed products are large enough that they can be much more easily deformed than emulsion droplets by the hydrodynamic forces commonly operating during processing (Murray et al. 2005).

Murray et al. (2005) mentions that coalescence does not cease immediately on expansion, but it occurs at a greatly reduced rate after expansion has ceased for a few tens of seconds, at most. In the system studied here the continuation of the coalescence events was very much release rate dependent. Murray et al., (2005) argues further that the persistence of some coalescence events after expansion has ceased, points to relaxation mechanisms within the adsorbed film that have longer time scales than the time of the interfacial deformation (Murray et al., 2005).

In the experiments discussed in this chapter, coalescence events still persisted long after pressure release had stopped, and the duration for which these events lasted was directly related to the speed of the pressure release, *i.e.* quick release, few extra coalescence events were seen after the release, but with a slow release, many slow coalescence events were witnessed after the release, which in addition lasted for a longer time period.

It can be speculated that in actual industrial processes the coalescence rate in a foam might be a lot higher. As the base mix is loaded into the aerator, this is then pressurised and only subsequently aerated creating the foam once it is under pressure (Murray et al., 2005). The bubbles (and their interfacial covering) will have been formed under the higher barrel pressure, but when this is then released, the rapid expansion and the lack of material covering the bubble might cause considerable coalescence in the aerated mix. The Linkam pressure system described in this chapter, can only partially explain

coalescence dependence as it relates to pressure releases. It would not be right to compare the dynamics taking place in the Linkam pressure cell, to those that take place industrially. The work is nevertheless important in elucidating the principles behind fast and slow pressure release rates. So if a comparison between the Linkam system and industrial processes were made, it must be noted that the foams in the Linkam pressure cell were formed at atmospheric pressure and will thus react differently to both pressurisation and depressurisation. Upon pressurisation the bubble surface and the protein covering, will crumble and contract. It will then relax again once the pressure has been taken off. This process is most likely not witnessed in the industrial setting, to the extent it is here. The initial protein ‘crumpling’ or folding during pressurisation is probably not seen at all, as the foam will have been formed under pressure. This will consequently lead to a different coalescence profile taking place in both cases. But as it was nevertheless stressed before, it is the main concern of this work to capture the principle understanding of the processes taking place during a pressure release event and not necessarily to mimic the event exactly. A very quick release event from relatively high pressures of 6 bar will not affect the bubble microstructure as much as a very slow release rate will. A very slow release of pressure that only experiences a very small drop in pressure will not affect the microstructure either. On the other hand a large drop in pressure at a very slow release rate, will detrimentally affect the microstructure.

From the disproportionation experiments it can be seen that disproportionation takes place at a faster rate in an environment containing Nitrous oxide than it does with air as an aerating agent. This is to be expected as nitrous oxide is about 20 times more soluble than air (see table: Table 5.1). In both cases disproportionation at the high pressure of 11 bar absolute takes place faster than disproportionation at 6 bar, and disproportionation at 6 bar, in turn takes place faster than disproportionation at atmospheric pressure (1 bar absolute). At high pressure, buoyancy issues in relation to bubble behaviour might have an influence on the mean volume and its more rapid increase in size. The imaging interface at the higher pressure of 11 bar, gets depressed, more than what would take place at 6 bar or 1 bar, and this facilitates, previously unseen bubbles, to rise to the surface, and then be imaged as the experiment progresses. The explanation for this is that with added pressure, bubbles which were originally uniformly spread across the interface, shrink and are made smaller by the pressure, creating “bubble-free” spaces at the interface. These spaces are then filled progressively with bubbles which had previously remained unseen at the start of the experiment and which through buoyancy rise to the surface and are then imaged. They are only buoyed to the surface relatively slowly due to the viscosity of the model mix. A possible solution to the creaming and buoyancy issues has already been discussed in the conclusion section of the previous chapter, and will not be discussed further.

Due to the viscosity of the mix, it can be argued that in contrast to some of Murray’s experiments, the interface of the bubbles in this case is only

replenished very slowly if at all with the surface active species (protein/emulsifier mix).

It must not be disregarded that at higher pressures the drive for disproportionation will of course be higher than at the lower pressures, as dissolution and incorporation of small bubbles will happen much more rapidly.

Most of the figures for the bubble numbers counted during the disproportionation experiments show a decrease throughout the 5 hours in which sampling took place. This is to be expected, as smaller bubbles shrink and are lost from the sample when they are incorporated into larger ones. The fact that the bubble numbers increase slightly on some occasions is most likely an artefact of the “tessellation” of the bubble. On the other hand it should not unduly affect the Bubble volume quoted. If a bubble has a very hazy border, which only tends to happen with very big bubbles, the Matlab script will, on rare occasions, draw small objects around the bubble which are then counted as separate bubbles, but they are in reality only very small specs. As it is fully automated there is no way of removing this error, but this error was not commonplace.

Comparing the graphs for bubble numbers in this chapter to those in the previous chapter (where single and pressure cycling experiments were carried out), there isn't always a loss of bubbles in the disproportionation experiment. This experiment is only testing small changes over a very long period of time.

In the previous chapter quite disruptive changes which took place over a short period of time were being assessed, and thus a change in bubble numbers was more marked. Bubble buoyancy issues played a role in the disproportionation experiments, where much larger bubbles were progressively pushed to the surface as the experiment proceeded. In the coalescence experiment, buoyancy only became an issue, due to harsh coalescence, or it might have been an issue if the experiment took place over longer time-scales, which was not the case.

Different gases show different aeration times, different resultant foam microstructures and also different disproportionation behaviour. Disproportionation behaviour for air and argon is nearly the same, which is not unsurprising seeing that at 25 °C both their solubilities in water are nearly the same, see Table 5.1 (Sander, 1999). Both gases show nearly the same slopes at each of the three different pressures tested. On the other hand carbon dioxide could not have reacted more differently. The negative slope at 1 bar absolute is in fact a true reflection of the microstructural rearrangements taking place at that pressure. The figure of bubble count also reflects this. The sample had lost all its structure by the end of the 5 hour run. This led to a more detailed investigation into the effects of this gas (and it is the gas with the highest solubility of the 5 used in this study). In Figure 5.24 an overnight run was set up, where the carbon dioxide aerated sample was inverted mechanically and continuously for 17 hours. This sample was then subjected to the normal 5 hour disproportionation experiment, under ambient pressure. Despite the big bubble sizes present in the foam, a size increase due to disproportionation was still

measured. During the standard experiment the mean bubble volume with carbon dioxide is nearly double that in oxygen. At 6 bar absolute the disproportionation behaviour is nearly double that present in oxygen. Disproportionation at 11 bar of all five gases tested, is the highest in carbon dioxide. Carbon dioxide disproportionation at the higher pressures of 6 and 11 bar was not carried out in the overnight sample, as the sample would not have allowed it, and as such at 1 bar pressure the microstructure was extremely fragile. An effect that was not considered at the time the experiments were carried out with carbon dioxide was to check the samples' pH, as this might have had implications for the behaviour of the protein within the system.

The disproportionation trends for helium and nitrous oxide are particularly interesting, in that both graphs at 1 bar show the highest disproportionation when compared to the other 5 gases. But even more curious is that Nitrous oxide is 66 times more soluble than helium. For helium, disproportionation is almost double that of air and argon (although air and argon are nearly three and a half times more soluble than helium). In comparison, for nitrous oxide it is nearly 20 times. Nitrous oxide shows the highest disproportionation at 6 bar and the second highest at 11 bar after carbon dioxide, although this is not too surprising, seeing that both Nitrous oxide, followed by Carbon dioxide are the two most soluble gases used in the study (compare solubilities: Table 5.1). Helium at 6 bar reacts similarly to air, but at 11 bar disproportionates at double the rate of air or argon, which is curious as helium is the least soluble gas of the five.

It might be argued that the aeration method with which different gases were incorporated into the mix was a somewhat crude method for incorporating these gases. Clearly this critique would be well founded if all the disproportionation traces were the same. As it has been demonstrated they are indeed different, which is evidence to the fact that the target gases were by and large incorporated into the viscous mix. Pre-sparging the mix with the gas also helped to saturate the mix in readiness for whipping, results without pre-sparging (data collected but not presented) are not as conclusive and the trends are somewhat more erratic.

The data collected with the vane instrument before the disproportionation experiments and results obtained after the 5 hour time period do not show any difference in bulk microstructural deformation. It might also be the case that disproportionation is actually taking place within the system but that the changes are too subtle for the vane geometry and the technique employed, to be able to detect a difference.

For the shear experiments, comparing the results in Figure 5.30 to those in Figure 5.31, the 30 minute time point seems to be when most of the break-up and coalescence (both in the shear cell and in the vane) takes place. Although at first sight the results seem contradictory, this might prove not to be so. The results in Figure 5.25 show that a lower shear rate (i.e 100 s^{-1}) has the effect of dramatically increasing the mean bubble volume. This might have happened

under the “shear breakdown” regime too, but might not have led to the characteristic overarching bubble, which would only have appeared under shear for a longer time. On the other hand the mean bubble volume only increased very slowly at the faster shear rate (of 200 s^{-1}), but only took a short time to show “breakdown” in Figure 5.31. This can be explained by Figure 5.28, where the sample microstructure broke down almost always after a shear rate of around 125 s^{-1} , and this, after only 10 minutes shear. Breakdown at 125 s^{-1} happened regardless of the target shear rate under investigation.

The observations made with the pressure release experiments run counter-intuitive to what might be expected, but the phenomenon might be explained by the following: a quick release, expands the interface in a short time-frame and thus protects it from further deformations or bubble interactions, but a slow release only stretches the interface very slowly for a longer time-frame, allowing it to deform with each added release wave, and thus when the release has ceased, the interface is still able to deform further which it continues to do. It can be argued further, that a slow release process is exposing the sample to dynamic bubble surface changes, for a longer period of time when compared to the short release, which only allows the bubble a shorter period of time to coalesce with other bubbles, and the deformation of the interface stops very quickly too. The fast pressure release rate exposes the sample only briefly to the destabilising influence, and once this has stopped, little extra coalescence takes place, and thus a quick pressure release can be seen to be protective against extra coalescence events.

5.6 *Concluding remarks*

It can be said that the microstructural behaviour of our model system was revealed through the shear, pressure release and disproportionation experiments. Behaviour in one experiment helped underpin the understanding in the following sections and experiments.

The model foam developed seems fairly robust to extraneous influences if these happen to be large and fast as these caused the least damage to the bubbles. This statement is applicable if the disruption is either due to shear or pressure. On the other hand, if these changes were slow and subtle, they were much more detrimental to the foam composition.

Both in the pressure release experiments and in the shear experiments with the vane rheometer, small progressive changes, had a more detrimental effect on the foam microstructure than large and quick changes did. This can even be seen between the two different shear experiments that were carried out. The one that was sheared in a linear fashion where shearing started off slowly and then progressed to reach its full speed towards the end of the run, which was more detrimental to the final foam than the one that sheared the foam in a continuous fashion at the full shear speed for the entire duration. In the linear regime the slowest shear rate was the one that created the biggest mean increase in volume, and the fastest, the least. In the continuous mode it was not

that clear cut. The slowest again elucidated the biggest increase in mean volume, but it was then later followed by the fastest shear rate, and finally the second fastest shear rate showed the least change.

If, on the basis of these findings, recommendations were to be made to the ice-cream industry, it must be said that any process should avoid particularly slow extrusion speeds. Ideally the fastest feasible speed obtainable (which would of course be process dependent) should be chosen. It would also be advisable to avoid any un-necessary “stops and starts” as these have a dramatic destabilising effect on the resultant microstructure.

Contrary to what was cited in the current literature, where it is said that coalescence could be considerably accelerated by a rapid drop in pressure, with catastrophic bursting of bubbles taking place over the time scale of the pressure drop, the experiments in this chapter suggest that this mainly takes place if the pressure drop is slow, a fast pressure drop seemingly has more of a protective effect on the resultant bubble microstructure.

When considering the choice of gas to use within an aerosol canister, argon would be ideal if one were interested in quick structuring of a product after extrusion through the nozzle (as argon was the gas that whipped the model mix the fastest, by almost halving the whipping time which was normally around 30 minutes – the new whipping time empirically assessed!). An argon foam though, would have no extra added benefit in protecting against

disproportionation phenomena, when compared to a foam filled with air. Both these foams reacted similarly when allowed to disproportionate at ambient pressure.

Helium as a new carrier gas would not be a viable option either, as disproportionation takes place at nearly double the rate than it does in air, when assessed at 1 bar absolute pressure.

It is possible, using the Linkam setup, to assess any gas for its viability as a nitrous oxide replacement within pressurised aerosol containers, giving the setup a high degree of versatility.

6 Conclusions

Due to the fact that Emlea Full Fat and Elmlea light both have different fat ratios, different buttermilk levels, and Elmlea light has one more stabiliser, it was therefore difficult to conclude which reaction within the whipping dynamics was just purely due to the fat level alone. Hence why the reformulated mixes had an identical continuous phase but the only ingredient that varied between the formulations was the ratio of hard to liquid oil.

In the reformulated emulsions there was always a constant trade-off between the following attributes: whipping kinetics, bubble size (structure), bulk effects, mouth-feel and viscosity; with none of the six reformulated samples able to adequately show desirable properties in all of the attributes. Taking these trade-offs into account, the mix that was able to show good whipping kinetics, good bubble size and desirable mouth-feel and viscosity, (but show somewhat reduced bulk effects during slumping) was mix 3. This formulation must therefore be the mix in the optimum formulation space (with 20% hardened oil and 14% liquid oil).

Within the pressure stability work, pressure induced changes had a considerable impact on foam microstructure which ultimately will affect its processing. It will also have an impact on the stability and texture of the finished aerated product. The methodology covered in this thesis offers new routes to

follow these changes and add a new insight into the dynamics of foam behaviour under increasingly complicated situations.

7 Further Work

Scope for further investigation with model food foams might be with in situ measurements of the processes taking place dynamically, in which the bubbles might be visualised immediately post-shear and still under pressure. Work by Balerin *et al.*, (2007) (described in section 1.2.10) goes some way to do this, but there is scope for possible refinement to their methodology. In their experiment a pilot scale foaming line was equipped with a range of on-line probes, including flow-meters, pressure, temperature and multiple light scattering sensors. The combination of these sensors has allowed them to measure bubble sizes under pressure, at different stages of the process but focusing particularly after the mixing geometry. By doing this they mention that they image static (i.e. stopped) foams. The relaxation while static with subsequent further shear once the foam was set in motion again would surely have a marked and detrimental influence on the final microstructure of the foam that was imaged.

In the experiments it is elucidated that well characterised model fluids were aerated using a continuous dynamic foaming device, in which stable foams were obtained, with a range of bubble sizes not dissimilar to those of actual food foams (Balerin *et al.*, 2007). A useful extension to their work would be research and

further experiments on actual food foams and real systems and, if technically feasible, with mixed systems being dynamically sheared and which would not require the process to be stopped and started.

Taking the current Linkam pressure cell setup, in an attempt to eliminate the pseudo-creaming effects seen with low air phase volume foams, it might be possible to try imaging these using an inverted confocal setup. This would ensure that micrographs of the foam were taken from below the glass crucible and not from a creamed layer on the foam surface. One possible problem with this method might be that the thickness of the serum layer might not allow the foam to be imaged.

Further work with creams might determine their behaviour when subject to pressure changes. Experiments similar to those carried out in chapters 4 and 5 could be performed, where the cream is subjected to a pressure drop or pressure cycling event and this would assess the cream for its robustness to further processing of this kind. It would be interesting to see how the coalescence profile of a cream structure might differ from that of an ice-cream model mix, and whether the cream would show any coalescence at all under such harsh treatment regimes.

Some further work with the whipped creams might involve experimenting with slumping under cool conditions, to simulate refrigerator storage, prior to serving. This would be quite challenging to perform, as one would have to control for condensation build-up on the camera lens.

Another experiment could involve imaging only one slumping tower at a time, whereby the cream would be placed within the centre of a cylindrical vessel and the experiment started. As the experiment progressed, and the tower beginning to lean on its preferred axis, the container could be rotated to obtain a side-on view.

A series of controlled Tribology experiments could be performed, where the friction is tested as a function of cream whipping time and overrun measurement. One could test an optimally whipped sample and an overwhipped one.

Further experiments could be performed, testing the tribometers' response to the creams as a function of temperature and/or force.

Reference List

- Allen, K.E., Murray, B.S. and Dickinson, E. (2008) Development of a model whipped cream: Effects of emulsion droplet liquid/solid character and added hydrocolloid. *Food Hydrocolloids* **22**: 690-699.
- Arbuckle, W.S. (1986) *Ice-cream*. New York: Van Nostrand Reinhold.
- Balerin, C., Aymard, P., Ducept, F., Vaslin, S. and Cuvelier, G. (2007) Effect of formulation and processing factors on the properties of liquid food foams. *Journal of Food Engineering* **78**: 802-809.
- Bamforth, C.W. and Milani, C. (2004) The foaming of mixtures of albumin and hordein protein hydrolysates in model systems. *Journal of Science and Food Agriculture* **84**: 1001-1004.
- Belitz, H.D., Grosch, W., Schieberle, P., Burghagen, M.M. (2004) *Food chemistry*, 3rd Ed., (Translated by Burghagen, M.M.), Springer.
- Bell, A., Gordon, M.H., Jirasubkunakorn, W. and Smith, K.W. (2007) Effects of composition on fat rheology and crystallisation. *Food Chemistry* **101**: 799-805.
- Ben and Jerry website (2006) From Cow to Cone: Vermont's Finest production process, (text version), from: http://www.benjerry.com/our_company/research_library/production [accessed: 09.06.06].
- Bisperink, C.G.J., Ronteltap, A.D. and Prins, A. (1992) Bubble-Size Distributions in Foams. *Advances in Colloid and Interface Science* **38**: 13-32.
- Bolotin, P.A., Baranovsky, S.F., Chernyshev, D.N. and Evstigneev M.P. (2007) Spectrophotometric study of the solution interactions between riboflavin, sodium salicylate and caffeine. *International Journal of Physical Sciences* **2**: 68-72.
- Bruhn, C.M. and Bruhn, J.C. (1988) Observations on the Whipping Characteristics of Cream. *J. Dairy Sci.* **71**: 857-862.
- Business Wire (2008) Business Services Industry: Starbucks and Unilever Sign Licensing Agreement to Grow Super-Premium Starbucks Ice Cream Business, Business Wire, Sept 15, 2008, from: http://findarticles.com/p/articles/mi_m0EIN/is_2008_Sept_15/ai_n28094939?tag=content;coll [accessed: 10.01.09]
- Calvert, J.R. and Nezhati, K. (1987) Bubble-Size Effects in Foams. *International Journal of Heat and Fluid Flow* **8**: 102-106.

-
- Camacho, M.M., Martinez-Navarrete, N., and Chiralt, A. (2001) Stability of whipped dairy creams containing locust bean gum/[lambda]-carrageenan mixtures during freezing-thawing processes. *Food Research International* **34**: 887-894.
- Campbell, G.M. and Mougeot, E. (1999) Creation and characterisation of aerated food products. *Trends in Food Science & Technology* **10**: 283-296.
- Cosway, D. (2008) Manufacturing industry section: Ice cream, science with a chocolate topping, *Chemistry and Industry*, Feb 25, 2008, available online under: http://findarticles.com/p/articles/mi_hb5255/is_4/ai_n29418248 [accessed: 10.01.09]
- Dairycrest website (2008) Buttermilk Powder, Ingredient Datasheet, Dairycrest, from: www.dairycrest.co.uk [accessed: 15.10.2008]
- Damodaran, S. (2004) Adsorbed layers formed from mixtures of proteins, *Curr. Opin. Colloid Interface Sci.* **9**:328-339.
- Danisco personal communication (2008) Best dissolution method and Krafft point of Lactem emulsifier [May 2008]
- Danisco website (2009) Products and ingredients: emulsifiers, from: http://www.danisco.com/cms/connect/corporate/products%20and%20services/product%20range/emulsifiers/pge/pge_en.htm [accessed: 06.03.09]
- Davies, E., Dickinson, E., and Bee, R.D. (2001) Orthokinetic destabilization of emulsions by saturated and unsaturated monoglycerides. *International Dairy Journal* **11**: 827-836.
- de Vicente, J., Stokes, J.R., and Spikes, H.A. (2006) Soft lubrication of model hydrocolloids. *Food Hydrocolloids* **20**: 483-491.
- Dimitreli, G. and Thomareis, A.S. (2008) Effect of chemical composition on the linear viscoelastic properties of spreadable-type processed cheese. *Journal of Food Engineering* **84**: 368-374.
- DMI website (2005) Dairy Management Incorporated: Buttermilk Powder, Ingredients and Features, from: www.innovatewithdairy.com [accessed: 16.10.08]
- Drewett, E.M. and Hartel, R.W. (2007) Ice crystallization in a scraped surface freezer. *Journal of Food Engineering* **78**: 1060-1066.
- Dubey, U.K. and White, C.H. (1997) Ice Cream Shrinkage: A Problem for the Ice Cream Industry. *J. Dairy Sci.* **80**: 3439-3444.

-
- Dutta, A., Chengara, A., Nikolov, A.D., Wasan, D.T., Chen, K. and Campbell, B. (2004) Destabilization of aerated food products: effects of Ostwald ripening and gas diffusion. *Journal of Food Engineering* **62**: 177-184.
- Eisner, M.D., Jeelani, S.A.K., Bernhard, L. and Windhab, E.J. (2007) Stability of foams containing proteins, fat particles and nonionic surfactants. *Chemical Engineering Science* **62**: 1974-1987.
- Eisner, M.D., Wildmoser, H. and Windhab, E.J. (2005) Air cell microstructuring in a high viscous ice cream matrix. *Colloids and Surfaces A: Physicochemical and Engineering Aspects* **263**: 390-399.
- Ettelaie, R., Dickinson, E., Du, Z. and Murray, B.S. (2003) Disproportionation of clustered protein-stabilized bubbles at planar air-water interfaces. *Journal of Colloid and Interface Science* **263**: 47-58.
- European Commission website (2006) Case No COMP/M.3975 - Cargill/Degussa Food Ingredients, Lecithin, Article 8 (1), REGULATION (EC) No 139/2004, Brussels, 29 III 2006 C(2006) 1034 final, 29/03/2006, from: <http://eur-lex.europa.eu> [accessed: 10.10.2008].
- Færgemand, M., Pedersen, B.V., Olesen, S.K. and Krog, N. (2003) Emulsifier Functionality probed by interfacial rheology, Proceedings of the 3rd International Symposium on Food Rheology and Structure, 535-536.
- Ferrando, M. and Spiess, W.E.L. (2000) Review: Confocal scanning laser microscopy. A powerful tool in food science. *Food Science and Technology International* **6**: 267-284.
- Garrett, P.R. (1993) Recent developments in the understanding of foam generation and stability. *Chemical Engineering Science* **48**: 367-392.
- Goff, H.D. (1997) Colloidal aspects of ice cream--A review. *International Dairy Journal* **7**: 363-373.
- Goh, E.M. (2002) Applications and uses of palm and palm kernel oils in speciality products. *Malaysian Oil Science and Technology* **11**: 46-52.
- Golding, M. and Pelan, E. (2008) Application of Emulsifiers to Reduce Fat and Enhance Nutritional Quality. In *Food emulsifiers and their applications*. Hasenhuettl, G.L., and Hartel, R.W. (eds). Springer, 327-348.
- Graf, E. and Mueller, H.R. (1965) Fine structure and whippability of sterilised cream. *Milchwissenschaft* **20**: 302-308.

-
- Heertje, I. (1993) Microstructural studies in fat research. *Food Structure* **12**: 77-94.
- Hui, Y. H. (2006) Handbook of food science, technology, and engineering, CRC Press
- Igoe, R.S. (1983) *Dictionary of food ingredients*, van Nostrand and Reinhold Company, seen on the food resource page of: The College of Health and Human Sciences, Oregon State University, From: <http://food.oregonstate.edu/glossary/c/cornsirup.html> [accessed: 27.02.09]
- IFR website (2009) Institute of Food Research, Norwich, Orogenic displacement of Proteins, from: <http://www.ifr.ac.uk/SPM/Proteins.html> [accessed: 11.06.09]
- IUPAC website (1997) Krafft point definition, *Goldbook: Compendium of Chemical Terminology*, 2nd Edition, from: <http://www.iupac.org/goldbook/K03415.pdf> [accessed: 24.03.09]
- Jakubczyk, E. and Niranjana, K. (2006) Transient development of whipped cream properties. *Journal of Food Engineering* **77**: 79-83.
- Keys, A., Anderson, J.T., and Grande, F. (1965) Serum cholesterol response to changes in the diet : IV. Particular saturated fatty acids in the diet. *Metabolism* **14**: 776-787.
- Kokelaar, J.J. and Prins, A. (1995) Surface rheological properties of bread dough components in relation to gas bubble stability. *Journal of Cereal Science* **22**: 53-61.
- Krog, N. J. (1997) Food emulsifiers and their chemical and physical properties, in: S. E. Friberg, K. Larsson (Eds.) *Food Emulsions*, 3rd ed., Marcel Dekker, , pp. 141-188.
- Leser, M.E. and Michel, M. (1999) Aerated milk protein emulsions -- new microstructural aspects. *Current Opinion in Colloid & Interface Science* **4**: 239-244.
- Luengo Hendriks, C. L., Rieger, B., van Ginkel, M., van Kempen, G. M. P. and van Vliet, L. J. (2006) *DIPimage: a Scientific Image Processing Toolbox for MATLAB*, <http://www.qi.tnw.tudelft.nl/DIPLib>, 1999-2006.
- Mackie, A.R., Gunning, A.P., Wilde, P.J. and Morris, V.J. (1999) Orogenic Displacement of Protein from the Air/Water Interface by Competitive Adsorption. *Journal of Colloid and Interface Science* **210**: 157-166.

Malone, M.E., Appelqvist, I.A.M., and Norton, I.T. (2003) Oral behaviour of food hydrocolloids and emulsions. Part 1. Lubrication and deposition considerations. *Food Hydrocolloids* **17**: 763-773.

Malvern Instruments website (2009) Application Note: The use of modern rheometers in characterising the behaviour of foods, Bohlin Application note: MRK609-01, from: www.malvern.co.uk, [last accessed: 01.03.09].

McClements, D.J. (2004) Protein-stabilized emulsions. *Current Opinion in Colloid & Interface Science* **9**: 305-313.

Morrison, A., Kimsey, I.M., Marks, H. (1992) Whippable Non-dairy creams, US Patent number, 005149557 A.

Murray, B. S., Campbell, I., Dickinson, E., Maisonneuve, K., Nelson, P. V. and Söderberg, I. (2002a) Technique for studying the effects of rapid surface expansion on bubble stability, *Langmuir*, **18**:5007-5014.

Murray, B. S., Cattin, B., Schüler, E. and Sonmez, Z. O. (2002b) Response of Adsorbed Protein Films to Rapid Expansion, *Langmuir*, **18**:9476-9484.

Murray, B. S. (2002) Interfacial rheology of food emulsifiers and proteins, *Curr. Opin. Colloid Interface Sci*, **7**:426-431.

Murray, B.S., Dickinson, E., Lau, C.K., Nelson, P.V., and Schmidt, E. (2005) Coalescence of protein-stabilized bubbles undergoing expansion at a simultaneously expanding planar air-water interface. *Langmuir* **21**: 4622-4630.

Narine, S.S. and Humphrey, K.L. (2004) A comparison of lipid shortening functionality as a function of molecular ensemble and shear: microstructure, polymorphism, solid fat content and texture. *Food Research International* **37**: 28-38.

Narine, S.S. and Marangoni, A.G. (1999) Relating structure of fat crystal networks to mechanical properties: a review. *Food Research International* **32**: 227-248.

Niranjan, K. (1999) An introduction to bubble mechanics in foods. In *Bubbles in Food*. Campbell, G.M., Webb, C., Pandiella, S.S., and Niranjan, K. (eds). St. Paul, Minesota: Eagan Press, 3-9.

Olympus web (2008) Theory of confocal microscopy: Fluorophores for confocal microscopy, Olympus Corporation 2004-2008, from: <http://www.olympusconfocal.com/theory/fluorophoresintro.html> [last accessed: 08.08.08].

-
- Perry, R.H. and Green, D.W. (1997) *Perry's Chemical Engineers' Handbook*. Internatinal edition: McGraw-Hill.
- Pernetti, M., van Malssen, K.F., Flöter, E., and Bot, A. (2007) Structuring of edible oils by alternatives to crystalline fat. *Current Opinion in Colloid & Interface Science* **12**: 221-231.
- PCS Instruments website (2008) Tribology machines, Traction machines, Testing Fuels, from: <http://www.pcs-instruments.com/index.shtml> [accessed: 15.10.2008]
- PhotochemCAD web (2008) Program and chemical database developed by Du, H., Fuh, R.A. and Lindsey, J.S., of Carnegie Mellon Univesity and North Carolina State University, Copyright 1998, (based on an early DOS version by Corkan, L.A. (1989)), from: <http://omlc.ogi.edu/spectra/PhotochemCAD/html/du98.html> [last accessed: 07.08.08]
- Pugnaroni, L.A., Ettelaie, R. and Dickinson, E. (2005) Brownian dynamics simulation of adsorbed layers of interacting particles subjected to large extensional deformation. *Journal of Colloid and Interface Science* **287**: 401-414.
- Ranken, M.D., Baker, C. and Kill, R.C. (1997) *Food Industries Manual*, 24th Edition, Springer Verlag.
- Richardson, G., Bergenstahl, B., Langton, M., Stading, M. and Hermansson, A.M. (2004) The function of [alpha]-crystalline emulsifiers on expanding foam surfaces. *Food Hydrocolloids* **18**: 655-663.
- Roller, S. and Jones, S.A. (1996) *Handbook of Fat replacers*. CRC Press.
- Russ, J.C. (1995) *The Image Processing Handbook*, second ed., CRC Press.
- Sander, R. (1999) Compilation of Henry's Law Constants for Inorganic and Organic Species of Potential Importance in Environmental Chemistry (Version 3), from: <http://www.mpch-mainz.mpg.de/~sander/res/henry.html> [accessed: 27.06.09].
- Smith, A.K., Goff, H.D. and Kakuda, Y. (2000) Microstructure and rheological properties of whipped cream as affected by heat treatment and addition of stabilizer. *International Dairy Journal* **10**: 295-301.
- Soille, P. (1999) *Morphological Image Analysis. Principles and Applications*. Springer Verlag.

Stanley, D.W., Goff, H.D. and Smith, A.K. (1996) Texture-structure relationships in foamed dairy emulsions. *Food Research International* **29**: 1-13.

Stauffer, C.E. (1999) *Emulsifiers*. St. Paul, Minnesota: Eagan Press.

Subramanian, R., Muthukumarappan, K., and Gunasekaran, S. (2006) Linear Viscoelastic Properties of Regular- and Reduced-Fat Pasteurized Process Cheese During Heating and Cooling. *International Journal of Food Properties* **9**: 377-393.

ten Grotenhuis, E., Paques, M. and van Aken, G.A. (2000) The Application of Diffusing-Wave Spectroscopy to Monitor the Phase Behavior of Emulsion-Polysaccharide Systems. *Journal of Colloid and Interface Science* **227**: 495-504.

Tcholakova, S., Denkov, N.D., Ivanov, I.B., and Campbell, B. (2006) Coalescence stability of emulsions containing globular milk proteins. *Advances in Colloid and Interface Science* **123-126**: 259-293.

van Aken, G.A., Blijdenstein, T.B.J., and Hotrum, N.E. (2003) Colloidal destabilisation mechanisms in protein-stabilised emulsions. *Current Opinion in Colloid & Interface Science* **8**: 371-379.

Wildmoser, H., Scheiwiller, J., and Windhab, E.J. (2004) Impact of disperse microstructure on rheology and quality aspects of ice cream. *Lebensmittel-Wissenschaft und-Technologie* **37**: 881-891.

Windhab, E.J., and Wildmoser, J. (2005) Low Temperature extrusion process and device for energy optimized and viscosity adapted micro-structuring of frozen aerated masses. Patent Number: WO/2005/070225, filed: 20-1-2005.

Xu, W., Nikolov, A., and Wasan, D.T. (2005) Shear-induced fat particle structure variation and the stability of food emulsions: I. Effects of shear history, shear rate and temperature. *Journal of Food Engineering* **66**: 97-105.

Appendix 1

A1.1 Functionality of the ingredients for the whipped creams

Due to the complexity of the reformulated mixes, and the addition of many different ingredients, the individual components making up the mix, will be discussed separately in the following sections.

A1.1.1 Lecithin

Lecithin acts as an emulsifier within food ingredient formulations. Emulsifiers derive their name from the ability to stabilise emulsions, and they contain a mix of hydrophilic (water-loving) and hydrophobic (oil-loving) substances. Lecithin is classed a ‘natural’ emulsifier, as in its basic production, fluid lecithin only requires physical operations to manufacture it. These might be centrifugation or degumming processes. Lecithin is the only marketed *natural* emulsifier. By contrast, *synthetic* emulsifiers (e.g. mono- or diglycerides) are artificially created compounds that are produced through chemical reactions. Lecithin is a by-product generated in the process of crushing oilseeds. These are generally soybeans. The vast majority of the lecithin sold on the market is extracted from soy oil (95%). Functions of lecithin are generally not limited to its emulsifying properties, but it also has an impact on flavour and other product characteristics. In many applications, lecithin’s multiple functionalities are used co-currently in the product. Lecithin is added in small quantities to food and animal feed products, cosmetics and pharmaceutical products (EC web, 2006).

Although it generally represents less than 1% of total production costs, it is usually essential to the industrial process and can radically change the quality of a final product. Different types of lecithin can be produced by the crushing of soybeans into soy meal and crude soy oil. The crude soy oil can be separated into degummed soy oil and so-called 'wet gums'. This process is then what is termed the 'degumming' process (EC web, 2006).

Wet gums are then further processed to 'crude' fluid lecithin by a drying process which takes place through evaporation. This crude fluid lecithin extracted in the mills is not yet suitable for use in most applications. Particularly in food applications, since variations in the degumming process and the quality and origin of the soybeans result in some heterogeneity (e.g. in viscosity). Therefore, the producers usually refine the crude lecithin by blending different crude lecithins and by adding fatty acids in order to reduce the viscosity. These operations produce 'standardised' or 'basic' fluid lecithin.

Different operations can then be applied to this basic fluid lecithin creating differences in the composition and functionalities of fluid lecithin (e.g. enzymatic modification, hydrogenation) (EC web, 2006).

Fluid lecithin can be further refined by removing the oil still present in the fluid lecithin. This operation produces lecithin in granule and/or powder form, the

‘deoiled’ lecithin (which is also termed: ‘pure’ lecithin), which consists almost only of emulsifying molecules. This type was the one used in this study. Different technologies can achieve this result. The conventional method uses acetone which yields a mix of powder and granules. Another technology is based on the use of CO₂ and yields only powder. Typical applications for deoiled lecithin are food applications (oil and fat spreads, instant products, bakery) and the health and nutrition sectors (food additives, sports nutrition) (EC web, 2006).

A1.1.2 Lactem

Food produced at the industrial scale requires the use of emulsifiers as processing aids to facilitate the uniform quality of an end product and also to ensure a long shelf life of the finished product. The functions of emulsifiers in foods are many and diverse: they facilitate emulsification, they promote controlled destabilisation of the oil phase and they help interact with the carbohydrates and the fat crystallisation process (Færgemand *et al.*, 2003).

In dairy products emulsifiers are usually typically present together with milk proteins and interactions with the proteins and the emulsifiers cannot be excluded. The interactions can be of two forms: competitive or cooperative. Competitive interactions can be described as those that result in protein desorption from the air bubble interface, whereas cooperative interactions are those where proteins and emulsifiers are co-adsorbed at the interface (Færgemand *et al.*, 2003).

Whether the emulsifier reacts in either a cooperative or competitive fashion is to some extent governed by the ratio of the emulsifier to the protein in the mix. But there are also clear differences between different types of emulsifiers and their respective ability to participate either in cooperative or competitive interactions. Therefore, within many food products several different emulsifiers are used, dependent on the products' final usage. If the product is to form a stable emulsion during quiescent storage for example, but then destabilise subsequently during whipping, as is the case with vegetable oil whipping cream alternatives (Færgemand *et al.*, 2003), like Elmlea, then various combinations of different emulsifiers need to be added to the formulation in order to facilitate this behaviour.

From the formulation in patent number: 005149557 A, by Morrison et al. (1992), granted to Unilever, it is suggested that both a stabilising and a destabilising emulsifier be used to obtain the desired quiescent stability; but yet allow the formation of partially coalesced structures during aeration. It is recommended that one of each be used. In the patent, soy lecithin was classed as a destabilising emulsifier and lactem was classified as a stabilising emulsifier. In addition it was stipulated that preferably one of each be used when formulating a non dairy whipping cream, and further options were given for alternate emulsifiers that could have been used. But the patent recommended Lactem and Lecithin as their preferred options.

A1.1.3 Buttermilk Powder (BMP)

The Buttermilk Powder used in this study is made from the liquid fraction which is obtained when sweet cream is churned during the manufacture of butter. The buttermilk is concentrated under vacuum and then spray dried, producing the resultant Buttermilk Powder (Dairycrest web, 2008). In the Elmlea formulation Buttermilk Powder is mainly added to the cream to form a palatable and organoleptically acceptable product. It is used partially for its flavour enhancing properties. It can impart flavour notes from sweet to sour. Beyond its versatility as a flavour compound it also adds concentrated calcium, protein and other important nutrients to the mix. Buttermilk Powder also brings several desirable properties to food formulations. It aids in emulsification as the proteins in the dry buttermilk act at oil/water interfaces, aiding in the formation and stabilisation of the fat emulsions. It can aid in foaming and water binding. In foaming, the dry buttermilk helps diffuse the protein to the air/water interfaces and reduces surface tension while also partially unfolding the protein. Encapsulated air bubbles form a stable and elastic film. Finally the water-holding capacity of buttermilk proteins is used to create desired textures within viscous food products (DMI web, 2005).

A1.1.4 Xanthan

Xanthan gums are a new breed of hydrocolloids which are collectively categorized as fermentation or biosynthetic gums. The microorganisms produce three distinct types of polysaccharides: extracellular polysaccharides, structural

polysaccharides and intracellular storage polysaccharides. The extracellular polysaccharides secreted are often complex in terms of their primary structure compared with more traditional gums. This frequently results in them having novel gelling and solution properties. The novel rheological behaviour of xanthan solutions has made the commercialisation of Xanthan gum a success. Xanthan is an extracellular polysaccharide from the microorganism *Xanthomonas campestris* an organism originally isolated from the rutabaga plant (a member of the cabbage family). Current commercial production of Xanthan gum is brought about through large-scale aerobic fermentation. Once fermentation is completed, the broth is pasteurised, followed by precipitation with isopropyl alcohol, then dried and milled to the desired particle size distribution (Roller and Jones, 1996).

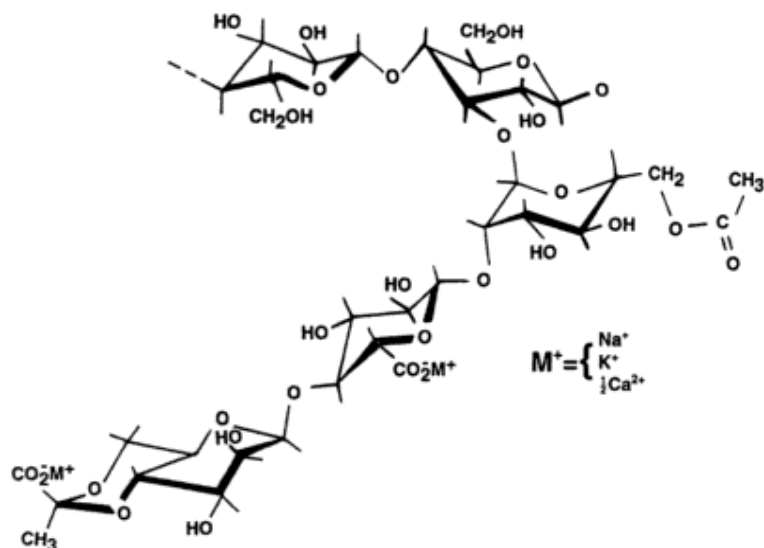


Figure A.1.1 Primary repeating structure of Xanthan from:(Roller and Jones, 1996)

Xanthan in terms of its conformation in solution is different from most other polysaccharide thickeners in that it usually exists as a rod-like conformationally ordered structure rather than as a random coil. This confers Xanthan its unique solution and gelling properties. The solutions are extremely pseudoplastic and show a different shear-thinning behaviour compared to solutions containing random coiled polysaccharides. Its pseudoplasticity results in Xanthan possessing high viscosities when not under the influence of a shear force (Roller and Jones, 1996).

The origins of the unusual solution properties of Xanthan lie in its molecular structure, which determines its conformational behaviour. It is generally believed that the weak gel-like properties of Xanthan solutions occur as a result of weak side by side associations of ordered chain sequences from different molecules to give a tenuous three-dimensional intermolecular network. With other polysaccharide gels the bonding in the junction zones needs to be strong in order to counter the considerable loss of conformational entropy as the fluctuating random coil chain is incorporated into the ordered junction zone. The gels that are consequently formed are quite strong. In Xanthan however, weak side-by-side enthalpically favoured associations can occur between different molecules without substantial loss of conformational entropy as the Xanthan chains are already conformationally ordered. Consequently the gel structure is only weakly bonded and can be easily disrupted by application of shear (Roller and Jones, 1996).

A1.1.5 Sodium Caseinate

Caseinate is the soluble form of casein prepared by reacting acid casein curd with an appropriate alkali e.g. NaOH. The caseinate dispersion containing 20 to 25% solids is then spray dried or roller dried to a moisture content of about 5%. Sodium caseinate is the most widely used caseinate and a number of grades with different viscosities can be manufactured (Ranken et al., 1997).

Acid casein is by its nature insoluble and is therefore not often used in food products in this form. However, an increasing number of food processors now prefer to buy acid and convert it to the sodium form themselves; this not only gives economic advantages but provides a more effective means of preparing a caseinate solution rather than trying to dissolve the very fine, poorly dispersible, sodium caseinate powder (Ranken et al., 1997).

Solubility may be generally defined as the amount of protein that goes into solution or into colloidal dispersion under specified conditions (of pH, ionic strength, protein concentration and temperature). Unlike whey proteins which exhibit excellent solubility over the entire pH range, caseinates (alkali dispersions of casein used in commercial applications) are almost insoluble in the region of their isoelectric point (pI: pH 4.0-5.0). However outside of this region caseinates possess excellent solubility (Hui, 2006).

Caseins possess high surface hydrophobicity with a well balanced distribution of hydrophilic and hydrophobic domains and possess a high degree of conformational flexibility which allows them to interact strongly at the air-water interface (Hui, 2006).

Due to their limited secondary structure, the caseins possess excellent heat stability. Solutions of sodium caseinate may be heated up to 140 °C for 60 minutes without precipitation (Hui, 2006).

Caseinates are used almost exclusively in the food industry. Sodium caseinate is superior to most food proteins in its emulsifying and water binding ability and is used for this purpose as an ingredient in the manufacture of meat products, coffee whiteners and whipped toppings (Ranken et al., 1997).

A1.1.6 Palm Oil

Palm oil and palm kernel oil are ideal raw materials for the production of speciality fats. Palm oil contains about 50% of the long-chain saturated fatty acids of which palmitic acid constitutes about 44% (Goh, 2002)

Table A.1.1 Percentage of fatty acids present in Cocoa Butter and Palm Oil.

| Fatty Acids | | Cocoa Butter | Palm Oil |
|--------------------------|------|--------------|----------|
| Myristic acid | 14:0 | | 1 |
| Palmitic acid | 16:0 | 26.5 | 44 |
| Stearic acid | 18:0 | 35 | 4.5 |
| Oleic acid | 18:1 | 35 | 39 |
| Linoleic acid (omega-6) | 18:2 | 3 | 10 |
| Linolenic acid (omega-3) | 18:3 | | 0.5 |
| Total Saturated | | 61.5 | 49.5 |

From: (Goh, 2002)

Palm kernel oil and coconut oil are the two lauric oils which are of commercial importance. These two oils are interchangeable in many applications because of their property similarities. However, palm kernel oil contains a higher amount of oleic acid than coconut oil. This makes palm kernel oil suitable for hydrogenation (hardening) in the production of speciality fats with different end-use melting points and hardness. Palm and palm kernel oils, like most of the other vegetable oils in their original state, have a limited application when utilised as such. Hence their properties have to be modified in order to extend the range of their utilisation (Goh, 2002).

Fractionation, hydrogenation and interesterification are commonly used for the production of speciality fats. Hydrogenation is carried out to remove the unsaturation of fatty acids and hence to increase the oxidative stability and melting

point of the oils. Depending on the extent of hydrogenation, the oils and fats can be modified to products of varying hardness, thus giving the oil a wider utility range (Goh, 2002).

Speciality fats produced from palm and palm kernel oils, especially the hydrogenated fats, are very stable against oxidation (Goh, 2002) This oxidative stability renders them resistant to rancidity which could impart “off-flavours” in many food products elaborated with them as an ingredient.

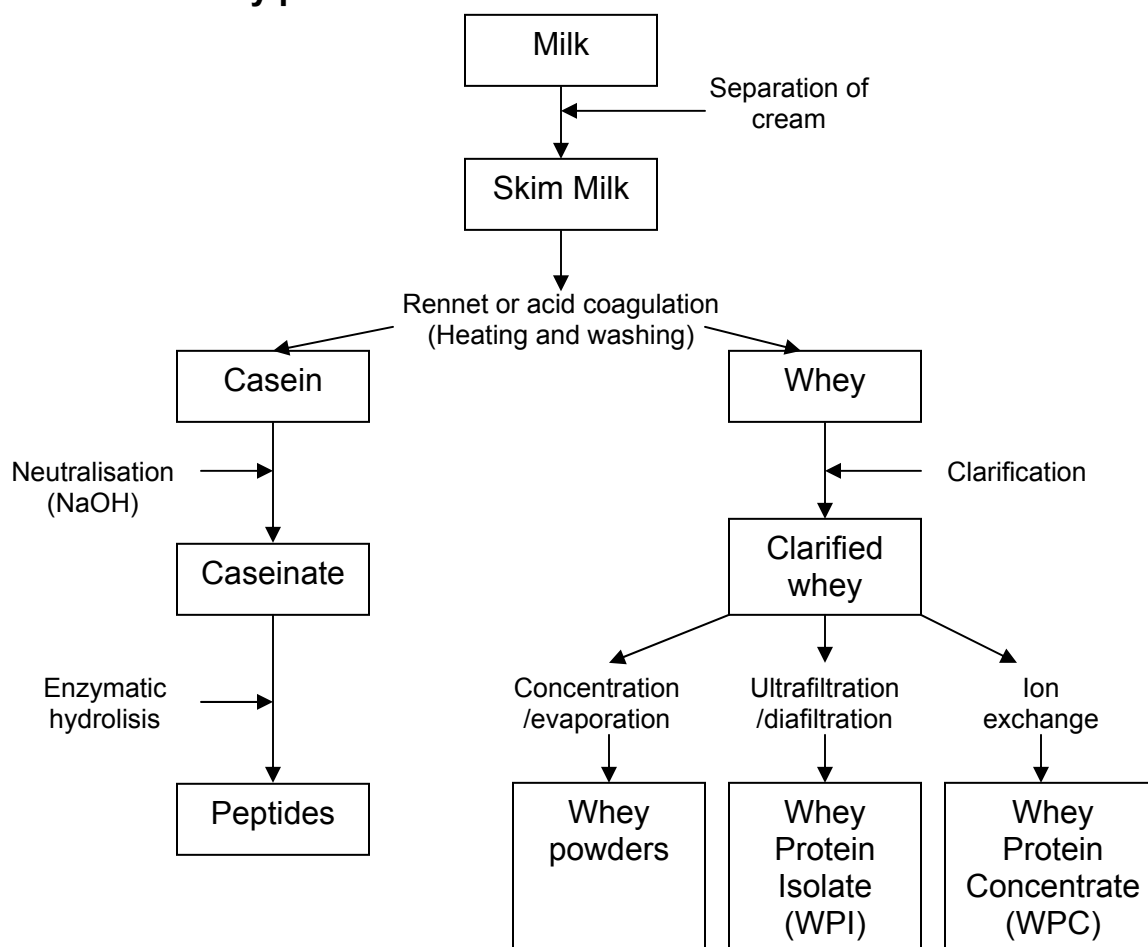
A1.2 Selection of the ingredients for the foam model mix

A1.2.1 Corn syrup

Corn syrup is a corn sweetener which is a viscous liquid containing maltose, dextrin, dextrose, and other polysaccharides. It is obtained from the incomplete hydrolysis of corn starch. It is classified according to the degree of conversion which is expressed as the dextrose equivalent (DE), which is the measure of sweetness of the corn syrup as compared to that of a sucrose syrup.

Generally the greater the degree of conversion that has taken place, the sweeter the syrup will be. Corn syrup is used as a replacement for sucrose but it is less sweet than sucrose. It can control crystallization in candy making, contribute body in ice cream, amongst other things freeze point depression, and provide pliability in confections (Igoe, 1983).

A1.2.2 Whey powder



Source: Hui (2006)

Figure A.1.2: Production routes of whey products and caseinate from Milk

Not only does milk comprise various proteins with unique intrinsic properties, the milk proteins themselves are commercially available in many different forms. Furthermore milk proteins may be modified by physical, chemical or enzymatic means, possibly resulting in significant improvements in one or more functional properties. However, physical and enzymatic methods of modification are currently preferred over chemical methods (Hui, 2006).

Randomly coiled structures such as caseins generally display greater viscosity in solution than whey proteins which have a compact globular structure (Hui, 2006)

Whey is produced as a by-product of cheese and casein manufacture. There are many possible products and manufacturing processes, which can be derived from milk, some of which are outlined in Figure A.1.2. The First step involves separation and selective concentration of residual fat and casein by centrifugation. This is followed by concentration of the whey proteins by the use of membrane separation (ultrafiltration and diafiltration). The protein stream is further concentrated by evaporation and then spray-dried to produce whey protein concentrate with an approximate protein concentration of 85%. Alternatively, further fractionation and concentration of the whey proteins may be performed using ion exchange to produce whey protein isolates (containing approximately 95% protein). The protein products described have a wide range of food ingredient and industrial applications, many utilising the emulsifying water and fat-binding properties of the proteins (Hui, 2006).

Whey proteins also adsorb rapidly to, unfold and re-orientate at the oil-water and air-water interfaces forming emulsions which are only slightly less stable than those formed by caseins under the same conditions. Whey proteins are readily

denatured above 70 °C, leading to aggregation, and depending on pH and protein concentration, precipitation or gelation (Hui, 2006).

A1.2.3 Polyglycerol Ester of Fatty acid (PGE)

Polyglycerol esters are produced from esterification of polyglycerols with fatty acids. Polyglycerol esters are often used in combination with distilled monoglycerides. Variations in the emulsifier are obtained through the type of fatty acids they contain and also polyglycerol. In addition further variations can be created with the degree of esterification they are subjected to. One of the main application areas for PGE is in the fine bakery area, where the polyglycerol esters provide improved cake batter performance, crumb structure and cake volume (Danisco web, 2009). They form a particularly stable foam. PGE's Krafft point is 60 °C and it will form the α -gel form after subjected to cooling at 5 °C.

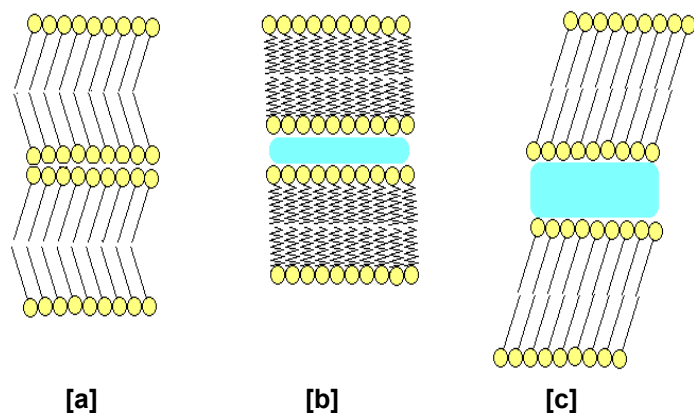


Figure A.1.3: Transition of PGE from its stable β -crystalline state [a], through to a liquid lamellar solution [b] into its final, α -gel form.

Appendix 2

A2.1 DSC Raw data (without baseline subtraction)

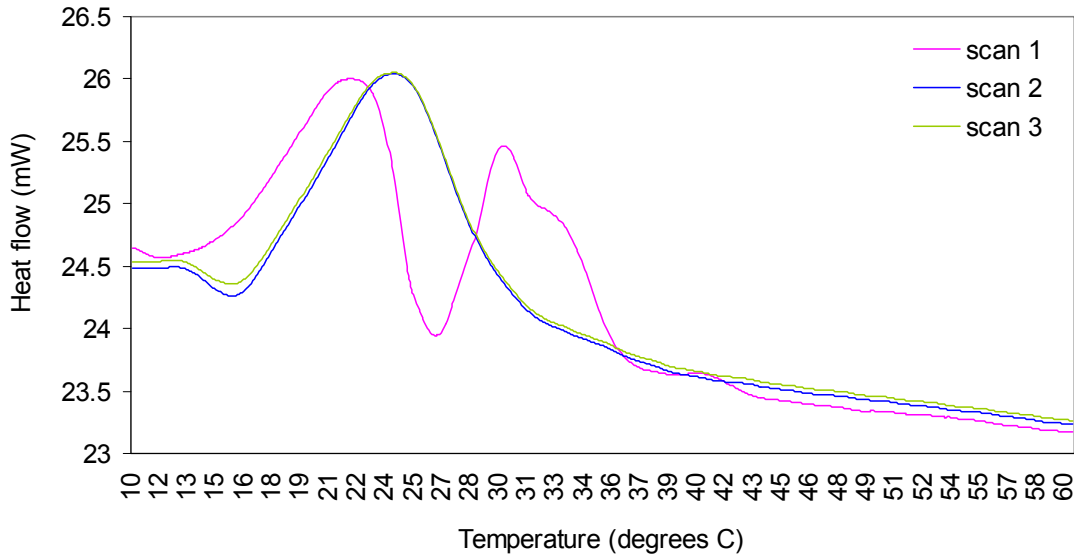


Figure A.2.1: DSC measurement of Elmlea light double cream at a sampling rate of 5°C per minute. Without baseline subtraction.

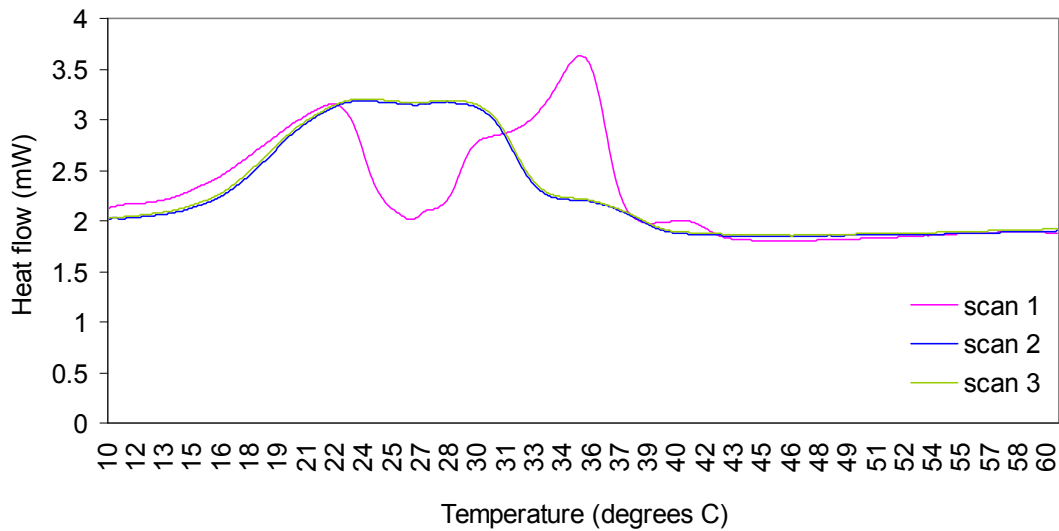


Figure A.2.2.: DSC measurement of Elmlea full fat double cream at a sampling rate of 5°C per minute. Without baseline subtraction.

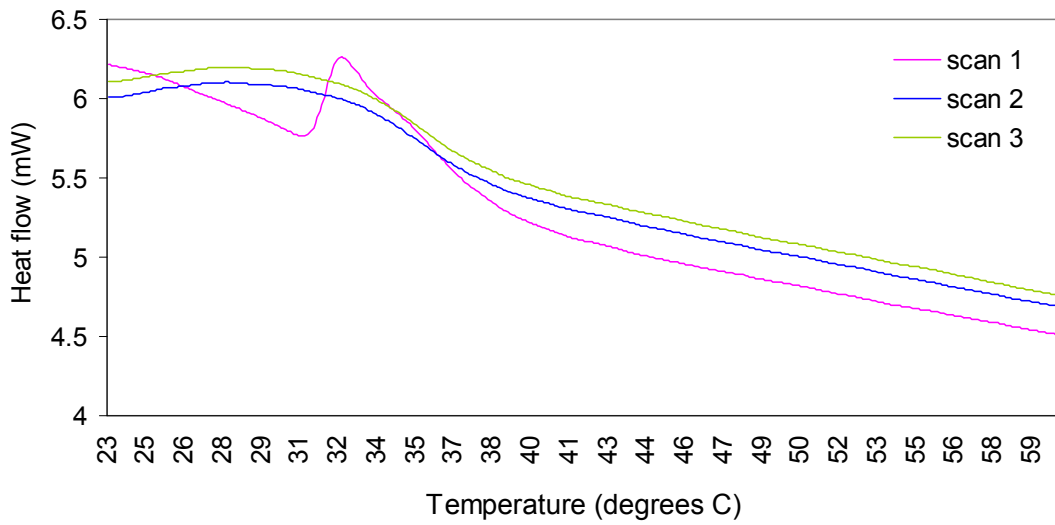


Figure A.2.3: DSC measurement of J. Sainsbury's double cream at a sampling rate of 5°C per minute. Without baseline subtraction.

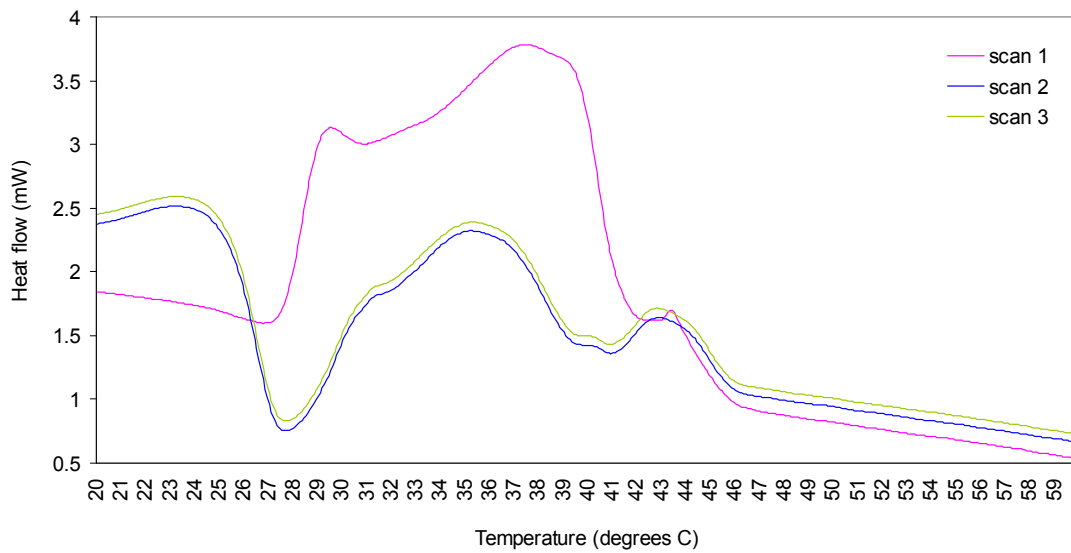


Figure A.2.4: DSC measurement at a sampling rate of 5°C per minute of pure hard palm oil which was used for all the re-formulated mixes. Without baseline subtraction.

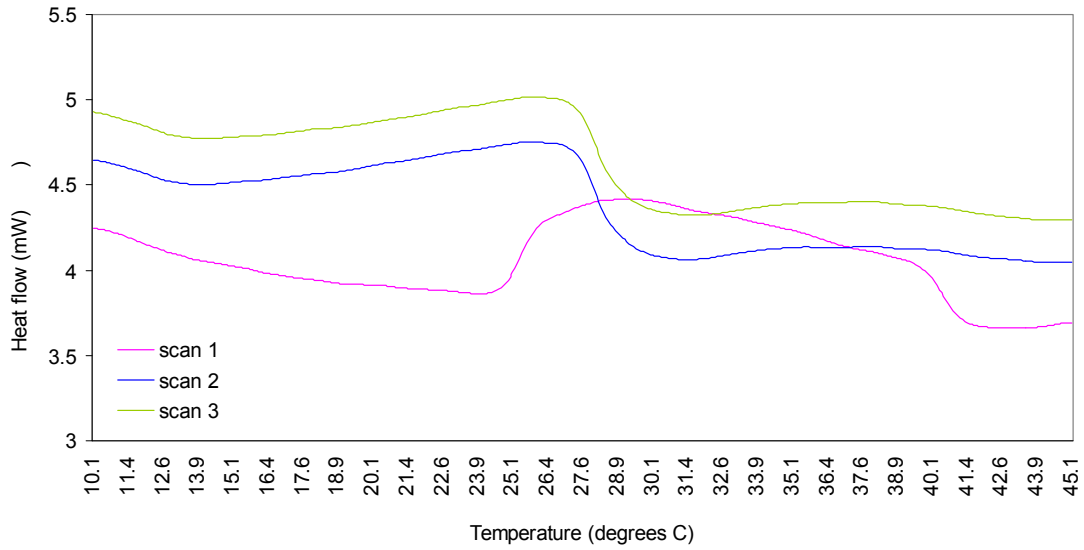


Figure A.2.5: DSC measurement of a re-formulated mix at a sampling rate of 5°C per minute. Mix Number 6 with 34% hard oil and no liquid oil fraction. Without baseline subtraction.

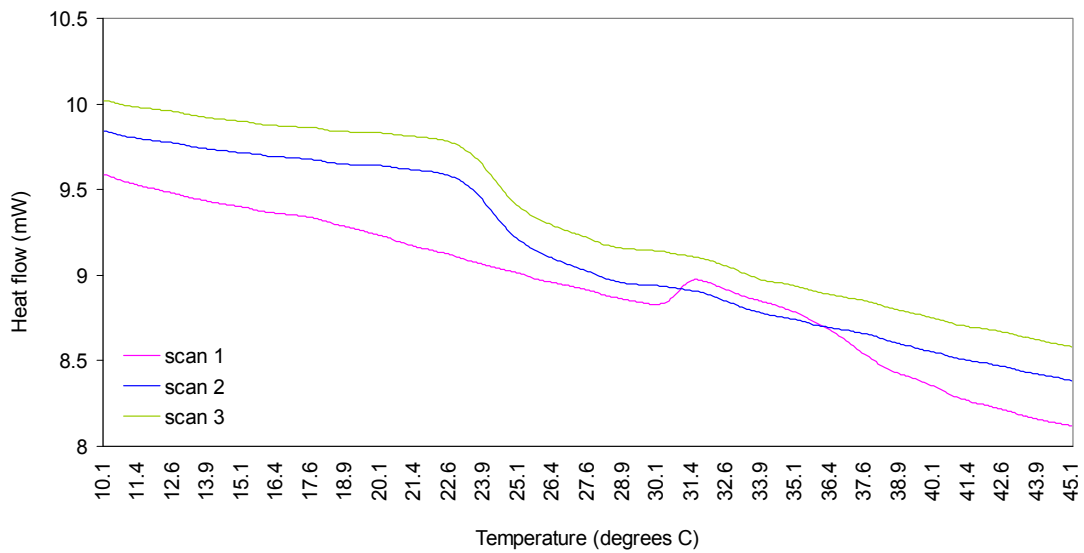


Figure 2.6: DSC measurement of a re-formulated mix at a sampling rate of 5°C per minute. Mix Number 3 with 20% hard oil and 14% liquid oil fraction. Without baseline subtraction.

Appendix 3

A3.1 Further bubble sizing data

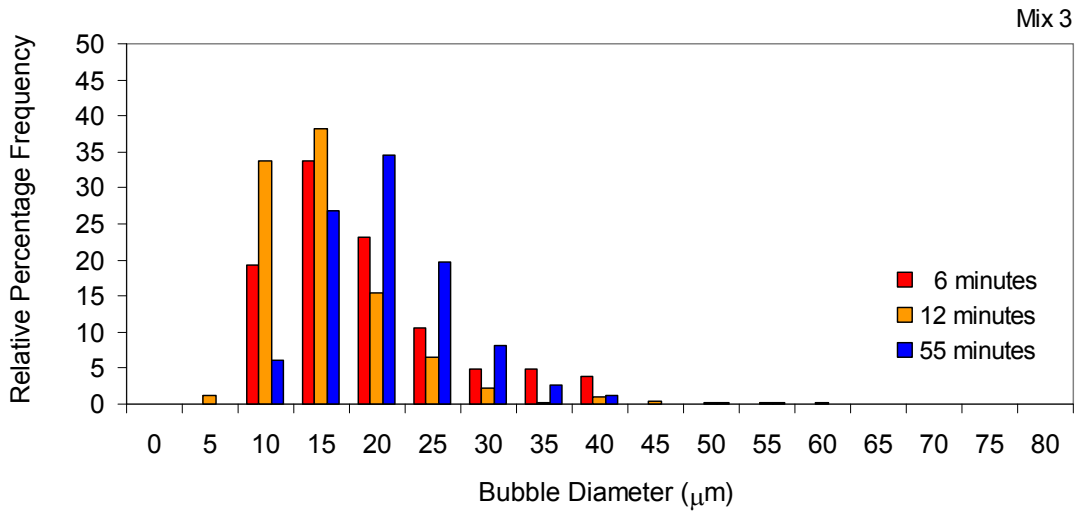


Figure A.3.1: Bar graph of Mix 3, illustrating the normalised bubble size distribution as a function of whipping time. Hard oil and liquid oil are 20 and 14 percent respectively.

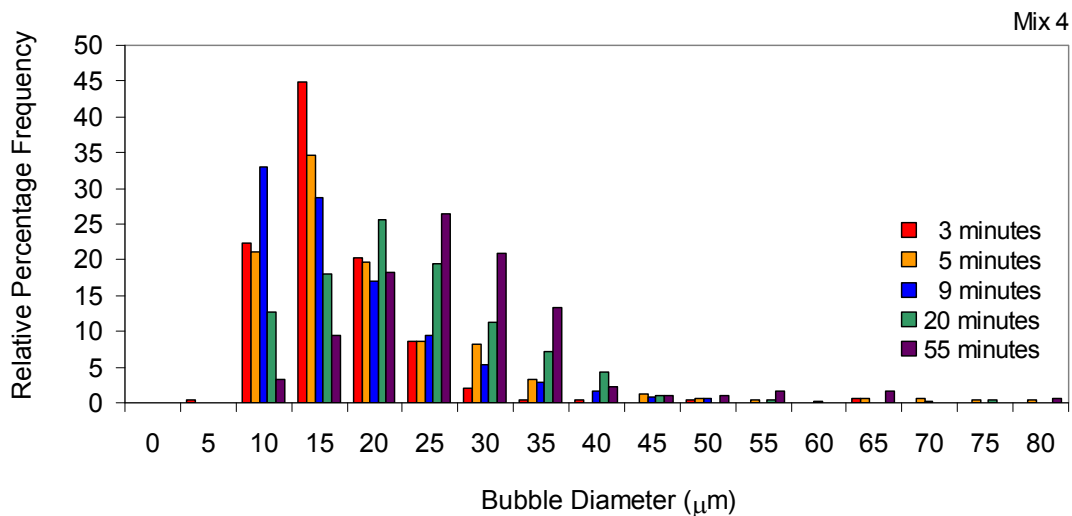


Figure A.3.2: Bar graph of Mix 4, illustrating the normalised bubble size distribution as a function of whipping time. Hard oil and liquid oil are 25 and 9 percent respectively.

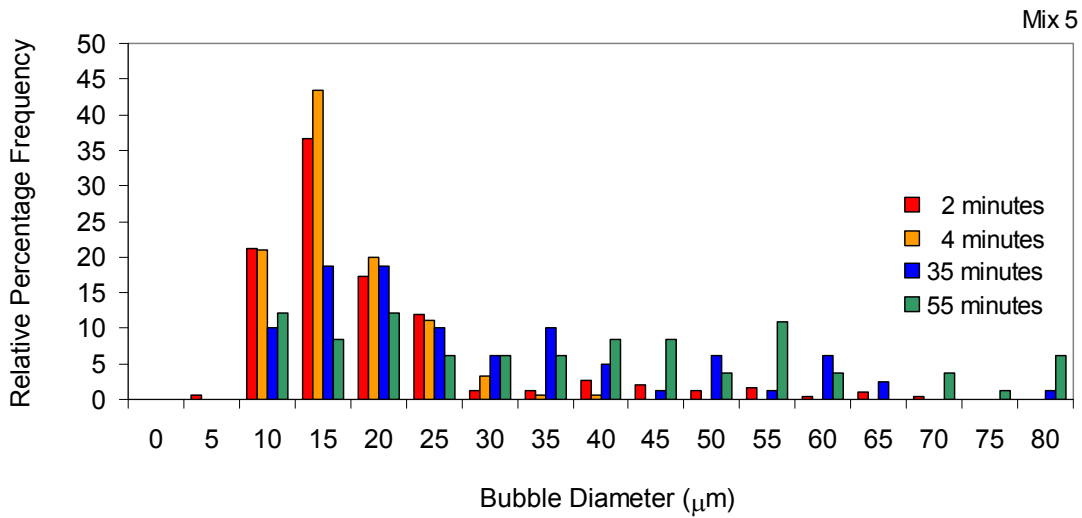


Figure A.3.3: Bar graph of Mix 5, illustrating the normalised bubble size distribution as a function of whipping time. Hard oil and liquid oil are 30 percent and 4 percent respectively.

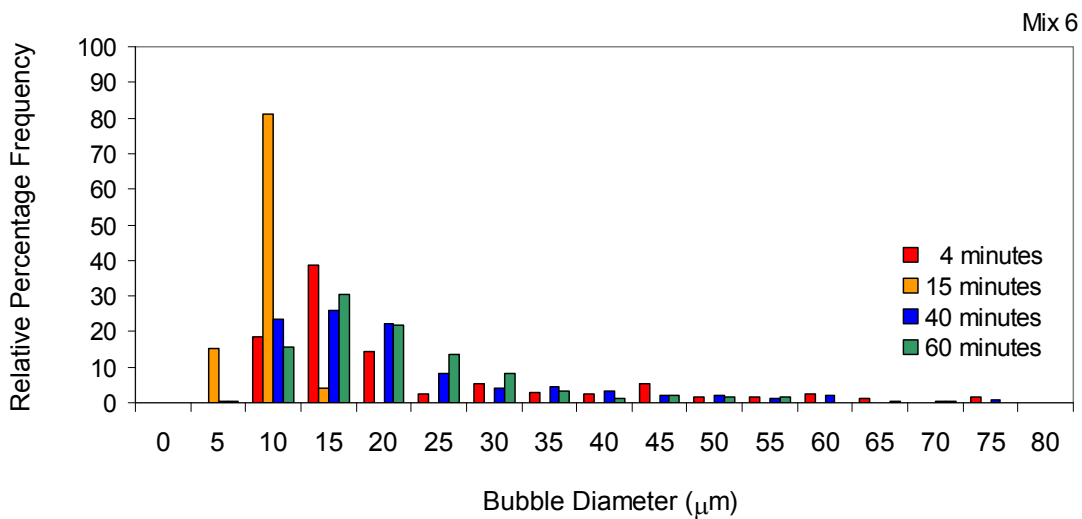


Figure A.3.4: Bar graph of Mix 6, illustrating the normalised bubble size distribution as a function of whipping time. Hard oil content is 34 percent with no liquid oil present.

Appendix 4

A4.1 Analysis of fat content with a Differential Scanning Calorimeter

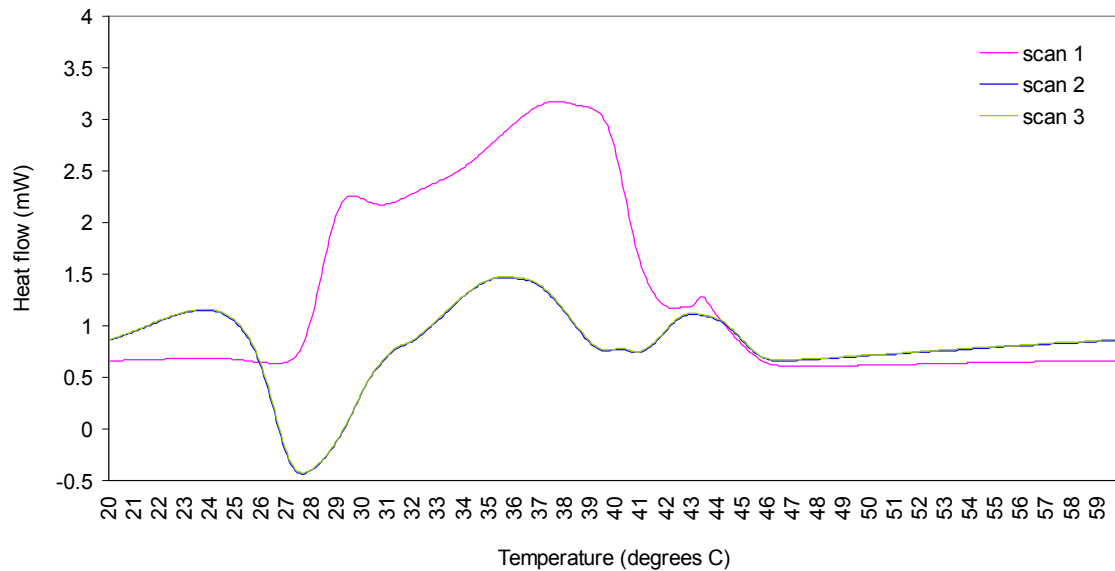


Figure A.4.1: DSC measurement at a sampling rate of 5 °C per minute of pure hard palm oil which was used for all the re-formulated mixes. Traces include baseline subtraction.

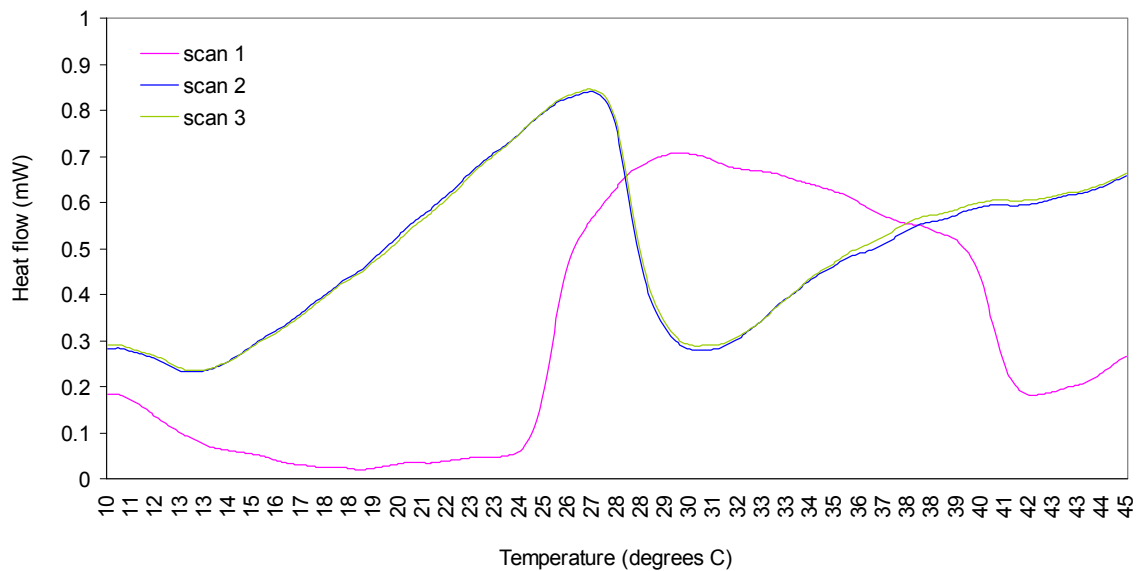


Figure 4.2: Mix Number 6 with 34% hard oil and no liquid oil fraction. DSC measurement of the re-formulated mix at a sampling rate of 5 °C per minute. Traces include Baseline subtraction.

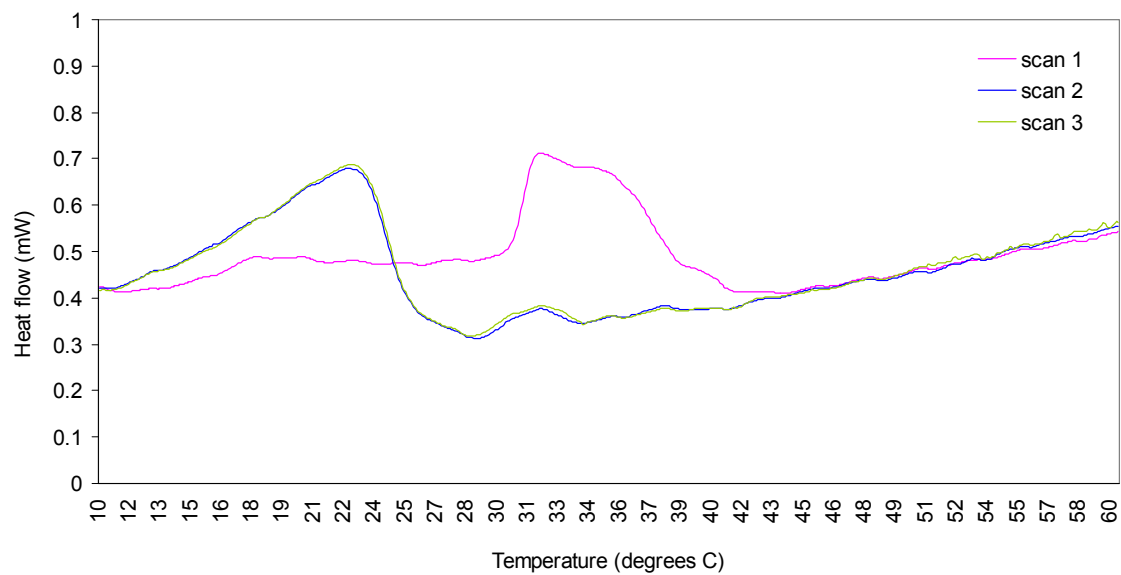


Figure A.4.3: Mix Number 3 with 20% hard oil and 14% liquid oil fraction. DSC measurement of the re-formulated mix at a sampling rate of 5 °C per minute. Traces include Baseline subtraction.

Table a.4.1 Peak analysis of the thermal behaviour of the reformulated creams within the DSC

| Analysis to Figure A.4.1 (Sil-palm oil. Base ingredient) | | | | |
|--|--------|------------|------------|----------|
| | | | Peak onset | Peak end |
| scan 1: | peak 1 | 5.55 J/min | 27.5 °C | 46 °C |
| scan 2 | | 2.89 J/min | 28 °C | 47 °C |
| scan 3 | | 2.89 J/min | 28 °C | 47 °C |
| Analysis to Figure 4.2 – Mix 3 | | | | |
| | | | Peak onset | Peak end |
| scan 1: | peak 1 | 1.56 J/min | 24 °C | 42 °C |
| scan 2 | | 0.97 J/min | 13 °C | 30 °C |
| scan 3 | | 0.97 J/min | 13 °C | 30 °C |
| Analysis to Figure A.4.3 – Mix 6 | | | | |
| | | | Peak onset | Peak end |
| scan 1: | peak 1 | 0.44 J/min | 10 °C | 30.5 °C |
| | peak 2 | 0.21 J/min | 30.5 °C | 43 °C |
| scan 2 | | 0.59 J/min | 10 °C | 28 °C |
| scan 3 | | 0.59 J/min | 10 °C | 28 °C |

Appendix 5

A5.1 Publications